THE ROLE OF METAMORPHIC AND GEOCHEMICAL FACTORS IN THE FORMATION OF GEM CORUNDUM, SPINEL, AND HAÜYNE IN METACARBONATES OF THE LAKE HARBOUR GROUP, BAFFIN ISLAND, CANADA

by

PHILIPPE MAXIME BELLEY

B.Sc., University of Ottawa, 2014

A DISSERTATION SUBMITTED IN PARTIAL FULFILLMENT OF
THE REQUIREMENTS FOR THE DEGREE OF

DOCTOR OF PHILOSOPHY

in

THE FACULTY OF GRADUATE AND POSTDOCTORAL STUDIES

(Geological Sciences)

THE UNIVERSITY OF BRITISH COLUMBIA
(Vancouver)

April 2019

The following individuals certify that they have read, and recommend to the Faculty of Graduate and Postdoctoral Studies for acceptance, the dissertation entitled:

The role of metamorphic and geochemical factors in the formation of gem corundum, spinel, and haüyne in metacarbonates of the Lake Harbour Group, Baffin Island, Canada

Submitted by Philippe Maxime Belley in partial fulfillment of the requirements for the degree of Doctor of Philosophy in Geological Sciences.

Examining Committee:

Dr. Lee A. Groat
Supervisor

Dr. James K. Mortensen
Supervisory Committee Member

Dr. Lori Kennedy
Supervisory Committee Member

Dr. Tom Troczynski
University Examiner

Dr. Maya Kopylova
University Examiner

Dr. Ian Graham
External Examiner
University of New South Wales

Abstract

The Lake Harbour Group (LHG) metacarbonates on Baffin Island contain occurrences of the gemstones sapphire (corundum), spinel (including cobalt-blue), and lapis lazuli (blue haüyne-rich rock). This dissertation uncovers the regional geologic processes (*e.g.*, metamorphic history, metasomatism, protolith geochemistry) that influence gemstone potential by developing genetic models for the LHG gem mineral occurrences. Both barren and gem-bearing metacarbonates were studied using field examination and sampling, petrological (optical) and scanning electron microscope petrography, and whole rock geochemistry. Boron isotope geochemistry, thermodynamic modelling, and age-dating (zircon U-Pb and mica ^{40}Ar-^{39}Ar) were employed for selected occurrences.

Corundum formation was made possible by three equally important sequential metamorphic reactions: (1) formation of nepheline, diopside, and K-feldspar (inferred) at granulite facies peak metamorphic conditions; (2) partial retrograde replacement of the peak assemblage by phlogopite, oligoclase, calcite, and scapolite; and (3) retrograde break-down of scapolite + nepheline to form albite, muscovite, corundum, and calcite. The corundum-forming reaction only occurs in a <100 °C window. Spinel and haüyne formed at granulite facies peak metamorphic conditions, and spinel remained stable through upper amphibolite facies retrogression.

The corundum, spinel, and haüyne occurrences are interpreted to have different sedimentary protoliths with the exception of a few metasomatic spinel occurrences. The protoliths of the occurrences are interpreted to be: [A] impure dolomitic limestone (spinel); [B] dolomitic marl (spinel, corundum); [C] magnesite-rich evaporitic marl (spinel); and [D] evaporite (halite and anhydrite)-bearing dolomite-rich marl (haüyne). The meta-marls have Al/Si

abundances comparable to that expected in a siliciclastic mud. Calc-silicate rocks barren of gem minerals have lower Al/Si (sandier protoliths). Spinel-bearing calc-silicates have higher Al/Si relative to that of sapphire- and haüyne-bearing rocks. High abundances of Al to Si are crucial to spinel formation in Mg-rich calc-silicates. Spinel formation in impure dolomitic marbles requires low K activity and does not require high Al/Si. Cobalt enrichment at two spinel occurrences is localized and interpreted to represent geochemical features of the protolith.

The genetic models provide broad gemstone exploration criteria for carbonate-bearing metasedimentary sequences such as the LHG.

Lay Summary

Marble and associated rocks are major producers of commercial gemstones around the world. Such rocks occur on southern Baffin Island, and contain gem sapphire, spinel, and lapis lazuli. This thesis uses a collection of analytical methods to identify the large- and small-scale geological factors that result in gemstone formation. Factors leading to gem formation include changes in pressure and temperature conditions during metamorphism and having favourable chemical compositions in the initial sedimentary rocks. Sapphire formed via a three-step metamorphic process, most likely to occur near a regional fault, which transformed a magnesium-rich mixed mud and limestone rock into a sapphire-bearing metamorphic rock. Spinel formed from the metamorphism of impure magnesium-rich limestones and mixed mud-dolomite rock, where spinel formation is dependent on low potassium concentrations and high aluminium relative to silicon. Lapis lazuli formed from a mixed mud-carbonate rock containing evaporite salt impurities. These research results have helped develop exploration criteria.

Preface

This dissertation is an original independent work by the author, Philippe Belley. All discussions and conclusions represent my own independent work. Portions of the thesis have been published or submitted as manuscripts in peer-reviewed journals. Much of the data presented in Chapter 3 was collected by previous workers and re-interpreted in the present dissertation. Co-authors provided several figures, as described below.

Chapters 1 and 2

Portions of Chapter 1 and the totality of Chapter 2 appear in the papers listed below in Chapters 3 and 4.

Chapter 3

Chapter 3 was published in the 2017 Gem Materials special issue of *The Canadian Mineralogist*, volume 55, pages 669-699 in the paper entitled "Origin of scapolite-hosted sapphire (corundum) near Kimmirut, Baffin Island, Nunavut, Canada by Philippe M. Belley (present author), T.J. Dzikowski, A. Fagan, J. Cempirek, L.A. Groat, J.K. Mortensen, M. Fayek, G. Giuliani, A.E. Fallick, & P. Gertzbein. T.J. Dzikowski contributed some petrographic observations (petrography was largely re-done independently by the present author) and collected electron microprobe (EPMA) data. A. Fagan (in his capacity with True North Gems Inc.) provided the geological map of the TNG Inc. property near Kimmirut. J. Cempirek collected EPMA data on, and re-calculated the formula of oxy-dravite. J.K. Mortensen conducted TIMS analysis of zircon. M. Fayek conducted the B isotope analysis of oxy-dravite using SIMS. The oxygen isotopic composition of corundum was measured by A.E. Fallick. Mica Ar-Ar data

was collected by Andrea Cade. The discussion is the complete independent work of the present author (Philippe Belley). Andrew Fagan provided a useful suggestion on Al-silicate/corundum stability that improved the discussion. The Al-Mg-Ca ternary plot was provided by G. Giuliani. The REE and oxygen isotope plots are after Dzikowski (2013).

Chapter 4

Chapter 4 has been accepted with revision in *The Canadian Mineralogist*. The paper, by Philippe M. Belley and Lee A. Groat, is entitled "Metacarbonate-hosted spinel on Baffin Island, Nunavut, Canada: Insights into the origin of gem spinel and cobalt-blue spinel." Chapter 4 is the complete independent work of the present author (Philippe Belley). Lee Groat provided useful comments which improved the quality of Chapter 4 and the manuscript.

Chapter 5

Some of the new contributions on lapis lazuli were included in the spinel paper (Ch. 4), where lapis lazuli was compared to other metacarbonates.

Chapter 6

An adapted version of Chapter 6 will be submitted as a manuscript to a peer-reviewed journal.

Table of Contents

List of Tables

List of Figures

Acknowledgments

I wish to thank the following individuals and organizations that provided assistance, knowledge, and support during the course of my PhD.

Dr. Lee Groat (supervisor) always made himself available to discuss plans and share wisdom. Your mentorship has been very important to me. My committee, Drs. James Mortensen and Lori Kennedy, offered useful advice and criticism, as did my committee at the time of candidacy (J. Mortensen, M. Raudsepp, and K. Hickey). My scientific and grant writing skills reached new levels thanks to Mackenzie Parker. Many useful comments were provided by External Examiner Dr. Ian Graham, and University Examiners Drs. Maya Kopylova and Tom Troczynski.

I owe a great deal of gratitude to Brad Wilson, who was instrumental in the planning and executing of field work on southern Baffin Island, and with whom I have had many interesting discussions on the subject of Canadian gemstone occurrences.

I am very grateful to the staff and management of True North Gems Inc. for granting access to their mining claim, providing data, maps, and for discussions about the geology of the property. The Qikiqtani Inuit Association (QIA) and staff at the Katannilik Territorial Park allowed access to Inuit-owned and park lands, respectively. I thank the community of Kimmirut for welcoming us to their home, allowing access to municipal lands, and providing much needed help in the field. ᓇᔨᕋᒃ.

In the sapphire study (Chapter 3), several co-authors provided useful data and figures (see *Preface*) which have been used in the present dissertation. Allison Brand provided assistance to Lee Groat in the field. Andrea Cade helped in sample preparation and data collection for Ar-Ar geochronology. Ryan Sharpe assisted Mostafa Fayek with boron isotope analysis. Corundum-

bearing samples from Pitcairn, NY were provided by Dr. George Robinson. Andrew Fagan, Jan Cempirek, Donald Lake, David Turner provided useful suggestions. Helpful comments from Mackenzie Parker, *Canadian Mineralogist* guest editor Dr. Dan Marshall, and reviewers Drs. Yannick Branquet and Eloise Gaillou improved the quality of Chapter 3. In the spinel study (Chapter 4), I wish to thank Holly Steencamp for the Hall Peninsula marble sample, and Glenn Poirier for help with EPMA analysis. Helpful comments from *Canadian Mineralogist* associate editor Matthew Steele-MacInnis, reviewers D. Skipton, B. Rondeau, B. Dyck, and one anonymous reviewer improved Chapter 4.

Financial support was provided by the Dr. Eduard Gübelin Scholarship, a UBC Four-Year Fellowship, UBC tuition awards, a Northern Scientific Training Program in the form of a grant, and by the Natural Sciences and Engineering Research Council of Canada in the form of a Discovery Grant (to Prof. Lee Groat, funding reference 06434) and Canada Graduate Scholarships (CGS-M and CGS-D3). Additional funding was provided by the Mineralogical Association of Canada (Foundation Scholarship), the International Mineralogical Association (Outstanding PhD Student Award), and the Walker Mineralogical Club (Peacock Prize).

My time in Vancouver was a lot of fun thanks to my friends DJ Lake, Jaimy Henman, and Ashley Shapiro. I will remember our crazy gem hunting, camping, and snow sculpting adventures forever. I thank Joel Grice, André Lalonde, Michel Picard, John Montgomery, Michael Bainbridge, Rob Woodside, and George & Susan Robinson for their friendship and encouragement of my pursuit of mineralogy. Most importantly, I would not be here were it not for the tireless support of my parents, Michel and Aline, who have always been there for me.

Chapter 1. Introduction and Literature Review

1.1 Introduction

Sapphire (gem-quality corundum), Mg-Al spinel, and lapis lazuli (a rock principally composed of haüyne, ideally $Na_3Ca(Si_3Al_3)O_{12}(SO_4)$) are mined for their use in jewelry. Many sapphire deposits, and all *in situ* spinel and lapis lazuli deposits occur in metacarbonates, but there are few detailed petrologic and geochemical studies on such deposits, especially with regards to sapphire and spinel, for the following reasons: (a) gem deposits are rare, and some varieties of gemstones (*e.g.*, cobalt-blue spinel) are only known from a few localities; (b) many marble-, skarn-, or calc-silicate hosted sapphire and spinel deposits are mined from eluvial deposits formed in part from the weathering of carbonate minerals (*e.g.*, Mogok District, Myanmar; Luc Yen District, Vietnam; Tanzania) while other deposits are alluvial (*e.g.*, Ratnapura, Sri Lanka); (c) many gem deposits are located in politically sensitive areas with limited access (*e.g.*, Myanmar, Afghanistan); and (d) most deposits are mined on an artisanal scale, where no geological records or samples are kept but samples can sometimes be collected *in situ* during production.

Metacarbonates in the Precambrian Lake Harbour Group (LHG), southern Baffin Island, of high metamorphic grade (granulite and upper amphibolite), are recognized for their outstanding gem potential (Gertzbein 2003). High-quality gem sapphire (LeCheminant *et al.* 2005, Dzikowski 2013, present research), low-grade lapis lazuli (Hogarth 1971, Hogarth & Griffin 1978), violet spinel, and highly prized vivid cobalt-blue spinel (Wilson 2014) are known to occur in the LHG, especially in the well-explored Kimmirut area.

The gem-bearing rocks of southern Baffin Island offer a unique opportunity to conduct detailed petrological work on a diverse suite of *in situ* gem occurrences within a single geologic

terrane. Such gem occurrences are typically rare and seldom well-exposed. The goal of this study is to develop an understanding of the conditions responsible for the formation of these gem occurrences and to establish deposit models and to formulate exploration strategies.

This goal will be achieved by building on existing petrogenetic models together with developing new models for the genesis of gem corundum, spinel, and lapis lazuli in LHG metacarbonates. These models will be constrained by an estimate of protolith composition, the nature of metasomatism, metamorphic history, and trace element geochemistry.

The research comprises three parts: (1) Development of a genetic model for Kimmirut-type sapphire from geochemical, isotopic and petrographic data, and by using thermodynamic modelling to determine the timing and *P-T* conditions of key mineral assemblage transformations; (2) Development of a genetic model for LHG gem spinel occurrences based on petrology, estimates of the protolith composition (where applicable), and trace element geochemistry (spinel chromophore concentrations) with a focus on determining the possible sources of cobalt-enrichment relative to other chromophores; (3) An evaluation of the lapis lazuli protolith building upon previous research, and measuring Li and other trace element concentrations in lapis lazuli bearing meta-evaporite at Soper River, Baffin Island (Hogarth & Griffin 1978) to provide a basis for the comparison of lapis lazuli meta-evaporite to other metacarbonate-hosted gem occurrences in the LHG.

These new or improved genetic models are expected to facilitate gem exploration in Baffin Island and elsewhere by creating a set of criteria for recognizing areas of high gem potential. In addition, this research will contribute to our general understanding of gem deposits and their relation to regional geology, metamorphic conditions, and protolith geochemistry.

1.2 Geology of study area

1.2.1 Regional geology

The sapphire-, spinel-, and haüyne-bearing rocks occur near Kimmirut, in Markham Bay, and on the Hall Peninsula (Fig. 1.1), in a sequence of marble and calc-silicate rocks structurally overlying garnet psammite, meta-semipelite, metapelite, and rare orthoquartzite. The marble, calc-silicate rock, and metaclastic rocks form the Lake Harbour Group (LHG) supracrustal suite (Scott 1997, Scott *et al.* 1997, 2002). The LHG is interpreted to be the sedimentary cover sequence of the Meta Incognita microcontinent, which was accreted to the southern margin of the Rae Craton by the Trans-Hudson Orogeny (THO; St-Onge *et al.* 2009). Detrital zircon ages indicate a Paleoproterozoic (rarely Archean) sediment source for LHG sediments and suggest a depositional age for the LHG older than *ca.* 1.93 Ga (corresponding to the youngest detrital zircon age, Scott *et al.* 2002). Sparse mafic/ultramafic sills up to 200 m thick and 5.6 km in maximum dimension intrude the LHG and were affected by peak granulite-facies metamorphism (St-Onge *et al.* 2015).

The supracrustal rocks of the THO, including the LHG, were subjected to multiple deformational and metamorphic events (see St-Onge *et al.* 2007). In deformation event D_0, which post-dates the deposition of the LHG and pre-dates emplacement of the Cumberland batholith, basement rocks were imbricated with cover rocks. The Cumberland batholith, an Andean-type granitic batholith, was emplaced from 1865 +4/-2 to 1848 ± 2 Ma. The Narsajuaq oceanic arc was accreted to Meta Incognita (deformation event D_{1A}), and the suture closed between 1845 ± 2 and 1842 +5/-3 Ma. Prograde granulite-facies metamorphism (M_{1A}) occurred *ca.* 1849 – 1835 Ma as a result of crustal thickening (accretion of the Narsajuaq arc) and heat advection (emplacement of the Cumberland batholith). A high-temperature thermal perturbation

(M_{1B}), *ca.* 1833-1829 Ma, represents either continued mineral growth in the late stages of M_{1A} or a distinct thermal event related to felsic intrusions. Retrograde upper-amphibolite facies metamorphism (M_2) occurred from 1820 ± 1 Ma to 1813 ± 2 Ma with reactivation and further shortening of the Soper River suture (D_2) which separates Meta Incognita from the Narsajuaq terrane. Recrystallization to S_2 assemblages was noted to be most significant in samples with strong foliation and occurring contiguous to D_2 thrusts. This localized recrystallization is interpreted by St-Onge *et al.* (2007) as being driven by deformation-enhanced fluid circulation. Lastly, post-D_2 thermal and fluid activity occurred *ca.* 1797 – 1785 Ma, possibly related to late felsic intrusive rocks of similar age and speculated to be a potential cause of minor greenschist facies retrogression (secondary chlorite, epidote, sericitization). Pressure-temperature determinations for the Lake Harbour Group rocks by St-Onge *et al.* (2007) are as follows: S_{1A} mineral assemblages provided *P-T* values of *ca.* 810 °C and 8.0 kbar; thermobarometry of S_2 mineral assemblages indicate metamorphic conditions of upper amphibolite facies, *ca.* 720 °C and 6.2 kbar. LHG rocks, including marbles and calc-silicates, in the western part of the Hall Peninsula were metamorphosed to granulite facies (~850-890 °C, 6.1-7.35 kbar) during 1850-1825 Ma (Skipton *et al.* 2016).

1.2.2 Lake Harbour Group marble and calc-silicate rocks

Marbles and calc-silicate schists showing centimeter- to meter-scale compositional layering comprise a significant portion of the Lake Harbour Group (Scott 1997). The LHG metacarbonate and calc-silicate rocks commonly contain calcite, diopside, phlogopite, forsterite, serpentine, amphibole, spinel, graphite, pyrite, pyrrhotite, or scapolite with the occasional occurrence of apatite, titanite, wollastonite, humite, plagioclase, or magnetite (Blackadar 1967, Scott 1997, Herd *et al.* 2000, St-Onge *et al.* 2000). Grain sizes range from fine to very coarse.

Nepheline and K-feldspar occur in calc-silicate bands and marble on Aliguq Island, 165 km NW of Kimmirut (Butler 2007). Layering in the marbles is generally convoluted, probably due to ductile flow (Scott 1997), and silicate-rich lithologies occur as both stratigraphically continuous layers and boudins or pods (Butler 2007).

1.3 Broad research questions and significance

Some high-grade, metacarbonate-rich terranes contain multiple gem spinel (Hughes 1997), ruby (Garnier *et al.* 2008 and references therein), sapphire (Hughes 1997), and uncommon lapis lazuli deposits, such as that in Vietnam (Chauviré *et al.* 2015, Pham *et al.* 2013, Blauwet 2006), Afghanistan (Faryad 2002), Tajikistan (Hughes & Pardieu 2006), and Myanmar (Pardieu 2014, Themelis 2008). Other terranes of similar metamorphic grade and abundance of metacarbonates are not necessarily known to contain any significant gemstone occurrences. Such an example is the Central Metasedimentary Belt (CMB, Grenville Province, Ontario-Quebec; Rivers 2015, Corriveau 2013), from which noteworthy coloured gemstone occurrences are not yet known, but the CMB is known to contain spinel and corundum of poor colour and quality (*e.g.*, Wilson 2014, Belley *et al.* 2016) in addition to gem-quality skarn-hosted grossular (Belley & Bourdeau 2014).

The metacarbonate rocks of the Lake Harbour Group, Baffin Island contain numerous and significant gemstone occurrences which are of particular significance due to the size and quality of gemstones (sapphire up to 7.81 carats), the occurrence of rare coloured stones (vibrant cobalt-blue spinel), and in some cases, the extent of mineralization (low-grade lapis lazuli/haüyne). These well-exposed gem occurrences offer a unique opportunity for research: A comprehensive study of the genesis of metacarbonate-hosted gemstones of diverse mineralogy in a single geologic terrane. The present dissertation seeks to determine the ways in which regional

geologic phenomena influence gemstone potential (*e.g.*, metamorphic history, metasomatism, intrusions, and protoliths) by means of creating genetic models for gem corundum, spinel, and lapis lazuli in the LHG.

An understanding of these regional-scale controls on gem formation in high-grade metasedimentary belts helps clarify the origin of coloured stones that have fascinated human societies for millennia and facilitate exploration. The present research contributes new information on the effects of metamorphic history, protolith composition, and chromophore distribution on gemstone genesis which enhances our general understanding of metamorphic gem formation.

1.3.1 Part 1 - Corundum

Calc-silicate-hosted sapphire occurrences near Kimmirut, Baffin Island, comprise a new type of gem corundum deposit (see section 1.4.1 for a review of known deposit types). Developing an understanding of corundum genesis in these scapolite-rich rocks represents an important new contribution to the understanding of gem-quality sapphire formation and helps predict the potential for such deposits in the LHG and other high-grade marble-rich terranes.

Kimmirut sapphire was previously studied by LeCheminant *et al.* (2005) and Dzikowski (2013), but their early interpretations did not fully explain the origin of corundum in these calc-silicate pods. LeCheminant *et al.* (2005) proposed that the calc-silicate pods formed from contamination of a syenitic intrusion and were subsequently metamorphosed. Dzikowski (2013) contradicted the previous study, suggesting a mixed evaporite-black shale protolith, where the corundum-bearing assemblage was formed during retrograde metamorphism from the possible break-down of nepheline + scapolite, nepheline + anorthite, or anorthite.

The goal of the present research is to produce a robust deposit model for Kimmirut sapphire using a combination of new data and a different approach to solving the complex petrogenesis of sapphire-bearing calc-silicate rock using additional mineralogical and textural observations, petrography, X-ray powder diffraction, and boron isotope geochemistry. The approach to protolith determination used in the present study yielded different results from previous workers. The geochronology of mineralization (U-Pb of zircon, $^{40}Ar/^{39}Ar$ of micas) was re-interpreted, yielding different results to previous authors.

1.3.2 Part 2 - Spinel

Several areas in the world are producing gem spinel, and much of this spinel is recovered from eluvial or alluvial deposits. Interest in spinel gemstones has increased significantly in the early 21st century (Pardieu *et al.* 2008); however, the geology of spinel has yet to receive attention from geoscientists – in significant contrast to gem corundum geology (*e.g.*, Giuliani *et al.* 2014). Giuliani *et al.* (2017) noted that "[g]eological investigations of gem spinel deposits in marble are scarce" and that "[s]everal questions remain regarding their genesis, particularly: (1) their age and the *P-T-x* conditions of formation; (2) the relationship between oxygen isotopic composition of spinel and the nature of fluid-rock interaction with marbles; and (3) the sources of Al and other trace elements incorporated in spinel." The potential for gaining new insight into gem spinel genesis from small *in situ* occurrences that are not being mined for gem material (giving a much larger sample size) has been overlooked. The present dissertation presents the first comprehensive gem spinel deposit model, which is based on fourteen occurrences in the Lake Harbour Group, including two cobalt-blue spinel occurrences, and seeks to determine geochemical controls on whether or not spinel forms in a metacarbonate rock.

Spinel of an intense red colour (chromium chromophore) and vibrant cobalt-blue colour (cobalt chromophore) are of greatest commercial interest. Ruby (Cr-bearing corundum) deposit models suggest that Cr enrichment is a result of Cr-rich sediment deposited coevally with carbonates and the concentration of Cr in organic matter (Garnier *et al.* 2008). At Revelstoke, British Columbia, Cr was enriched in gneiss layers that reacted with marble to form corundum (Dzikowski *et al.* 2014). The enrichment of cobalt in concentrations sufficient to turn spinel bright blue has yet to be adequately explained. In the most detailed petrologic study on cobalt-blue spinel to date, Chauviré *et al.* (2015) suggested that Co and Ni were enriched in cobalt-blue spinel from F- and Cl-bearing evaporite-contaminated metamorphic fluids sourcing these metals from evaporite or amphibolite. This hypothesis will be evaluated for the Kimmirut occurrences.

The effect on chromophore element distribution in minerals associated with spinel, including preferential incorporation of elements in some phases over others, has yet to be studied or assessed as a potential control on the colour of gem spinel. For example, does an abundance of sulphide minerals (*e.g.*, pyrite, pyrrhotite) preferentially incorporate Co, thus limiting its availability to spinel? Or is the effect negligible at Co concentrations in typical cobalt-blue spinel-containing rocks?

1.3.3 Part 3 - Lapis lazuli

Meta-evaporite compositions are diverse (*e.g.*, Moine *et al.* 1981), and major element rock compositions can overlap with normal sediments. Concentrations of trace elements, most notably Li, offer good potential for meta-evaporite identification, however Li tends to be poor in dolomite-rich evaporite-related rocks (Moine *et al.* 1981). The trace element composition of lapis lazuli at Soper River will be used as a check primarily for Li concentrations in an example of Precambrian meta-evaporite in the LHG. Furthermore, the protolith composition of lapis lazuli

will be estimated based on whole rock chemical composition to establish differences and similarities with the composition of other metacarbonates containing gem minerals.

1.4 Background on gem corundum

1.4.1 Geology of gem corundum deposits

Gem corundum (sapphire: blue, purple, pink, colourless, yellow, *etc.*; ruby: red) occurs in a variety of geological environments where Al is in excess relative to Si (*i.e.*, Si is a limiting reactant in aluminosilicate formation), and where *P-T-x* conditions favor corundum stability (Giuliani *et al.* 2014). Gem corundum occurs in igneous rocks (syenite, monzonite, xenocrysts in basalt and lamprophyre), metasomatic rocks (skarn, biotitite, desilicated pegmatite and gneiss), metamorphic rocks (marble, mafic granulite, amphibolite, aluminous gneiss), and anatexite (Fig. 1.2, Giuliani *et al.* 2014, Simonet *et al.* 2008). Since this research pertains to metacarbonate-related gem deposits specifically, these are described in greater detail below.

Metamorphic gem corundum deposits form under amphibolite and granulite facies conditions at 500 to 800 °C temperature and 2 to 10 kbar pressure (Fig. 1.3, Giuliani *et al.* 2014). Four types of metacarbonate-related deposits have been defined (see reviews by Giuliani *et al.* 2014 and Simonet *et al.* 2008): (1) Endoskarns where magma intrudes marble and becomes desilicated, such as the pargasite-phlogopite-hosted ruby occurrence at the edge of mafic dykes at Mahenge, Tanzania; (2) Exoskarns where pegmatite or granite intrudes marble or calc-silicate rocks, such as in Myanmar (Themelis 2008), Sri Lanka (scapolite-corundum-spinel zoned skarn, Silva & Siriwardena 1988), and Madagascar (diopsidite and scapolitite/marble); (3) Stratiform gem corundum mineralization in calcite-dolomite marble, typically formed from the retrograde break-down of spinel, and at some localities suggested to be metamorphosed evaporite lenses

(Garnier *et al.* 2008); (4) Impure marble containing gneiss or silicate-rich layers, which react with the marble under peak metamorphic conditions (*e.g.*, Dzikowski *et al.* 2014).

1.4.2 Colour of corundum

Pure corundum (Al_2O_3) is colourless, and colourless sapphire gemstones are less sought after than yellow, blue, and red, in order of increasing value. Yellow colouration in corundum is caused by $O^{2-} \rightarrow Fe^{3+}$ charge transfer. Corundum is made blue by the presence of Fe and Ti, which cause the colour by intervalence charge transfer ($Fe^{2+} \rightarrow Ti^{4+}$; Fritsch & Rossman 1988). Ti^{4+} preferentially pairs with Mg^{2+} relative to Fe^{2+}, and Mg^{2+} preferentially pairs with Si^{4+} relative to Ti^{4+}; therefore, Si and Mg trace concentrations control the availability of Ti^{4+} to Fe^{2+}, and thus influence the colour of corundum (Emmett *et al.* 2017). Red hues (*i.e.*, ruby or pink sapphire) are caused by the presence of Cr^{3+} (Fritsch & Rossman 1987).

1.4.3 Previous studies on Kimmirut sapphire deposits

LeCheminant *et al.* (2005) suggested that formation of the corundum-bearing calc-silicate rocks at the Beluga and Bowhead occurrences involved a contaminated syenitic magma emplaced in marble late in the D_2 deformation event. The nepheline- and diopside-rich assemblage was proposed to have been formed by the reaction of syenitic magma with LHG marble and possibly evaporites, followed by retrogression forming phlogopite-oligoclase-scapolite at the expense of diopside and nepheline, and a second retrograde event resulting in the fracture-controlled alteration of nepheline to form corundum. In a study of nepheline-bearing LHG metacarbonates on Aliguq Island, Butler (2007) determined that nepheline-K-feldspar formed late based on textural relations with forsterite, diopside, and phlogopite. Butler (2007) proposed that this assemblage formed at peak metamorphic conditions (*ca.* 800 °C and 8 kbar) at low X_{CO2} (≤ 0.15) by the reaction 3 albite + 3 calcite + phlogopite → K-feldspar + 3 nepheline +

3 diopside + H_2O + 3 CO_2. Dzikowski (2013) suggested that the protolith for the Beluga and Bowhead calc-silicate pods was evaporite-black shale deposited in the LHG carbonate shelf and proposed the following paragenetic sequence: (1) prograde diopside + nepheline (≤ 810 °C, 8.3 kbar); (2) alteration of the peak assemblage by NaCl-bearing fluids (at < 710 °C, 6 kbar) forming phlogopite-oligoclase 'symplectites' with late scapolite rims; (3) introduction of hydrous fluids, post-D_2, causing the break-down of nepheline and either scapolite or anorthite to form albite, muscovite, and corundum or alternatively, the introduction of Na-bearing hydrous fluids breaking down anorthite to albite and corundum.

Lepage & Davison (2007) reported the use of ultraviolet LED technology to explore for fluorescent scapolite, which they assumed would coexist with gem corundum in the Kimmirut area. Turner *et al.* (2017) investigated the potential application of hyperspectral imaging in exploration for Kimmirut-type gem corundum deposits.

In Chapter 3, this dissertation re-evaluates the data presented by Dzikowski (2013) with additional isotopic and petrographic data, and applies the results to change, refine, and generate new interpretations on the origin and petrogenesis of gem corundum in Kimmirut-type deposits.

1.5 Background on gem spinel

1.5.1 Geology of gem spinel deposits

Mg-Al spinel is a common constituent of marble and metasomatic rocks associated with marble, however it is seldom of gem quality due to its typically unattractive dark colour (*e.g.*, Van Velthuizen 1993, Belley *et al.* 2016) and small crystal size. Gem-quality Mg-Al spinel, which is most prized when intense red, pinkish-red, or cobalt-blue in color, is mined at several localities worldwide, most of which occur in marble metamorphosed at high metamorphic grade: (1) red and pinkish-red spinel is mined in marble and eluvial deposits in karsts at Mogok and

Namya, Myanmar (Pardieu 2014, Themelis 2008); (2) pinkish red spinel, the largest crystal having been found to date weighing 54 kg and the largest gemstone weighing 50 carats, is mined from marble and eluvial deposits near Ipanko, Tanzania (Pardieu 2008); (3) red, pink, blue, and cobalt-blue spinel is mined from granulite-facies marble and contiguous eluvial and alluvial deposits in the Luc Yen District, Vietnam (Chauviré *et al.* 2015, Pham *et al.* 2013, Senoble 2010, Blauwet 2006); (4) blue, purplish-blue, and greyish cobalt-blue spinel is mined from alluvial placer deposits in Ratnapura, Sri Lanka (Shigley & Stockton 1984, personal communication M. Ikram); and (5) red and pink gem-quality spinel occurs in marble and magnesian skarns (at the contact of gneiss and marble) at Kuh-i-Lal, Tajikistan (Kievlenko 2003, Hughes & Pardieu 2006).

Giuliani *et al.* (2017) identified several questions that remain regarding gem spinel genesis, notably about the *P-T-x* conditions of formation and the sources of Al and trace elements incorporated in spinel. Most of these questions have been addressed in the present dissertation, with the notable exception of Cr-bearing red spinel, which has not been found in the Lake Harbour Group on Baffin Island.

1.5.2 Colour of spinel

Spinel color is determined by the concentration of Fe, Cr, Co, and to a lesser degree, V, in addition to the coordination and charge of Fe (D'Ippolito *et al.* 2015). As total Fe content increases in spinel, it grades in color from colorless to pale lilac (*e.g.*, 0.58-0.65 wt. % $FeO_{total\ Fe}$, Kleišmantas & Daukšytė 2016), sky blue, green, deep green (Hålenius *et al.* 2002) and black (Van Velthuizen 1993). Pink and red spinel is primarily colored by Cr^{3+} in concentrations of at least 0.1 wt. % Cr_2O_3, and color saturation is largely determined by Fe content (Kleišmantas & Daukšytė 2016). Kleišmantas & Daukšytė (2016) suggested that V contributes yellow or brown

hues to spinel in concentrations over 0.4 wt. % V_2O_3. It should be noted that the study of Kleišmantas & Daukšytė (2016) compared spinel chemical compositions directly with colour without supporting the observed colour-composition trends using absorption spectra. Cobalt-poor spinels containing Fe are typically blue (octahedral Fe^{3+}), purplish-blue (tetrahedral Fe^{2+}), or greenish blue (higher total Fe), and $^{T}Co^{2+}$ absorption bands can be detected in spinel at Co concentrations greater than 10 µg/g (D'Ippolito *et al.* 2015). Natural spinel with a significant Co color contribution was first noted by Shigley & Stockton (1984). Vibrant cobalt-blue spinel from Vietnam has a Fe/Co ratio of 10, a Co concentration of 1236 µg/g, ~2500 µg/g Ni, ~1100 µg/g Cr, and ~1000 µg/g Zn. The Cr content of this spinel gives it a very slight purplish tinge when viewed in incandescent light (Chauviré *et al.* 2015). Based on trace element and light absorption data, Chauviré *et al.* (2015) estimated that the visible light molar absorptivity of cobalt in spinel is ~20× more important than that of iron.

1.5.3 Previous studies on Lake Harbour Group spinel

Spinel occurrences in Nunavut have not yet been the subject of scientific research. Wilson (2014) noted spinel from the following localities within the LHG: (1) violet crystals up to 3 cm in marble near the Soper River lapis lazuli occurrence near Kimmirut; (2) blue and violet spinel crystals up to 3 cm at Waddell Bay; (3) violet crystals up to 4.5 cm in a mica exploration trench on Soper Lake, near Kimmirut; (4) violet crystals in 'chondrodite' at Soper Falls, north of Kimmirut; (5) violet crystals up to 5 cm at Glencoe Island (see also Grice *et al.* 1982); (6) cobalt-blue, opaque fragments up to 1 cm at the Qila occurrence, near Kimmirut; and (7) cobalt-blue, occasionally transparent and heavily fractured crystals up to 2.7 cm at the Trailside occurrence, also near Kimmirut. Small faceted gemstones, almost all under 0.50 carats (with the exception of

an opaque 2.14 carat Qila spinel cabochon) have been produced from these localities (Wilson 2014).

1.6 Background on lapis lazuli

1.6.1 Lazurite vs. haüyne

Lapis lazuli is commonly reported to be composed of the sodalite group minerals lazurite and/or haüyne. Lazurite is the sulphide end-member, ideally $Na_6Ca_2(Al_6Si_6O_{24})S_2$, and haüyne is the sulphate end-member, $Na_3Ca(Al_4Si_4O_{12})(SO_4)$. Multiple studies indicate the occurrence of lazurite, however in examples where sulphate and sulphide content was determined in the mineral, the sulphate member rather than sulphide is the dominant species, including at Sar-e-Sang, Afghanistan and Soper River, Baffin Island, Canada, (Hassan *et al.* 1985, Fleet *et al.* 2005, Moore & Woodside 2014) with some examples being sulphite-dominant (Tauson *et al.* 2012). Therefore, natural examples of "lazurite" are in fact all haüyne.

1.6.2 Geology of lapis lazuli deposits

Lapis lazuli is a royal blue rock composed primarily of haüyne and is used as an ornamental stone and in jewelry. Three economic lapis lazuli deposits (Afghanistan, Russia and Chile) are well-known known, as are a number of small deposits or deposits where the rock is too impure to be of commercial interest.

At Coquimbo, Chile, lapis lazuli composed primarily of haüyne, wollastonite, calcite, diopside, pyrite, and scapolite occurs in lenses up to 2 × 0.1 m (locally up to 0.4 m in thickness) in three skarn zones up to 300 m wide. The deposit formed from the contact metamorphism and metasomatism of limestone by granite (Coenrads & Canut de Bon 2000).

Smaller occurrences of lapis lazuli formed by contact metamorphism and metasomatism include Cascade Canyon in California, USA (quartzite/limestone protolith; Housley 2012 and

references therein), Latium, Italy (limestone xenoliths in leucitic tuff, Hogarth & Griffin 1975), and at Italian Mountain, Colorado, USA (subgreywacke/dolostone protolith; Hogarth & Griffin 1980).

Two deposits, Tultui and Malo Bystrinsky, occur near Lake Baikal, Russia (Hogarth 1979). An unspecified deposit near Lake Baikal is reported to have formed by contact metasomatism of marble by alkaline igneous rocks (Deer *et al.* 2004 and references therein).

The lapis lazuli deposit at Sar-e-Sang, Afghanistan was regionally metamorphosed, possibly subjected to metasomatism, and the lapis lazuli is found in three distinct modes of occurrence: (1) At the contact with granite and pegmatite, lenses up to 40 × 2 m with K-feldspar-quartz-plagioclase cores surrounded by calc-silicate rock composed of diopside, forsterite, phlogopite, tremolite, grossular, *etc.*, and an exterior rim of calcite, diopside, haüyne, nepheline, and afghanite. (2) Lenses up to 450 × 6 m consisting of an alternating sequence of calcite-diopside-haüyne, diopside, and phlogopite-diopside calc-silicate rocks thought to represent original bedding. (3) Lenses of haüyne up to 2 × 0.3 m occurring between granite or pegmatite and marble (Faryad 2002 and references therein). The Sar-e-Sang deposit is considered to be a meta-evaporite contained within a metamorphosed shallow marine sediment sequence (Faryad 2002).

At the Edwards Zn-Pb mine, Edwards, New York, two pods of lapis lazuli up to 2.4 × 0.9 m were found during mining. The core of the pods is composed of haüyne, calcite, actinolite, diopside, and pyrite and is surrounded by a pyrite-rich actinolite layer, a phlogopite layer, and at the contact with dolomitic marble, high-grade sphalerite (Lessing & Grout 1971). A cobble of impure lapis lazuli (haüyne in diopsidite) was found in gravel from glacial till in Ottawa,

Ontario, and likely originates from the nearby Central Metasedimentary Belt (unpublished data, P.M. Belley; personal communication Michael Bainbridge).

1.6.3 Geology of the Soper River lapis lazuli occurrence

Along the Soper River, north of Kimmirut, Nunavut, impure lapis lazuli (North and Main occurrences) occurs in five zones (four of which are located at the Main occurrence), up to 168 m long, interbedded with marble. The lapis lazuli rock is composed of varying concentrations of haüyne (up to 42.2 vol. %), diopside, plagioclase, and calcite with locally abundant phlogopite, nepheline, tremolite, and scapolite, and common subordinate pyrite (Hogarth 1971). It is proposed to be a regionally metamorphosed evaporite-limestone (Hogarth 1971, Hogarth & Griffin 1978).

Hogarth & Griffin (1978) convincingly proposed that the Soper River lapis lazuli is a meta-evaporite citing the following evidence: (1) The lapis lazuli has well-developed layering parallel to the regional foliation, suggesting that it is metasedimentary; (2) the area has a scarcity of intrusive rocks, which does not support a contact metasomatic origin; and (3) the abundances of Na, K, S, Cl, Br, F, and Fe are consistent with evaporite-related sediments.

1.7 Figures

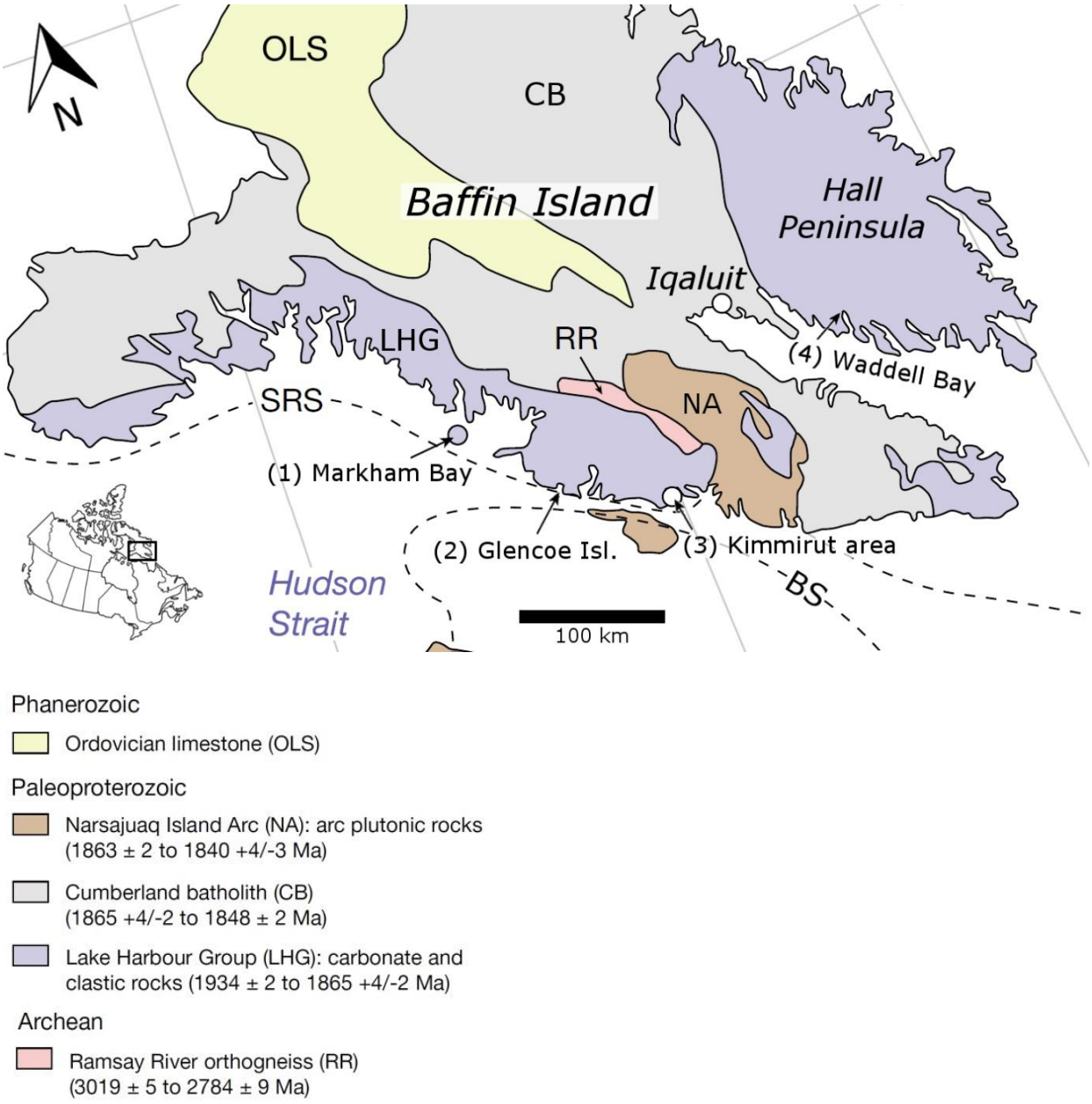

Figure 1.1: Geology of southern Baffin Island and location of the study areas. Crustal sutures separating structural domains are represented by dashed lines. BS: Bergeron suture; SRS: Soper River suture. Modified after St-Onge *et al.* (2000) and Butler (2007); ages from St-Onge *et al.* (2001).

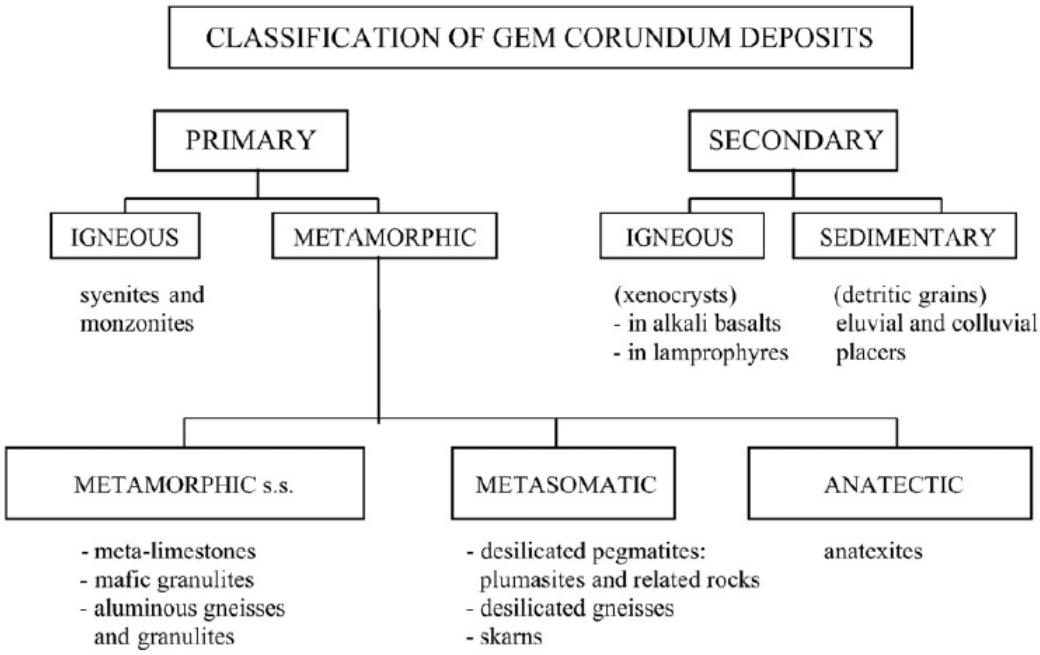

Figure 1.2: Classification of gem corundum deposits (after Simonet *et al.* 2008).

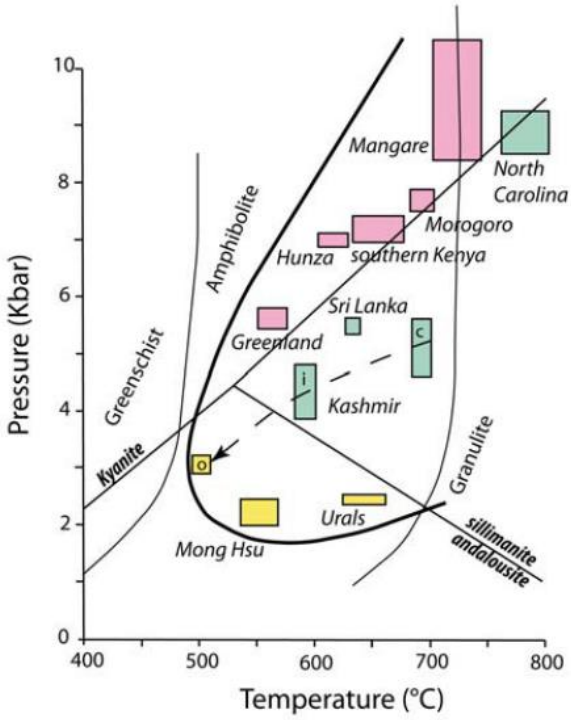

Figure 1.3: *P-T* conditions for the formation of corundum in various metamorphic deposits (after Giuliani *et al.* 2014).

Chapter 2. Methods

2.1 Sapphire

2.1.1 Petrography and Mineral Identification

Approximately 25 kg of representative rock samples were collected by Lee Groat, Paul Gertzbein and others at the Beluga sapphire occurrence and to a lesser degree at the nearby Beluga occurrence (calc-silicate with no sapphire). Samples were studied in the petrological microscope and scanning electron microscope (SEM) from ~16 thin-sections (3 Bowhead). Mineral phases that were not analyzed with electron probe microanalysis (EPMA) were identified using energy dispersive spectroscopy (EDS) in the SEM, or standard X-ray powder diffraction (XRPD) techniques (noted in text).

2.1.2 Chemical analysis

Chemical analyses for all minerals with the exception of tourmaline were performed by Dzikowski (2013) with a CAMECA SX-50 electron microprobe (at the University of British Columbia) in wavelength-dispersion (WD) mode. Full data sets are in appendices of Dzikowski (2013). The operating voltage was 15 kV, with 20 nA beam current and 5 µm beam diameter. Counts were collected for 20 s for each element with the exception of F and Cl (50 s) and La, Ce, Pr, Nd, Sm, Gd, Th, and U in zircon (60 s). The following standards were used (all *K*α lines): synthetic phlogopite (F), albite (Na), synthetic phlogopite (Mg and Si in phlogopite, K in micas), diopside (Mg, minerals other than phlogopite), kyanite (Al in diopside and micas), corundum (Al in corundum), anorthite (Al in other minerals), zircon (Si in zircon), barite (S), scapolite (Cl), orthoclase (K in micas, Si in muscovite, nepheline, muscovite, and scapolite), rutile (Ti), synthetic V (V), synthetic magnesiochromite (Cr), synthetic rhodonite (Mn), and synthetic fayalite (Fe). The following additional standards were used for zircon (all *L*α lines except U*M*α):

$Y_3Al_5O_{12}$ (Y), zircon (Zr), Ca-Al-Si-glass (Drake & Weill 1972; La, Pr, Nd, Sm, Gd), CeO_2 (Ce), ThO_2 glass (Th), and UO_2 glass (U). Matrix correction calculations were done with using the 'PAP' $\phi(\rho Z)$ method (Pouchou & Pichoir 1985).

Chemical analysis of tourmaline was performed with a CAMECA SX100 instrument at Masaryk University, Brno, Czech Republic. The operating voltage was 15 kV with 10 nA beam current and 5 μm beam diameter. Counts were collected for 10 s with the following exceptions: 15 s (V), 20 s (Mg, Cr, Ca, Zn), 30 s (Cl), 40 s (K), and 60 s (F). The following standards were used (all *K*α lines): topaz (F), albite (Na), pyrope (Mg), sanidine (Al, Si, K), fluorapatite (P), vanadinite (Cl), wollastonite (Ca), titanite (Ti), scandium vanadate (V), chromite (Cr), spessartine (Mn), almandine (Fe), and gahnite (Zn). B_2O_3 concentrations of 10.63 wt. % were estimated for matrix correction of tourmaline data. Matrix correction was done using the X-PHI method (Merlet 1994).

2.1.3 Boron isotopes

The boron isotope composition of tourmaline was determined at the University of Manitoba with a Cameca IMS 7f ion microprobe using secondary-ion mass spectroscopy (SIMS), a primary O- beam (5 nA accelerated at 12.5 kV), with a 15 μm beam diameter, a sample accelerating voltage +10kV, electrostatic analyzer +10 kV, and ETP 133H electron multiplier coupled with an ion counting system having an overall deadtime of 21 ns. The entrance slit was set at 36 μm with a mass resolving power of 1450. Counts for ^{11}B, ^{10}B, and ^{30}Si were collected in succession for 50 cycles with 1 s measurements of each isotope per cycle, 30 s pre-sputter, and 0 V offset. The analytical procedure was similar to that used by Chaussidon & Albarède (1992). Instrumental mass fractionation (IMF) and analytical quality were assessed by replicate analyses of an elbaite tourmaline reference material (No. 98114, see below);

repeatability of the reference material was 0.4‰. Precision (1σ) for the unknown sample during the sessions was ±0.3‰. The boron isotope composition is expressed in delta notation, as a per mil deviation from boric acid standard NIST RM 951 ($^{11}B/^{10}B = 4.0437 \pm 0.0033$, Catanzaro *et al.* 1970): $\delta^{11}B = ([^{11}B/^{10}B]_{sample}/[^{11}B/^{10}B]_{SRM951} - 1)*1000$.

For the analysis of Beluga oxy-dravite, elbaite standard No. 98114 ($^{11}B/^{10}B = 4.0014 \pm 0.0007$, Leeman & Tonarini 2001) was used. Ludwig *et al.* (2011) reported no significant matrix effects for B isotope analysis of tourmaline (using dravite, elbaite, and schorl standards) with SIMS. Cabral *et al.* (2012) found a 1‰ to 2‰ IMF offset with elbaite, comparable to overall uncertainty and therefore not significant. However, a +1.6‰ discrepancy in Leeman & Tonarini (2001) standard elbaite No. 98114 relative to dravite No. 108796 was deemed significant by MacGregor *et al.* (2013).

2.1.4 Oxygen isotopes of corundum

The oxygen isotope composition ($^{18}O/^{16}O$) of corundum was measured at the Isotope Geosciences Unit, Scottish Universities Environmental Research Centre, Glasgow, Scotland using the laser fluorination method of Giuliani *et al.* (2005). Precision (1σ) of analyses on a quartz standard is ±0.1‰. Data is reported in delta notation as a per mil deviation from the $^{18}O/^{16}O$ value of Vienna Standard Mean Ocean Water (VSMOW) standard NIST RM 8535.

2.1.5 Whole-rock geochemistry

Whole rock major and trace elements were analyzed by ALS Chemex in Vancouver, Canada using a combination of inductively coupled plasma mass spectrometry (ICP-MS) and atomic emission spectroscopy (ICP-AES). Carbon was determined by combustion furnace, and samples were subjected to a lithium borate fusion for resistive elements, a four acid digestion, and aqua regia digestion. Precision of major element analyses, carbon, sulphur and chlorine is

5%. Precision of trace element, boron, and fluorine analyses is 10% with the exception of mercury (15%) and copper (7%).

2.1.6 Radiometric dating

Zircon crystals were analyzed using conventional ID-TIMS (isotope dilution thermal ionization mass spectrometry) at the Pacific Center for Isotopic and Geochemical Research (PCIGR), University of British Columbia, using the methods described by Mortensen *et al.* (1995) and Beranek & Mortensen (2011). Errors attached to individual analyses were calculated using the numerical error propagation method of Roddick (1987), and decay constants are those recommended by Steiger & Jäger (1977). Compositions for initial common Pb were taken from the model of Stacey & Kramer (1975). The zircon grains were strongly air abraded prior to dissolution in order to try to minimize the effects of post-crystallization Pb loss.

Muscovite and phlogopite were analyzed for $^{40}Ar/^{39}Ar$ dating in the Noble Gas Laboratory of the PCIGR. Mineral separates were hand-picked, washed in acetone, dried, wrapped in aluminum foil, and stacked in an irradiation capsule with a neutron flux monitor (Fish Canyon Tuff sanidine, 28.02 Ma, Renne *et al.* 1998) and 1071 Ma hornblende HB3Gr as an age check (which yielded a flat J-curve and an age of 1069 ± 2 Ma). The samples were irradiated at the McMaster Nuclear Reactor in Hamilton, Ontario, for 90 MWH, with a neutron flux of approximately 6×10^{13} neutrons/cm^2/s. Analyses (n = 45) of 15 neutron flux monitor positions produced errors of <0.5% in the J value. At PCIGR, the mineral separates were step-heated at incrementally higher powers in the defocused beam of a 10W CO_2 laser (New Wave Research MIR10) until fused. The gas evolved from each step was analyzed with a VG5400 mass spectrometer equipped with an ion-counting electron multiplier. All measurements were corrected for total system blank, mass spectrometer sensitivity, mass discrimination, radioactive

decay during and subsequent to irradiation, atmospheric Ar contamination, and the effect of irradiation on Ca, Cl, and K. The plateau and correlation ages were calculated using Isoplot v3.09 (Ludwig 2003). Errors are quoted at the 2-sigma (95% confidence) level and are propagated from all sources except mass spectrometer sensitivity and age of the flux monitor. The best statistically justified plateau and plateau age were picked based on the following criteria: (1) three or more contiguous steps comprising more than 50% of the ^{39}Ar; (2) probability of fit of the weighted mean age greater than 5%; (3) slope of the error-weighted line through the plateau ages equals zero at 5% confidence; (4) ages of the two outermost steps on a plateau are not significantly different from the weighted-mean plateau age (at 1.8σ, six or more steps only); and (5), the outermost two steps on either side of a plateau must not have nonzero slopes with the same sign (at 1.8σ, nine or more steps only).

2.2 Spinel

2.2.1 Sampling, petrography and mineral identification

The sampling strategy used in the field on southern Baffin Island was to extract samples from each unique lithology at a spinel occurrence (both spinel-bearing and spinel-absent rocks, with as representative a sample as possible) and, where possible, to sample nearby marble, calc-silicate, and other rocks for geochemical comparisons.

Rock samples were examined in thin-section using an petrological microscope and scanning electron microscope (SEM). Mineral phases that were not analyzed with electron probe microanalysis (EPMA) were identified using energy dispersive spectroscopy (EDS) in the SEM, or standard X-ray powder diffraction (XRPD) techniques (noted in text).

2.2.2 Electron probe microanalysis

Minerals analyzed with EPMA were extracted using hand tools directly from the rock samples (of which parts were used for whole rock geochemical analysis), mounted in epoxy pucks, and polished. Chemical compositions were obtained with a JEOL JXA-8230 electron microprobe (University of Ottawa) in wavelength-dispersion (WD) mode. The operating voltage was 20 kV, with 20 nA beam current and 5 μm beam diameter. Counts were collected for 20 seconds for each element with the exception of F (30 seconds). The following standards were used (all *Ka* except for Ba *La*): Sanidine (Si, Al, K, Ba), albite (Na), diopside (Ca, Mg), dolomite (Ca and Mg in carbonates), hematite (Fe), olivine (Fe, Mg and Si in forsterite), pyrrhotite (Fe and S in sulphides), chromite (Cr, Co, Al in forsterite and spinel, Mg in spinel), rutile (Ti), tephroite (Mn), pentlandite (Ni), vanadinite (V), gahnite (Zn), tugtupite (Cl), and fluorite (F). Matrix correction calculations were done using the Armstrong/Love-Scott $\phi(\rho Z)$ method (Armstrong 1988).

2.2.3 Whole-rock geochemistry

Whole rock major and trace elements were analyzed by ALS Canada Ltd in Vancouver, Canada. Samples were crushed and pulverized. Major elements (Si, Al, Fe, Ca, Mg, Na, K, Ti, Mn, in addition to Ti, P, Sr, Ba) were determined by inductively coupled plasma – atomic emission spectroscopy (ICP-AES) following fused bead preparation and acid digestion. Loss on ignition was determined by heating samples in a furnace at 1000 °C. Total sulphur and carbon were determined by Leco furnace. The following elements were measured by inductively coupled plasma – mass spectrometry analysis (ICP-MS) following Li borate fusion and acid digestion: Ba, Sr, Cs, Cr, V, Y, REE, Hf, Zr, Nb, Ta, Th, U, W, Rb, Ga, Ge, and Sn. The elements As, Bi, Hg, In, Re, Sb, Se, and Tl were determined by ICP-MS. The following elements

were measured by ICP-AES following Li borate fusion and four acid digestion: Ag, Cd, Co, Cu, Li, Mo, Ni, Pb, Sc, and Zn. Boron was determined for selected samples using ICP-MS following NaOH fusion. Chlorine and F were determined for selected samples using ion chromatography following KOH fusion. Precision of major element analyses, carbon, sulphur and chlorine is 5%. Precision of trace element, boron, and fluorine analyses is 10% with the exception of mercury (15%) and copper (7%).

2.2.4 Thermodynamic modelling

Pseudo-sections were generated with Perple_X version 6.8.1 (Connolly 2009) using the default thermodynamic database (*hp02ver.dat*), the default computational file, and the CORK fluid equation of state (Holland & Powell 1991, 1998), with calculations assuming a saturated CO_2-H_2O fluid, using a constrained 2d grid computational model, and the following solution models: GlTrTsPg for clinoamphiboles; Sp(GS) for spinel; O(SG) for forsterite; Bio(HP) for phlogopite; Cpx(l) for diopside; and Scap for scapolite. A humite-rich sample could not be modeled due to the lack of humite in the thermodynamic databases (clinohumite is present, but is structurally and chemically different to humite).

The accuracy and precision of calculated phase diagrams is sensitive to uncertainty related to petrographic variations at hand sample and thin-section scales, *e.g.*, displacement of equilibria by ±1 kbar for a moderate degree of modal proportion uncertainty (20% relative threshold, Palin *et al.* 2016). Spinel-bearing rocks on Baffin Island tend to be very coarse-grained, and heterogeneous in texture and mineral abundance. Therefore, only highly representative samples were selected for thermodynamic modelling (samples 2A-SPL-2, 3A-1, 3E-3-A, and 3F-2). The nature of the spinel occurrences and the limited volume of sampling may nonetheless be a source for error, since the chosen samples may not perfectly represent the total

equilibration volume. Sample 3F-1 was excluded due to the high abundance of sericitization, which may have affected the bulk composition. Bulk rock compositions used in the calculations were obtained from whole rock analysis of crushed 0.3-0.6 kg hand samples. Whole rock concentrations of Fe (sample 2A-SPL-2 only) and Ca were corrected to compensate for the presence of pyrrhotite and apatite, respectively, which have been excluded from the effective bulk composition.

2.3 Lapis lazuli

2.3.1 Whole-rock geochemistry

Two whole rock Soper River lapis lazuli samples were analyzed using the same method as the spinel study.

Chapter 3. Origin of scapolite-hosted sapphire (corundum) near Kimmirut

3.1 Results summary

Gem-quality corundum (sapphire) occurs in scapolite-rich calc-silicate rock hosted in marble of the Lake Harbour Group near Kimmirut, southern Baffin Island. A deposit of blue and colourless gem corundum (Beluga occurrence) is compared to a similar calc-silicate pod generally lacking corundum but containing nepheline (Bowhead occurrence) and located 170 m to the SSW. Corundum formation was made possible by three equally important sequential metamorphic reactions: (1) formation of nepheline, diopside, and K-feldspar (inferred) at granulite facies peak metamorphic conditions; (2) partial retrograde replacement of the peak assemblage by phlogopite, oligoclase, calcite, and scapolite (Me_{50}-Me_{67}) as a result of CO_2-, H_2O-, Cl-, F-bearing fluid influx at 1782.5 ± 3.7 Ma (*P-T* < 720 °C, 6.2 kbar); and (3) retrograde break-down of scapolite + nepheline (with CO_2- and H_2O-bearing fluid) to form albite, muscovite, corundum, and calcite. Late, low-temperature zeolite mineralization is common in corundum-bearing zones. Based on thermodynamic models, the corundum-forming reaction only occurs in a <100 °C window with an upper limit determined by scapolite-nepheline stability, and a lower limit determined by the formation of Al-silicate rather than corundum. The protolith is inferred to be dolomitic argillaceous marl with no evidence to suggest the initial presence of evaporites. The enrichment of trace metals V and Cr, and the depletion of Co, Ni, and Mn suggest reducing diagenetic conditions in the initial sediment. Beluga calc-silicate rock is strongly depleted in REE (Total REE ~ 18 µg/g). Oxy-dravite $\delta^{11}B$ (+3.9 ± 0.7‰) is consistent with a marine boron source. The oxygen isotope composition of corundum ($\delta^{18}O_{VSMOW}$ = 16.4 ± 0.1‰) is comparable to that of corundum in marble or desilicated pegmatite associated with marble. Phlogopite and muscovite $^{40}Ar/^{39}Ar$ ages and calculated closure temperatures

(considered estimates) are *ca.* 1640 Ma (T_c = 455 to 515 °C) and 1510 Ma (T_c = 410 to 425 °C), respectively. In the Lake Harbour Group, the most prospective areas for gem corundum exploration are expected to be contiguous to the thrust fault separating the Lake Harbour Group and Narsajuaq terranes, where the retrograde, amphibolite facies overprint of the granulite peak assemblages was most pervasive.

3.2 Chapter introduction

Gem-quality blue corundum (sapphire) accounts for a significant portion of the gemstone market and prices continue to rise in response to demand (Shor & Weldon 2009, Genis 2016). For this reason, there is considerable interest in understanding the genesis of gem-quality corundum and constraining the types of environments in which it forms. Improved exploration methodologies based on sapphire genetic models will aid in the development of a Canadian colored gemstone industry that will be competitive on the world market and could be applied in exploration efforts worldwide.

Gem corundum deposits have been found in syenite, monzonite, kimberlite, lamprophyre, basalt (xenocrysts), gneiss, amphibolite, marble, skarn, and various contact metasomatic rocks (Simonet *et al.* 2008, Dzikowski *et al.* 2014, Giuliani *et al.* 2014). Gem-quality blue and colorless corundum was discovered in 2002 near Kimmirut, southern Baffin Island, Nunavut, Canada, and subsequent exploration led to the discovery of blue, colorless, yellow, and pink gem corundum showings (True North Gems 2007). These occurrences are the first reported examples of gem corundum hosted in scapolite-rich calc-silicate pods in marble. The present study examines two calc-silicate pods, the Beluga deposit, which is blue-corundum-bearing, and the Bowhead occurrence, a nearby calc-silicate pod in which corundum is rare, with the objective of determining the cause and timing of mineralization, and the nature of the protolith.

3.3 Exploration History

The area around the Beluga and Bowhead calc-silicate pods was extensively explored by True North Gems, Inc. (TNG) from 2002 to 2009 after the initial discovery of the Beluga sapphire occurrence in 2002 by Seemeega and Nowdluk Aqpik, prospectors from Kimmirut. Ultraviolet light prospecting for fluorescent scapolite assisted in the discovery of 8031 scapolite showings in and around the Beluga Project property, in addition to 45 named spinel outcrops, and 44 named corundum localities (some of which consist of multiple contiguous showings). The distribution of corundum, scapolite, and spinel showings is plotted on a geological map of the TNG property in Fig. 3.1.

Several corundum occurrences produced notable gems as part of the exploration and deposit assessment work: the Beluga South occurrence produced 34 yellow sapphire gemstones totalling 6.98 carats, notably including two yellow stones weighing 1.47 carats and 1.09 carats (Fig. 3.2A), in addition to colorless and pale blue stones. The Aqpik occurrence produced two virtually flawless colorless stones, 2.50 carats and 2.59 carats in weight, and a pale blue, lightly included 7.81 carat gemstone (Fig. 3.2B). Some of the Aqpik rough sapphire turned blue as a result of heat treatment. One heat-treated, rich blue cushion-cut stone weighs 2.43 carats (Fig. 3.2A). The Beluga occurrence is the most important gem corundum occurrence found in Nunavut to date, containing grades of gem sapphire rough between 33 g/t (4.29 t bulk sample) and 19 g/t (22.5 t bulk sample). Colorless, pale blue, and more commonly saturated to dark blue corundum occurs as crystals up to *ca.* 7 cm long. One of the more notable stones in the bulk sample is a 1.17 carats, deep blue, extra fine sapphire gemstone (Figs. 3.2) showing even color when viewed through the table facet, but which in fact is primarily colorless with a central, dark blue patch (Wilson 2014). Lastly, pinkish corundum was found at one location.

In total, 2607 polished corundum gemstones, totalling 169.95 carats (33.99 g), were cut from gem rough recovered by regional and bulk sampling. The great majority of these gemstones originated from the Beluga deposit.

3.4 Results

3.4.1 Outcrop descriptions

The Beluga (N 62.828734°, W 69.894072°; Fig. 3.3) and Bowhead (170 m to the SSW) occurrences are marble-hosted calc-silicate pods with surface exposures of 4.2 × 3.7 m and 2 × 1.5 m, respectively. Contacts with the host marble are sharp, with the exception of parts of the Beluga pod, where euhedral crystals of dark brownish-purple diopside (1-3 cm) or yellowish-grey scapolite (1-5 cm) occur in very coarse pale-orange calcite between the calc-silicate rock and marble. The rock in the calc-silicate pods is beige with abundant 1 to 6 cm spots of brown mottling. Beige areas are primarily composed of scapolite, albite, muscovite, calcite, and corundum at Beluga, and scapolite-nepheline-calcite at Bowhead. The brown mottling is phlogopite-rich with oligoclase and diopside. The relative abundance of the light- and dark-coloured assemblages is variable: for example, at Beluga, the darker assemblage ranges between 10 and 90% on a decimeter scale but overall represents roughly half of the total rock volume based on visual estimation.

3.4.2 Petrography and mineral compositions

3.4.2.1 Beluga occurrence

The calc-silicate rock at Beluga is coarse to very coarse-grained (5 mm to > 5 cm) and commonly consists of randomly oriented centimeter-scale crystals, occasionally with maximum

dimensions *ca.* 4 - 7 cm. The calc-silicate rock can be divided into three distinct mineral assemblages (Fig. 3.4): (1) dark areas composed of phlogopite, oligoclase, diopside, and subordinate calcite; (2) light-colored, scapolite-rich zones, where scapolite is frequently altered to a mixture of fine-grained silicate minerals, generally separating the first assemblage from the corundum-bearing assemblage; and (3) pods or zones of light-colored corundum-albite-muscovite-calcite assemblage containing small amounts of graphite and pyrrhotite.

Dark brown, Fe-, F-, and Ti-bearing phlogopite (Table 3.1), pale grey oligoclase (Ab_{80}; Table 3.2), and subordinate calcite occur as graphic oriented intergrowths ranging in size from several millimeters to 2 cm across. Phlogopite-oligoclase symplectite up to 3 mm across is uncommon. The oriented intergrowths form coronae around irregularly-shaped grains of purplish-brown Al-bearing, Si-poor diopside (Fig. 3.5) from several millimeters to 3 cm in size (0.31 Al *pfu*, 0.12 Na *pfu*; Table 3.3), and are uncommonly pseudomorphic after diopside. The replacement of diopside by phlogopite-oligoclase is substantial (*ca.* 30-80%) with considerable local variation, and small relict diopside grains occur sparsely in the phlogopite-oligoclase. Minor pale-orange calcite is present in the coronae and is infrequently visible in hand sample. Titanite (<0.5 mm), zircon (Table 3.4), and apatite (0.1 mm) are uncommon. The phlogopite-oligoclase intergrowths are locally associated with 1-3 cm masses of equigranular, medium-grained oligoclase with subordinate phlogopite and calcite.

Anhedral, coarse-grained to very coarse-grained crystals of pale yellowish-grey to grey scapolite occur around the phlogopite-rich coronae. The scapolite averages 57 mol. % meionite component with considerable variation (Me_{50} – Me_{62}; Table 3.5) and minor silvialite component (average 0.014 SO_4 *pfu*). Much of the scapolite is pervasively replaced by milky white, fine-

grained mixtures (Fig. 3.6) of the following mineral phases, identified via X-ray powder diffraction: albite with variable quantities of prehnite, analcime, and thomsonite, and small amounts of calcite and muscovite. The altered scapolite retains its cleavage in hand sample. Uncommon, microscopic fractures cutting scapolite contain albite, calcite, and probable Mg-chlorite; other such fractures contain analcime. Unaltered scapolite fluoresces bright yellow when exposed to long- and short-wave ultraviolet radiation. Pristine scapolite, easily seen when exposed to UV, is generally restricted to the periphery of phlogopite-oligoclase mineralization and as isolated 'pods' within the light-coloured zones, where intensely altered scapolite is always contiguous to corundum-bearing zones (Figs. 3.6, 3.7). Phlogopite crystals associated with scapolite, occurring on the periphery of phlogopite-oligoclase intergrowths, have well-developed basal faces and no embayed grain boundaries with scapolite, which suggests that these minerals form a stable assemblage.

Small pods and zones, ranging in size from 0.5 × 1 cm to more than 4 × 10 cm, are composed of fine- to coarse-grained grey end-member albite (Ab_{98}; Table 3.2), silvery-grey muscovite (Table 3.1), idiomorphic blue corundum, pale-yellow calcite (Fig. 3.6), subordinate graphite, and uncommon grains of anhedral pyrrhotite (<6 mm). Oxy-dravite (Table 3.6) occurs very uncommonly at Beluga, and was only a significant constituent of a corundum-bearing pod in one sample, where it occurs as a 40 × 32 mm friable medium-brown mass near two dark brown, short-prismatic, euhedral crystals of the same mineral (up to 32 mm in length). The corundum-bearing zones locally constitute up to 70% of the rock volume, estimated from visual inspection of outcrop. Parts of the calc-silicate rock with high abundance of phlogopite-oligoclase-diopside (~90% of rock volume) tend to have little or no corundum mineralization. The corundum-bearing zone contains open cavities where the rock surface, including euhedral

corundum, is entirely covered by a 1-2 mm thick coating of prismatic thomsonite with local analcime and grey, scalenohedral calcite. Some cavities contain thin thomsonite prisms up to 8 mm in length with analcime and calcite crystals no larger than 2.5 mm. LeCheminant *et al*. (2005) noted thomsonite seemingly penetrating a corundum crystal. The surface of those corundum crystals enclosed in albite-muscovite-calcite and those enclosed in thomsonite are identical in morphology and show no corrosion or alteration.

The corundum crystals are euhedral and tapered along the c axis; their faces are striated perpendicular to c. Most crystals have dimensions in the range of 8 - 14 mm long and 1 – 4 mm wide, but larger crystals are not infrequent (2-4 cm long) and length:diameter aspect ratios range from approximately 3:1 to 9:1. The largest crystal recovered intact at Beluga measured 7.7 × 2.1 cm (LeCheminant *et al.* 2005). The corundum is royal blue, dark blue, or dark greyish blue in hand sample. When observed in cut cross-sections or gemstones, the corundum varies from colorless and pale blue to bright blue, dark blue, or dark blue with a grey tinge in well-defined oscillatory zoning patterns and irregular sector zoning. The corundum has good transparency and is sparsely included by calcite and apatite. Gem quality is principally controlled by the degree of fracturing. The corundum at Beluga contains an average of 0.08 wt. % TiO_2 (range 0.00 – 0.30 wt. %) and 0.07 wt. % FeO (range 0.02 – 0.13 wt. %), and there is a weak positive correlation between Fe and Ti content (correlation coefficient = 0.26; see Dzikowski 2013 for spot analyses data).

Rare rutile, sanbornite, thorianite, monazite, and uraninite are noted from the Beluga calc-silicate pod (Dzikowski 2013, LeCheminant *et al.* 2005).

3.4.2.2 Bowhead occurrence

Mineralization in the Bowhead calc-silicate pod is relatively similar to that at Beluga with the notable exception that it is largely devoid of corundum mineralization whereas nepheline is common. LeCheminant *et al.* (2005) noted trace corundum in the surface exposure. The rock at Bowhead is composed of coarse to very coarse-grained phlogopite-oligoclase intergrowths (partly replacing diopside), diopside, scapolite, calcite, and nepheline. The diopside and phlogopite at Bowhead are slightly poorer in Ti and Fe relative to Beluga (Tables 3.1 & 3.3). The oligoclase is slightly more calcic than that at Beluga (Ab_{76}; Table 3.2), and the same is true of scapolite (average Me_{60}, range Me_{50}-Me_{67}; Table 3.5). Both nepheline and scapolite have irregular curved boundaries with calcite. Some scapolite grains appear to embay nepheline. Scapolite rims of variable thickness, some of which are very thin and difficult to observe in low magnification, occur around nepheline grains contiguous to calcite (Fig. 3.8). Multiple nepheline grains are proximal to phlogopite-oligoclase intergrowths bordering diopside. The extent of diopside replacement by phlogopite-oligoclase in the nepheline-bearing Bowhead samples (~15-30%) is inferior to the average level of replacement at Beluga and calcite is a major component of the nepheline-bearing rock, whereas it is less abundant at Beluga. A single, 50 µm-wide nodule of muscovite (Table 3.1) and end-member albite (Ab_{98}; Table 3.2) was found in scapolite.

3.4.3 Whole rock composition – Beluga deposit

The Beluga calc-silicate pod is primarily composed of SiO_2 (Table 3.7; *ca.* 46 wt. %), CaO (17 wt. %), Al_2O_3 (14 wt. %), and MgO (10 wt. %). The rock is richer in Na than K (average Na_2O = 2.71 wt. %, K_2O = 2.02 wt. %, Na/K = 2.04) and contains 2.02 wt. % total Fe and 0.98 wt.% TiO_2. The atomic ratio of Al/Si is 0.36. Loss on ignition is on the order of 5%, where CO_2 is the principal volatile. The rock is relatively enriched in V (Table 3.8; 237 µg/g)

and, to a lesser degree, Cr (108 µg/g). The Beluga occurrence is very poor in Co (2.5 µg/g), Ni (5 µg/g), and Cu (5 µg/g). Fluorine is relatively abundant (1260 µg/g). The concentration of B is ~ 80 µg/g, and Cl ~545 µg/g. The average total rare earth element (REE) concentration is relatively low, 18.1 µg/g, and the rock is slightly enriched in LREE with a smooth, flat HREE chondrite-normalized signature and variable negative Eu anomaly (see discussion).

3.4.4 Boron and oxygen isotope compositions

The oxygen isotopic composition ($\delta^{18}O_{VSMOW}$) of corundum from the Beluga occurrence is 16.4 ± 0.1‰. Oxy-dravite has an average boron isotope composition ($\delta^{11}B$) of +3.9 ± 0.7‰ (Table 3.9).

3.4.5 Zircon U-Pb geochronology

Zircon was recovered from the phlogopite-oligoclase portion of rock from the Beluga occurrence. The zircon in the sample displays a range of morphologies, including coarse, irregular grains with rounded edges and sharp-faceted, stubby prismatic to equant grains. All the grains are clear to translucent but range from medium to dark brown in color. Five single grains (mostly *ca.* 130 µm in maximum dimension) were selected for analysis, including one coarse (>180 µm diameter), dark brown, translucent grain fragment with all rounded or broken edges (fraction A); two single, clear, stubby euhedral, prismatic brown grains (fractions B & C); and two single, clear, slightly elongate brown prismatic grains (fractions D & E). The five zircon fractions contain relatively high U concentrations (608-1258 µg/g) and have low Th/U ratios (0.06-0.12; Table 3.10). The analyses are slightly to strongly discordant (2.4-13.3%) but define a linear array, interpreted to reflect mainly recent Pb loss from a single age of metamorphic zircon, with calculated upper and lower intercepts (calculated using Model 1 of Ludwig 2003) of 1782.5 ± 3.7 Ma and -6 ± 140 Ma, respectively, with calculated MSWD = 0.23 (Fig. 3.9).

3.4.6 Ar-Ar ages of mica and estimate of T_c

Two ^{40}Ar-^{39}Ar data collections from Beluga phlogopite (Appendix A) produced: (1) a flat spectrum yielding a plateau age of 1635.9 ± 8.4 Ma (Fig. 3.10A) where data corresponding to 91.4% of the ^{39}Ar volume was used, and (2) a non-ideal saddle-shaped spectrum with a flat minimum yielding a plateau age of 1646.8 ± 8.6 Ma (Fig. 3.10B) where 63.7% of the data was used. Two analyses of muscovite (Appendix A) yielded the following plateau ages: (1) 1511.7 ± 8.4 Ma using 34% of the ^{39}Ar volume (Fig. 3.10C), and (2) 1510.4 ± 8.3 Ma using 78% of the ^{39}Ar volume (Fig. 3.10D). Closure temperatures were calculated using CLOSURE v1.2 (Brandon *et al.* 1998) and different sets of activation energies and frequency factors for phlogopite and muscovite (Table 3.11). Using the activation energies and frequency factors of Villa (2010) and Harrison *et al.* (2009), we estimated the cooling rate to be on the order of *ca.* 0.35-0.75 °C/Ma, and the closure temperatures of phlogopite and muscovite to be *ca.* 455-515 °C and 410-425 °C, respectively. The accuracy of these results is limited by the quality of the models, the validity of underlying assumptions (size of diffusion domain), and the use of only two minerals as geothermometers.

3.5 Discussion

3.5.1 Paragenetic sequence and metamorphic history

Butler (2007) suggested the following possible nepheline-forming reactions for rocks on Aliguq island:

$$\text{dolomite} + \text{albite} \rightarrow \text{diopside} + \text{nepheline} + 2\ CO_2 \quad (1)$$

$$\text{phlogopite} + 3\ \text{calcite} + 3\ \text{albite} \rightarrow 3\ \text{diopside} + 3\ \text{nepheline} + \text{K-feldspar} + 3\ CO_2 + H_2O \quad (2)$$

Based on the inclusion of nepheline by diopside, phlogopite, and forsterite, Butler (2007) ruled-out reaction (1), since it occurs at lower metamorphic grade than a forsterite-bearing

assemblage. The implied late formation of nepheline and its intergrowth with K-feldspar led Butler (2007) to infer that nepheline formed from reaction (2). A thermodynamic model of the reaction presented by Butler (2007) suggests that at 8 kbar pressure, reaction 2 only occurs at $X_{CO2} < 0.15$. The reaction produces CO_2 at a ratio of 3:1 relative to H_2O, and therefore the reaction would be self-limiting under these *P-T* conditions unless X_{CO2} was buffered by a large supply of H_2O-dominant metamorphic fluid. In the Beluga and Bowhead calc-silicate pods, the break-down of diopside to a mixture of phlogopite, oligoclase, and calcite clearly implies the retrograde reversal of the peak metamorphic assemblage in reaction 2. Thermodynamic modelling of reaction 2 in a TWQ v1 *P-T* phase diagram (Fig. 3.11A; Berman 1988, 1991) places the phase boundary out of range of the peak metamorphic grades, thus low X_{CO2} (as per Butler 2007, Fig. 3.11B) is required to form the nepheline-bearing assemblage. Reaction 2 is significantly more consistent with the whole rock composition and mineral parageneses compared to reaction 1. The expected whole rock composition based on the mineral proportions in reaction 1 differs significantly from the measured composition of Beluga calc-silicate rock: the abundance of K relative to Na (whole rock K/Na = 0.49) cannot be accounted for by the relatively small K concentrations found in nepheline (Bowhead nepheline K/Na = 0.16). Potassium feldspar was not observed in samples from Beluga or Bowhead, but it has been noted in other corundum-bearing calc-silicate pods in the area (Hansen 2008). Therefore, the presence of K-feldspar in the peak metamorphic assemblage is inferred from its suggested role in metamorphic reactions, its coeval relationship with nepheline in calc-silicate rocks elsewhere in the LHG (Butler 2007), and since it can account for whole rock K concentrations higher than expected for the peak metamorphic paragenesis partly preserved in Beluga and Bowhead calc-silicate rock.

Zircon recovered from phlogopite-oligoclase coronae have a concordia intercept age of 1782.5 ± 3.7 Ma, interpreted as the age of zircon neocrystallization and break-down of the peak metamorphic assemblage during the post-D_2 fluid incursion as suggested by St-Onge *et al.* (2007) in *P-T* conditions slightly lower than M_2 metamorphism (720 °C, 6.2 kbar). The timing of this retrograde mineralization is consistent with slow cooling rates estimated from phlogopite-muscovite ages (0.35-0.75 °C/Ma, estimated from running multiple iterations for closure temperatures in CLOSURE v1.2 calculations using phlogopite and muscovite). The extent to which the retrograde mineral assemblage replaces the peak assemblage (*i.e.*, reversed reaction [2]) is dependent on the availability of CO_2 and H_2O in fluids introduced during this episode of retrograde metamorphism.

Scapolite appears stable with phlogopite since the phlogopite crystals possess well-developed basal faces, and neither mineral embays the other: thus we infer that the scapolite is part of the phlogopite-oligoclase-calcite assemblage, although since it is not present within the phlogopite coronae, it may have formed slightly later from destabilization of nepheline not consumed in the phlogopite-forming reaction. The higher X_{Ca} of scapolite (Me_{50-67}) relative to oligoclase (An_{19-24}) is consistent with compositional data for coexisting scapolite-plagioclase pairs in metamorphic rocks, but F and Cl contents of phlogopite ($X_{Mg} \approx 0.93$, F ≈ 1.39 – 1.96 wt. %, Cl = 0.02 wt. %) are significantly different from values in biotite associated with scapolite in these metasediments ($X_{Mg} \approx 0.6$, F ≈ 0.6 wt.%, Cl ≈ 0.2 wt.%; Mora & Valley 1989). At the Bowhead occurrence, rims of scapolite separate nepheline and calcite; this suggests that during the first episode of retrograde metamorphism, scapolite formed from the reaction of nepheline with calcite. The availability of NaCl in fluid stabilizes scapolite relative to plagioclase in the presence of calcite (Ellis 1978), but the effect of fluid Cl content on the relative stability of

nepheline-scapolite-calcite is unknown. In corundum-bearing calc-silicate rock at Pitcairn, New York, rims of NaCl-bearing scapolite separating nepheline from calcite or apatite imply the formation of scapolite from the reaction of nepheline with calcite or apatite and CO_2- and Cl-bearing fluid (P.M. Belley, unpublished data). We suggest that scapolite formation at Beluga and Bowhead may have been limited by Cl availability, whereas fluid Na content may not be a controlling factor since the nepheline is Na-rich. Therefore, the extent of scapolite formation at the expense of nepheline and calcite may be controlled by the availability of Cl introduced to the system concomitant with CO_2- and H_2O-influx during retrograde metamorphism.

Pods and zones of albite, muscovite, calcite, and corundum are always surrounded by pervasively albitized (Ab_{98}) scapolite. A similar phenomenon is observed on a centimetre scale around small corundum-bearing zones in scapolite at Pitcairn, New York, but muscovite is not present at this locality (P.M. Belley, unpublished data). This consistent spatial relationship, together with the presence of calcite in the fine-grained alteration, suggests that the carbonate-bearing scapolite is a reactant in corundum-forming reaction (3), below. Reaction (3) excludes graphite and pyrrhotite, two minerals occurring in the corundum-bearing assemblage at Beluga which probably formed as a result of carbonate and sulphate (released from scapolite break-down) reduction, respectively.

Scapolite (Me_{57}) + 0.84 nepheline + 0.60 H_2O + 2.02 CO_2 → 0.76 corundum + 2.35 calcite + 2.14 albite + 0.60 muscovite + 0.66 Cl (3)

Reaction (4), an approximation of reaction (3), was used to model in TWQ due to limitations in scapolite solid solution and the inclusion of muscovite in the reaction:

$$\text{meionite} + 3\ \text{nepheline} + 3\ CO_2 \rightarrow 3\ \text{corundum} + 4\ \text{calcite} + 3\ \text{albite} \qquad (4)$$

The phase boundary for reaction (4) is in the 650-700 °C range for 2.5-4 kbar pressure (Fig. 3.11A). The phase boundary temperature for the break-down reaction of scapolite and nepheline with CO_2 is probably overestimated by the TWQ thermodyamic model, since Kimmirut scapolite is richer in Na (Me_{50-67}) and end-member meionite becomes stable at higher temperature relative to Na-bearing scapolite (Goldsmith & Newton 1977). Moreover, the TWQ modeled reaction does not take into account the formation of muscovite, an important constituent of the albite-calcite-corundum assemblage at Beluga, however this may not be an important control on mineralization, since muscovite is absent in a similar retrograde corundum-calcite-albite assemblage at Pitcairn, NY.

Zeolites, whose presence is characteristic of low-grade metamorphism, formed in corundum-bearing zones at Beluga relatively late (<1500 Ma, since mica closure temperatures indicate that temperatures were above zeolite facies conditions at this time), and are accompanied by the dissolution of calcite, or the break-down of scapolite or possibly relict nepheline, resulting in the creation of open space.

Uncommon oxy-dravite crystals occur near the border of phlogopite-oligoclase and the corundum-bearing zone. Due to the wide *P-T* stability range of tourmaline (van Hinsberg *et al.* 2011) and the lack of mineral textures that could provide information on its paragenesis, the position of oxy-dravite in the paragenetic sequence could not be determined.

3.5.2 Controls on corundum genesis

At Kimmirut, corundum was formed by the following sequence of events, determined from the petrography and modeled reactions discussed in section 3.5.1: (1) formation of a nepheline-diopside-rich peak metamorphic assemblage; (2) high-temperature partial retrogression of this assemblage where some nepheline is preserved and where scapolite forms at its expense; and (3) introduction of CO_2-H_2O-bearing fluid at slightly lower temperature, causing nepheline and scapolite to react, forming albite, calcite, corundum, and muscovite. Muscovite formation is expected to be controlled by the availability of K (from nepheline) and H_2O (fluid) and is probably not essential to the corundum-forming reaction. Corundum mineralization is extensive at the Beluga occurrence whereas it is rare at Bowhead, where the nepheline is largely unaltered. Since the occurrences are separated by a distance of only 170 m, it is evident that local variations play an important role in controlling the reaction.

Corundum forms from the break-down of nepheline + scapolite is predicted to occur in a narrow temperature range with upper and lower limits controlled by nepheline + scapolite stability and corundum *vs.* Al-silicate stability, respectively. Al-silicate forms by reaction (5):

$$2 \text{ meionite} + 3 \text{ nepheline} + 6\ CO_2 \rightarrow 8 \text{ calcite} + 6\ Al_2SiO_5 + 3 \text{ albite} \qquad (5)$$

A TWQ thermodynamic model (Fig. 3.11A) indicates a 70-90 °C window in which nepheline and meionite would break down to form corundum rather than Al-silicate for expected pressures in a barrovian retrograde *P-T* path. The actual position of this window in *P-T* space could only be determined with improved thermodynamic models for Na-bearing scapolite.

3.5.3 A possible magmatic origin?

LeCheminant *et al.* (2005) proposed that the Beluga and Bowhead calc-silicate pods formed from syenitic magma that intruded, and were contaminated by marble during D_2 deformation. Partly contaminated syenitic intrusions have not been noted in the area, but they would be expected given the widespread occurrence of scapolite-bearing and corundum-bearing calc-silicate pods in LHG marble near Kimmirut. Some scapolite-rich pods are small (*ca.* 1 m in maximum dimension) and isolated within the regional marble (Hansen 2008). Moreover, the contacts between marble and the calc-silicate rocks are generally sharp with no apparent zoning. The author (PMB) has observed multiple granite pegmatites in marble throughout the Central Metasedimentary Belt, Grenville Province, where metamorphic grades were in upper amphibolite to granulite facies, and these dikes typically have no to minor contamination in the form of Ca-Mg-bearing silicate minerals. The dikes typically have thin metasomatic aureoles at their contact with marble (*e.g.*, tremolite around zircon-rich pegmatite near Bryson, Québec), or are contiguous with coarsely crystalline vein- or pod-like bodies of clinopyroxene and feldspar/scapolite with calcite-rich cores (*e.g.*, rocks in the Lac Tortue area, ZEC Bras-Coupé Désert, Québec). Compared to these examples, the Beluga and Bowhead calc-silicate pods are remarkably uniform, despite local variations in mineral abundance. Th/U ratios in Beluga zircons ($Th/U_{avg} = 0.08$) are within the range considered to be characteristic for metamorphic zircon ($Th/U < 0.1$) by Rubatto *et al.* (1999), although Möller *et al.* (2003) cautioned against attributing the origin of zircon using Th/U. Lastly, the paragenetic sequence of the Beluga and Bowhead calc-silicate pods appears most consistent with a metamorphic origin where the peak metamorphic assemblage was subjected to two distinct stages of high-temperature retrograde

metamorphism, and the inferred peak *P-T* formation of nepheline was noted in carbonate-bearing metasediments in another region of the LHG (Butler 2007).

3.5.4 Nature of the protolith

Beluga calc-silicate rock plots between LHG metapelites and psammites in Al/Si and Na/K ratios (Fig. 3.12A), is slightly Fe-depleted relative to shale and metapelites (Fig. 3.12B), and contains a TiO_2 concentration (~1 wt. %) consistent with a shale/pelitic component (Fig. 3.12D). The rock is significantly richer in CaO and MgO than LHG clastic metasediments and intrusive rocks but with similar concentrations to LHG lapis lazuli metaevaporite layers in marble (Fig. 3.12C). These data suggest a protolith of mixed clastic and carbonate composition, where the clastic component is an intermediate between the pelitic and psammitic sediments, *i.e.*, a silty clay. While a small quantity of halite could explain the greater abundance of Na relative to K, the relative abundance of these elements at Beluga is consistent with an intermediate between LHG metapelite and psammite, and the Na/K value at Beluga (~2) is significantly lower than that at the Soper River lapis lazuli metaevaporite (~ 5 to 19; Hogarth & Griffin 1978). Metamorphic reactions resulted in significant decarbonation of the rock, but initial carbonate content can be estimated by subtracting an estimated MgO and CaO siliciclastic contribution (an intermediate of LHG metapelite-psammites, 2 wt. % CaO, 3-6 wt. % MgO) from the total bulk CaO and MgO, and recalculating the difference as calcite and dolomite with a second iteration correcting assumed initial CaO and MgO values for the amount of original allochthonous material (*i.e.*, 1.6 wt. % CaO, 2.6-5.2 wt. % MgO). The resulting estimation is a protolith with *ca.* 19 wt. % dolomite and 13 wt. % calcite to 29 wt. % dolomite and 7 wt. % calcite. Therefore, the most likely protolith based on major element bulk composition is a silty or sandy dolomitic argillaceous marl, although a thinly interlayered dolostone-shale sequence is equally possible

given the coarse size of metamorphic recrystallization. It should be noted that the initial relative abundance of Na *vs.* K may have been affected by diagenetic processes, notably albitization of detrital feldspars (*e.g.*, Baccar *et al.* 1993).

The trace-element composition of Beluga calc-silicate rock is not as simple to interpret and it is important to consider that the complex metamorphic history of the deposit may have obscured the original trace element signature in the protolith. Vanadium (237 µg/g) is significantly enriched relative to Cr (108 µg/g), while Co, Ni, and Cu (≤ 5 µg/g) are extremely depleted. The V concentration at Beluga is similar to V-rich LHG metapelite and psammite, while Cr is consistent with shale, argillite, or marl, and Co, Ni, and Cu concentrations are closer to that of marble (Fig. 3.13). According to Tuttle *et al.* (2000), "aluminum and titanium are mostly bound to phases that are relatively unreactive in marine environments; therefore, both of these elements provide a good estimate of the amount of allochthonous detritus." Using this assumption, V, Cr, and Ni concentrations in Beluga rock, LHG metapelite, and psammite are plotted against the expected clastic contribution of trace elements in average shale (Fig. 3.14). The comparison with shale suggests significant V enrichment, typical detrital Cr contribution, and significant Ni (and by proxy, Co and Cu) depletion. One LHG psammite (95-C084 of Thériault *et al.* 2001) shows similar V-enrichment, expected Cr, and a weaker Ni-depletion (29 µg/g).

A study of transition metal behavior in response to different early diagenetic environments of modern sediments (Shaw *et al.* 1990) demonstrated the trapping of Ni and Co with manganese oxides, which are enriched and preserved in the oxic zone of sediments and released under reducing conditions. In contrast, near-anoxic reducing conditions (*e.g.*, in organic-matter-bearing sediment) favor the enrichment and preservation of Cr, V, and Mo, where

accumulation of Cu is moderately enriched in response to reducing conditions and closely correlated with biogenic material flux (*i.e.*, the Cu binding capacity of sediment decreases in slowly accumulating sediments where a smaller fraction of biogenic detritus survives). In strongly reducing H_2S-rich environments which favour high V/(Ni+V) ratios, maximum molar V/(Ni+V) are on the order of ~ 0.85 (black shale-carbonate sequences of Wenger & Baker 1986) – significantly lower than that at Beluga (V/(Ni+V) ≈ 0.98). Vanadium is strongly enriched in the Beluga calc-silicate rock, and Cr well-preserved. Molybdenum concentration is below detection level (<2 µg/g), but considering the low concentration in average shale (2 µg/g; Carmichael 1989) and significant dilution by the carbonate component in the protolith, Mo enrichment may not be detectable. Low MnO (0.01 wt. %) relative to a sample of LHG marble (0.17 wt. %; Butler 2007), average shale, and average marine carbonate (0.08 wt. %, 0.07 wt. %; Carmichael 1989) is consistent with the proposed mechanism of Co and Ni depletion, but many LHG metapelites and psammites contain low MnO with highly variable Ni (Fig. 3.13).

The extremely low REE concentrations relative to other lithologies in the LHG and Meta Incognita peninsula (Fig. 3.15) could partly be explained by early, reducing diagenetic conditions since REE also concentrate on Mn oxides, although REE could be preserved in phosphate in anoxic conditions (Takahashi *et al.* 2015). The V-enriched, Ni-depleted LHG psammite is far richer in total REE (~335 µg/g) relative to Beluga (~18 µg/g), which does not support this hypothesis. In LHG metapelites, concentrations of V, Ni, and Cr show some degree of positive correlation. Diagenetic processes could potentially dissolve phosphate minerals and mobilize REE. Given the complex metamorphic history of the Beluga calc-silicate rock, the attribution of early diagenetic processes to observed trace element profiles carries high uncertainty.

The oxygen isotope composition of corundum at Beluga is slightly higher than for corundum in desilicated pegmatite in marble, and at the low end of the marble range (Fig. 3.16). A $\delta^{18}O$ value of +16.4‰ is consistent with the equilibration of oxygen isotopic composition with marble, and it is higher than for corundum in skarn developed in marble (Giuliani *et al.* 2014).

3.5.5 On evaporites

Dzikowski (2013) suggested that the Beluga and Bowhead protoliths contained an evaporitic component. Here, we compare the bulk composition of Beluga calc-silicate rock with the geochemistry of evaporite-bearing argillites, dolomitic marls, and mixed sulfate rocks. These evaporite-bearing or evaporite-related sediments, in comparison with common platform sediments, have high Mg, high Mg/Ca ratios (except Ca-sulfate-rich rock), low Fe contents, high K with low Na (except halite-bearing rocks), and specifically in argillites, high Li, F, and B/Al (Moine *et al.* 1981). The Al-Mg-Ca geochemical signature of Beluga calc-silicate rock is within the range of platform marl and clay-shale, and just outside the compositional domain for evaporites and metaevaporites (Fig. 3.17). Hypothetically, the evaporite-associated sediment best matching the bulk major element composition of Beluga rock is argillaceous marl (clay/silt with dolomite and calcite) containing halite (Na > K), but Na-K contents are also consistent with a mixed clastic component (*i.e.*, intermediate between LHG metapelites and psammites, Fig. 3.12A). The boron concentration at Beluga (80 µg/g) is similar to that of average shale (100 µg/g; Carmichael 1989) but far lower than in argillaceous evaporitic rocks (200-400 µg/g; Moine *et al.* 1981). The whole-rock B measurements at Beluga may be affected by localized oxy-dravite mineralization (*i.e.*, oxy-dravite is very uncommon, but one sample contains a ~8 cm cluster). The concentration of Li at Beluga (15 µg/g) is far lower than the range for most evaporitic rocks (45 – 300 µg/g), however Li concentrations are low in Mg-clay-poor, dolomite-

rich sedimentary rocks associated with evaporites (Moine *et al.* 1981). Beluga F content (1260 µg/g), mostly held in phlogopite, is comparable to evaporitic argillite (1000-2000 µg/g; Moine *et al.* 1981) and approximately double that of shale (500-740 µg/g; Carmichael 1989). Beluga calc-silicate rock is also enriched in Cl (~500 µg/g) relative to shale (160-180 µg/g; Carmichael 1989). Fluorine-rich phlogopite and Cl-rich scapolite are retrograde assemblages: F and Cl are not highly compatible constituents within the major mineral phases in the peak assemblage (nepheline, diopside, K-feldspar), therefore it can be surmised that these elements were probably introduced with metamorphic fluids during retrograde metamorphism.

The boron isotope composition of oxy-dravite is similar to tourmaline with B sourced from marine boron. Due to the overlap of tourmaline $\delta^{11}B$ in marble, evaporite-associated metapelite, and B-rich metaevaporite (Fig. 3.18), an evaporitic protolith cannot be inferred from the data.

In summary, bulk rock major and trace element data are consistent with non-evaporitic marine platform sediments. There is no evidence to support an evaporitic origin of the protolith, although the possibility that the protolith contained a small evaporite component cannot be ruled out.

3.5.6 Implications for gem corundum exploration

Since corundum mineralization is dependent on two episodes of amphibolite facies retrograde metamorphism in Beluga- and Bowhead-like rocks, parts of the LHG with pervasive amphibolite-facies retrograde overprinting of peak metamorphic assemblages would be more prospective than areas with well-preserved, peak granulite facies assemblages. In the LHG, domains with pervasive amphibolite facies retrograde metamorphism are restricted to the

periphery of the thrust fault between the LHG and the Narsajuaq terrane (see Fig. 5 of St-Onge *et al.* 2000).

Kimmirut-type gem corundum deposits are produced by a very specific *P-T* history and protolith composition, and therefore are probably rare compared to gem corundum deposits with simpler paragenetic sequences and more common protoliths (especially marble-hosted deposits, see Giuliani *et al.* 2014). A corundum occurrence similar to the Kimmirut deposits is located in Pitcairn, New York, USA, where purplish-red, opaque corundum occurs with albite and calcite formed at the expense of scapolite and nepheline (unpublished data, P.M. Belley; Chamberlain *et al.* 2015).

3.6 Conclusions

In Lake Harbour Group calc-silicate rocks near Kimmirut, Nunavut, corundum formation was made possible by three equally important sequential metamorphic reactions: (1) formation of nepheline, diopside, and K-feldspar (inferred) at peak metamorphic (granulite facies) conditions from a metamorphosed dolomitic argillaceous marl precursor; (2) partial retrograde replacement of the peak assemblage by phlogopite, oligoclase, calcite, and scapolite as a result of CO_2-, H_2O-, Cl-, F-bearing fluid influx at 1782.5 ± 3.7 Ma, ~30 Ma younger than the end of M_2 metamorphism (therefore *P-T* < 720°C, 6.2 kbar); and (3) retrograde break-down of scapolite + nepheline (+ CO_2 + H_2O) to form albite, muscovite, corundum, and calcite. As evidenced by the abundance of corundum at Beluga and its near absence at Bowhead (170 m away), conditions favouring the alteration of scapolite-nepheline were locally heterogeneous. The corundum-forming reaction only occurs in a <100°C window with a lower limit determined by the formation of Al-silicate rather than corundum. Thermodynamic models of these reactions are inconsistent with known metamorphic conditions in the LHG, but do not take into account

variations in the composition of major phases. They are interpreted to be overestimates of phase boundary *P-T* since they exceed estimates based on the paragenetic sequence and the regional metamorphic history. The inferred mineral reactions are in strong agreement with petrologic observations, mineral assemblages, and bulk composition.

Phlogopite and muscovite $^{40}Ar/^{39}Ar$ ages and calculated closure temperatures are *ca.* 1640 Ma (T_c = 455 to 515°C) and 1510 Ma (T_c = 410 to 425°C), respectively. The late formation of thomsonite, analcime, and prehnite at Beluga is expected to be considerably younger than the muscovite closure age.

Local-scale and outcrop-scale field observations, combined with bulk and trace element geochemistry, suggests that the Beluga and Bowhead calc-silicate pods are metasedimentary. The relative abundances of Ca, Mg, Al, Si, Ti, and Fe are consistent with dolomitic argillaceous marl, where the siliciclastic component is an intermediate between that of LHG metapelites and psammites (*i.e.*, sandy or silty clay). Significant V enrichment, high Cr, and very low Ni, Co, and Cu may be related to early diagenetic processes such as a slow sedimentation rate and reducing conditions caused by the presence of organic matter.

The Li and B concentrations do not suggest an evaporite-related protolith, although concentrations of these elements in evaporite-associated sediments can be low. The Na/K ratios are intermediate between LHG metapelites and psammites. High F and Cl concentrations (*ca.* 1260 and 500 µg/g, respectively) appear to have been introduced by metamorphic fluid during retrograde metamorphism. Tourmaline boron isotopes are consistent with a marine boron source but cannot be used to distinguish between normal marine and hypersaline environments. Therefore, data do not suggest that the Beluga protolith was evaporite-related; *i.e.*, Beluga whole rock geochemistry is within the range expected in non-evaporitic marine shelf sediments.

However, the possibility that an initial, minor evaporitic component was present in the protolith cannot be rejected. We infer a similar origin for the Bowhead calc-silicate rock due to its mineralogical and geological similarity to the Beluga occurrence.

In the Lake Harbour Group, the most prospective areas for gem corundum exploration are expected to be contiguous to the thrust fault separating the LHG and Narsajuaq terranes, where the retrograde, amphibolite facies overprint of the granulite peak assemblages is most pervasive.

3.7 Tables

Table 3.1: Average composition of phlogopite and muscovite from the Beluga and Bowhead calc-silicate pods. After Dzikowski (2013).

Wt.%	phlogopite Beluga *n* = 41	phlogopite Bowhead *n* = 18	muscovite Beluga *n* = 12	muscovite Bowhead *n* = 2
SiO_2	39.79	40.99	44.96	45.00
TiO_2	2.53	1.84	0.04	0.04
Al_2O_3	15.58	15.01	37.39	38.47
Cr_2O_3	0.03	0.01	0.01	0.00
MgO	23.32	25.12	0.02	0.08
CaO	0.02	0.01	0.01	0.14
BaO	0.04	0.06	0.01	0.09
MnO	0.03	0.02	0.02	0.00
FeO	2.92	2.14	0.04	0.03
Na_2O	0.27	0.31	0.81	1.76
K_2O	10.56	10.63	10.68	8.96
F	1.39	1.96	0.00	0.00
Cl	0.02	0.02	0.02	0.04
H_2O*	3.57	3.36	4.46	4.51
O=F,Cl	-0.59	-0.83	0	-0.01
Total	99.48	100.65	98.46	99.11
Normalized to 12 anions with OH* + F + Cl = 2				
Si (*apfu*)	2.820	2.860	3.020	2.985
Ti	0.135	0.097	0.002	0.002
Al (IV)	1.180	1.140	0.980	1.015
Al (VI)	0.121	0.094	1.980	1.993
Cr	0.002	0.001	0.001	--
Mg	2.463	2.613	0.002	0.008
Ca	0.002	0.001	0.001	0.010
Ba	0.001	0.002	0.000	0.002
Mn	0.002	0.001	0.001	--
Fe	0.173	0.125	0.002	0.002
Na	0.037	0.042	0.105	0.226
K	0.955	0.946	0.915	0.758
F	0.312	0.432	--	--
Cl	0.002	0.002	0.002	0.004
OH*	1.686	1.565	1.998	1.996
∑cations	7.891	7.922	7.009	7.001

*Calculated, OH = 2 – F – Cl

Table 3.2: Average composition of plagioclase and nepheline from the Beluga and Bowhead calc-silicate pods. After Dzikowski (2013).

Wt.%	oligoclase Beluga *n* = 42	albite Beluga *n* = 9	oligoclase Bowhead *n* = 8	albite Bowhead *n* = 5	nepheline Bowhead *n* = 20
SiO_2	63.27	66.31	62.65	68.16	43.49
Al_2O_3	23.27	20.61	23.74	19.96	34.45
MgO	0.13	0.07	0.00	0.00	0.00
CaO	3.93	0.41	4.96	0.38	2.37
MnO	0.01	0.00	0.01	0.02	0.00
FeO	0.05	0.02	0.03	0.01	0.00
Na_2O	9.23	11.61	8.82	11.33	15.69
K_2O	0.19	0.11	0.07	0.10	3.92
Total	100.08	99.14	100.28	99.96	99.92
Norm.	8 O	8 O	8 O	8 O	4 O
Si (*apfu*)	2.793	2.932	2.766	2.978	1.035
Al	1.211	1.074	1.235	1.028	0.966
Mg	0.009	0.005	--	--	--
Ca	0.186	0.019	0.235	0.018	0.061
Mn	0.000	--	0.000	0.001	--
Fe	0.002	0.001	0.001	0.000	--
Na	0.790	0.995	0.755	0.960	0.724
K	0.011	0.006	0.004	0.006	0.119
Or	0.01	0.01	0.00	0.01	
Ab	0.80	0.98	0.76	0.98	
An	0.19	0.02	0.24	0.02	

Table 3.3: Average composition of diopside from the Beluga and Bowhead calc-silicate pods. After Dzikowski (2013).

	Beluga	Bowhead		Beluga	Bowhead
Wt.%	*n* = 18	*n* = 9		Normalized to 6 anions	
SiO_2	51.24	51.99	Si (*apfu*)	1.856	1.888
TiO_2	1.29	0.78	Ti	0.035	0.021
Al_2O_3	7.25	5.76	Al	0.310	0.247
Cr_2O_3	0.02	0.01	Cr	0.001	0.000
MgO	14.24	15.01	Mg	0.769	0.813
CaO	22.52	23.28	Ca	0.874	0.906
MnO	0.04	0.03	Mn	0.001	0.001
FeO	1.59	1.20	Fe	0.048	0.036
Na_2O	1.69	1.56	Na	0.119	0.110
Total	99.88	99.62	∑cations	4.013	4.022

Table 3.4: Composition of zircon from the phlogopite-oligoclase portion of Beluga calc-silicate rock.

Wt.%	*n* = 2
SiO_2	33.54
ZrO_2	65.34
HfO_2	1.36
La_2O_3	0.01
Ce_2O_3	0.01
Pr_2O_3	0.07
Nd_2O_3	0.02
Sm_2O_3	0.13
Gd_2O_3	0.03
ThO_2	0.05
UO_2	0.00
Total	100.56

Table 3.5: Average composition of scapolite from Beluga and Bowhead calc-silicate pods with standard deviation and minimum/maximum me% compositions. See Dzikowski (2013) for full data set.

	Beluga	σ	Min.**	Max.**	Bowhead	σ	Min.**	Max.**
Wt.%	*n* = 67				*n* = 15			
SiO_2	49.04	1.78	49.90	46.84	47.95	1.35	49.54	45.44
Al_2O_3	26.30	1.00	25.52	27.09	26.21	0.75	25.31	27.58
MgO	0.06	0.22	0.00	0.00	0.00	0.01	0.00	0.00
CaO	14.34	1.77	13.03	15.13	15.10	1.17	14.02	17.38
MnO	0.01	0.02	0.00	0.00	0.01	0.02	0.00	0.01
FeO	0.02	0.03	0.10	0.00	0.02	0.02	0.00	0.08
Na_2O	5.52	0.93	6.12	4.97	5.31	0.66	5.87	4.16
K_2O	0.45	0.18	0.49	0.39	0.33	0.08	0.39	0.24
SO_3	0.12	0.05	0.08	0.09	0.12	0.08	0.20	0.06
Cl	2.59	0.92	3.65	2.30	2.65	0.57	3.24	1.66
CO_2*	1.82	1.02	0.31	1.90	1.71	0.70	0.71	2.66
O=Cl	-0.58	0.21	-0.82	-0.52	-0.6	0.13	-0.73	-0.37
Total	99.69	0.81	98.37	98.19	98.81	0.49	98.55	98.9
				Normalized to Al + Si = 12				
Si (*apfu*)	7.353		7.487	7.136	7.189		7.490	6.996
Al	4.647		4.513	4.864	4.631		4.510	5.004
Mg	0.013		--	--	0.000		--	--
Ca	2.304		2.095	2.470	2.426		2.271	2.867
Mn	0.001		--	--	0.001		--	0.001
Fe	0.003		0.013	--	0.003		--	0.010
Na	1.605		1.780	1.468	1.544		1.721	1.242
K	0.104		0.094	0.076	0.076		0.075	0.047
SO_4	0.014		0.009	0.010	0.014		0.023	0.007
Cl	0.658		0.928	0.594	0.673		0.830	0.433
CO_3*	0.328		0.063	0.396	0.313		0.147	0.560
Me(%)	57		50	62	60		50	67

*Calculated assuming CO_3 + Cl + SO_4 = 1

** Examples of minimum and maximum Me(%) analyses

Table 3.6: Average composition of oxy-dravite at the Beluga occurrence.

Wt.%	Beluga *n* = 7	Site	Normalized to 15 Y + Z + T cations	
SiO_2	36.18	T	Si (*apfu*)	5.844
TiO_2	0.36	T	Al	0.156
B_2O_3[a]	10.76		B[a]	3.000
Al_2O_3	37.10	Z	Al (Z)	6.000
V_2O_3	0.03	Y	Ti	0.044
Cr_2O_3	0.01	Y	Al	0.906
FeO	1.14	Y	V	0.004
MnO	0.00	Y	Cr	0.001
ZnO	0.02	Y	Fe^{2+}	0.154
MgO	7.84	Y	Mn	--
CaO	0.46	Y	Zn	0.002
Na_2O	2.82	Y	Mg	1.888
K_2O	0.04	X	Ca	0.080
F	0.30	X	Na	0.883
Cl	0.00	X	K	0.008
O=F,Cl	-0.13	X	Vacancy	0.029
Total	99.68	V	OH[b]	2.950
		V	O[b]	0.050
		W	F	0.153
		W	Cl	0.000
		W	O[b]	0.847

[a]Boron calculated assuming ideal 3 B *apfu*
[b]OH-O calculated by cation charge balance

Table 3.7: Whole rock major element composition, Beluga occurrence. After Dzikowski (2013).

Wt.%	BA-1	BA-2	BA-3	BA-4	BA-5	Average
SiO_2	45.19	45.86	46.07	45.37	46.54	45.81
TiO_2	0.92	1.07	1.03	0.93	0.95	0.98
Al_2O_3	15.26	11.47	13.3	15.32	14.92	14.05
Cr_2O_3	0.01	0.01	0.01	0.01	0.01	0.01
Fe_2O_3	1.47	1.83	1.53	1.43	1.47	1.55
FeO	1.16	1.42	1.16	1.16	1.09	1.2
MnO	0.02	0.03	0.03	0.02	0.02	0.02
MgO	9.28	11.46	10.53	9.59	9.87	10.15
CaO	15.82	18.86	17.62	16.07	16.92	17.06
SrO	0.02	< 0.01	0.01	0.03	0.02	0.02
BaO	0.02	0.01	0.02	0.02	0.02	0.02
Na_2O	2.96	2.43	2.68	2.94	2.55	2.71
K_2O	2.45	1.55	1.86	2.37	1.88	2.02
P_2O_5	0.03	0.02	0.02	0.02	0.02	0.02
LOI	5.58	4.56	4.37	5.1	3.95	4.71
Total	100.19	100.58	100.24	100.38	100.23	100.33
H_2O-	0.04	0.01	0.06	0.04	0.02	0.03
H_2O+	0.89	0.66	0.66	1.12	1.22	0.91
C	1.15	0.95	0.93	1.05	0.66	0.95
CO_2	4.2	3.5	3.4	3.8	2.4	3.46
Mol.%						
P	0.009	0.006	0.006	0.006	0.006	0.006
Si	15.338	15.805	15.832	15.293	15.900	15.634
Ti	0.235	0.277	0.266	0.236	0.244	0.252
Al	6.104	4.659	5.387	6.086	6.008	5.651
Cr	0.003	0.003	0.003	0.003	0.003	0.003
Fe^{3+}	0.375	0.475	0.396	0.363	0.378	0.398
Fe^{2+}	0.329	0.409	0.333	0.327	0.311	0.343
Mn	0.006	0.009	0.009	0.006	0.006	0.006
Mg	4.696	5.888	5.395	4.819	5.027	5.164
Ca	5.753	6.964	6.488	5.804	6.194	6.238
Sr	0.004	< 0.002	0.002	0.006	0.004	0.004
Ba	0.003	0.001	0.003	0.003	0.003	0.003
Na	1.948	1.624	1.786	1.921	1.689	1.793
K	1.061	0.681	0.815	1.019	0.819	0.879
H-	0.091	0.023	0.138	0.090	0.046	0.068
H+	2.015	1.517	1.513	2.518	2.780	2.072
C	1.953	1.638	1.599	1.770	1.128	1.622
C	1.946	1.647	1.595	1.749	1.119	1.612
O	58.132	58.373	58.435	57.983	58.336	58.252

Table 3.8: Whole rock trace element composition, Beluga occurrence. After Dzikowski (2013).

µg/g	BA-1	BA-2	BA-3	BA-4	BA-5	Average
Rb	80.2	47.1	56	71.2	55.9	62.08
Cs	3.5	1.9	2.5	3.2	2.1	2.64
Sr	305	131.5	230	368	423	291.5
Ba	64.9	38.5	49.7	51	69.5	54.72
Sc	11.8	13.8	12.3	9.9	11.2	11.8
V	218	263	236	221	247	237
Cr	110	130	100	100	100	108
Zr	196.0	248.0	212.0	198.5	220.0	215.0
Hf	6	8	7	7	7	7
Nb	4	3	4	3	3	3.4
Ta	0.5	0.5	0.5	<0.5	0.5	0.5
Mo	<2	<2	<2	<2	<2	<2
W	1	1	1	2	3	~ 2
Co	2.4	3.2	2.3	2.5	2.3	2.5
Ni	5	6	5	5	6	5.4
Cu	5	7	6	5	<5	~ 5
Zn	32	35	31	29	34	32
Ag	<1	<1	<1	<1	<1	<1
Ga	27	27	26	27	28	27
Tl	<0.5	<0.5	<0.5	<0.5	<0.5	<0.5
Sn	3	3	3	3	3	3
Pb	<5	<5	<5	<5	<5	<0.5
Re	0.002	0.003	<0.002	0.003	<0.002	~ 0.002
Se	3	9	4	4	3	4.6
Te	<0.05	0.27	0.07	0.06	<0.05	~ 0.1
Y	3.5	3.9	3.7	3.3	3.5	3.6
La	2.7	2.7	2.7	2.9	2.6	2.7
Ce	6.4	6.4	6.2	5.5	5.7	6.0
Pr	0.8	0.9	0.9	0.9	0.8	0.9
Nd	3.9	4.3	4.3	3.5	3.7	3.9
Sm	1.2	1.4	1.3	1.1	1.2	1.2
Eu	0.2	0.2	0.2	0.2	0.3	0.2
Gd	0.9	1	1	0.9	0.9	0.9
Tb	0.1	0.2	0.2	0.1	0.1	0.1
Dy	0.8	0.9	0.8	0.7	0.8	0.8
Ho	0.1	0.2	0.2	0.1	0.2	0.2
Er	0.4	0.5	0.4	0.4	0.4	0.4
Tm	<0.1	0.1	0.1	<0.1	<0.1	~ <0.1
Yb	0.4	0.5	0.4	0.4	0.4	0.4
Lu	0.1	0.1	0.1	<0.1	0.1	0.1
Th	1	1	1	1	1	1
U	1.7	1.8	2.1	1.7	1.7	1.8
Li	17.6	14.2	13.9	14.5	16.2	15.3
Be	1.84	2.01	1.93	1.78	1.84	1.88
B	60	60	90	100	80	78
F	1580	1050	1240	1390	1030	1260
Cl*	570	230	690	800	460	550
Cl**	490	270	620	810	510	540

*Neutron activation analysis, ** Specific ion electrode analysis

Table 3.9: Boron isotope composition of oxy-dravite from the Beluga occurrence.

$\delta^{11}B$ (‰)	σ (‰)
4.6	0.3
4.3	0.3
4.4	0.3
3.7	0.3
4.2	0.3
2.8	0.3
2.7	0.3
3.3	0.3
3.9	0.3
4.4	0.3
4.4	0.3
Average	
3.9	0.7

Table 3.10: U-Pb analytical data for zircon from the Beluga occurrence.

Sample description[1]	A: N2, +180,t	B: N2, +134,s,c	C: N2, +134,s,c	D: N2, +134,e,c	E: N2, +134,e,c
Wt. (mg)	0.090	0.033	0.011	0.032	0.023
U (ppm)	1233	608	632	776	1258
Pb^{2} (ppm)	355	169	170	229	385
$^{206}Pb/^{204}Pb$ (meas.)[3]	3977	1294	1569	15970	1344
Tot. common Pb (pg)	513	277	76	30	418
% $^{208}Pb^{2}$	1.5	2.0	2.1	1.6	3.0
$^{206}Pb/^{238}U^{4}$ (± % 1s)	0.29734(0.19)	0.28611(0.14)	0.27582(0.17)	0.30505(0.07)	0.31143(0.11)
$^{207}Pb/^{235}U^{4}$ (± % 1s)	4.4700(0.26)	4.3091(0.42)	4.1416(0.36)	4.5840(0.09)	4.6856(0.39)
$^{207}Pb/^{206}Pb^{4}$ (± % 1s)	0.10903(0.14)	0.10923(0.35)	0.10890(0.28	0.10899(0.03)	0.10912(0.33)
$^{206}Pb/^{238}U$ age (Ma; ± % 2 s)	1678.1(5.5)	1622.1(3.9)	1570.3(4.8)	1716.3(2.1)	1747.7(3.2)
$^{207}Pb/^{206}Pb$ age (Ma; ± % 2 s)	1783.3(5.0)	1786.6(12.8)	1781.1(10.1)	1782.6(1.2)	1784.8(12.0)
Discordance %	6.7	10.4	13.3	4.2	2.4
Th/U (calc.)	0.057	0.078	0.083	0.063	0.116

[1]N2 = non-magnetic at 2° side slope on Frantz magnetic separator; grain size given in microns; t = translucent; c = clear; s = stubby prismatic grains; e = slightly elongate prismatic grains.

[2]Radiogenic Pb; corrected for blank, initial common Pb, and spike.

[3]Corrected for spike and fractionation.

[4]Corrected for blank Pb and U, and common Pb.

Table 3.11: Estimated cooling rate and closure temperatures for phlogopite and muscovite at the Beluga occurrence using different determinations of activation energy (E_a) and frequency factor (D_0) for phlogopite (Phl) and muscovite (Ms) and calculated in closure v1.2.

Ms data	Phl data	Ms E_a (kJ/mol)	Ms D_0 (cm^2/s)	Phl E_a (kJ/mol)	Phl D_0 (cm^2/s)	Phl - Ms ~ ΔT_C (°C)*	Phl - Ms ~ Δt (Ma)**	Estimated cooling rate (°C/Ma)	Phl T_C (°C) Approx.	Ms T_C (°C) Approx.
Robbins (1972), Hames & Bowring (1994)	Giletti (1974)	180	4×10^{-4}	242	242	67	124	0.54	400	330
Robbins (1972), Hames & Bowring (1994)	Villa (2010)[B]	180	4×10^{-4}	299.4	205	131	124	1.06	470	340
Robbins (1972), Hames & Bowring (1994)	Villa (2010)[B]	180	4×10^{-4}	359.2	93611	180	124	1.45	525	345
Harrison *et al.* (2009)[A]	Giletti (1974)	268	20	242	242	-20	124	n/a		
Harrison *et al.* (2009)[A]	Villa (2010)[B]	268	20	299.4	205	44	124	**0.35**	**455**	**410**
Harrison *et al.* (2009)[A]	Villa (2010)[B]	268	20	359.2	93611	93	124	**0.75**	**515**	**425**

A 750 µM SPHERICAL RADIUS (APPROXIMATING A 500 µM CYLINDER RADIUS) WAS USED AS THE EFFECTIVE DIMENSION OF THE DIFFUSION DOMAIN
[A] ESTIMATE OF D_0 FOR 5 KBAR [B] TWO POSSIBLE SETS OF E_A AND D_0 FROM A RE-EVALUATION OF GILETTI'S (1974) EXPERIMENTS
* 0.01-10°C/MA COOLING RATE RANGE (VALUE IS A 9 DATA POINT AVERAGE) ** (PHL-A) – (MS-B)

3.8 Figures

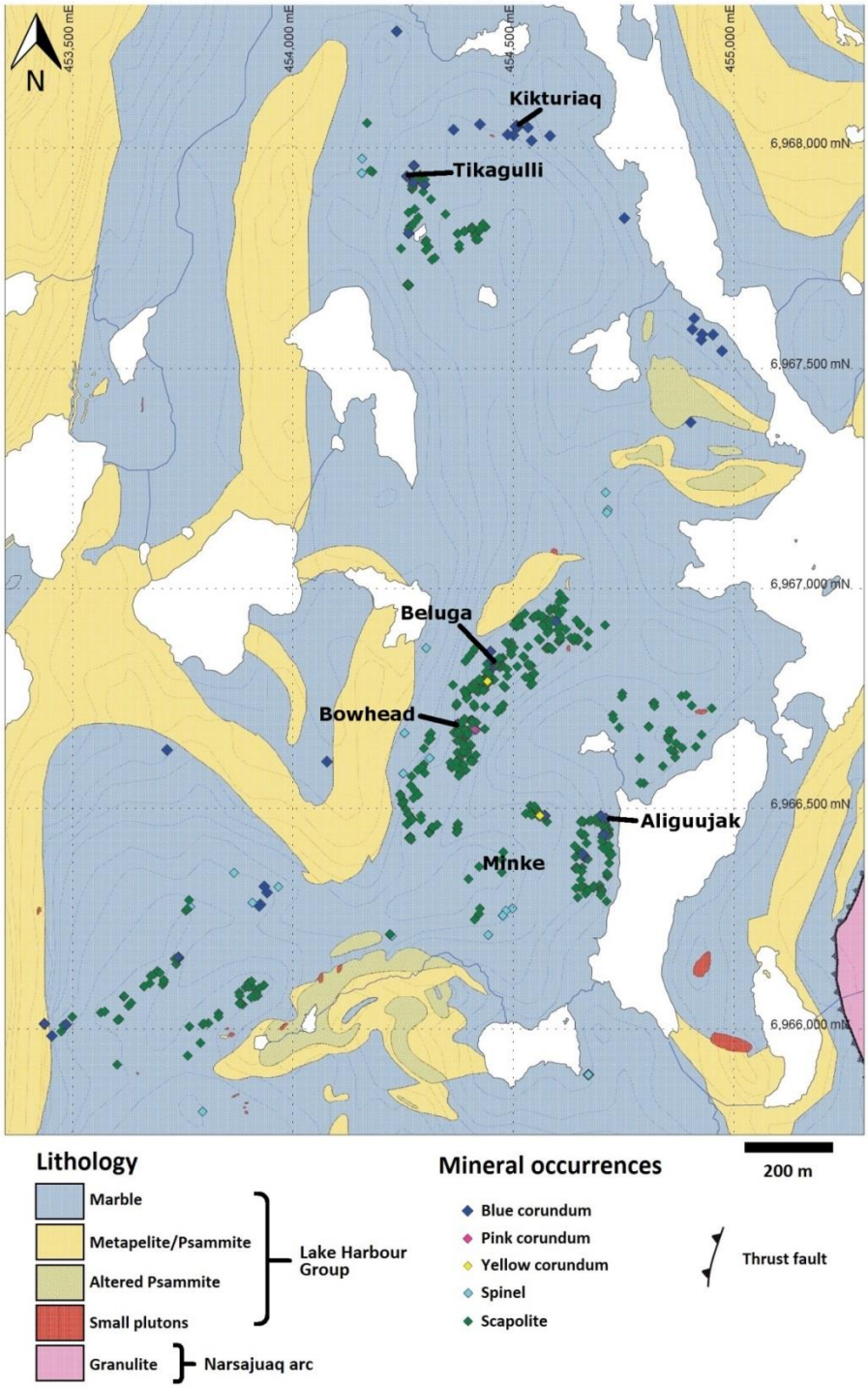

Figure 3.1: Bedrock geology map of the True North Gems property with markers for scapolite, spinel, and corundum occurrences found during the 2006 mapping season. The most important mineralized areas are named. Small plutons consist of granite or ultramafic plugs. UTM zone 19 V (NAD83). Map courtesy of True North Gems Inc.

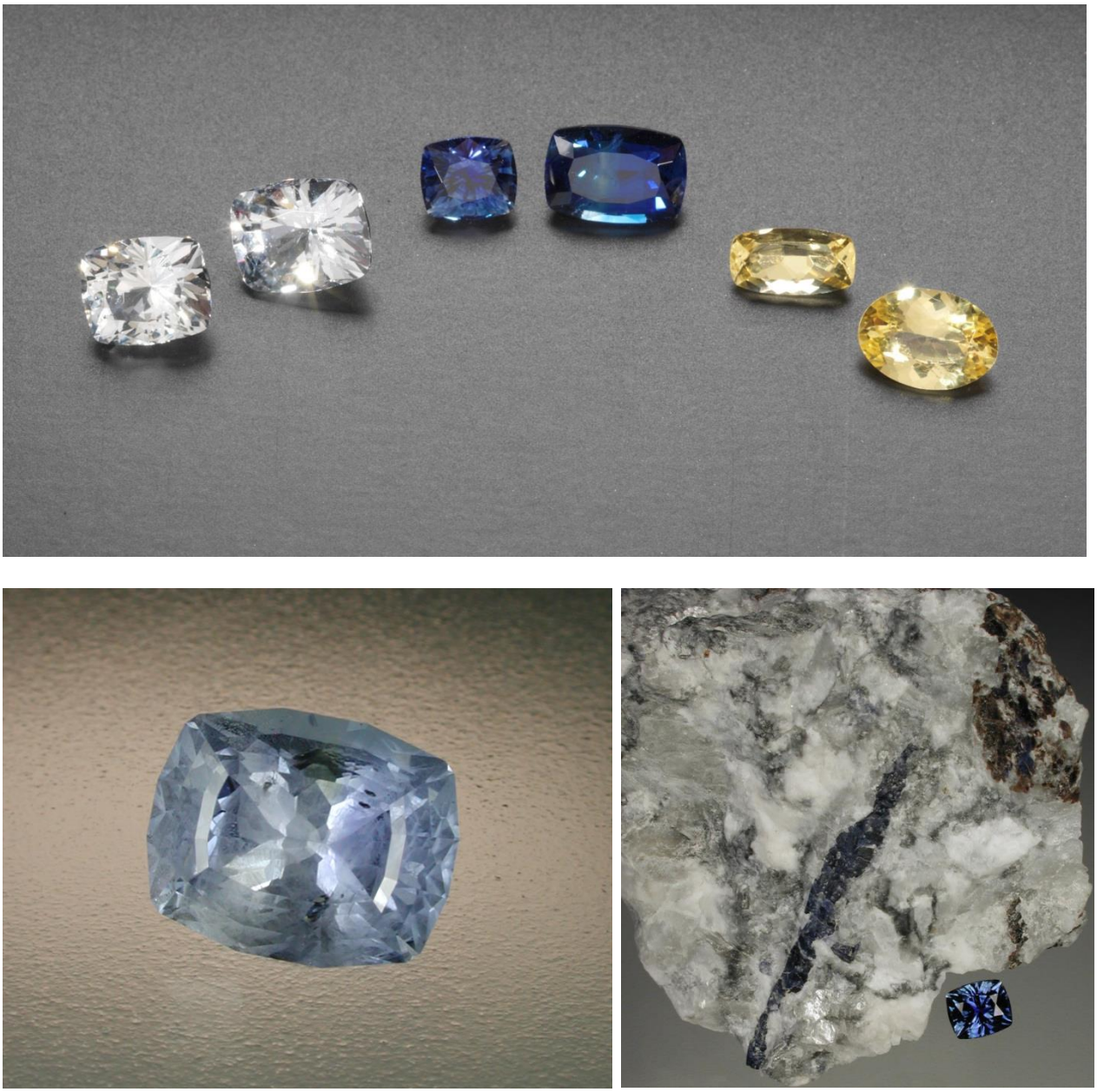

Figure 3.2: (A: top) Corundum (sapphire) gemstones from the Kimmirut occurrences. Left: colorless sapphire, Aqpik occurrence, 2.50 and 2.59 ct. Top centre: deep blue, extra fine sapphire, 1.17 ct, from the Beluga occurrence, and a heat-treated, rich blue 2.43 ct sapphire from Aqpik. Right: yellow sapphire, Beluga South occurrence, 1.09 ct and 1.47 ct. Photograph courtesy of True North Gems Inc. (B: lower left) lightly included, light blue sapphire (7.81 ct) from the Aqpik occurrence. Photograph by Brad Wilson. (C: lower right) dark blue corundum crystal, 36 × 4 mm, in calc-silicate rock, and a 1.17 ct sapphire gemstone from the Beluga occurrence. Photograph by Brad Wilson, courtesy of True North Gems Inc.

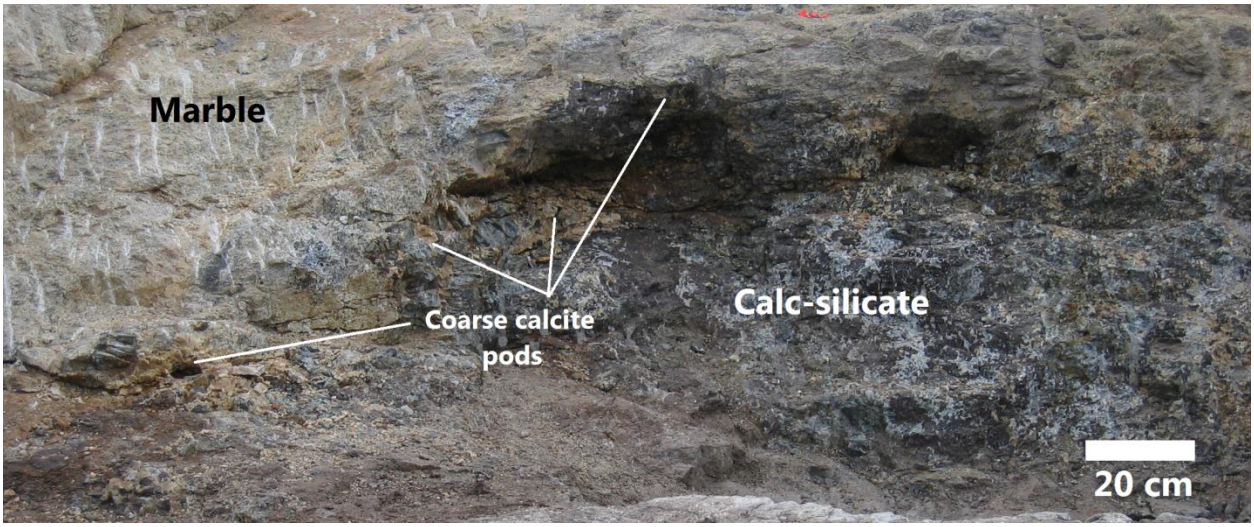

Figure 3.3: Contact between marble and sapphire-bearing calc-silicate rock at the Beluga occurrence. Note the variation in the distribution of light-colored and dark mineral assemblages within the calc-silicate pod, and the undulate nature of the contact with coarsely crystalline marble. The calc-silicate pod is surrounded by very coarse-grained marble, and no foliation is apparent in the outcrop.

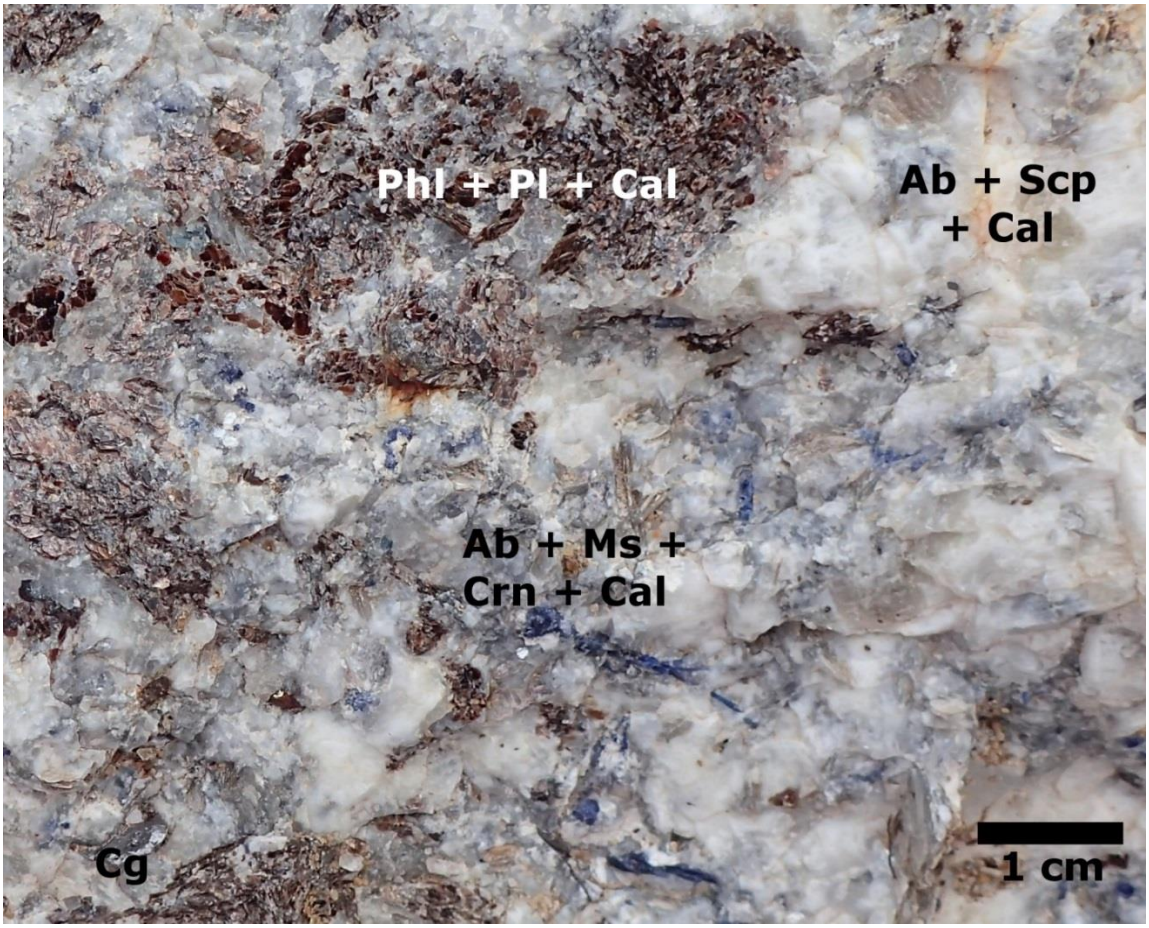

Figure 3.4: Corundum-bearing calc-silicate rock *in situ* at the Beluga pit. Phlogopite-oligoclase (Phl + Pl) intergrowths occur near partly albitized scapolite (Ab + Scp) and albite, muscovite, and blue corundum (Ab + Ms + Crn). The corundum- and phlogopite-bearing assemblages contain calcite. Minor graphite (Cg) is present.

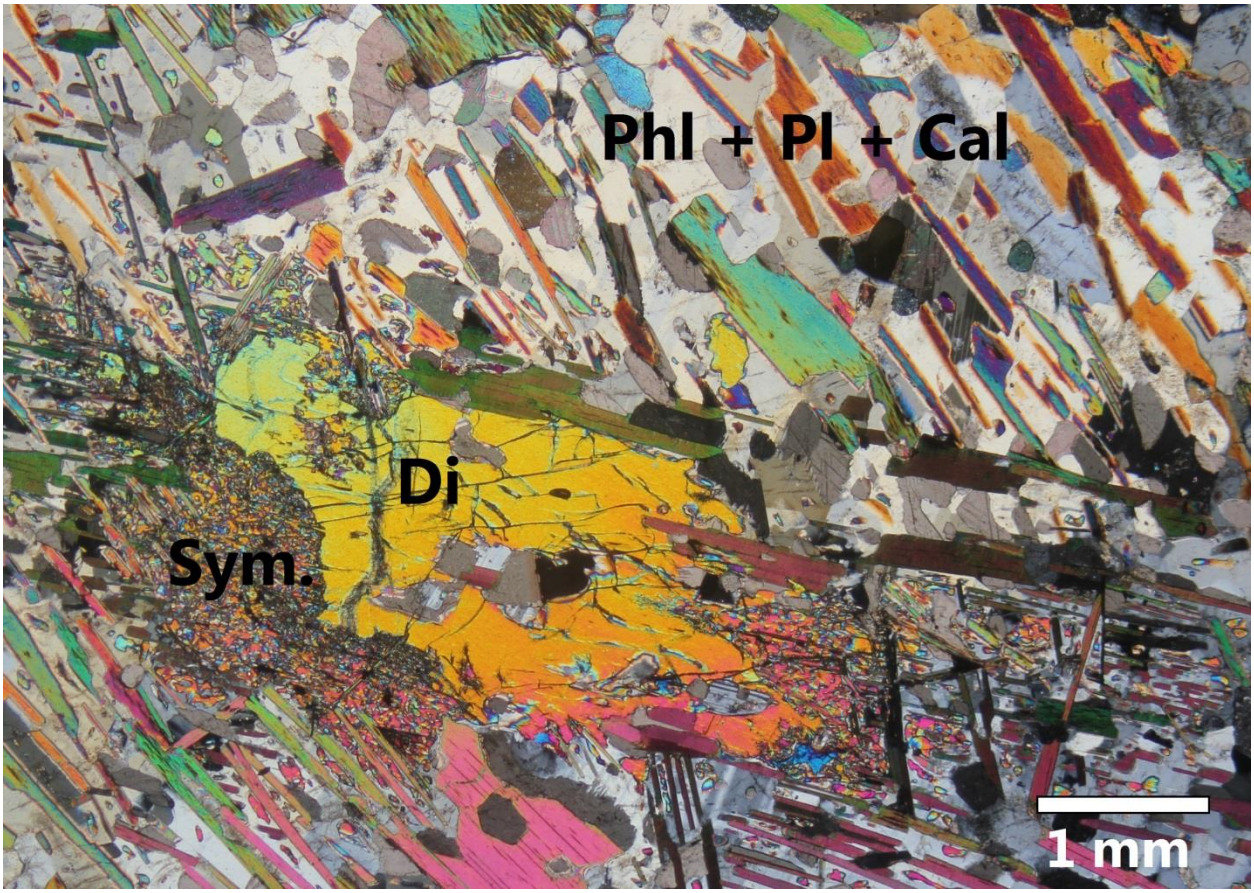

Figure 3.5: Diopside (Di) surrounded by phlogopite-oligoclase symplectite and coarser oriented intergrowths of phlogopite (Phl), oligoclase (Pl), and calcite (Cal). Beluga occurrence. Cross-polarized light.

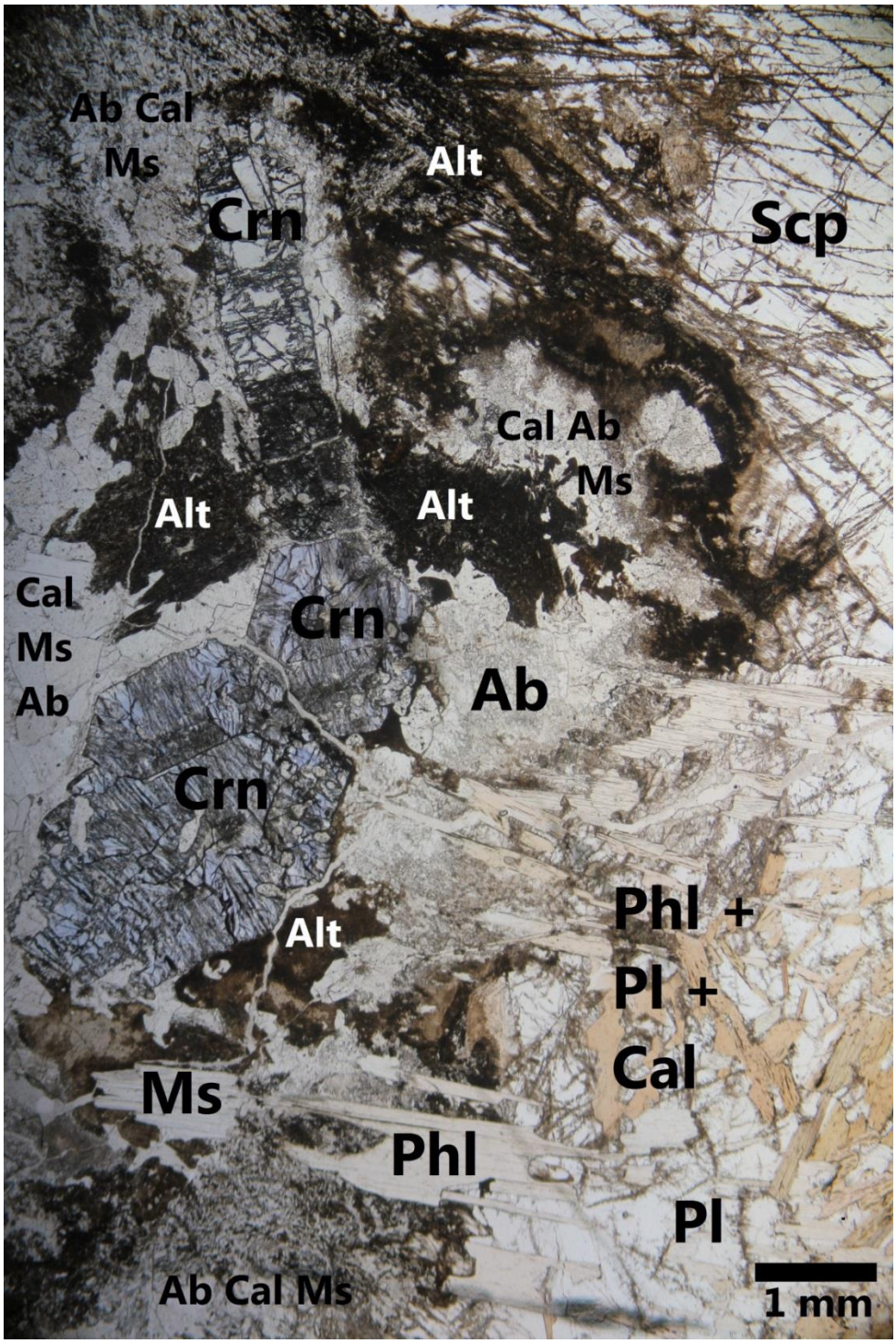

Figure 3.6: Contact between coarse-grained scapolite (Scp), phlogopite-oligoclase-calcite (Phl-Pl-Cal), and the corundum-bearing zone. The latter zone contains idiomorphic corundum (Crn) with albite (Ab), calcite (Cal), and muscovite (Ms) of variable grain size. Dark zones of fine-grained alteration (Alt) consist of mixtures of the following minerals in variable abundance: albite, calcite, muscovite, analcime, prehnite, and thomsonite. Beluga occurrence. Plane polarized light.

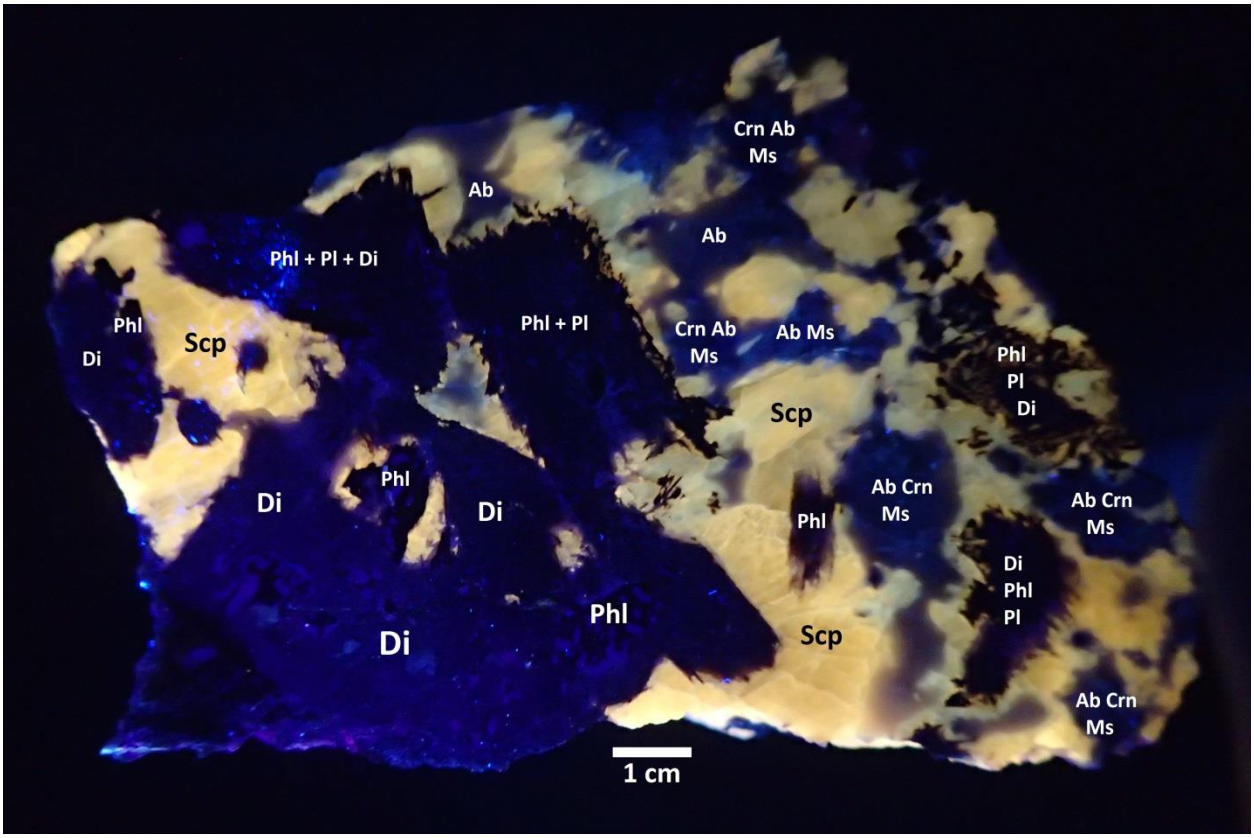

Figure 3.7: Beluga calc-silicate rock under shortwave ultraviolet light showing the fluorescent scapolite (yellow; Scp), variable diopside-phlogopite-oligoclase assemblages (Di-Phl-Pl), albitized scapolite (Ab), and albite-corundum-muscovite assemblages (Ab-Crn-Ms). Minor calcite is present. Purple coloration is an artefact of the UV light source.

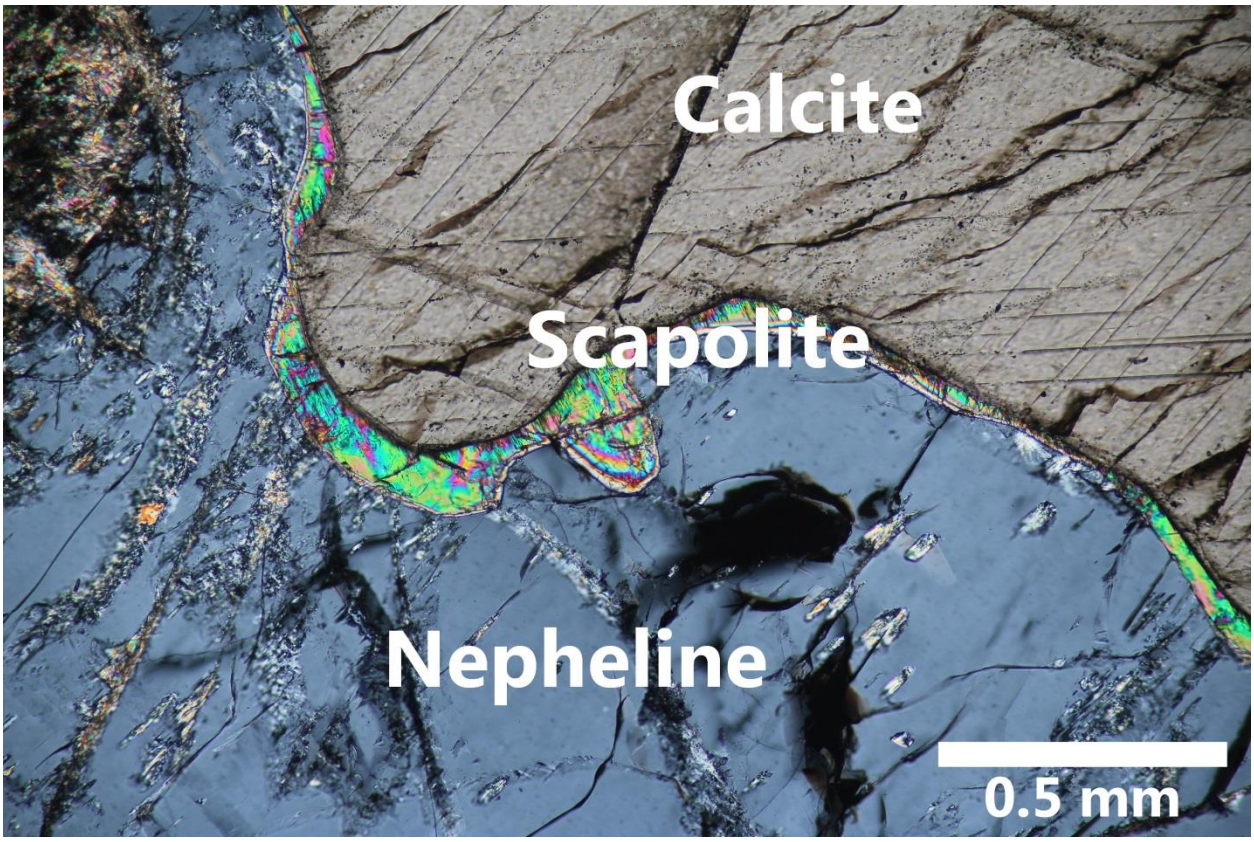

Figure 3.8: Thin scapolite rim between a grain of nepheline and calcite, which suggests that scapolite formed from the reaction of calcite and nepheline and post-dates the nepheline-bearing mineral assemblage. Bowhead occurrence. Cross-polarized light.

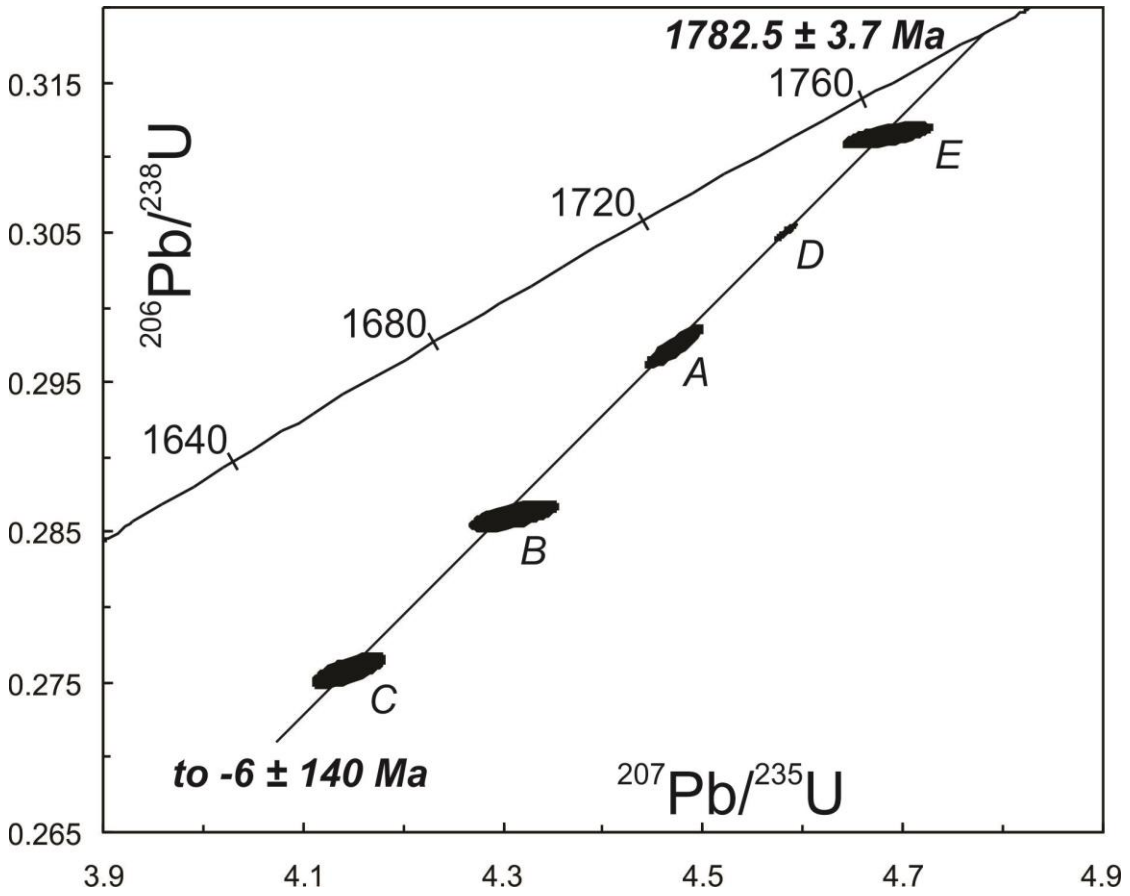

Figure 3.9: U-Pb concordia diagram for zircon recovered from the phlogopite-rich assemblage at the Beluga occurrence calculated using Model 1 of Ludwig (2003). Error ellipses represent 2σ. See Table 10 and text for U-Pb data and sample descriptions.

A (Phlogopite)

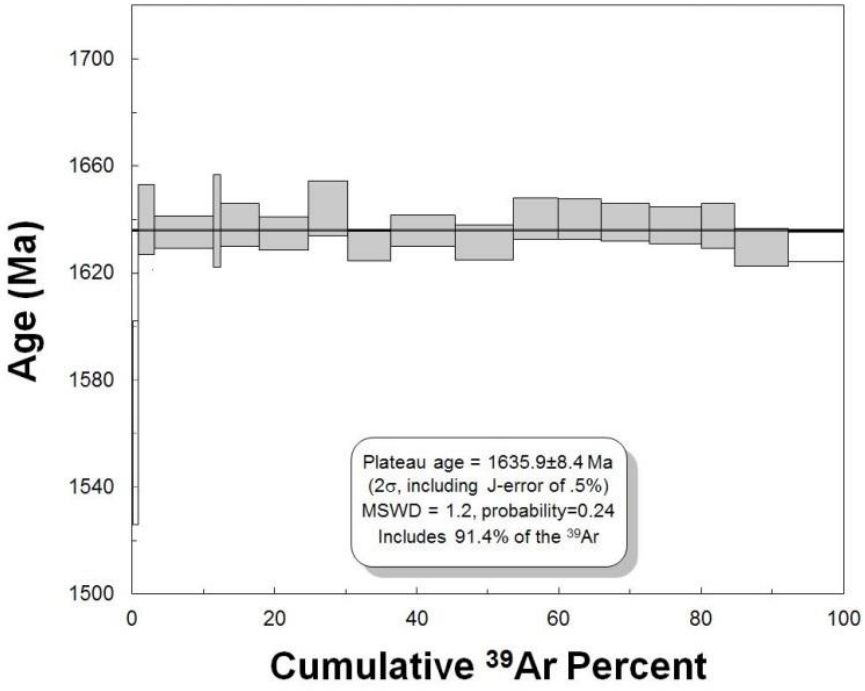

B (Phlogopite)

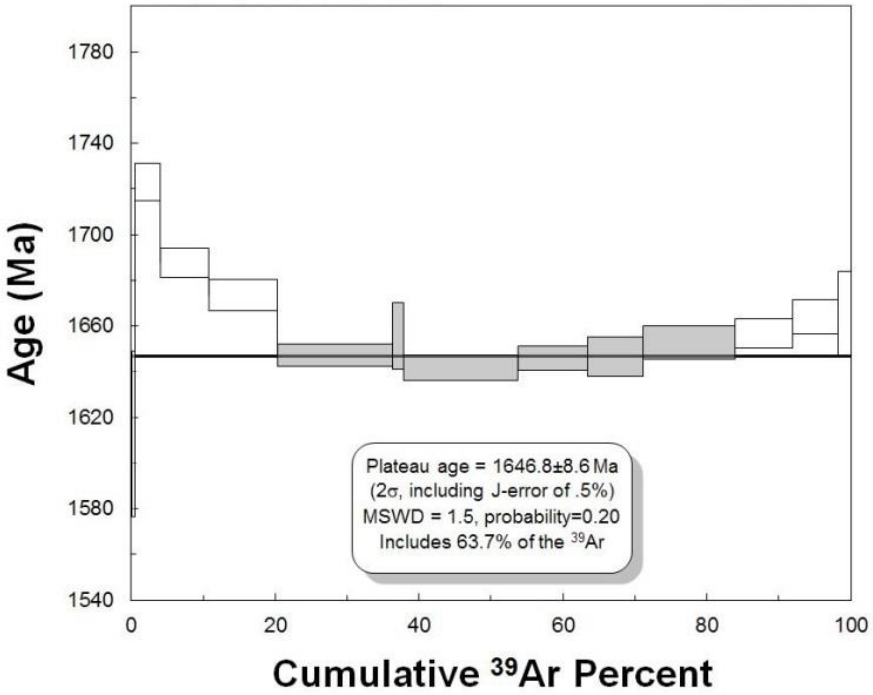

Figure 3.10 A-B: $^{40}Ar/^{39}Ar$ age spectra of phlogopite from the Beluga occurrence. Box heights are 2σ. Plateau steps are filled and rejected steps are open. After Dzikowski (2013).

C (Muscovite)

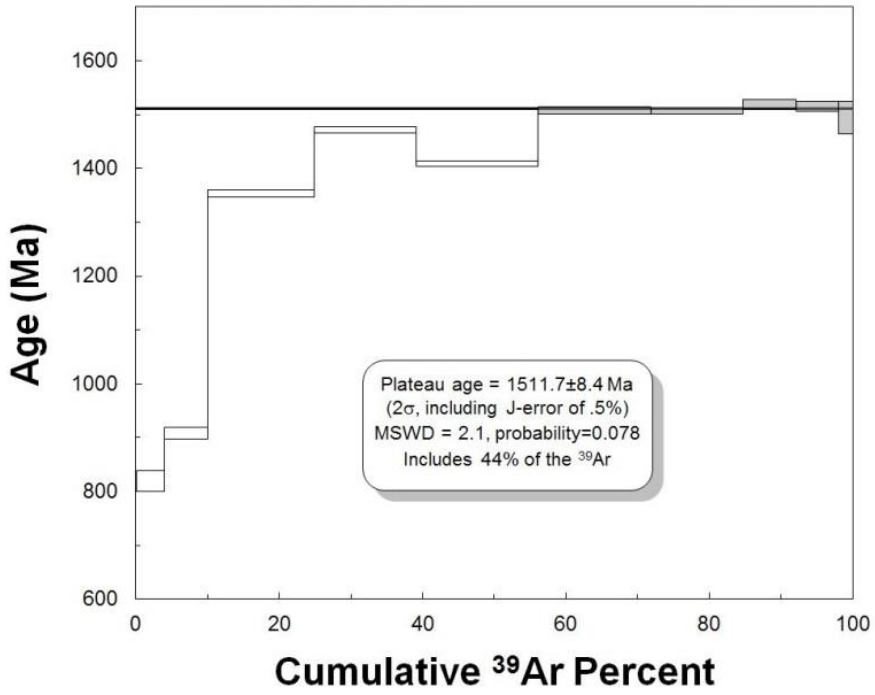

D (Muscovite)

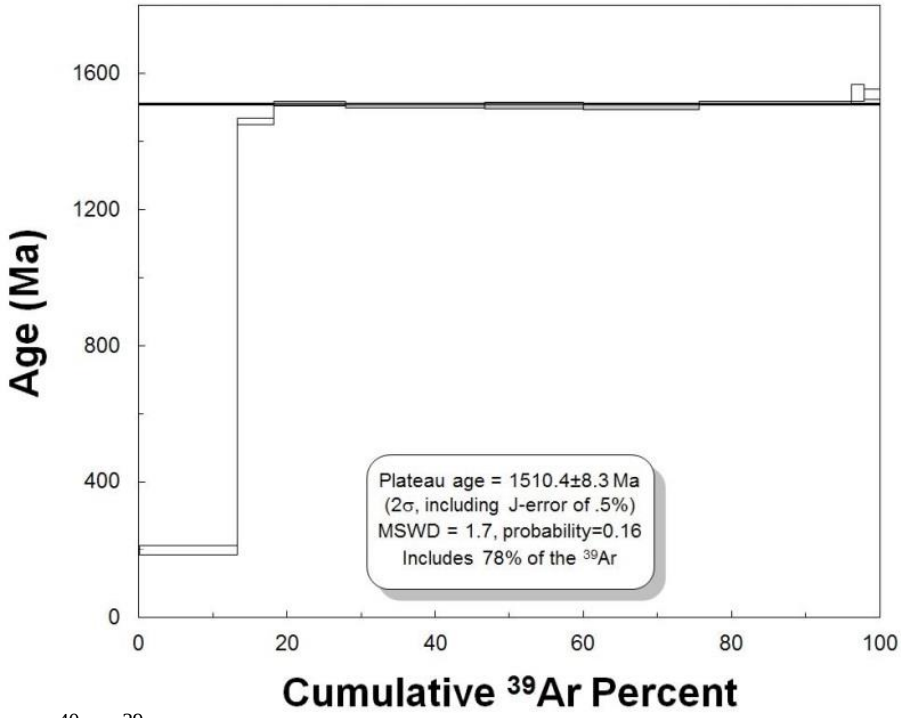

Figure 3.10 C-D: $^{40}Ar/^{39}Ar$ age spectra of muscovite (Ms; C, D) from the Beluga occurrence. Box heights are 2σ. Plateau steps are filled and rejected steps are open. After Dzikowski (2013).

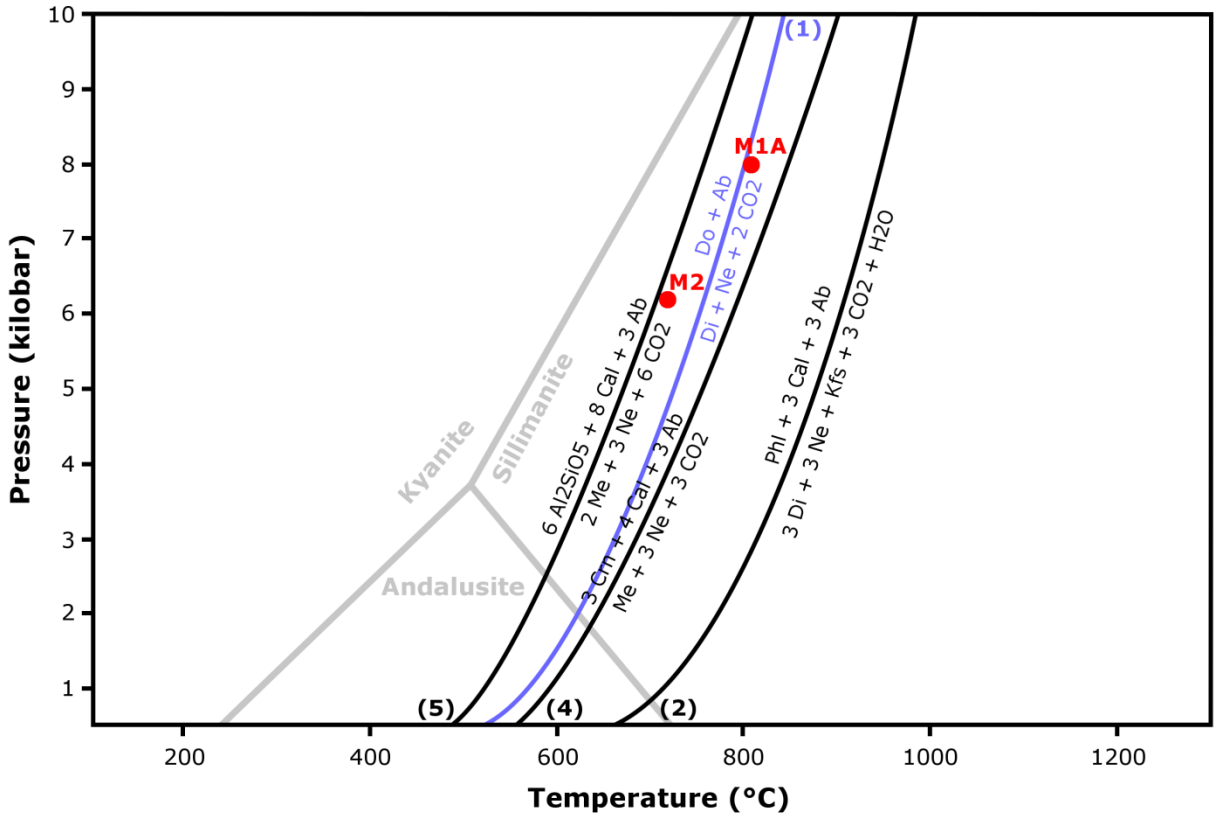

Figure 3.11A: Mineral reactions modeled in TWQ v1 (Berman 1988, 1991). Based on the paragenetic sequence of Bowhead and Beluga calc-silicate rock (present study) and metasediments on Aliguq Island (Butler 2007), the diopside (Di), nepheline (Ne), and K-feldspar (Kfs) assemblage is suggested to be possible at M_{1A} metamorphic conditions but low X_{CO2} (see Fig. 3.11B). Alternatively, the formation of nepheline and diopside from albite (Ab) and dolomite (Dol) is consistent with regional *P-T* conditions but differs significantly from the paragenetic sequence at Beluga and Bowhead. The peak assemblage is partly replaced by phlogopite (Phl), calcite (Cal), and albite at conditions slightly below that of M_2. The meionite (Me) – nepheline break-down reactions are probably overestimates since the measured scapolite compositions contain significant Na. The latter minerals break down to form corundum (Crn), calcite, and albite at higher temperature than a similar reaction forming Al-silicate, calcite, and albite. Regional *P-T* conditions after St-Onge *et al.* (2007). See text for a detailed discussion of mineral reactions and paragenetic sequence in the context of regional metamorphism.

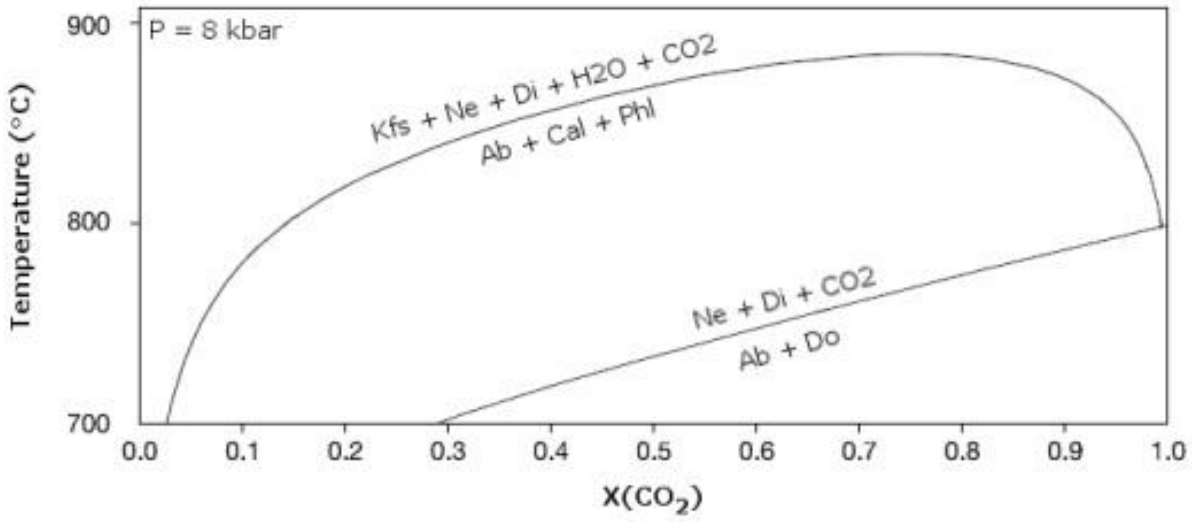

Figure 3.11B: Mineral reactions modeled in TWQ (Berman 1988, 1991) modified after Butler (2007) at peak metamorphic pressure (8 kbar, St-Onge *et al.* 2007). The nepheline-bearing assemblage occurs at low X_{CO2} at the peak metamorphic temperature (810°C, St-Onge *et al.* 2007).

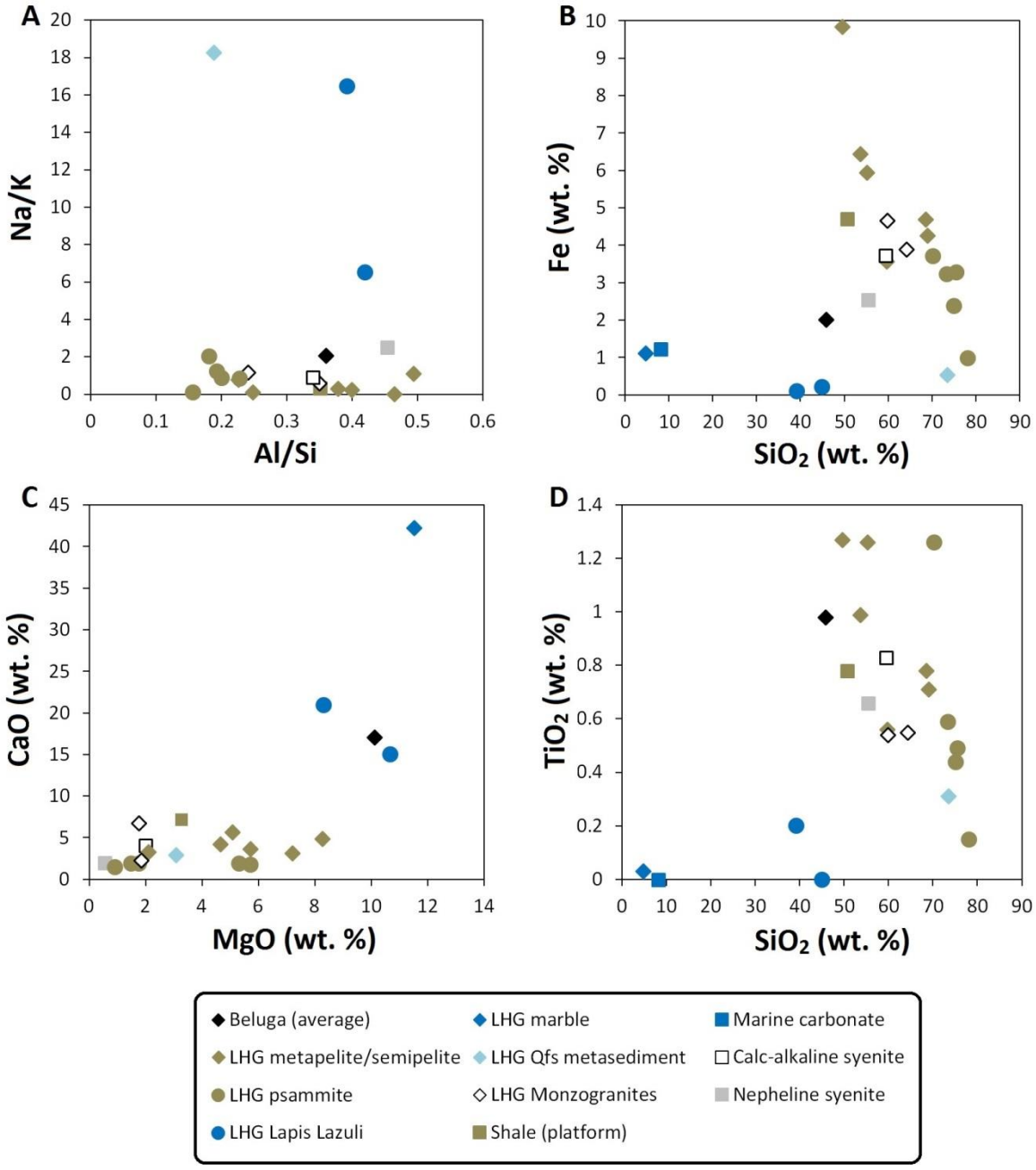

Figure 3.12: Comparison of Beluga calc-silicate rock major element composition with selected representative Lake Harbour Group metasediments (Thériault *et al.* 2001, Butler 2007), monzogranites (Butler 2007), lazurite/haüyne-bearing metaevaporites (Hogarth & Griffin 1978), averages for platform sediments (Carmichael 1989), and averages for syenite (Nockolds 1954).

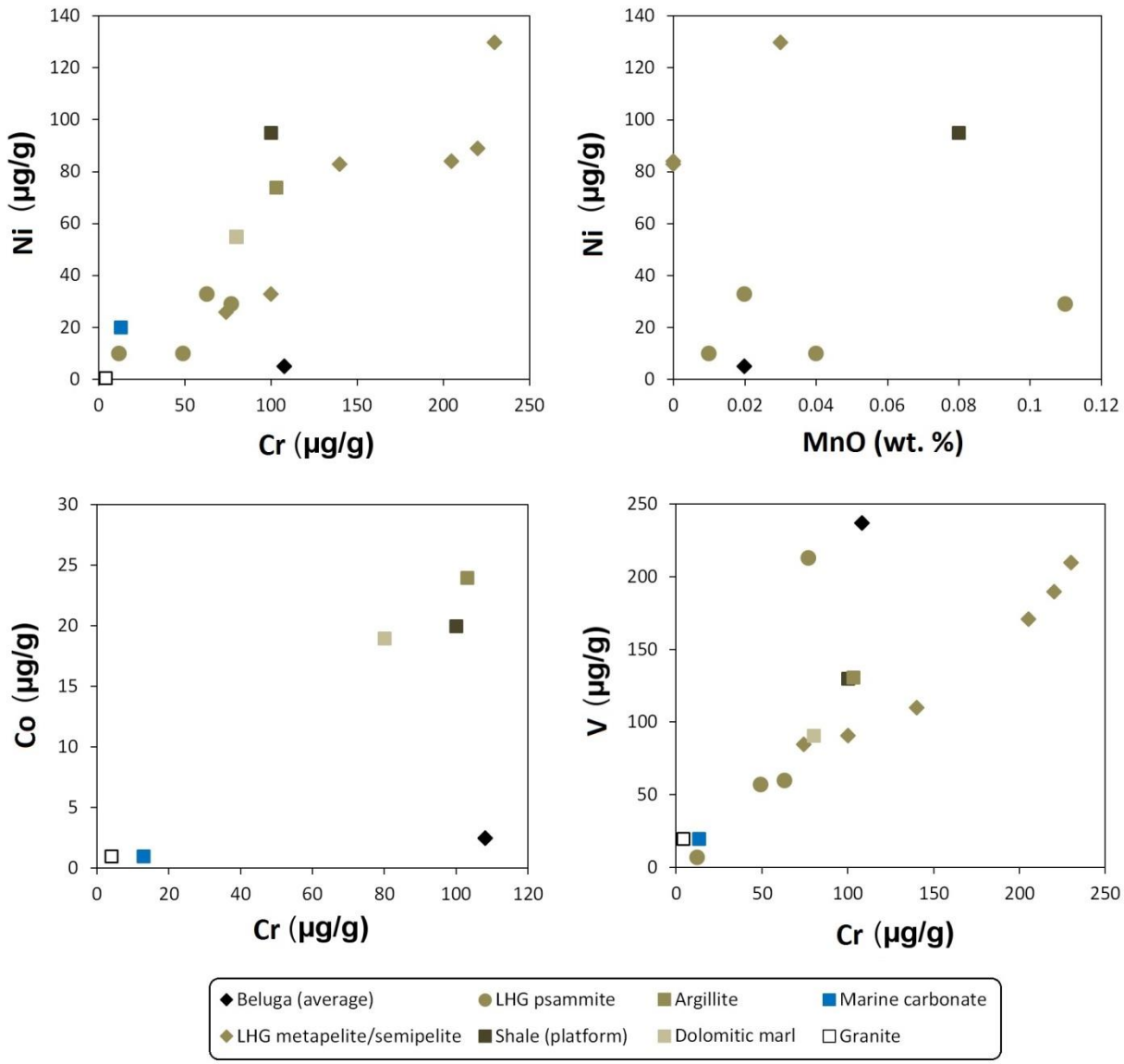

Figure 3.13: Abundance of selected trace metals in Beluga calc-silicate rock compared to representative LHG metasediments (Thériault *et al.* 2001), sediments (Carmichael 1989, Moine *et al.* 1981 and references therein), and average granite (Carmichael 1989).

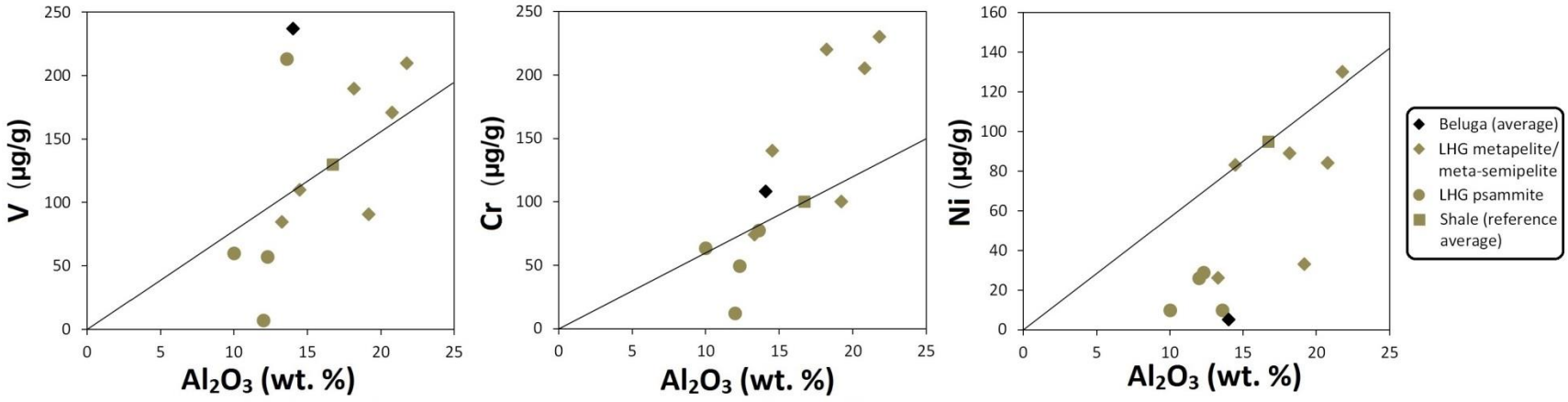

Figure 3.14: Abundance of V, Cr, and Ni relative to Al_2O_3. Line represents expected concentration of metals relative to alumina by varying amount of allochthonous detritus based on metal-Al_2O_3 ratios from a shale average (Carmichael 1989). Selected examples of metapelite and psammite from the Lake Harbour Group (Thériault *et al.* 2001) are included for comparison.

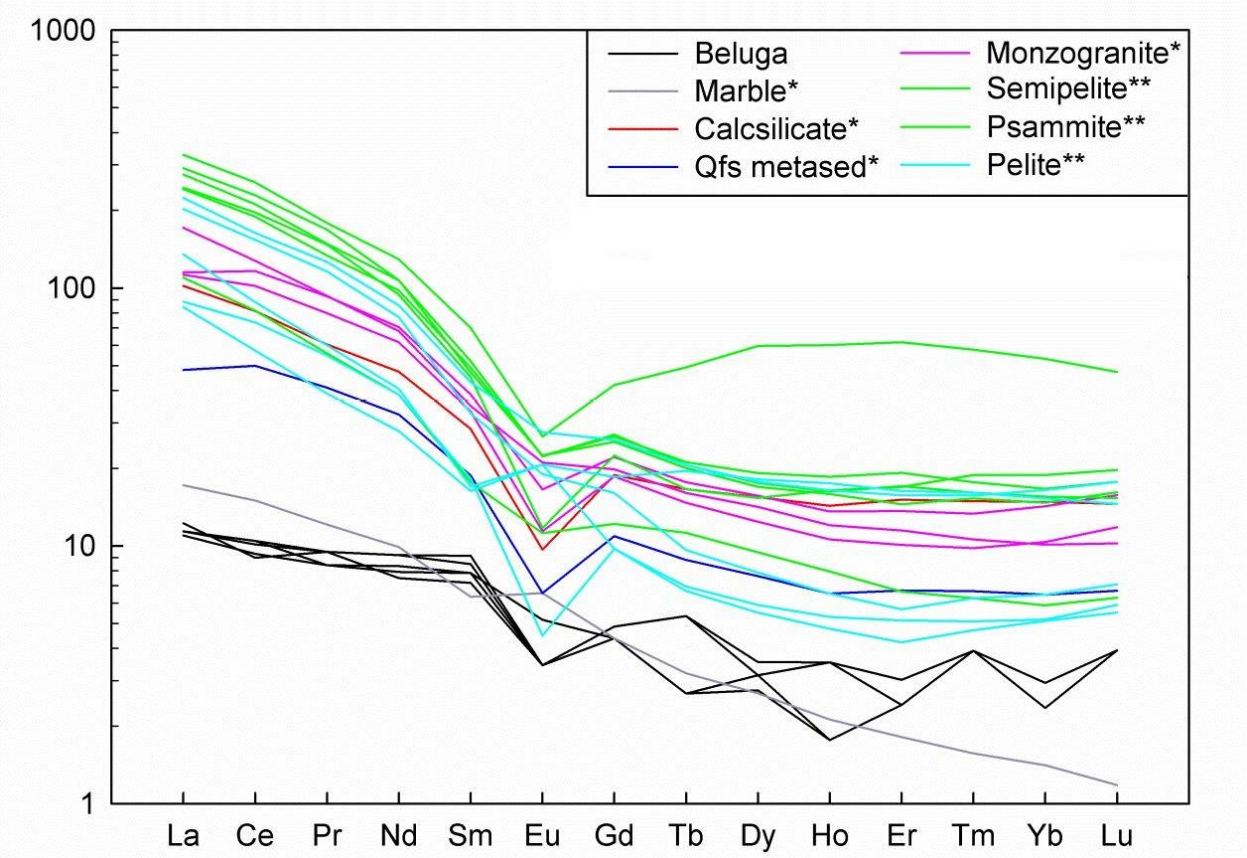

Figure 3.15: Chondrite-normalized (values of Taylor & McLennan 1985) REE trace element profile of Beluga calc-silicate rock compared to rocks from the Lake Harbour Group (*Butler 2007, **Thériault *et al.* 2001). After Dzikowski (2013).

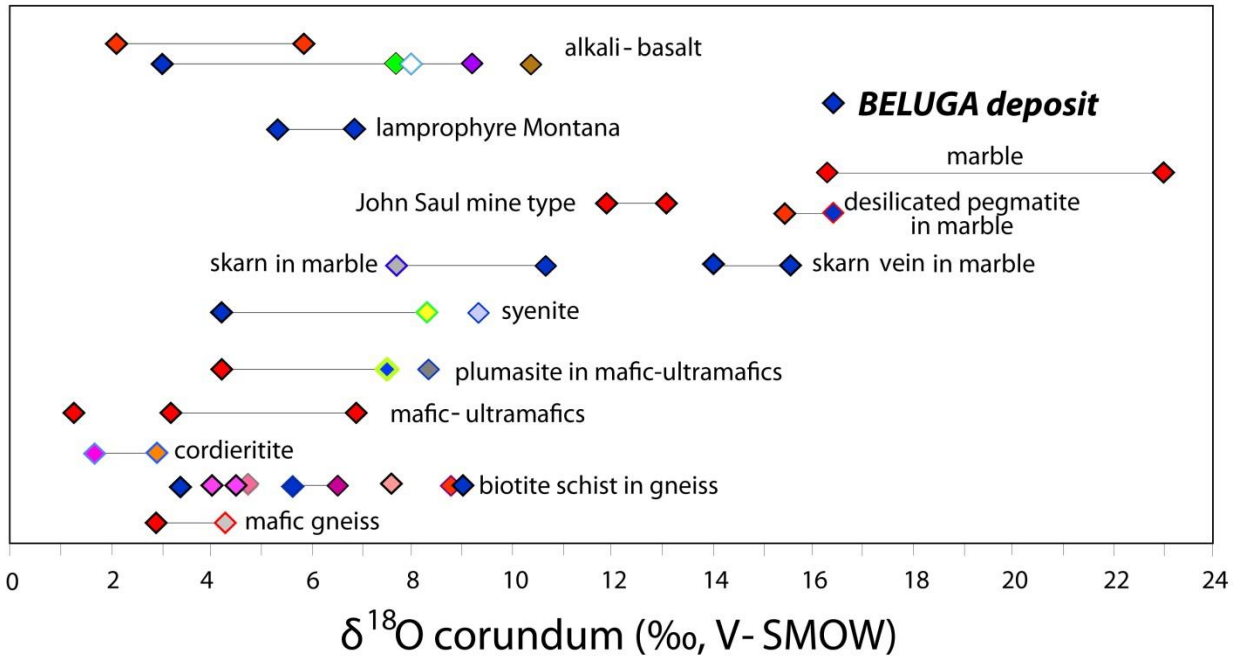

Figure 3.16: Oxygen isotope composition of Beluga corundum compared to values from different types of gem corundum deposits (modified after Giuliani *et al.* 2014). Color in diamonds represent the colour of gem-quality corundum from different deposits (red = ruby, others = colored sapphire). Diagram courtesy of G. Giuliani.

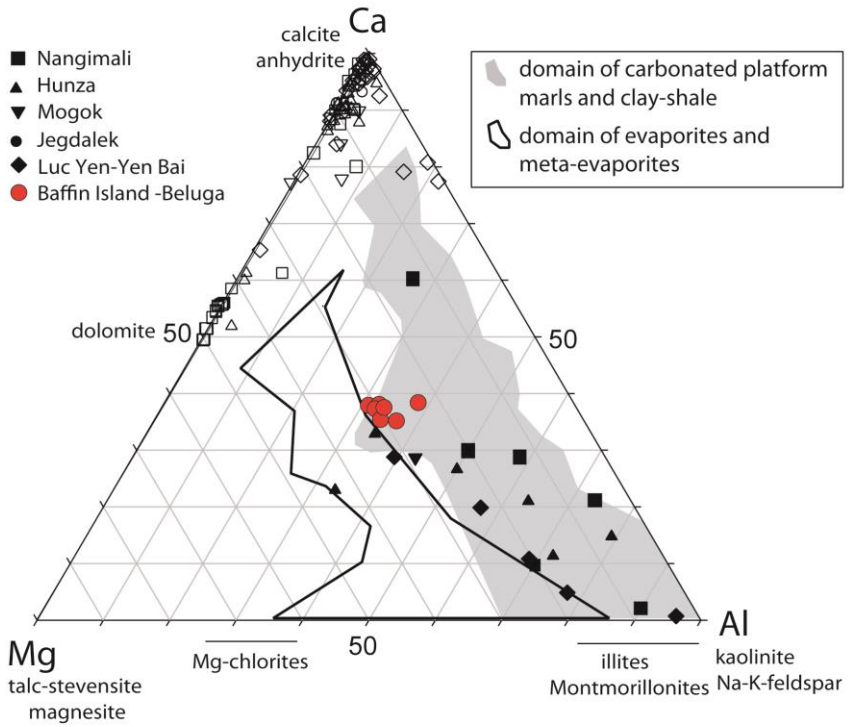

Figure 3.17: Al-Mg-Ca diagram showing the distribution of the calc-silicate rock from the Beluga corundum deposit relative to domains for platform marls and clay-shale, evaporites, and meta-evaporites (modified after Moine *et al.* 1981) and in comparison to marbles (open symbols) and intercalated schists and gneisses (full symbols) from ruby-bearing marbles in central and south-east Asia (after Garnier *et al.* 2008). Diagram courtesy of G. Giuliani.

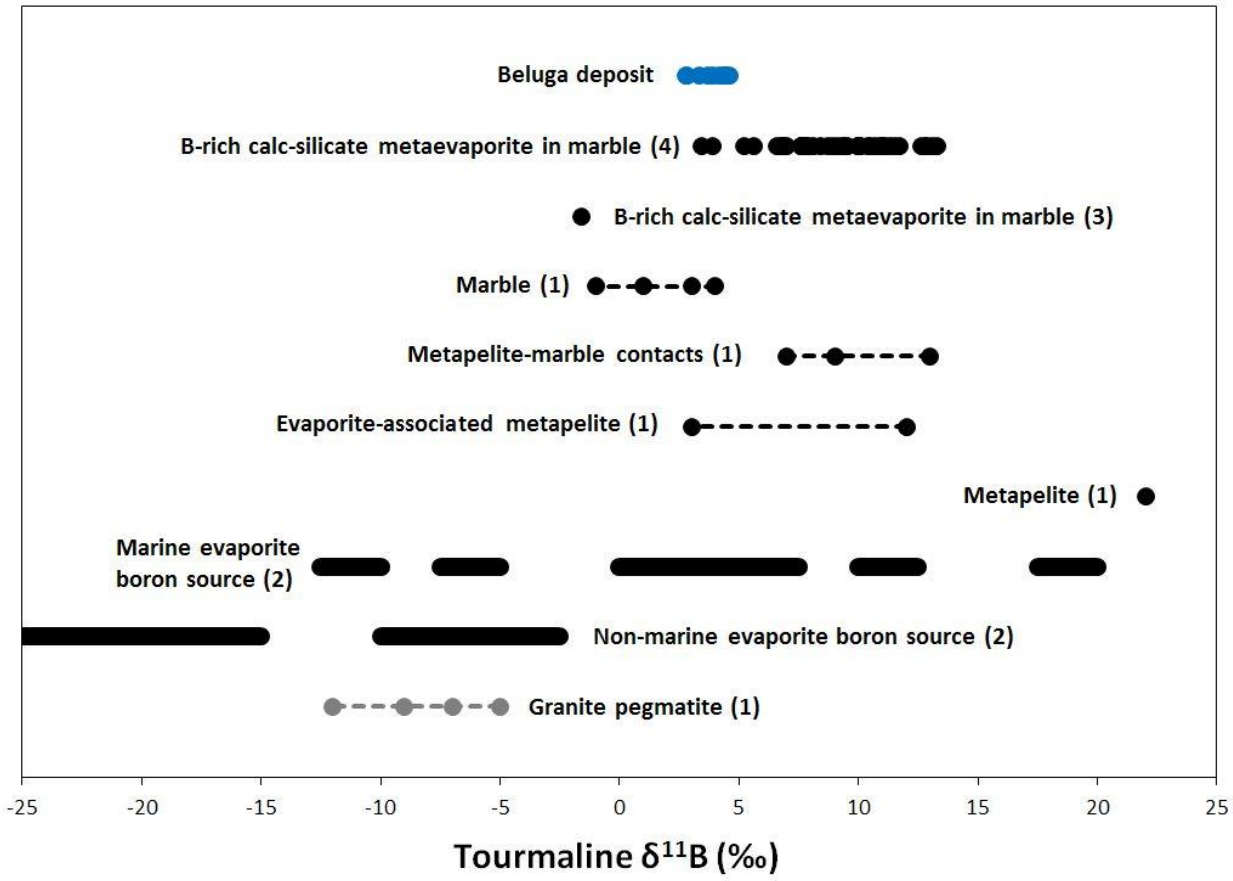

Figure 18: Boron isotope composition of Beluga oxy-dravite compared to tourmaline from different environments. Sources of data: (1) Swihart & Moore 1989; (2) Palmer 1991; (3) serendibite-rich calc-silicate rock interpreted to be metamorphosed illite layer deposited in a hypersaline environment (Grew *et al.* 1991); (4) serendibite-rich calc-silicate rock similar to the latter, but with both prograde and retrograde tourmaline (Belley *et al.* 2014).

Chapter 4. Metacarbonate-hosted spinel on Baffin Island: Insights into the origin of gem spinel and cobalt-blue spinel

4.1 Results summary

Fourteen spinel occurrences were sampled in the Lake Harbour Group (LHG), southern Baffin Island, Nunavut, Canada, and studied using a combination of petrography, whole rock geochemistry, microprobe analysis, and where possible, geochronology. Spinel at most occurrences is blue to violet in colour, and generally not of gem quality. Two spinel occurrences near Kimmirut contain facet- and cabochon-gem quality vivid blue, cobalt-enriched (0.03-0.07 wt.% CoO) spinel. The spinel mostly occurs in metasedimentary (*sensu stricto*) deposits, with the exception of two metasomatic occurrences in Markham Bay. All spinels occur in marble and calc-silicate/silicate-rich metacarbonate rocks. Minerals occurring with spinel as part of a stable assemblage include calcite, dolomite, phlogopite, pargasite, diopside, humite, forsterite, scapolite, anorthite, graphite, and pyrrhotite. Spinel formed under peak granulite facies metamorphic conditions. The spinel at two localities is partly replaced by retrograde corundum.

Spinel-bearing metacarbonates are interpreted to have the following protoliths: (1) impure dolomite-bearing and dolomitic limestone; (2) dolomitic marl; and (3) evaporitic magnesitic marl. Spinel genesis in Mg-bearing metacarbonates is favored by: (1) the low abundance of silica relative to alumina, the primary control on whether spinel forms in most calc-silicate rocks; (2) low potassium activity limiting the formation of phlogopite and thus leaving Al available for spinel formation; (3) low X_{CO2} in marbles; and (4) insufficient quantities of Mg or dolomite reactant in diopsidite limiting Al incorporation into phlogopite to form spinel.

The spatial distribution of Co enrichment at the cobalt-blue spinel occurrences is indicative of highly localized enrichment, with possibly only small scale (≤ 1 m) diffusion during

metamorphism. Cobalt and Ni are interpreted to have been enriched in the original sediment, or during diagenesis or low-grade metamorphism. Concentrations of Co (especially) and Ni are anomalously high (up to 29 µg/g, conservatively twice the expected cobalt concentration in a comparable metasediment), while concentrations of Fe, Mn, V, Cr, and Cu are much lower than expected; a chemical signature that speculatively could be caused by diagenetic processes prior to metamorphism.

Pyrrhotite strongly partitions Fe relative to spinel, therefore an abundance of sulfide is expected to improve the attractiveness (therefore commercial value) of spinel by decreasing the amount of Fe incorporated into spinel (thus preventing overly dark colors).

Marbles containing abundant metamorphosed dolomitic marl (magnesian calc-silicate) layers offer the best potential for gemstone discoveries in southern Baffin Island. Small, sometimes localized variations in whole rock Al/Si and K/Al, or fluid X_{CO2} could result in the occurrence of spinel. Other significant gemstone occurrences on Baffin Island (sapphire and lapis lazuli) are hosted in relatively similar rock types.

4.2 Chapter introduction

Interest in spinel gemstones has increased significantly in the early 21st century (Pardieu *et al.* 2008); spinel with an intense red color (chromium chromophore) and vibrant cobalt-blue color (cobalt chromophore) are the most valuable. The enrichment of cobalt in concentrations sufficient to turn spinel bright blue has yet to be adequately explained. In the most detailed petrologic study on blue gem spinel to date, Chauviré *et al.* (2015) suggested that Co and Ni were enriched in cobalt-blue spinel from F- and Cl-bearing metamorphic fluids (partly derived from evaporites) sourcing these metals from evaporite or amphibolite. The enrichment of Cr in metacarbonates is better understood; research on ruby (Cr-bearing corundum) deposit models

suggest that the Cr enrichment is a result of Cr-rich sediment deposited coevally with carbonates and the concentration of Cr in organic matter (Garnier *et al.* 2008). At Revelstoke, British Columbia, Cr was enriched in gneiss layers that reacted with marble to form corundum (Dzikowski *et al.* 2014).

Very few areas in the world are producing gem spinel, and much of this spinel is recovered from eluvial or alluvial deposits. Perhaps because of this, the geology of spinel has yet to receive attention from geoscientists – in significant contrast to gem corundum geology (*e.g.*, Giuliani *et al.* 2014). Moreover, the potential for gaining new insight into gem spinel genesis from small *in situ* occurrences that are not being mined for gem material (giving a much larger sample size) has been overlooked. This research will produce the first general gem spinel deposit model, based on 14 spinel occurrences in the Lake Harbour Group, Baffin Island, Nunavut, Canada (Table 4.1), containing violet, blue, and black spinel in addition to two cobalt-blue spinel occurrences and comparisons to similar, spinel-barren rocks.

4.3 Results

4.3.1 Petrography

4.3.1.1 Markham Bay

A. Spinel Island

This spinel occurrence is located on "Spinel Island" (Fig. 4.1; as named in this study, although it has no official name) just north of MacDonald Island, by the water in a diopsidite (calc-silicate) band at the contact between syenogranite pegmatite and dolomite-and-phlogopite-bearing calcite marble on the eastern tip of the island (N 63.69753° W 72.60063°; Fig. 4.2). A 55 meter portion of the calc-silicate band (1.5-2.5 m thick, strikes 089°, dip 80°) on the SE tip of the island contains spinel. The band has been truncated by erosion to the east, and re-appears on the

easternmost point of the island, where the diopsidite rarely contains small (< 1 cm) black spinel crystals. At the spinel occurrence, the calc-silicate band extends 30 meters to the west, where at its extremity, it occurs between lineated and foliated granitoid metaplutonic rocks (similar to that of Butler 2007 at the nearby Aliguq Island). The diopsidite in this area is medium-grained and devoid of spinel. South to north "lithosection" descriptions of the lithologies are presented in Tables 4.2A and B. At a point 40 meters south of the diopsidite band, only visible at low tide, coarse-grained monzogranite occurs south of the marble, and is surrounded by a metasomatic zone of diopsidite with large (3-20 cm) light brown phlogopite crystals and yellowish calcite. The monzogranite, which is different in composition to the pegmatite (more albite, presence of clinopyroxene and ilmenite, lack of titanite and rutile; sample 1A-MG), is coarse-grained, composed principally of albite, K-feldspar, quartz with subordinate clinopyroxene (intermediate between diopside and hedenbergite), ilmenite, trace apatite and zircon. Zircon, in addition to rare allanite and monazite were observed by use of a SEM and are generally < 20 μm in largest dimension. Marble west of the monzogranite contains small pods of white diopsidite and green talc/serpentine mixture.

Spinel at this locality occurs as dark blue to black euhedral crystals up to 9 cm in size. The spinel is too dark to have value as a gemstone, but the locality has produced museum-quality mineral samples. Spinel crystals typically have equal development of octahedral and dodecahedral faces, and small trapezohedral {3 1 1} faces.

The spinel-bearing diopsidite is heterogeneous in both grain size and mineral abundance (Fig. 4.3A). It is very coarse to pegmatitic in calcite-rich zones, and medium-grained to very coarse in calcite-poor, diopside-dominant zones. Some portions of the rock contain over 30 volume % phlogopite. Euhedral spinel crystals averaging 1-3 cm (up to 9 cm) are most common

in pods of white calcite (5-35 cm), and are associated with euhedral, greenish-grey diopside prisms (1-3 cm diameter, 2-8 cm long) and dark brown phlogopite (up to 4 cm; Fig. 4.3B). Pink end-member anorthite is locally common and has been observed in association with spinel. Rare, euhedral thorianite crystals up to 1 mm occur with spinel (personal communication, B. Wilson; identified with qualitative EDS).

The main assemblage was not subjected to significant retrograde alteration; only a negligible amount of pargasitization around the diopside and weak (15%) sericitization of the anorthite are apparent. The notable exception is a small zone (< 1 m) in the diopsidite band where the spinel is partly altered to corundum and other minerals, and where anhedral, greyish-green tremolite crystals up to 3 cm long are present. One microscopic inclusion of titanite was observed in the tremolite. Fractures in the partly altered spinel can contain corundum, sericite, probable chlorite, and/or gahnite. Very small amounts of zinc sulphide are associated with the corundum and chlorite alteration. The exterior of one spinel is penetrated by euhedral corundum crystals together with Mg-chlorite, which grades into a thin corona of margarite followed by zoisite/clinozoisite, and then tremolite (Fig. 4.3C; minerals identified by EDS).

B. Unnamed Island

Small quantities of black spinel occur in a metasomatic phlogopite- and calcite-bearing diopsidite on the edge of a small unnamed island located between “Spinel Island” and Aliguq Island (Fig. 4.1; N 63.70581° W 72.57546°). The majority (>95%) of the metasomatite is devoid of spinel, and instead contains abundant and large (1–15 cm, average 3 cm) euhedral, black amphibole crystals associated with dark brown phlogopite (≤10 cm) in calcite and diopside, especially bordering a network of calcite veins (Fig. 4.4). This calc-silicate unit occurs over an area of 10 by 3 meters on the edge of the island. Black, octahedral spinel crystals (1–30 mm)

with small dodecahedron faces occur in calcite just below the low tide mark. Microscopic chlorapatite (< 200 μm) was identified with semi-quantitative EDS.

4.3.1.2 Glencoe Island

Multiple spinel occurrences are present on the north side of Glencoe Island (Fig. 4.5) in marble and calc-silicate rocks following a band of steeply-dipping marble in gneiss (the marble strikes approximately 104° in the NW part, and 124° in the SE part of the island). The geology of Glencoe Island was briefly described by Grice *et al.* (1982). The dominant rock type is biotite-quartz-feldspar gneiss with or without almandine with a band of calcite marble, up to 20 m wide, extending almost the full length of the north side of the island. K-feldspar-quartz pegmatites up to 2 m wide cross-cut the gneiss roughly perpendicular to the foliation.

A. Main occurrence

Spinel occurs in calc-silicate pods in a 2-meter thick band of very coarse phlogopite-bearing serpentine marble (2A-M; N 63.08516° W 71.44985°). The serpentine occurs as pseudomorphs after what were presumably subhedral forsterite crystals, now entirely replaced. The serpentine marble contains trace graphite and, in one area, a very rich seam of graphite (10 × 80 cm) occurs with diopsidite. The band of marble is exposed on the side of a small embayment on the north side of the island and continues into the water (Fig. 4.6A). The contact between marble and siliceous host rocks strikes 110° and dips 68°. To the east end of the outcrop, the south contact of the marble is bound by psammite (2A-PS) and the north contact by dark green diopsidite (2A-DI). The psammite is principally composed of quartz, plagioclase (An_{80}), and orthopyroxene ($X_{Mg} \approx 0.75$) with subordinate pyrrhotite (< 2 vol. %) and graphite, and trace amounts of K-feldspar, titanite, and monazite. Parts of the psammite are very rich in quartz. Approximately 10-30 vol. % of the orthopyroxene is altered to a fine-grained hydrous Mg-

silicate. The dark green diopsidite is dominantly composed of diopside with subordinate phlogopite. It contains 1-2 vol. % pyrite, graphite, and trace concentrations of pyrrhotite and chalcopyrite.

Spinel was first noted from this locality by Grice *et al.* (1982), who reported finding crystals up to 5 cm across. A 0.39 carat violet gemstone was faceted from a spinel from this location (Wilson 2014). Violet (as in sample 2A-SPL-1 and 2A-SPL-2) to dark greyish-violet (as in 2A-SPL-3) spinel crystals occur in calc-silicate pods ranging in size from 10 to 30 cm in maximum dimension. The pods tend to be unequally proportioned and are randomly oriented. The calc-silicate pods are composed of different assemblages in randomly distributed zones (Fig. 4.6B), such as: diopside, phlogopite-diopside, calcite-diopside-phlogopite-spinel (± pyrrhotite), and less commonly, anorthite-diopside (± calcite). Anorthite occurs in some of the spinel-bearing pods but was not observed in direct contact with spinel. Trace graphite occurs in all zones. Calcite-poor zones are medium- to very coarse-grained, and contain varying quantities of greenish-grey diopside and brown phlogopite. Very coarse-grained anorthite-diopside is less common. The calc-silicate rocks contain trace amounts of zircon, apatite, and Ba-rich K-feldspar.

Spinel occurs only in and around calcite-rich zones, where grain sizes are generally between 4 and 25 mm. Spinel crystals are subhedral to euhedral, with equal development of octahedral and dodecahedral faces, but generally too fractured for gem cutting. Color ranges from pale violet to dark greyish-violet. Uncommon fractures in spinel are lined with chlorite and trace zinc sulphide.

B. Marble beach occurrence

Dark blue, euhedral spinel crystals up to 2 cm in maximum dimension occur in pods of silicate-bearing marble (< 25 cm) within a few blocks on marble over weathered marble outcrop

near the bay on the NE side of the island (N 63.07965° W 71.44720°). The spinels are transparent, but fractured and too dark to produce large gemstones. Their morphology resembles that of spinel at the main occurrence. In the silicate-bearing marble pods, crystals range between 5 mm and 3 cm in size, the majority of grains being 5-10 mm. The silicate-bearing pods are composed of calcite, phlogopite, grey diopside, and spinel in order of decreasing abundance.

C. Contact occurrence

Dark greyish violet spinel occurs in a 1 meter thick steeply-dipping diopsidite between marble and gneiss and, locally, between marble and a 30-cm thick dyke of Kfs-Qtz pegmatite oriented sub-parallel to foliation (N 63.08924° W 71.47921°). Spinel has two modes of occurrence: (1) as ≤ 5 mm octahedra associated with very coarse-grained greenish grey diopside and dark brown phlogopite in white calcite pods (≤ 5 cm); and, (2) as elongated anhedral porphyroblasts up to 4 × 2 cm surrounded by a thin layer of medium-grained phlogopite in massive, medium-grained diopsidite. The latter spinels are elongated along the foliation, however the orientation of the phlogopite is variable.

D. Marble gulch occurrence

White marble is exposed on a vertical wall in a gulch near the crest of a ridge (N 63.08957° W 71.48546°). The marble is composed of medium-sized grains with small quantities of forsterite, pargasite, trace graphite and apatite. A 1-3 cm layer of dolomite-bearing calcite marble contains greyish-violet octahedral spinel crystals up to 2 mm in size with 5 vol. % yellow forsterite (slightly serpentinized), local green euhedral amphibole (≤ 6 mm), and trace diopside. When associated with amphibole or diopside, the forsterite is strongly embayed by the former minerals (Fig. 4.7). Although the embayed grain boundaries could have formed by grain boundary migration, it is possible that the minerals do not form a stable assemblage and that

diopside and amphibole formed during retrograde metamorphism. No coronas or reaction textures were observed.

4.3.1.3 Kimmirut area

Six spinel occurrences in the Kimmirut area were sampled for study (Fig. 4.8). Smaller occurrences of spinel (comparable to the Soper Lake Camp occurrence; see below) are common throughout the area. Two occurrences, Trailside and Qila, are located on True North Gems Inc.'s Beluga sapphire property and are significant for the exceptionally vivid blue color of the spinel.

A. Soper River occurrence

Violet spinel occurs in a 100 × 30 m area (N 62.964986° W 69.795387°; total 230 × 60 m total marble exposure) of dolomitic marble (3A-1) on the west side of Soper River, just east of the lapis lazuli occurrence (whole rock samples 3A-LAPIS-1, 3A-LAPIS-2) described by Hogarth (1971). The marble is coarse to very coarse-grained and is dominantly composed of carbonate (> 99 vol. %) consisting of white dolomite with 5 to 60 vol. % pale grey calcite. It strikes apparently NE and dips roughly 45°, but the coarse grain size, lack of distinct banding, and weathered exposure has obscured the attitude. Accessory minerals averaging 1-2 mm in maximum dimension (up to 6 mm) are much dispersed. From most to least abundant (relatively similar concentrations), they are: (1) white, rounded, fine-grained diopside and dolomite pseudomorphs after an unknown mineral; (2) lime green, euhedral pargasite; (3) violet euhedral spinel octahedra, less commonly with dodecahedral faces (Fig. 4.9); (4) diopside; (5) pyrrhotite; (6) rare graphite and phlogopite. Pargasite appears to consume grains of diopside, however unaltered diopside grains occur in close proximity (< 5 mm). Phlogopite is uncommon in the marble and was not observed in association with spinel. Wilson (2014) reported spinel crystals

up to 3 cm from this occurrence. The largest spinel observed by the author at Soper River measures 6 mm across.

B. Soper Falls occurrence

Spinel occurs in bright orange humite pods (up to 25 cm) in a low humite-bearing marble outcrop (Fig. 4.10; N 62.902903° W 69.839723°). The marble contiguous to the pods contains 20 % humite by volume and no spinel. The pods are aligned NNW; the marble is steeply-dipping, and the pod-bearing layer is traceable for 6 m, after which the weathered rock is covered in soil. Humite (≤ 5 vol. %) occurs in marble as far as 30 meters away from the occurrence. All rock in close vicinity (60 m) to the occurrence is marble, with the exception of a silicate rock included in the marble (K-feldspar, scapolite, diopside with subordinate quartz, calcite, trace apatite and Fe-oxide).

The humitite consists of bright orange, very coarse-grained but highly fractured, fluorine-dominant humite (93-95 vol. %) with greyish-violet spinel octahedra (average 2 mm, up to 9 mm, 3-5 vol. %, generally associated with carbonate; Fig. 4.11A), white carbonate (magnesite >> dolomite, 2 vol. %), coarse pearly white talc (in 5-15 mm pods with carbonate, <1%, identified with XRPD), green pargasite (up to 2.5 × 1 cm), and uncommon pale grey diopside (partly replaced by tremolite) and pyrrhotite. Pargasite occurs in masses and thin veins cross-cutting humite rock. The pargasite appears to have formed at the expense of humite (Fig. 4.11B). Very thin rims of retrograde clinochlore occur around spinel. Dolomite is occasionally present around humite grains in magnesite and in fractures in magnesite; the dolomite appears to post-date the humite-spinel-magnesite stable assemblage (Fig. 4.11C). Talc has a similar grain size to magnesite, and does not appear to form at the expense of humite or magnesite (Fig. 4.11B). Talc is never in contact with spinel.

C. Soper Lake Camp marble

Medium-grained white calcite marble is exposed on the edge of Soper Lake (N 62.871727° W 69.867925°) and contains 4 vol. % yellow forsterite, 1% pyrrhotite, <1% octahedral violet spinel, trace phlogopite, and graphite. The spinel is too small, fractured, and low in abundance to signal gem potential. One Ca-Mg amphibole crystal (EDS) was observed in contact with forsterite. Similar amphiboles are common in marble in this area. Rare titanium oxide, apatite, and one grain of zirconolite were identified with SEM-EDS.

D. Soper Lake mica mine

Spinel occurs in a pegmatitic forsterite-phlogopite-carbonate rock exposed in a mica mine trench (N62.86540° W69.87154°; Fig. 4.12A). The trench is 21 m long and oriented N15°E. Samples of this silicate rock (3D-1 spinel-phlogopite-forsterite-calcite, 3D-2 forsterite-carbonate) were extracted for petrography and bulk rock geochemistry, however these are not representative of the average rock due to its extremely coarse-grained and heterogeneous nature. The mica 'ore' consists of very coarse-grained greyish-green forsterite (75-98 vol. %, estimate for entire rock unit) with dispersed brown phlogopite porphyroblasts (10–36 cm; ~ 5 vol. %) and randomly oriented pods of very coarse-grained white carbonate (dolomite and calcite, 2-10 vol. %, pods generally 5-15 cm in size) containing euhedral forsterite (≤ 3 cm) and, less commonly, dark greyish purple spinel octahedra up to 4.5 cm across (~ 0.5 vol. %; Fig. 4.12B), and trace graphite. Rare amphibole, pyrrhotite, and a 15 × 100 µm grain of probable dissakisite-(Ce) were identified using SEM-EDS. Some of the forsterite-rich rock locally has up to 60 vol. % carbonate. Forsterite is moderately serpentinized, between 10 and 30% by volume. Spinel gemstones have been cut from this occurrence (0.23 carat, very dark purple stone, Wilson 2014)

but the vast majority of spinel is not of gem quality, and no gem quality fragments were observed during field work for this study.

To the east of the pegmatitic zone is marble. The unit contiguous to the band (3D-M1) is a coarse-grained forsterite-bearing marble with ~ 20 vol. % yellow forsterite, subordinate pale brownish-yellow phlogopite, trace dark violet spinel, and graphite. The medium- to coarse-grained marble (3D-3) several meters east of the pegmatitic zone consists of calcite (with dolomite exsolution) with 10-50% silicate, primarily phlogopite with subordinate forsterite, and trace graphite and pyrrhotite.

E. Qila occurrence

The Qila spinel occurrence is located approximately 1 km south of the Beluga sapphire pit. Incredibly vivid, cobalt-blue spinel occurs in a pargasite-rich calc-silicate pod and underlying marble (Fig. 4.13A). The calc-silicate rock forms the cap of a 1.2 m wide, 0.5 m high outcrop that has been eroded on all sides. Calcite-rich pargasite rock and spinel-bearing marble occur in the layers below, but are not exposed anywhere else in the vicinity of the exposure.

The calc-silicate rock (3E-1) is very coarse-grained, consisting of pargasite, scapolite, phlogopite, carbonate, and spinel. *In situ* sampling of this zone was not permitted by the claim holder, but carbonate associated with spinel in float from the same unit consisted of dolomite. Subhedral spinel octahedra (2–10 mm across) are clustered in zones of higher concentration, sometimes with carbonate (Fig. 4.13B). The scapolite is meionite-dominant (Me_{69}) with a thin exterior zone of sodic scapolite (Me_{29}, EDS). Fractures in the scapolite are lined with Mg-chlorite. One grain of pargasite contained a microscopic diopside inclusion and rare pyrite grains up to 10 µm.

Some parts of the calc-silicate rock are underlain by a coarse-grained pargasite-calcite rock (3E-2), but the latter is very discontinuous. The principal mineral components of the coarse to very coarse-grained rock are pargasite (50 vol. %), calcite (45%; including minor dolomite exsolution), pale brownish-yellow phlogopite (5%), sky blue spinel (< 1%), and trace graphite, zircon, and apatite. One diopside grain in calcite, with a zone of pargasite (undulose contact) was observed in thin-section. Rarely, K-feldspar and Mg-Al-silicate (probable clinochlore) partly replace phlogopite.

The marble underlying the pargasite-rich rocks consists of medium- to coarse-grained calcite (with dolomite exsolution) and approximately 6 volume % of other minerals, most commonly (in order of decreasing abundance): forsterite, pargasite, spinel, diopside, apatite, and phlogopite (3E-3-A). Isolated parts of the marble are richer in phlogopite relative to other silicates and contain only trace spinel (3E-3-B). The marble contains rare graphite and zircon. Forsterite grains commonly have diopside coronae, the exterior of which is sometimes replaced by pargasite (Fig. 4.14). Unaltered forsterite, partly altered forsterite, isolated diopside, and isolated amphibole occur in close proximity to each other (few mm) showing that equilibrium was not reached. Forsterite is commonly observed in contact with phlogopite. Diopside and amphibole were observed in contact with spinel. Since accessory minerals are widely dispersed in the marble, the paragenetic relationship between spinel and other silicate minerals cannot be ascertained. Spinel occurs as subhedral, vivid blue octahedra measuring 0.5-1 mm across. The blue color is not as intense as in the calc-silicate pod, but more vivid than in the calcite-rich pargasite rock.

Two marbles were sampled within 30 meters of the Qila spinel occurrence. The first marble sampled (3E-M1) is coarse dolomitic marble with dispersed forsterite (Fo grains have

diopside coronae, and local F-rich pargasite, EDS), spinel, amphibole, diopside, graphite, and apatite. A 6 mm purple spinel analyzed with EPMA has Co below the detection limit (< 0.03 wt. % CoO). The second marble (3E-M2) is coarse-grained, white calcite marble with less than 2 volume % of phlogopite, forsterite (variably serpentinized, in association with phlogopite, and having diopside coronae), and subhedral green diopside.

F. Trailside occurrence

The Trailside spinel occurrence is located approximately 1 kilometer north of the Beluga sapphire pit. Cobalt-blue spinel occurs in two calc-silicate pods hosted in phlogopite-bearing marble. The main pod measures 3 × 2 meters. The calc-silicate pod contains irregularly distributed zones of different rock types, listed in order of decreasing abundance: diopside + phlogopite + carbonate + quartz (3F-4); sericite + phlogopite + clinochlore + calcite + spinel (3F-1); diopside + calcite; phlogopite + calcite; and phlogopite + calcite + spinel (3F-2).

The diopside-phlogopite-carbonate rock is principally composed of greenish-grey, very coarse-grained massive diopside with subordinate dolomite, phlogopite, quartz, and calcite. Trace apatite and zircon were observed in SEM. The phlogopite-calcite rock is coarse-grained with small amounts of fine-grained albite, and rare titanium oxide. The phlogopite is poikiloblastic (calcite inclusions) and randomly oriented.

The main mineral components of spinel-bearing, mottled pale grey and brown calc-silicate rock (3F-1; Fig. 4.15) are sericite, phlogopite, calcite, clinochlore, albite, and spinel. Discontinuous, medium-brown phlogopite-rich bands occur throughout the rock. Cobalt-blue spinel is dispersed throughout the rock (≤ 1 vol. %) with slightly higher local concentrations. Two distinct mineral assemblages are apparent in thin-section (petrological microscope and

SEM): (1) a coarse-grained assemblage of brown phlogopite, yellowish calcite, and cobalt-blue spinel; and (2) a fine-grained assemblage of muscovite (sericite), clinochlore, calcite, albite, corundum, and pyrite. Titanium oxide was observed in SEM. Sericite-clinochlore mixtures (identified with X-ray powder diffraction) occur as pseudomorphs after subhedral crystals of a completely altered unknown mineral (an abundant, rock-forming component of the zone). Fine-grained alteration principally consists of sericite with up to 10% albite, and locally common clinochlore, with subordinate calcite. Muscovite and corundum are locally coarser-grained (crystals up to 0.6 mm). One grain of albite was observed in contact with phlogopite, where the phlogopite showed no alteration to muscovite or chlorite. Phlogopite and spinel are commonly surrounded by clinochlore. Spinel is altered to corundum and clinochlore in zones and along fractures (≤ 15 vol. %; Fig. 4.16). Pyrite associated with corundum-chlorite alteration is cobalt-bearing (see *Mineral Compositions* below). Vivid blue spinel occurs as subhedral octahedra averaging 4 mm across, rarely up to 2.7 cm. A small amount of spinel is of gem quality but due to the high degree of internal fracturing, the largest gemstone produced from this locality to date weighs 0.16 carats (Fig. 4.17; Wilson 2014).

Cobalt-blue spinel also occurs in a medium-grained (1-3 mm), foliated phlogopite-calcite-spinel rock (3F-2; found as float above the outcrop; Fig. 4.18). The rock is composed, by volume, of pale beige carbonate (60%, calcite >> dolomite), pale brown phlogopite (35%), and vivid blue spinel (5%) with minor dolomite, scapolite (Me_{47}, EDS), corundum and trace Fe-oxide and Ba-rich K-feldspar. Alteration of spinel to corundum is generally negligible (average < 5 vol. %).

The second spinel-bearing pod, located 24 meters SSW from the first, is smaller in size relative to the first pod and contains smaller spinel crystals (≤ 1 mm). Two samples of marble

were sampled in the vicinity of the spinel occurrence; samples 3F-M1 and 3F-M2. Marble 3F-M1 is calcite (with dolomite exsolution) marble with 5% phlogopite, 3% forsterite, trace diopside, and rare microscopic spinel and Fe-oxide. The forsterite is weakly serpentinized. One forsterite crystal is rimmed by a layer of diopside, and appears to have been replaced by diopside to some degree (Fig. 4.19). The second marble sample (3F-M2) is very coarse-grained white carbonate with ~ 1% phlogopite (2 mm crystals).

Two spinel-free calc-silicate pods occur 48 meters south of the main spinel-bearing pod (3F-CS1, 3F-CS2, 3F-CS3). The rock ranges from a medium to very coarse grain size and the mineralogy consists primarily of diopside and phlogopite with subordinate dolomite, calcite, and quartz. In calc-silicate sample 3F-CS1, one crystal of calcic magnesian amphibole occurs with quartz and calcite as an inclusion in diopside. Sample 3F-CS2 also contains subordinate scapolite (Me_{55}, EDS), trace plagioclase (An_{19}, EDS), and rare zircon.

4.3.1.4 Waddell Bay occurrence

A sample of coarse-grained pale orange calcite containing euhedral pale grey diopside, bluish-violet spinel, and dark brown phlogopite collected by Bradley Wilson was given to the authors for study. Wilson (2014) reported that blue and violet spinel crystals (combination of octahedral, dodecahedral, and trapezohedral faces) up to 3 cm occur with phlogopite and diopside in coarse-grained calcite marble. Wilson (2014) also reported that the largest faceted gem spinel from this location weighs 0.23 carats.

4.3.1.5 Unspecified occurrence on Hall Peninsula

A sample of spinel-bearing marble from an unspecified location on the Hall Peninsula was given to the authors for study. The marble is a coarse-grained white calcite marble with 3% pale yellow forsterite, 1% dark greyish violet spinel (2 – 4 mm crystals), < 1% pale brown

phlogopite, and rare titanium oxide. Forsterite shows no alteration or reaction rims. Amphibole and calcite were observed as inclusions in spinel in thin-section. A phlogopite-calcite-diopside and a calcite-spinel inclusion occur in amphibole. The lack of obvious reaction textures and the dispersed nature of the silicates prevent definitive paragenetic sequence determination.

4.3.2 Mineral compositions

Spinel and principal associated phases were analyzed with EPMA. Grains of each mineral were extracted from the same rock sample so that element concentrations in different minerals of a specific assemblage can be accurately compared. Sample numbers refer to suites of minerals extracted from a single rock sample with the following exception: Sample 3A-1, which includes dolomite, calcite, pyrrhotite, amphibole, and diopside extracted from two rock samples, while a third sample (3A-2) contained spinel in contact with pargasite in calcite. Minerals at locality 3A (Soper River) were generally too dispersed to be extracted from the same rock samples.

4.3.2.1 Spinel

Spinels in metacarbonates on Baffin Island are all Mg-dominant (spinel *sensu stricto*; Tables 4.3A-D), with a median X_{Fe} (Fe/[Mg+Fe]) of 0.07, a minimum of 0.03, and maximum of 0.18. Black spinel from the unnamed island in Markham Bay is richest in Fe (X_{Fe} = 0.18), followed by very dark blue spinel from Spinel Island (X_{Fe} = 0.14). Spinels with $X_{Fe} \approx 0.1$ tend to be slightly dark but can be of gem quality (*e.g.*, Glencoe Island main occurrence and Trailside). The spinels poorest in Fe, which are pale violet in color, are the pyrrhotite-associated Soper Camp spinel and the dolomite-hosted spinel in marble near Qila (X_{Fe} = 0.03).

Vanadium concentrations are commonly below the detection limit (< 0.03 wt. % V_2O_3) with a median of 0.04 wt. % V_2O_3. Baffin Island spinels have a median of 0.06 wt. % Cr_2O_3, the highest value (0.14 wt. %) found in dark purple spinel from the Soper Lake mica mine. MnO

concentrations vary between below detection limit (< 0.03 wt. %) and 0.1 wt. % (median 0.045 wt. %). Spinels with the highest X_{Fe} (localities Markham Bay and two localities on Glencoe Island) also contain the highest Mn concentrations, however the values do not correlate perfectly. Cobalt is below detection limit (< 0.03 wt. % CoO) in all samples except at Qila and Trailside (0.03-0.07 wt. % CoO), where the spinel is vivid blue in color. Nickel was only detected in the Qila spinel (0.03-0.04 wt. % NiO, detection limit 0.03 wt. %). ZnO was measured in the majority of samples (detection limit 0.03 wt. %) with a median of 0.13 wt. %. Spinel from the main occurrence on Glencoe Island is particularly enriched in Zn (2.32-4.25 wt. % ZnO) relative to other Baffin Island spinels.

A violet and a dark greyish-violet spinel from two different calc-silicate pods from the Glencoe main occurrence had slightly different major element concentrations: 2.32 and 4.25 wt. % ZnO, < 0.02 and 0.04 wt. % V_2O_3, but relatively similar FeO (4.88 *vs.* 4.23 wt. %), respectively.

At the Soper Lake mica mine, spinel in phlogopite "ore" is richer in chromium relative to spinel in the contiguous Fo-Spl marble (0.14 and 0.05 wt. %, respectively), while the spinel in marble contains more ZnO (0.18 in the marble *vs* 0.12 wt. %).

Three vivid blue spinel samples were extracted from different lithologies at Qila: calc-silicate rock, pargasite-calcite rock, and spinel-bearing marble. Spinel from the calc-silicate rock is richer in ZnO (0.16 wt. %), Fe (X_{Fe} = 0.07), CoO (0.07 wt. %), and NiO (0.04 wt. %) relative to spinel from the other rock units (0.05 wt. % ZnO, X_{Fe} = 0.05, 0.03 wt. % CoO, ≤ 0.03 wt. % NiO). A pale violet spinel recovered from dolomitic marble near the Qila outcrop contains 0.09 wt. % ZnO, a lower X_{Fe} (0.03), and no detectable NiO or CoO (< 0.03 wt. %). This pale violet spinel is much richer in V_2O_3 (0.04 wt. %) than the cobalt blue spinel at Qila (< 0.02 wt. %).

Cobalt-blue spinels from the Trailside occurrence are all Cr-, V-, and Ni-poor (below detection limits), contain ~ 5 wt. % FeO, and 0.06 wt. % CoO. Spinel in the silicate rock contains roughly half (0.05 wt. %) the amount of ZnO compared to spinel in the calcite-phlogopite-spinel rock (0.13 wt. %).

4.3.2.2 Forsterite

Olivines in the Baffin Island spinel-bearing metacarbonate samples are all end-member forsterite (Fo_{97} – Fo_{99}; Table 4.4). Forsterite associated with cobalt-bearing, vivid blue spinel in the Qila marble contains up to 0.03 wt. % CoO. Greenish and grey forsterite from the same sample of Qila spinel-bearing marble vary slightly in FeO (2.39 and 2.28 wt. %) and MnO (0.05 and 0.07 wt. %) concentrations, respectively.

4.3.2.3 Diopside

Diopside associated with spinel (Table 4.5A-B) is very Na-poor (< 0.01 *apfu*), with the exception of low concentrations at Qila (0.026 *apfu*) and Waddell Bay (0.043 *apfu*). They generally contain 0.116-0.235 Al *pfu* except for Al-poor diopside from Soper Falls, Soper River (~ 0.03 *apfu*), and in the diopside-dolomite pseudomorph at Soper River (0.003 Al *pfu*). All diopsides are relatively Fe-poor; X_{Mg} ranges between 0.95 and 0.99. The most Fe-rich diopside originates from localities with the darkest colored, most Fe-rich spinel.

4.3.2.4 Amphibole

All amphiboles are pargasite with the exception of tremolite replacing diopside at Spinel Island and Soper Falls (Tables 4.6A-C). Tremolite from Spinel Island is the most Fe-rich (X_{Mg} = Mg/(Mg+Fe) = 0.93). Pargasite from the calc-silicate rock at Qila has X_{Mg} = 0.97 while all other amphiboles have X_{Mg} = 0.98 or 0.99.

Pargasite is generally TiO_2-poor (< 1 wt. %) with the exception of that at Glencoe Island marble gulch, Soper Lake Camp, and the Hall Peninsula marble occurrence, which have TiO_2 concentrations between 1.69 – 2.64 wt. %. The A-site is Na-dominant with X_{Na} = Na/(Na+K+Ca) ranging between 0.55 and 0.93 (lowest at Glencoe gulch, highest at Soper Falls). Pargasite from Qila is particularly rich in K_2O (up to 2.23 wt. %). Chlorine contents vary between 0.04 and 0.18 wt. %, and most fluorine concentrations are below detection limit (< 0.12 wt. %). Pargasite, which formed at the expense of F-rich humite, contains 0.42 wt. % F. Barium is generally below detection limit (< 0.06 wt. %) but up to 0.21 wt. % at Glencoe marble gulch.

Pargasite in marble at the Glencoe gulch occurrence contains small zones richer in TiO_2 (2.64 *vs.* 1.69 wt. %), poorer in Fe_2O_3 (0.43 *vs.* 0.60 wt. %), and poorer in K_2O (0.44 *vs.* 1.05 wt. %).

Pargasite in Soper River marble varies considerably in TiO_2 (0.23-0.58 wt. %) and Cl (0.08-0.18 wt. %) concentrations, with moderate variation in Na_2O (2.61-3.00 wt. %).

At Qila, pargasite in the calc-silicate rock is richer in the following components relative to that in the pargasite-calcite rock: BaO (0.12 *vs.* 0.07 wt. %), K_2O (2.23 *vs.* 2.02 wt. %), and F (0.20 *vs.* < 0.12 wt. %). Pargasite in the pargasite-calcite rock contains more Na_2O (2.74 wt. %) than pargasite in the calc-silicate unit (2.04 wt. %).

4.3.2.5 Phlogopite

Phlogopites associated with spinel in metacarbonates on Baffin Island contain an average of 0.62 wt. % TiO_2 with a range of 0.09 – 1.60 wt. % (Tables 4.7A-E). FeO contents are 1.09 wt. % on average, ranging from 0.45 to 2.30 wt. %. Vanadium is below detection limit with the exception of the phlogopite associated with dark spinel at the Glencoe main occurrence (0.04 wt. %). The median BaO content is 0.83 wt. %; BaO values are above detection limits in all samples,

the lowest value being at Trailside (0.10 wt. %) and with Ba-rich outliers at Glencoe gulch and in the Hall Peninsula marble sample (4.04 – 6.64 wt. % BaO). Fluorine concentrations vary between below detection limit (< 0.12 wt. %) and 1.58 wt. %. Phlogopite richest in F is from the Qila calc-silicate rock (1.58 wt. %), Soper Lake mica mine (1.52 and 1.32 wt. %), and Spinel Island (1.22 wt. %).

At the Glencoe main occurrence, phlogopite associated with violet spinel differs in composition from that associated with the dark greyish violet spinel: they contain, respectively, 0.92 and 0.28 wt. % TiO_2, 1.51 and 1.27 wt. % FeO, and 2.21 and 1.40 wt. % BaO.

At the Soper Lake mica mine, phlogopite in the Fo-Spl marble is richer in FeO, Na_2O, BaO, and poorer in TiO_2 and F compared to phlogopite in the mica "ore."

Phlogopite occurs in the calc-silicate rock, the pargasite-calcite rock, and spinel-bearing marble at the Qila spinel occurrence. The phlogopites have the following compositional ranges, with the richest sample mentioned in brackets: 0.29-0.60 wt. % TiO_2 (calc-silicate), 0.51-0.80 wt. % FeO (calc-silicate), 0.51-0.95 wt. % BaO (Pargasite-Calcite rock), 0.11-0.72 wt. % Na_2O (Prg-Cal rock), 0.07-0.14 wt. % Cl (Pargasite-Calcite rock), and 0.42-1.58 wt. % F (calc-silicate). In the previously listed elements, the composition of phlogopite from the marble is intermediate between the calc-silicate and pargasite-calcite units with the exception of fluorine, where it is the least abundant.

Two phlogopite grains from the Trailside spinel-bearing silicate rock were analyzed. They are relatively similar, with the exception of different TiO_2 (0.09 – 0.32 wt. %), BaO (0.10-0.29 wt. %), and FeO (1.33-1.25 wt. %) contents. Phlogopite from the calcite-phlogopite-Spinel rock is, relative to that from the silicate rock, fairly comparable in TiO_2 and FeO concentrations.

Phlogopite from the calcite-phlogopite-spinel unit is richer in BaO (0.35 wt. %), Na_2O (0.44 wt. %), and Cl (0.07 *vs.* ≤ 0.02 wt. %).

In spinel-bearing marble from the Hall Peninsula, the Ba-rich (4.30 wt. % BaO) phlogopite contains slightly Ba-enriched zones (average 6.64 wt. % BaO) that correlate with slightly richer TiO_2 content.

4.3.2.6 Other Silicates and Oxides

The Soper Falls humite is F-dominant, containing 4.70 wt. % fluorine. It contains 1.18 wt. % Fe, and 0.43 wt. % TiO_2 (Table 4.8). The high total (103.07 wt. %) may be influenced by lower precision on F measurements.

A fragment of scapolite from the spinel-bearing calc-silicate pod at Qila is predominantly meionite (Me_{69}; Table 4.9) but thin exterior rims of marialite (Me_{29}) were identified using EDS. The measured composition of scapolite (EPMA data) is low since CO was not measured or accounted for.

Muscovite, part of a retrograde mineral assemblage at Trailside, contains small amounts of Na, Ca, Mg, and Ba (Table 4.10). Corundum replacing spinel as part of the same assemblage has the following composition as determined with EPMA (weight %): 100.76 Al_2O_3, 0.07 FeO, and 0.03 Cr_2O_3.

4.3.2.7 Calcite and Dolomite

Calcite (Table 4.11A-B) is the most common carbonate associated with spinel on Baffin Island. Dolomite commonly occurs as exsolution in calcite. Only Soper River marble, a spinel-bearing marble near Qila, and the Qila calc-silicate rock contain significant quantities of dolomite as part of the stable assemblage (*i.e.*, not exsolved dolomite within calcite; Table

4.12A-B). Small amounts of magnesite and dolomite, in addition to calcite, occur in humitite at Soper Falls.

Calcite contains from < 0.03 to 0.27 wt. % FeO, far less than dolomite (0.18 – 0.74 wt. %). Rock-forming abundances of dolomite and calcite occur together at Soper River; the dolomite is significantly richer in FeO relative to calcite (0.23 *vs.* 0.03 wt. %) but they have identical MnO concentrations (0.04 wt. %). MgO concentrations in calcite generally vary between 0.35 and 3.45 wt. % with the exception of exceptionally Mg-poor calcite at Spinel Island (0.03 wt. %). Calcite in the high range of MgO content has very fine dolomite exsolution, which is reflected in the EPMA data.

4.3.2.8 Pyrrhotite and Pyrite

Pyrite containing 1.79 wt. % cobalt (Table 4.13) occurs with corundum in altered spinel at the Trailside occurrence (the slightly low total weight % may be due to error since the grain was small, *ca.* 10 µm in maximum dimension). Pyrrhotite is the only sulphide mineral occurring with spinel as part of a stable assemblage. Pyrrhotite occurs in spinel-bearing calc-silicate pods at the Glencoe main occurrence, in spinel-bearing marble at Soper River and Soper Lake camp, and in the humitite at Soper Falls. Cobalt concentrations range from 0.06 to 0.11 wt. %; Ni varies from below detection limit (<0.03 wt. %) to 0.21 wt. %.

4.3.3 Whole-rock compositions

Whole rock major element (Tables 4.14A-C) and trace element (Tables 4.15A-D) compositions were obtained for selected rock samples. Of the number of samples analyzed, the results of six are considered somewhat qualitative due to limited sample size (very coarse-grained rock or extremely dispersed minerals not adequately represented in the collected samples): (1A-SG) Spinel Island syenogranite; (1A-SPL) Spinel Island spinel-bearing diopsidite;

(3D-2) Soper Lake mine rock from the main pit, which contains forsterite and carbonate, but no phlogopite or spinel; (3A-1) marble from Soper River consisting of two fairly representative marble samples from the spinel-bearing unit; (3E-1) Qila calc-silicate rock sample lacking the spinel and carbonate found in this rock unit; and (3F-1) Trailside silicate-rich rock with spinel that did not contain significant spinel or phlogopite (relative to the darker bands in rock, see petrography). The low total in humitite is due to the large amount of fluorine not included in the total. Similarly, Cl was not included in the total for lapis lazuli. Among others, the elements Sc, V, Cr, Mn, Fe, Co, Ni, and Zn are of particular interest to the study of gem spinel due to their abundance in the mineral and due to the role of Cr, Fe, Co, and V as chromophores which directly control the beauty, and therefore market value of gem spinel. Selected light elements (Li, B, Cl, F) are also discussed below.

4.3.3.1 Lithium

All marble samples and the Soper River lapis lazuli contain Li concentrations below detection limit (< 10 µg/g). Spinel-bearing rock at Spinel Island is relatively poor in Li (10 µg/g), however phlogopite is under-represented in the sample. Spinel-bearing calc-silicate rock and psammite at the Glencoe main occurrence contain between 10 and 30 µg/g Li. The Co-enriched calc-silicate pod at Qila contains 30 µg/g Li, while the spinel-bearing rock at Trailside is comparatively rich in Li (30-50 µg/g). The Co-rich Trailside diopsidite contains low Li (< 10 µg/g), and the spinel-free calc-silicate pods in the vicinity of Trailside contain 10 µg/g Li.

4.3.3.2 Boron, Chlorine, Fluorine

These elements were measured only in selected samples: Glencoe main spinel-bearing calc-silicate, Soper Lake Forsterite-Spinel-bearing marble, Soper Falls humitite, Soper River

spinel-bearing marble (B only), Qila Pargasite-Calcite rock, Trailside spinel-bearing silicate rock, Trailside area marble, and Soper River lapis lazuli.

The marbles and lapis lazuli are poorest in boron, 13-30 µg/g, with the exception of B-rich (129 µg/g) Forsterite-Spinel marble contiguous to the pegmatitic forsterite-phlogopite-carbonate-spinel rock at the Soper Lake mica mine. Spinel-bearing calc-silicate rock at the Glencoe main occurrence contains 21 µg/g B, much less than at Qila (95 µg/g), Trailside (196 µg/g), and Soper Falls (304 µg/g).

Lapis lazuli and the Soper Lake mine Forsterite-Spinel marble are poorest in F (560 and 510 µg/g). Spinel-bearing rock at the Glencoe main occurrence contains 1070 µg/g F. The Trailside cobalt-blue spinel bearing silicate rock and the phlogopite-bearing marble from the Trailside area contain similar F concentrations (2320 and 1970 µg/g). Pargasite-rich Qila calc-silicate rock is, unsurprisingly, much richer in F than the latter rocks (6960 µg/g). Soper Falls spinel-bearing humitite, which is dominantly composed of F-dominant humite, had a fluorine concentration exceeding the upper limit of quantification (> 2 wt. %).

Chlorine is least abundant in humitite and marbles (250-410 µg/g). The spinel-bearing silicate rock at Trailside contains 680 µg/g Cl, while the spinel-bearing rock at Glencoe main is slightly richer in the halogen (820 µg/g). The Qila pargasite-rich rock is, unsurprisingly, also richer in Cl with 1160 µg/g, and the Soper River lapis lazuli is richest in the element (3170 µg/g).

4.3.3.3 Chromium and Vanadium

LHG marble samples contain an average of 9 µg/g vanadium (5-17 µg/g range). In comparison, calc-silicate rocks, humitite, and lapis lazuli contain 22-53 µg/g V. Spinel-bearing rock at Spinel Island is relatively poor in V compared to the other calc-silicate rocks (14 µg/g).

Forsterite-carbonate rock from the Soper Lake mica mine contains very low V (5 µg/g), probably owing to the lack of spinel or phlogopite in the sample and thus, the value is likely not representative of the rock unit. The psammite at Glencoe Island contains 29 µg/g V, within range of the calc-silicate rocks, and the sulphide-rich diopsidite at the same location is exceptionally V-rich (457 µg/g). At the Qila cobalt-blue spinel occurrence, amphibole-rich units are richer in V (13 µg/g) relative to the marbles (≤ 5 µg/g). At the Trailside cobalt-blue spinel occurrence, phlogopite-calcite-spinel rock (3F-2) and diopsidite (3F-4) contain 17 and 16 µg/g V, respectively. Trailside sample 3F-1 is poorer in V (7 µg/g), likely a reflection of the low abundance of spinel and phlogopite in this sample relative to this rock unit.

Chromium concentrations in LHG marble, including those containing cobalt-blue spinel, are ~10 µg/g. Two spinel-bearing calc-silicate pods at Glencoe Island were found to contain 60 and 100 µg/g Cr. Spinel-bearing humitite is intermediate at 40 µg/g. Soper River lapis lazuli contains 30-50 µg/g Cr. Calc-silicate pods in the vicinity of the Trailside occurrence contain 20-30 µg/g Cr, while rocks at the Trailside occurrence are slightly poorer in the element (10-20 µg/g). The main calc-silicate pod at Qila (40 µg/g) is richer in Cr relative to other rocks at this occurrence (10 µg/g). As with vanadium, the low (10 µg/g) Cr concentrations in the Soper Lake mine forsterite-carbonate rock are probably not representative of the entire rock unit.

4.3.3.4 Manganese and Iron

Marbles and silicate-rich metacarbonates range in MnO content from 0.03-0.06 wt. % and 0.03-0.08 wt. %, respectively. Lapis lazuli is, in comparison, Mn-poor with 0.02 wt. % MnO. Glencoe Island sulphide-bearing psammite and diopsidite are both intermediate, with 0.04 wt. % MnO. Co-rich (9-29 µg/g) rocks at Qila and Trailside contain low to moderate (0.02-0.04 wt. %) MnO concentrations relative to other metacarbonates.

Iron concentrations are expressed as total Fe = Fe_2O_3. The Glencoe main occurrence diopsidite and psammite are, by far, the richest in Fe (5.36 and 4.89 wt. %, respectively). Silicate-rich metacarbonates are poorer in iron, ranging from 1.11-1.88 wt. % Fe_2O_3 with higher concentrations in the forsterite-carbonate rock at the Soper Lake mine (2.58 wt. %). Lapis lazuli is Fe-poor for a silicate-rich metacarbonate (~0.4 wt. %). Marbles contain less iron than calc-silicates, 0.31-0.94 wt. %. The Co-enriched rocks at Qila are relatively Fe-poor (0.33-0.82 wt. % Fe_2O_3) while those at Trailside are closer to the range for other metacarbonates in the LHG (0.44-1.14 wt. %).

4.3.3.5 Cobalt

Cobalt concentrations in the LHG metacarbonates are generally low: < 1 µg/g in lapis lazuli from Soper River; < 1 to 3 µg/g in marbles and impure marbles; and 2 to 6 µg/g in calc-silicate rocks. At the Glencoe Island main occurrence, sulphide-rich psammite and diopsidite are richer in Co, containing 7 and 16 µg/g respectively. Calc-silicate pods devoid of spinel in the vicinity of the Trailside occurrence are in the high range of cobalt concentrations for a calc-silicate rock (considering the lack of sulphides); 5 and 8 µg/g. Rocks containing cobalt-blue spinel, or spinel-free zones near these rocks (*i.e.*, Trailside diopsidite and Qila phlogopite-bearing, spinel-poor marble) are comparatively rich in cobalt; 16 µg/g on average, with a range of 9-29 µg/g. The cobalt concentration in the main calc-silicate pod sample (3E-1; pargasite, scapolite) is likely an underestimate, since a sample with spinel (the mineral in the assemblage that most strongly uptakes Co, as shown in the EPMA data) could not be taken due to sampling restrictions on the claim property. Similarly, the Trailside silicate rock (3F-1) was spinel-poor and did not contain a representative amount of the darker bands richer in phlogopite and spinel.

4.3.3.6 Nickel

Nickel concentrations in the LHG marble samples vary between < 1 and 4 µg/g. Concentrations of Ni in the lapis lazuli are below detection limit (< 1 µg/g). In silicate-rich metacarbonates, Ni concentrations vary between 2 and 23 µg/g with the exception of Soper Falls humitite (< 1 µg/g). The highest Ni concentration measured in the calc-silicates (23 µg/g) is in a pyrrhotite- and spinel-bearing rock from the Glencoe main occurrence. Nickel is fairly enriched in the Glencoe Island sulphide-bearing psammite (35 µg/g) and diopsidite (149 µg/g). Relative to most metacarbonates, rocks containing cobalt-blue spinel are richer in Ni, containing 22 µg/g on average (10-47 µg/g).

4.3.3.7 Copper

The LHG marbles sampled contain < 1 to 6 µg/g Cu, with the higher concentrations being in pyrrhotite-bearing samples. Copper was not detected in lapis lazuli (< 1 µg/g). In silicate-rich metacarbonates, copper concentrations range from 1 to 17 µg/g and, once again, the highest concentration is in sulphide-bearing rock (Glencoe Island 2A-SPL-2). Glencoe sulphide-bearing psammite and diopsidite are the rocks richest in copper with 62 and 55 µg/g, respectively. Rocks associated with cobalt-blue spinel contain negligible Cu (≤ 2 µg/g).

4.3.3.8 Zinc

Zinc is most abundant in the Glencoe main occurrence, where it occurs in concentrations between 230 and 308 µg/g in the spinel-bearing pods, serpentine marble, and sulphide-rich diopsidite; less so in the psammite (67 µg/g). At Spinel Island in Markham Bay, phlogopite-bearing marble is Zn-poor (< 2 µg/g) while the spinel-bearing rock contains 98 µg/g. Syenogranite pegmatite in contact with the spinel zone on Spinel Island in Markham Bay contains 7 µg/g Zn, and the nearby monzogranite, 14 µg/g.

Other LHG silicate-rich metacarbonates contain between 4 and 14 µg/g Zn. Marbles contain up to 5 µg/g. Rocks at the Qila cobalt-blue spinel occurrence are Zn-poor (≤ 2 µg/g) while the rock at Trailside varies considerably (two samples ≤ 3 µg/g, one spinel-rich sample containing 15 µg/g Zn). As in the case of cobalt concentrations, the low abundance of Zn in sample 3F-1 may reflect sampling bias.

4.3.3.9 Rare earth elements

Whole rock samples of Lake Harbour Group marbles and calc-silicate rocks have a similar chondrite-normalized REE profile to that for LHG metasediments reported by Thériault *et al.* (2001), characterized by fractionated LREE, relatively flat HREE profile, and a negative Eu anomaly. The profile for Glencoe Island psammite is similar, but with no Eu anomaly. Qila calc-silicate rock and diopsidite at and near the Trailside occurrence have a flat REE profile with negative Eu anomaly. The chondrite-normalized REE profile of Spinel Island monzogranite is very similar to that of the syenogranite pegmatite; both are downward sloping with increasing atomic number and have a positive Eu anomaly.

4.3.4 Pseudo-sections

T-X(CO_2) pseudo-sections at peak metamorphic conditions (P = 8 kbar, St-Onge *et al.* 2007) were calculated using Perple_X (Figs. 4.20 to 4.23) for the following samples: (2A-SPL-2) diopside-phlogopite-spinel-carbonate rock at the Glencoe Island main occurrence; (3A-1) dolomite-calcite marble with subordinate spinel, diopside-dolomite replacements after an unidentified mineral, pargasite, and phlogopite from the Soper River occurrence; (3E-3-A) calcite-dolomite marble containing forsterite, diopside, pargasite, spinel, phlogopite, and apatite from the Qila occurrence; and (3F-2) phlogopite-calcite-dolomite-spinel rock with trace scapolite from the Trailside occurrence. The following model systems were used: (2A-SPL-2) K_2O-CaO-

MgO-FeO-SiO2-Al_2O_3-H_2O-CO_2; (3A-1 and 3E-3-A) Na_2O-K_2O-CaO-MgO-FeO-SiO_2-Al_2O_3-H_2O-CO_2; and (3F-2) Na_2O-K_2O-CaO-MgO-FeO-SiO_2-TiO_2-Al_2O_3-H_2O-CO_2. Models that include Na result in the prediction that accessory aspidolite (Na end-member of phlogopite) is associated with phlogopite under certain conditions. The biotite solution model does not account for the substitution of Na for K, and thus the result is interpreted to reflect a small increase in phlogopite Na content. This is considered plausible because even in cases of extreme Na-enrichment in such micas, where the mineral species aspidolite is formed, the crystals contain mixed layers of variable Na and K content (*e.g.*, mixed aspidolite-phlogopite crystals associated with spinel in marble, Belley *et al.* 2016; mixed aspidolite-phlogopite-paragonite in ruby-bearing marbles, Garnier *et al.* 2004). No solution model was used for Mg incorporation in calcite, which may affect the positioning of phase boundaries separating calcite *vs.* calcite-dolomite bearing assemblages.

In calc-silicate sample 2A-SPL-1 (Glencoe Island main occurrence; Fig. 4.20), spinel is stable at all X_{CO2} at peak metamorphic conditions. The mineral assemblage noted in petrography is calculated to occur at X_{CO2} between *ca.*0.45 and 0.85.

At peak metamorphic conditions in the *T*-*X* pseudo-section for Soper River marble sample 3A-1 (Fig. 4.21), spinel occurs in the range *ca.* $0.09 \leq X_{CO2} \leq 0.57$. Spinel, forsterite, and pargasite occur as part of a stable assemblage without diopside between $X_{CO2} = 0.3$ and 0.5. The forsterite-out occurs at lower temperature, where the assemblage consists of pargasite, diopside, phlogopite, calcite, and dolomite.

Spinel-bearing marble from Qila (sample 3E-3-A) produced a similar pseudo-section to that of Soper River marble; spinel is only stable at lower X_{CO2} (~ 0.07 to 0.48, Fig. 4.22). At peak metamorphic conditions and with increasing X_{CO2}, the magnesian silicate assemblage

changes from containing forsterite, to forsterite-pargasite, to forsterite-pargasite-diopside, pargasite-diopside, and diopside.

In the phlogopite-calcite-spinel rock at Trailside (3F-2), spinel is expected to occur throughout the X_{CO2} range during peak metamorphism (Fig. 4.23, excluding partial melting at very low X_{CO2}). Trace scapolite occurs in this sample but was not observed in contact with spinel. Scapolite and spinel occur as part of a stable assemblage together with phlogopite, calcite, dolomite, and nepheline at $X_{CO2} \sim 0.95$. At lower temperature and high X_{CO2}, one assemblage consists of scapolite-phlogopite-calcite-dolomite. A spinel-free corundum-bearing assemblage also occurs at lower temperature.

4.4 Calculations

4.4.1 Sedimentary protolith composition estimation: Method and underlying assumptions

Classifying various LHG metasedimentary carbonates and impure carbonates can provide insights into protoliths that favor spinel genesis under high-grade metamorphic conditions. Metasedimentary rocks that are not the result of reaction with metasomatic fluids or plutonic rocks (*i.e.*, Markham Bay localities) are likely representative of the compositions of the sedimentary protoliths, although it should be reminded that sampling bias (discussed for specific samples in section 4.3.3; some examples have been excluded from composition estimation for this reason) and major element mobility during metamorphism will affect these results. Under the assumption that whole rock compositions are representative of the original rock, we qualitatively estimate the sedimentary composition of the protolith by: (1) calculating an estimate of siliciclastic sediment abundance using Al/Si (Fig. 4.24) to estimate mixing of "ideal" sandstone, shale, and kaolinite-rich claystone (for Al/Si values considerably higher than typical shale or clay); (2) using this estimate to calculate the expected CaO and MgO content of the

siliciclastic fraction; (3) calculating an estimate of original carbonate CaO and MgO by subtracting the former values from the totals; (4) calculating the estimated relative abundance of calcite, dolomite, and magnesite carbonate species in the protolith; and (5) re-calculation of the sediment weight percentages using the original protolith CO_2 content estimate and assuming that the shale/clay fractions contain 5 wt. % H_2O, which will account for mass loss during metamorphic devolatilization reactions. All non-siliciclastic CaO and MgO, in addition to CO_2 are considered part of the carbonate fraction. Siliciclastic CaO and MgO are assigned to their respective sediment fractions. Other elements, especially minor elements, are divided proportionally between the siliciclastic components. Lapis lazuli from Soper River is exceptionally Na-enriched – far more than would be possible in shale or clay. While Na is very mobile and could have been introduced during metamorphism, we attribute Na to halite in the original protolith calculation and add Cl, based on the identification of Soper River lapis lazuli as a meta-evaporite by Hogarth & Griffin (1978). Results are presented in Tables 4.16A-D.

4.4.2 Estimate of "expected" minor metal content

Comparing metasediment whole rock trace element abundances (or relative abundances, *e.g.*, metal/Al) to that of typical sedimentary rocks is a useful tool in assessing the geochemical properties of the metasedimentary rock, which is expected to reflect original protolith composition and potential chemical changes during diagenesis and metamorphism. Variations in some elements can imply a meta-evaporitic origin (*e.g.*, Moine *et al.* 1981) while variation in spinel chromophore concentrations can affect spinel color, and therefore its value as a gemstone (see discussion below). Metal/Al fractions are not an ideal method of comparison in the case of Lake Harbour Group spinel-bearing rocks since only some trace metals correlate with Al and the metasediments were probably a mixture of carbonate and siliciclastic sediments. Therefore, a

qualitative method of estimating the expected trace element composition of the metasediment samples is employed by calculating the expected relative trace element contribution of the various protolith components (estimated above) using trace element averages for sandstone, limestone (Turekian & Wedepohl 1961) and shales/clays (Parker 1967). Concentrations are corrected for the expected mass loss due to devolatilization during metamorphism estimated in Table 4.16 by the sum of the whole rock composition and additional CO_2 and H_2O estimated to have been lost by devolatilization. The qualitative "expected" trace element concentrations and the actual values relative to these expected concentrations (presented as a fraction) are shown in Tables 4.17A-B.

4.5 Discussion

4.5.1 Origin of spinel occurrences, parageneses, P-T conditions and timing

Spinel occurrences, with the exception of Markham Bay localities (and perhaps Waddell Bay), are interpreted to be metasedimentary (*sensu stricto*) due to their isolation within marble and paragneiss units with no proximal intrusive bodies or signs of large-scale metasomatism. Spinel at Markham Bay is interpreted to be of metasomatic origin.

4.5.1.1 Markham Bay

A. Spinel Island

Diopside, spinel, phlogopite, calcite and local anorthite form a stable assemblage with highly localized retrograde alteration consisting of tremolite and corundum with subordinate clinochlore, margarite, and clinozoisite/zoisite. Diopsidite is interpreted to have formed by the metasomatic reaction between feldspathic rock and marble; this metasomatic diopsidite band is thickest, best developed, and richest in spinel at the contact with pegmatitic syenogranite. Spinel is rare or absent in diopsidite contiguous to the foliated granitoid rocks. The occurrence of

diopsidite between marble and syenogranite suggests two possibilities: the intrusion of syenogranite into marble resulted in contact metasomatism forming diopsidite or, alternatively, that fluid influx at the syenogranite-marble boundary at high metamorphic grades resulted in a bimetasomatic reaction. Spinel genesis from the bimetasomatic reaction between feldspathic rock and dolomite-bearing marble is known from the Grenville Province in Québec (Belley *et al.* 2016). The locally more-extensive diopsidite development associated with the syenogranite could suggest that contact metamorphism resulted in the most intense metasomatism contiguous to the intrusion, and less so along nearby country rocks, however the presence of marble with no visible diopsidite on the middle western side of the syenogranite contradicts this hypothesis. Therefore, I propose that the diopsidite formed by structurally-controlled fluid influx at syenogranite/granitoid rock and marble boundaries resulting in a bimetasomatic reaction between these rocks. This reaction may have occurred at peak or near peak metamorphic conditions; similar mineral assemblages (*e.g.*, pseudo-section in Fig. 4.20) are stable at these conditions; but formation of the diopsidite during M_2 retrograde metamorphism (*ca.* 720 °C, 6.2 kbar, St-Onge *et al.* 2007) cannot be ruled-out with the available data. The syenogranite pegmatite may be related to the regionally significant Cumberland Batholith, but a 10 kg sample produced no zircons for age dating and therefore the timing of intrusion could not be determined. Chlorite, margarite, corundum and tremolite formed from the retrograde break-down of spinel and diopside following influx of H_2O and CO_2.

B. Unnamed Island

Spinel on the unnamed island occurs in parts of very coarse calcite veins that are free of amphibole. Elsewhere in the outcrop, coarse to pegmatitic amphibole occur within a crosscutting network of calcite veins in calc-silicate rock suggesting significant metasomatism. This rock unit

bears great resemblance to the metasomatic calc-silicate unit on the nearby Aliguq Island (Butler 2007).

4.5.1.2 Glencoe Island

A. Main occurrence

Spinel occurs in dispersed calc-silicate pods within a band of serpentine marble in a psammite sequence – it is clearly of metasedimentary origin. The pods are assumed to have been a siliceous layer within the marble that was boudinaged and displaced during metamorphism. The presence of forsterite in the marble, inferred from subhedral crystals replaced completely by serpentine, and of orthopyroxene in the psammite, indicates a high grade of metamorphism. Microscopic zircon crystals are common in the calcite-rich portion of one spinel-phlogopite-diopsidite sample. A *T-X* pseudo-section generated with Perple_X (Fig. 4.20) shows that a diopside-spinel-phlogopite-calcite-(dolomite) assemblage is stable at M_{1A} peak metamorphic conditions.

B. Marble beach occurrence

Calcite, phlogopite, diopside and spinel form a stable assemblage, which is relatively similar to the peak metamorphic assemblage at the main occurrence. The calcite-rich silicate pods are surrounded by marble (> 30 m), clearly indicating a metasedimentary origin.

C. Contact occurrence

Spinel and phlogopite-bearing diopsidite occurring between marble and gneiss is interpreted to have formed by contact metasomatism during metamorphism.

D. Marble gulch occurrence

The forsterite-spinel assemblage in a layer of this marble outcrop is consistent with granulite facies peak metamorphism. Retrograde break-down of forsterite-calcite to diopside-

dolomite, and the later alteration of diopside to pargasite subsequently occurred. In the retrograde reactions, equilibrium was not achieved on < 1 cm scale, even though parts of the marble layer contain large (6 mm) euhedral pargasite crystals. The lack of alteration in spinel suggests that it was stable during the retrograde formation of diopside and pargasite.

4.5.1.3 Kimmirut area

A. Soper River occurrence

Diopside-dolomite pseudomorphic mixtures in marble at Soper River probably formed from the break-down of forsterite and calcite, either because of increasing X_{CO2} or decreasing metamorphic grade (Fig. 4.21). The stability of a forsterite-pargasite-spinel-bearing assemblage (as observed in the samples, with forsterite inferred from the diopside-dolomite replacements after subhedral mineral grains) in Soper River marble is possible at peak metamorphic conditions and $0.3 \leq X_{CO2} \leq 0.5$.

B. Soper Falls occurrence

Spinel-bearing humitite could not be modeled with Perple_X due to the absence of humite in the thermodynamic database. Given the significant development of humite and its high volatile content (which are not likely present in such abundance during retrograde metamorphism, *e.g.*, retrograde assemblages described by Belley *et al.* 2017, St-Onge *et al.* 2007), it is probable that humite-spinel formed during prograde/peak metamorphism. Fluorine stabilizes humite-group minerals at high temperature (Grützner et al. 2015), and "[t]he stability fields for the individual humite minerals expand to more CO_2-rich fluid compositions with increasing fluorine content and decreasing total pressure" (Rice 1981). Retrograde dolomite and pargasite post-date the humite-spinel assemblage. Diopside and talc cannot be accurately placed into the paragenetic sequence. Diopside is weakly altered to tremolite, and spinel to clinochlore

indicating a minor amount of retrograde alteration to lower metamorphic grade assemblages. Magnesite appears to be part of the humite-spinel assemblage.

C. Soper Lake Camp marble

The peak metamorphic stable assemblage is interpreted to consist of forsterite, spinel, phlogopite, and pyrrhotite based on petrography, and the presence of forsterite is consistent with high-temperature granulite facies peak metamorphism. One amphibole crystal occurs in contact with forsterite, and does not appear to consume the forsterite; however, the small sample size of Fo-Amph contacts is insufficient to infer a stable assemblage.

D. Soper Lake mica mine

The exceptional crystal sizes (*i.e.*, phlogopite to 36 cm across) indicate a significant amount of element transport compared to other LHG metacarbonates. The coarse mineralized layer is poorly exposed due to mining and rock exposure is limited due to its proximity to Soper Lake. However, the lack of intrusive rocks in the vicinity suggests that the occurrence is metasedimentary; it is not known if the extreme coarsening could possibly have been the result of fluid influx from an unknown source. Apatite- and scapolite-bearing pegmatitic recrystallized marble occurs several kilometers to the east. These pods are extremely isolated within the marble sequence, which shows that localized extreme coarsening occurs in this region without a clear indication of intrusive rocks or metasomatic involvement.

E. Qila occurrence

In the calc-silicate pod at Qila (3E-1), pargasite, scapolite, spinel, phlogopite, and carbonate (dolomite, potentially calcite) form a stable assemblage. Spinel, calcite, phlogopite, and pargasite form a stable assemblage in the carbonate-rich zone below it (sample 3E-2). In the contiguous spinel-bearing marble, forsterite forms a stable assemblage with phlogopite, but

spinel was not observed in direct contact with either mineral due to the dispersed nature of non-carbonates. Both diopside and pargasite occur in contact with spinel and as isolated grains. Forsterite locally is rimmed by diopside coronae, some of which have an outer pargasite corona. At peak metamorphic conditions (810 °C, 8.0 kbar, St-Onge *et al.* 2007), a *T-X* pseudo-section (Fig. 4.22) indicates that forsterite, spinel, phlogopite, calcite, and dolomite form a stable assemblage at peak metamorphic conditions with X_{CO2} between ~ 0.07 and 0.27. An increase in X_{CO2} or decrease in metamorphic grade led to the formation of diopside and pargasite in a stable assemblage with forsterite, spinel, phlogopite, calcite and dolomite without crossing the spinel-out boundary. This new equilibrium assemblage led to the partial replacement of forsterite by diopside and pargasite.

F. Trailside occurrence

Spinel at Trailside occurs in two rock types, a silicate-rich rock (3F-1) and a carbonate-rich one (3F-2). In the silicate-rich unit, phlogopite, calcite, spinel, and a sericite-replaced unknown form a stable assemblage. The retrograde assemblage consists of muscovite, chlorite, calcite, albite, and corundum. It is hypothesized that sericite alteration completely replaced feldspar, scapolite or nepheline, which are known to occur in Kimmirut-area metacarbonates (Belley *et al.* 2017). Sericite replacement is significant, and may have resulted in a change in bulk composition, making thermodynamic modelling of this unit unreliable. Both scapolite and K-feldspar occur in trace quantities in sample 3F-2.

A *T-X* pseudosection for a representative sample of the phlogopite-calcite-spinel rock (3F-2; Fig. 4.23) shows that spinel was stable at peak metamorphic conditions. Unidimensional analysis of the predicted modal composition of the rock along a X_{CO2} path indicates that assemblages are dominantly composed of phlogopite and carbonate, with subordinate spinel and

other accessory minerals. At peak metamorphic conditions, scapolite and spinel are only expected to occur coevally at very high X_{CO2}. It is also possible that an accessory silicate was replaced by scapolite during retrograde metamorphism. Corundum formed at the expense of spinel during retrograde metamorphism.

4.7.1.4 Waddell Bay occurrence

The Waddell Bay spinel locality was not studied in the field, and thus little information can be extracted from the present samples. Phlogopite, spinel, diopside, and calcite formed coevally based on textural relations. The coarse-grained orange calcite is reminiscent of metasomatic calcite vein occurrences in the Grenville Province (P.M. Belley field observations in the Wakefield, Bryson, and Otter Lake areas, Quebec).

4.7.1.5 Unspecified occurrence on Hall Peninsula

Forsterite, spinel, and phlogopite are interpreted to have formed at peak metamorphic conditions followed by pargasite and diopside formation by either an increase in X_{CO2} or a decrease in metamorphic grade, similar to that observed in Qila marble.

4.5.2 Metasedimentary spinel protoliths

4.5.2.1 Protolith composition of calc-silicate rocks and marbles

Metasedimentary (*sensu stricto*) spinel occurrences in the LHG consist of magnesitic marl (Soper Falls humitite), dolomitic marl (calc-silicate rocks), and dolomitic and dolomite-bearing limestone protoliths (Fig. 4.25; Table 4.16A and B). Interestingly, other significant gemstone occurrences in the LHG are classified as meta-marl: the Beluga sapphire protolith is interpreted to be dolomitic marl (Belley *et al.* 2017), and the Soper River lapis lazuli an evaporite-bearing marl (Hogarth & Griffin 1978, present study). Since all three gem minerals

(spinel, corundum, and the feldspathoid haüyne) occur in silica-undersaturated rocks, high Al/Si (therefore siliciclastic mud but not sand) in marl protoliths would favor gem mineral genesis. Metamorphic reactions between intermixed carbonate and muddy sediments favor Si undersaturation at Al/Si abundances that would not result in corundum or spinel genesis in a metapelite with an identical Al/Si fraction (*i.e.*, in the metapelite with identical Al/Si, silica would be saturated). Nonetheless, the effect of *P-T* history on the mineral assemblage should not be disregarded, since it can also be an important control on whether spinel or corundum forms at all; this is true of the Beluga sapphire occurrence, where sapphire formation was only made possible by the localized retrograde break-down of nepheline and scapolite. While most spinel-bearing silicate rocks have Al:Si ratios corresponding to mud/clay (see Table 4.16, Fig. 4.24), spinel-bearing rock at the Trailside occurrence is exceptionally rich in Al relative to Si and is similar in Al/Si composition to kaolinite-rich claystone (*e.g.*, claystone sample AR-41 of López *et al.* 2005, Al/Si ≈ 0.7 g/g). The Trailside spinel-bearing rock, diopsidite, and diopsidite in the Trailside area contain elevated K/Al (0.4-0.8 mol/mol) due to their higher phlogopite content. This elevated K content relative to Al may be due to initial abundances of K-feldspar or illite in the protolith, or from K infiltration (a highly mobile element) with fluid during diagenesis/metamorphism. Trailside K/Al molar fractions are significantly higher than those of other calc-silicate rocks in the LHG (K/Al ≤ 0.3), average clay/shale (0.2, Parker 1967, Turekian & Wedepohl 1961), and sandstone (0.3, Turekian & Wedepohl 1961). López *et al.* (2005) noted arenite with K/Al = 0.9, likely owing to high K-feldspar content in the sandstone. Another possible origin for potassium enrichment in the spinel-bearing rocks is that it was sourced from the contiguous diopside-rich unit inferred to be metamorphosed sandstone (*i.e.*, the sandstone could have had a relatively high K/Al).

The relative proportion of sand and mud (estimated based on Al/Si relative abundance) does not appear to affect the occurrence of spinel so long as Al is sufficiently abundant in the rock; there is considerable overlap in the estimated protolithic composition of spinel-bearing, phlogopite-rich spinel-absent, and phlogopite-poor spinel-absent marbles (Fig. 4.25). Spinel genesis in marbles in the LHG samples is limited by high K and low Mg activities, as discussed below. A lack of Si relative to Al in a K-rich magnesian marble would also result in spinel formation.

LHG calc-silicate rock samples (including most spinel-bearing silicate rocks) have roughly the same molar abundance in Ca relative to Mg (Fig. 4.26) and thus the original carbonate fraction in the protolith is interpreted to have been predominantly dolomite (Tables 4.16A and B). Spinel-bearing humitite from Soper Falls is exceptionally Mg-rich and Ca-poor; it is interpreted to have been a magnesite-rich marl layer (an abundance of magnesian clays in the protolith could also explain the high Mg content), however the poor exposure did not allow for sampling of carbonate rocks in contact with the humitite. The possibility that Mg was enriched in the humitite unit and depleted in the contiguous marble should not be disregarded. Marble samples range from dolomitic to calcitic; most consist of dolomite-rich calcite marble.

4.5.2.2 Spinel and meta-evaporite

Garnier *et al.* (2008) and Giuliani *et al.* (2018) noted a relationship between selected metacarbonate-hosted gem deposits and evaporites (*i.e.*, lapis lazuli and East Asian ruby deposits). Giuliani *et al.* (2018) suggested that the presence of meta-evaporites or their indicators (*e.g.*, high salinity fluid inclusions, lazurite/haüyne, marialitic scapolites, tourmalinites, aspidolite, Warren 2016) could be used as exploration criteria for gem deposits in metamorphosed platform carbonate sequences. Hogarth & Griffin (1978) convincingly showed

that the Soper River lapis lazuli is a meta-evaporite citing the following evidence: (1) the lapis lazuli has well-developed layering parallel to the regional foliation, suggesting that it is metasedimentary; (2) the area has a scarcity of intrusive rocks, which does not support a contact metasomatic origin; and (3) the abundances of Na, K, S, Cl, Br, F, and Fe are consistent with evaporite-related sediments. Indeed, the Na and Cl concentrations in Soper River lapis lazuli (this study) are extraordinarily high (*i.e.*, ~6.6 wt. % Na_2O and 3170 µg/g Cl) relative to other Lake Harbour Group meta-marls (≤ 2.71 wt. % Na_2O and ≤ 1160 µg/g Cl, at Beluga sapphire and Qila, respectively) and a hypothetical shale-limestone mixture of average composition.

Most spinel occurrences on Baffin Island are interpreted to have dolomitic limestone and dolomitic marl protoliths that are consistent with typical non-evaporitic platform sediments transformed by subsequent diagenetic effects (*i.e.*, dolomitization). Evaporitic rocks typically have high Mg contents, relatively low Fe (caused by the widespread occurrence of Mg-rich clays), and evaporitic argillites are characterized by high K, Li, F, and B contents (with the exception of low Li concentrations in Mg-rich evaporites), and low Na contents (with the exception of halite-bearing evaporites; Moine *et al.* 1981). The abundance of Mg relative to Ca at most spinel occurrences is adequately explained by diagenetic dolomitization and does not imply an evaporitic origin. Compared to expected concentrations for a similar non-evaporitic protolith of "average" composition, metacarbonates are generally poorer in Li than expected (Tables 4.17A and B). Spinel-bearing rocks at Qila, Trailside, Soper Falls, and in Soper Lake mine spinel-bearing marble are richer than expected in B, F, and Cl. Spinel-bearing rock at the main occurrence on Glencoe Island and Trailside area marble are also higher than expected in F and Cl. High F and Cl contents reflect the presence of pargasite, phlogopite, humite, and/or scapolite. While the latter rock samples are enriched in F and Cl, these elements are volatiles

(expected to be highly mobile) and may not be representative of the protolith. Moreover, pore fluid salinity can significantly increase at high grades of metamorphism, such as in the amphibolite facies metamorphism of impure marbles and progressive granulite facies metamorphism (Yardley & Graham 2002), which would be expected to lead to increased incorporation of F and Cl relative to OH in phlogopite, pargasite and humite. In addition, a lack of mineral species that can readily incorporate evaporite-sourced volatiles may preclude a rock from retaining its evaporitic geochemical signature during metamorphism.

The composition of humitite at Soper Falls, compared to other LHG rock samples analyzed for the same elements, is much more extreme in concentrations of boron (304 μg/g), fluorine (> 2 wt. %), and magnesium (46.4 wt. % MgO), which we interpret as sufficiently above expected values so as to indicate a probable meta-evaporitic origin consistent with the criteria of Moine *et al.* (1981).

The presence of evaporites at most spinel occurrences is therefore unlikely, and evaporites are not genetically related to gem spinel: metamorphism of a protolith with the correct proportions of major elements, which occur in typical non-evaporitic carbonate platform sedimentary rocks, is the only criteria. Some geochemical aspects of evaporites noted by Moine *et al.* (1981) would, in theory, have a negative effect on gem spinel potential (*i.e.*, K enrichment, see *Geochemical factors in spinel genesis* below) or a positive one (*i.e.*, low Fe content, see *Controls on spinel color* below).

4.5.3 Geochemical factors in spinel genesis

Spinel-bearing calc-silicate rocks are richer in Al relative to Si compared to calc-silicate rocks devoid of spinel (Fig. 4.27A) in spite of having similar relative concentrations of Ca and Mg (see section above). The relative abundances of Al and Si appears to be an important control

on whether spinel could form; calc-silicate rocks with low Al/Si are at best silica-saturated (no silica undersaturated phases such as Al oxides, forsterite, haüyne; *e.g.*, sulphide-rich diopsidite at Glencoe Island), and at worst, are silica oversaturated (*e.g.*, quartz-bearing diopsidite near Trailside). Most calc-silicate rocks have K/Al molar fractions of 0.1-0.3 while the Trailside spinel-bearing rock, diopsidite, and diopsidite in the Trailside area contain elevated K/Al (0.4-0.8) due to their higher phlogopite content. Since all calc-silicate rocks studied contain Al > K, potassium activity is not expected to control whether or not spinel occurs. In silicate-rich metacarbonates adequate for thermodynamic modelling (Figs. 4.20, 4.23), spinel forms part of the stable mineral assemblage across the range of possible fluid X_{CO2} at peak metamorphic conditions. Therefore, the dominant geochemical control on spinel genesis in magnesian calc-silicate rocks under these *P-T* conditions (granulite facies, 810 °C and 8.0 kbar) appears to be the abundance of Si relative to Al. One exception applies to Qila (described below).

In contrast with calc-silicate rocks, spinel-bearing and spinel-absent marbles overlap in Al/Si and Ca/Mg ratios, but differ significantly in K/Al molar ratios. Spinel-bearing marbles are all very poor in potassium, while other marbles contain K/Al ≈ 1 (Fig. 4.27B). Phlogopite is part of stable mineral assemblages with spinel and forsterite, diopside, or pargasite. The proportions of these minerals are expected to obey the following equilibrium reactions:

(1) $3\ Di + Spl + 2\ Dol + 2\ K^{+}_{(aq)} + 4\ (H_2O,F) + CO_2 \leftrightarrow 2\ Phl + 5\ Cal$

(2) $6\ Fo + Spl + 7\ Cal + 2\ K^{+}_{(aq)} + 4\ (H_2O,F) + 7\ CO_2 \leftrightarrow 2\ Phl + 7\ Dol$

(3) $6\ Prg + 3\ Spl + 9\ Dol + 12\ K^{+}_{(aq)} + 12\ (H_2O,F) + 3\ CO_2 \leftrightarrow 12\ Phl + 21\ Cal$

In all three reactions, low K activity would favor spinel over phlogopite. The forsterite-spinel marbles contain sufficient calcite for the reaction to proceed, and thus K could be a limiting reactant preventing complete incorporation of Al into phlogopite. Similarly, in some

phlogopite-bearing marbles and in Qila calc-silicate rock, dolomite, pargasite, and spinel occur as a stable assemblage, leaving low K activity as a potential limiting factor in the phlogopite-forming reaction. The predominance of Na over K in the pargasites indicates a Na-dominant fluid composition and reinforces the low-K hypothesis. At the contact metamorphic occurrence at Spinel Island, spinel-, phlogopite-, and calcite-bearing diopsidite formed by the metasomatic reaction of a K-Al-Si-rich rock (syenogranite pegmatite, K/Al = 1.2) and phlogopite-bearing calcite marble. The contact metamorphic calc-silicate unit grades into marble, but the contact with unaltered marble has been eroded. However, all of the marble contiguous to the calc-silicate layer has been coarsely recrystallized to calcite with subordinate diopside and phlogopite. Therefore, in diopsidite at Spinel Island, insufficient Mg/dolomite rather than potassium probably prevented complete Al incorporation into phlogopite, which enabled the formation of spinel. Another key factor in spinel genesis in marbles is metamorphic fluid composition: at peak metamorphic conditions in the LHG, spinel only occurs at relatively low X_{CO2} (Fig. 4.21-4.22)

These controls on the presence or absence of spinel are by no means exhaustive, since mineral assemblages vary in composition (*e.g.*, scapolite at Qila; muscovite replacements after possible K-feldspar at Trailside; humite at Soper Falls), and the equilibrium reactions provided above demonstrate that other factors (such as calcite abundance in a forsterite-spinel assemblage) could be important controls on spinel formation in highly Mg-rich rocks.

4.5.4 Origin of cobalt enrichment at cobalt-blue spinel occurrences

4.5.4.1 The distribution of cobalt enrichment and genetic implications

The relatively elevated cobalt concentrations at Qila (9-29 µg/g) and Trailside (9-27 µg/g) vary on outcrop scale, but are isolated to these Co-enriched occurrences: (Qila area) one

impure marble sample contains only 3 µg/g Co (although Co/Fe and Co/Al are relatively high, see below) and a pale violet spinel from another nearby marble sample contains Co below the detection limit; (Trailside area) marbles contain ≤ 2 µg/g Co, and calc-silicate rocks 3F-CS2 and 3F-CS3 contain 5 and 8 µg/g Co, respectively. At Trailside, spinel in two contiguous lithologies contains similar Co concentrations (0.06 wt. % CoO), while spinel from the main calc-silicate pod at Qila (0.07 wt. % CoO) is much richer in the element than spinel in the pargasite-calcite rock and marble. There does exist some evidence for up to meter-scale trace element redistribution; the most notable example is the elevated scandium concentration in Trailside diopsidite (4 µg/g) relative to mica-, spinel-, carbonate-rock (1 µg/g), probably caused by the scavenging of Sc by diopside (diopside preferentially incorporates Sc relative to the associated minerals; PM Belley, unpublished distribution coefficients calculated from LA-ICP-MS data). However, while cobalt and nickel concentrations vary considerably by rock type, they are still relatively high in spinel-poor or spinel-free rock like phlogopite-rich marble at Qila (3E-3-B) and diopsidite at Trailside (3F-4). Thus, based on low Co content of local marbles and the Qila area spinel, it is abundantly clear that Co enrichment does not permeate metasedimentary rocks in the immediate area (~ 30 m radius) around the occurrences – although diffusion of trace elements may have occurred on a ≤ 1 m scale. Therefore, the vivid blue color of the spinel is made possible by highly localized Co-enrichment that is attributed to the protolith; *i.e.*, cobalt enrichment occurred prior to peak regional metamorphism, either as a result of Co-rich allochthonous sediment input or authigenic enrichment during sedimentation, diagenesis, or low-grade metamorphism. Chauviré *et al.* (2015) suggested that, at a cobalt-blue spinel occurrence in Vietnam, cobalt and nickel were mobilized from either the carbonate rocks or nearby amphibolitic rocks by evaporite-derived fluids to the spinel-bearing metacarbonate. This

explanation is inconsistent with observations made at Baffin Island cobalt-blue spinel occurrences.

4.5.4.2 Trace metal contents at Co-rich occurrences compared to other LHG rocks and expected protolith compositions

Cobalt concentrations in rocks at the Qila and Trailside occurrences (9-29 µg/g) are more elevated than in all analyzed LHG metacarbonates in this study (mostly ≤ 6 µg/g, with the exception of a Trailside area calc-silicate rock, 8 µg/g, and a sulphide-rich diopsidite on Glencoe Island, 16 µg/g). Co/Fe and Ni/Fe ratios show a significantly increased differentiation between Qila and Trailside compared to the other rocks (Fig. 4.28). The majority of LHG metasediments appear to form a trend where higher Fe concentrations are accompanied by progressively higher Co. In contrast, Qila and Trailside rock samples are richer in Co, show high variability in Co concentration, and occur in the low Fe range (Fig. 4.29). Cobalt concentrations at Qila and Trailside appear to increase sharply with slight increases in Fe, but the small sample size and high variability limit the reliability of this observation. Interestingly, the trend in Co/Fe *vs* Ni/Fe at Qila and Trailside has a similar slope to that of claystones, shales, and sandstones studied by López *et al.* (2005), but shows that cobalt is very strongly enriched relative to nickel (which itself is in the normal range to enriched) at Qila and Trailside (Fig. 4.28). Cobalt and nickel concentrations show no similar relations with Mn content. The Co-rich rocks at Qila and Trailside are generally above average in Co/Al, but are most distinguished from the other LHG metasediments by Co/Fe, which varies by an order of magnitude (Fig. 4.30).

Period IV metal content profiles vary considerably between shale, sandstone, and sedimentary carbonates. Shales and clays are richest in elements V to Zn, with the exception of Mn, which is more abundant in platform carbonates: average shales/clays contain 20 µg/g Co

and 95 µg/g Ni, in addition to 3.33 wt. % Fe, 670 µg/g Mn, and concentrations of Cu, Zn, Cr, and V from 57 to 130 µg/g (Parker 1967). Average sandstone is poor in Co and Ni (0.3 and 2 µg/g, respectively), Fe (~ 1 wt. %), Mn (50 µg/g), Cu (5 µg/g), and Zn, Cr, and V (16-35 µg/g; Turekian & Wedepohl 1961). Platform carbonates are poorer than the latter rock types in Co (0.1 µg/g), Fe (~0.4 wt. %), Cu, and Cr; with the same V concentration as an average sandstone, but more Ni and Zn than sandstone (Turekian & Wedepohl 1961). Limestone is also typically richer in Mn than both shales and sandstones. Unlike the previous authors, Graf (1962) noted higher average Co concentrations (4.3 µg/g) and Ni concentrations ranging between 7.5 and 17 µg/g in average sedimentary carbonate compositions from different regions. Even when considering the higher cobalt estimate for carbonates, which probably originate from higher Al content (since trace metals are primarily contained within the aluminous fraction of sediment, Schropp & Windom 1988), the calculated estimates for a completely average equivalent to the protoliths at Qila and Trailside contain 1/5 to ½ of the actual cobalt concentration (with two exceptions, sample 3E-2, which is poorer in Co, and 3F-1, in which spinel and phlogopite are under-represented). The main calc-silicate pod at Qila is twice as rich in Co as expected when using the 4.3 µg/g limestone value, despite sampling bias excluding spinel (the principal Co sink). The most anomalously high Co-Ni concentrations are in rocks with low Al/Si (samples 3E-3-A, 3E-3-B, 3F-4); it is possible that Co and Ni were redistributed to the mud-poor protoliths during diagenesis or low-grade metamorphism. In the case of sample 3F-4, the mud content may have been underestimated due to the lower representation of phlogopite relative to most of the diopside-rich zone. Relative to the protolith trace element concentration estimates (Tables 4.17A and B), the rocks at Qila and Trailside are poor in V, Cr, Fe, Mn, Cu, and Zn. The higher than expected Co (and close to expected Ni) concentrations, and lower Fe and Mn are particularly

interesting, since Co and Ni are typically incorporated coevally with either iron or manganese in oxides, hydroxides, or sulphides. It is important to note that LHG metacarbonate rocks are generally much poorer in post Period IV transition metals than expected from the calculated estimate (some exceptions in more sulphide-rich rocks, or high Zn at Glencoe Main). This is perhaps due to differences in the trace element composition of LHG sediments relative to the averages used in the estimate. The actual/estimate trace element values for Qila and Trailside are nonetheless much richer in Co-Ni, and poorer in other Period IV metals relative to other metacarbonates in the LHG.

4.5.4.3 Possible effects of metamorphism

In a comparative study of a single metasediment formation, Shaw (1954) found relatively constant concentrations of trace elements (including Li, V, Cr, Co, Ni, Cu, Pb) for low, medium, and high-grade metamorphosed rocks of a specific metapelite unit, with a minor decrease of Ni and Cu, and increase of Li and Pb correlating with K-metasomatism. A decrease in Ni could increase Co/Ni ratios, which are discussed below. However, given the results of Shaw (1954), we proceed under the assumption that trace metal concentrations were not significantly modified by high-grade metamorphism.

4.5.4.4 Possible explanations for the trace metal signature at Qila and Trailside

Since expected concentrations based on sediment averages do not adequately explain the Co-Ni enrichment (conservatively twice that expected in a similar protolith of average trace metal composition) together with low V, Cr, Fe, Mn, Cu and Zn abundances, the potential source of Co and Ni must have high Co/Al and very high Co/Fe and Ni/Fe ratios. We explore possible sources of Co enrichment.

Price (1972) measured maximum concentrations of approximately 900 µg/g Co and 950 µg/g Ni in syngenetic sedimentary pyrites; these are extreme deviations from the average concentrations (41 µg/g Co, 65 µg/g Ni). Even at the maximum outlier value for sedimentary pyrite Co, the Co/Fe ratio (19×10^{-4} g/g) is smaller than at Qila and Trailside (24×10^{-4} to 51×10^{-4} g/g), and sulphides are very rare at these occurrences (*i.e.*, no traces of original sulphides, although this could change with metamorphism). The average Co/Fe for sedimentary pyrites is 0.9×10^{-4} (Price 1972), considerably lower than all LHG metasediments analyzed in this study (1.7×10^{-4} to 8.2×10^{-4}). Moreover, Cu concentrations at Qila and Trailside suggest strong Cu depletion relative to the expected protolith composition; this is contrary to expected Cu concentrations in sediment deposited under euxinic conditions, where Cu would be preserved in sulphides. In Paleoproterozoic black shale-hosted sedimentary pyrite, the trace elements Ni, Cu, and As occur in higher concentrations than Co (Gregory *et al.* 2015). This is consistent with the interpretation that Co was not sourced from sedimentary pyrite.

Exceptionally Co-rich pyrite (Co/Fe = 0.011 g/g) containing a relatively low abundance of As, Pb, Zn, and Cu occurs at Pyrite Hill, Australia in a metamorphosed hydrothermal alteration zone within a granulite facies metasedimentary sequence (albite rock [interpreted to be metamorphosed tuffaceous rock], psammite, metapelite, amphibolite; Plimer 1977). However, the pyrite's very high Co/Ni (6.7, attributed to a volcanic exhalative origin by Plimer 1977) and its association with hydrothermal quartz are incompatible with a potentially similar mode of enrichment in cobalt-enriched rocks at Qila and Trailside, where Co enrichment is highly localized, the rocks generally have low silica contents, and much lower Co/Ni (0.6 to 1.5).

In sediments, Co and Ni can be leached from lower parts of the sedimentary sequence in suboxic conditions and become enriched in oxic sediments near the sediment-water interface

during early diagenesis (Heggie & Lewis 1984, Gendron *et al.* 1986, Shaw *et al.* 1990). These oxic conditions simultaneously result in the loss of Cr and V (while several factors influence the behaviour of Cu; Shaw *et al.* 1990). Stockdale *et al.* (2010) experimentally examined the association of Co with Fe and Mn in sediment columns, and suggest that Co is significantly more enriched in authigenic Mn oxides than Fe oxyhydroxides, but that Fe-Co maxima in some experiments were probably caused by sulphide formation by sulphate reduction. Co/Fe and Co/Mn ratios in Stockdale *et al.*'s experiment remain orders of magnitude smaller than that at Qila and Trailside.

Overall, Co-Ni enrichment in an oxic zone of sediments during early diagenesis best explains the unusually high Co-Ni and low Cr and V at Qila and Trailside with two exceptions: (1) Co-Ni would need to be sourced from underlying Co-Ni bearing units, but the surrounding rock is dominantly carbonate that is expected to contain little Co and Ni (*i.e.*, host marbles are Co-Ni poor, present study; average limestone is also Co-Ni poor, Turekian & Wedepohl 1961; while sulphides can occur in limestone/marble, high Co-Ni from sulphides would be expected to be accompanied with higher Fe concentrations); and (2) inconsistency with the relatively low Mn concentration. Furthermore, the much smaller Co/Fe and Ni/Fe values, and the apparent correlation of Co and Fe which cannot be adequately explained by the distribution of Fe-Co-rich phases in different lithologies, would suggest the concentration of Co and Ni in a Fe-bearing phase as opposed to Mn. In oxic conditions, if Co and Ni were concentrating primarily in Fe (oxy)hydroxide, higher whole rock Mn contents would nonetheless be expected; for example, particularly Fe-rich shallow marine ferromanganese concretions from the Black Sea have a Mn/Fe mass fraction of ¼ (Table 79 of Carmichael 1989). If Co and Ni were concentrating in authigenic sulphide, higher Cr, V, and Cu concentrations would be expected under these

conditions. Therefore, perhaps Co-Ni- and Mn initially concentrated in the oxic layer of sediment, which was later reduced during diagenesis, leading to the concentration of Co and Ni in Fe-sulphide, their diffusion to contiguous mud-poor units, and the loss of some Mn. There are, however, only traces of sulphide present at Qila and Trailside, and so for this hypothesis to be possible, sulphides must have been destroyed during metamorphism. Concentration of Co in Fe-oxide or siderite is rejected as a possible explanation since they would not result in coeval Mn loss.

Interestingly, meta-marl at the nearby Beluga sapphire occurrence shows the opposite geochemical trend to Qila and Trailside; it is enriched in V and Cr, and significantly impoverished in Co and Ni, which is interpreted to be the result of reducing early diagenetic conditions (Belley *et al.* 2017). An alternative hypothesis is that Beluga rock was initially enriched in Cr, V, Co, Ni (*i.e.*, deposition reduced euxinic conditions with formation of sedimentary pyrites containing Co and Ni) followed by subsequent dissolution of the sulphides during diagenesis or early metamorphism, resulting in loss of Co and Ni.

Cobalt enrichment during diagenesis or metamorphism could have been facilitated by high initial sediment Co content due to the sediment source composition. Ultramafic rocks, and laterites derived from their weathering (*e.g.*, Eliopoulos & Economou-Eliopoulos 2000), have elevated Co/Fe and Co/Mn values (*e.g.*, data of Turekian & Wedepohl 1961), however this is accompanied by very low Co/Ni (0.075, Turekian & Wedepohl 1961). Basaltic rocks, compared to other igneous rock types, are more similar to the average trace metal mass fractions for Qila and Trailside in Co/Fe (5.5×10^{-4} *vs* 35×10^{-4}), Co/Mn (320×10^{-4} *vs* 715×10^{-4}), Ni/Fe (15×10^{-4} *vs* 46×10^{-4}), Ni/Mn (870×10^{-4} *vs* 940×10^{-4}), and Co/Ni (0.37 *vs* 0.86). "Potential sources for detritus of the Lake Harbour Group […] have yet to be identified," but Sc/Th ratios in LHG

metapelites suggest at least partial derivation from ferromagnesian-rich sources (Thériault *et al.* 2001).

4.5.5 Controls on spinel color

4.5.5.1 Spinel composition

Most spinel in Lake Harbour Group metacarbonates are violet, often with greyish overtones; spinel at Spinel Island and Glencoe Beach is dark blue; spinel at Qila and Trailside is vivid blue; spinel at the Soper Lake mica mine is greyish-purple; and spinel in metasomatite on the unnamed island in Markham Bay is black.

The purple color in spinel from the Soper Lake mine is probably due iron in combination with its higher than average Cr_2O_3 concentration (0.14 wt. %), which produces a red hue in spinel even at low concentrations (0.1 wt. %, Kleišmantas & Daukšytė 2016). The dominant chromophore present in violet and blue spinel is assumed to be iron based on visible absorption spectra mesurements on gem spinels (see section 1.5.2). Vivid blue spinel from Qila and Trailside are colored vivid blue by cobalt (0.03 – 0.07 wt. % CoO) and likely has colour contribution of iron; the darker hue in Trailside spinel may be due to higher FeO contents (~ 5 wt. %) relative to Qila (~ 2.3 – 3.6 wt. %).

In LHG rocks, spinel is generally darker in color with increasing iron content: (1) lighter colored spinel contains 1.37-3.55 wt. % FeO; (2) spinel with slightly darker saturation contains 2.65-5.20 wt. % FeO, and were these materials sufficiently transparent and cut into gemstones 1 carat or larger, would appear overly dark, thus lowering their marketability; (3) spinel too dark to produce gemstones, 3.33-7.34 wt. % FeO; and (4) black spinel containing 8.61 wt. % FeO. While lower Fe concentrations (max 6 wt. % FeO, ideally < 4 wt. %) favor attractiveness in spinel (dark spinels have low commercial value), However, overlap between Fe concentrations and the

categories of spinel attractiveness in hand sample deserves further study (*i.e.*, quantifying visible light absorption spectra) before narrower conclusions can be made.

4.5.5.2 Relation of spinel Fe content to whole rock composition and mineral assemblage

Higher concentrations of iron in spinel result in darker coloration, which controls the mineral's attractiveness and potential value as a gemstone. Therefore, understanding the relationship between whole rock and spinel Fe concentrations could help in understanding rock types (protoliths or reactive components) that have the potential to produce high quality gem spinel. Iron is preferentially partitioned into spinel relative to the associated silicates (*i.e.*, spinel X_{Fe} is higher than that for any associated silicate; see EPMA data) and extremely strongly partitioned into spinel relative to carbonates. Paired whole rock and spinel Fe concentrations generally follow a linear correlation in that most spinel, have approximately 4.3× more Fe by weight % (Fig. 4.31). One exception exists: the spinel at Soper Falls is only about 1.5× richer in Fe. This may be explained by the high abundance of humite, in which Fe substitutes for Mg. While Fe is preferentially incorporated into spinel relative to humite, the distribution coefficient is not so significant as to negate the effects of a very high abundance of humite relative to spinel (~ 20× by volume).

It was established above that in LHG samples, only spinel with < 6 wt. % FeO appears sufficiently light colored to represent adequate gem material, or < 4.7 wt. % Fe. In most rocks described above, this would correspond to a Fe concentration of 1.09 wt. % Fe or less. "Expected" protolith composition estimates based on average shale, sandstone, and limestone are above the Fe threshold (~ 2 wt. % Fe; Tables 4.17A and B) for spinel-bearing calc-silicate rocks at Glencoe (3A-SPL-1), Qila (3E-2), and Trailside (3F-2), which suggests that lower-than-average Fe contents could be an important control on spinel gem quality in meta-marl. It should

be repeated that mineral assemblage and mineral abundances can have a significant effect on the concentration of Fe in spinel, as shown at Soper Falls. Iron sulphides may also limit Fe availability to spinel, and their abundance could favorably improve the gem-quality of spinel as a result of this preferential incorporation.

While the presence of coeval pyrrhotite or pyrite would improve spinel gem quality by preventing the latter from becoming overly dark, it may also limit or prevent the formation of vivid blue cobalt-enriched spinel, since cobalt is strongly partitioned in pyrrhotite relative to spinel (*e.g.*, see spinel-pyrrhotite pairs from the same rock samples in Tables 4.3 and 4.13).

4.5.6 Exploration criteria

The most significant gemstone occurrences in the Lake Harbour Group are all hosted in dolomitic meta-marls of variable composition (Beluga sapphire, Belley *et al.* 2017; Soper River lapis lazuli meta-evaporite, Hogarth 1971, Hogarth & Griffin 1978; spinel-bearing calc-silicates including cobalt-blue spinel). While dolomite-bearing marbles also contain spinel, the significantly higher spinel concentrations in calc-silicate rocks are more suitable for hard rock gem mining (the relative lack of fluvial environments make Baffin Island an unlikely source of placer-hosted gemstones). Regions with abundant calc-silicate layers intercalated with marble are highly prospective for gem deposits, and these layers could potentially be traced stratigraphically. Local variations in Al/Si and K/Al can lead to spinel genesis in rocks otherwise devoid of the mineral. The favorable geology, widespread abundance of metacarbonates, known gemstone occurrences, and excellent rock exposure make southern Baffin Island one of the most significant prospective areas for colored gem exploration – yet, due to its geographic isolation, one that has yet to be explored in any significant capacity.

The occurrence of two unique cobalt-blue spinel occurrences in the same area on Baffin Island is very promising in terms of gem potential. However, the origin of cobalt enrichment in metacarbonates remains poorly understood, making targeted exploration difficult.

4.6 Conclusions

4.6.1 Origin of spinel occurrences

Spinel occurrences in the Lake Harbour Group mostly consist of metasedimentary (*sensu stricto*) deposits, with the exception of the two occurrences in Markham Bay, which are metasomatic. The origin of the Waddell Bay spinel occurrence cannot be ascertained but may be metasomatic. Spinel-bearing calc-silicate rock at Spinel Island in Markham Bay formed from the reaction of syenogranite pegmatite with dolomite-bearing marble. All spinels occur in marble and calc-silicate/silicate-rich metacarbonate rocks. Minerals occurring with spinel as part of a stable assemblage include calcite, dolomite, phlogopite, pargasite, diopside, humite, forsterite, scapolite, anorthite, and pyrrhotite. Spinel is interpreted to have formed during peak granulite facies metamorphism. Spinel at Trailside and Spinel Island is locally replaced by retrograde corundum, chlorite, and other minerals.

4.6.2 Metasedimentary protoliths

Spinel-bearing metacarbonate rocks are interpreted to have the following protoliths: (1) impure dolomite-bearing and dolomitic limestone; (2) dolomitic marl; and (3) evaporitic magnesitic marl (Soper Falls humitite). The protoliths are relatively similar to the Beluga sapphire occurrence (dolomitic marl with lower Al/Si than in the spinel-bearing rocks) and the Soper River lapis lazuli rock (evaporitic marl). Spinel-bearing calc-silicate rocks have Al/Si relative abundances within range of sandy shale, shale, claystone, and kaolinite-rich claystone.

There is no compelling evidence for the presence of evaporites except at Soper Falls, where the humitite is particularly enriched in F, B, and Mg.

4.6.3 Geochemical factors in spinel genesis

Spinel genesis in LHG metacarbonates is favored by: (1) the low abundance of silica relative to alumina, the primary control on whether spinel forms in most calc-silicate rocks; (2) low potassium activity limiting the formation of phlogopite and thus leaving Al available for spinel formation; (3) low X_{CO2} in marbles; and (4) insufficient quantities of Mg or dolomite reactant in diopsidite limiting Al incorporation into phlogopite to form spinel.

4.6.4 Origin of cobalt enrichment at Qila and Trailside

The spatial distribution of Co-Ni enrichment at Qila and Trailside and the surrounding (~ 30 m) areas is indicative of highly localized enrichment, with possibly only small-scale (≤ 1 m) diffusion during peak metamorphism. This suggests that trace metal concentrations in cobalt-blue spinel bearing metacarbonates are a result of protolith composition and not due to the infiltration of metal-rich metamorphic fluids. Cobalt and Ni are therefore expected to have been enriched in the original sediment, or during diagenesis or low-grade metamorphism. Concentrations of Co (especially) and Ni are anomalously high (conservatively twice the expected cobalt concentration in a comparable metasediment), while concentrations of Fe, Mn, V, Cr, and Cu are much lower than expected; a chemical signature that, with the exception of low Fe and Mn, could be caused by element enrichment/depletion in the oxic layer of sediment during early diagenesis. I propose the possibility that later sulfide formation within the rock during low-grade metamorphism could have retained Fe, Co, and Ni and resulted in some loss of Mn (which would have been initially enriched together with Co and Ni in oxic conditions).

Ultimately, such explanations are speculative since the protoliths have undergone diagenetic, structural, and metamorphic transformations.

4.6.5 Controls on spinel color

Vivid blue spinel at Qila and Trailside are enriched in cobalt, containing 0.03-0.07 wt. % CoO. Spinels from other occurrences are blue and violet, and Fe is the probable chromophore. Lighter-colored spinels contain 1.37-3.55 wt. % FeO. Slightly darker spinels, which could only produce small gemstones (stones over a carat would likely be too dark for use as a gem), contain 2.65-5.20 wt. % FeO. Blue and violet spinels that are too dark for use as a gemstone contain 3.33-7.34 wt. % FeO. It is estimated that spinel should have concentrations below 6 wt. % FeO to have a chance of being suitable for use as a commercial gemstone.

Spinel Fe concentrations are generally 4.3× higher than in the host rock, with the exception of the very silicate-rich humitite rock at Soper Falls (1.5×). Considering the estimated 6 wt. % FeO cut-off for gem spinel, dolomitic marl protoliths would require < 1.09 wt. % Fe to have potential for gem-quality spinel. This value is lower than that expected for similar protoliths of "average" composition (~ 2 wt. % Fe).

Pyrrhotite strongly partitions Fe and Co relative to spinel, therefore an abundance of sulfide is expected to improve the gem quality/attractiveness of spinel by decreasing the amount of Fe incorporated into spinel (thus preventing overly dark colors), but would also prevent the formation of vivid blue, Co-enriched spinel in rocks that have suitable cobalt concentrations.

4.6.6 Exploration criteria

Marbles containing abundant metamorphosed dolomitic marl (magnesian calc-silicate) layers offer the best potential for gemstone discoveries in southern Baffin Island. Small, sometimes localized variations in whole rock Al/Si and K/Al could result in the occurrence of

spinel. Other significant gemstone occurrences on Baffin Island (sapphire and lapis lazuli) are hosted in relatively similar rock types. Meta-marl-rich units may be traceable stratigraphically.

4.7 Tables

Table 4.1: Spinel occurrences studied

Region	Locality	Location #
Markham Bay	**"Spinel" island**	**1A**
	Unnamed island	**1B**
Glencoe Island	**Main occurrence**	**2A**
	Marble beach occurrence	**2B**
	Contact occurrence	**2C**
	Marble gulch occurrence	**2D**
Kimmirut area	**Soper River occurrence**	**3A**
	Soper Falls occurrence	**3B**
	Soper Lake Camp marble	**3C**
	Soper Lake mica mine	**3D**
	Qila occurrence	**3E**
	Trailside occurrence	**3F**
Hall Peninsula	**Waddell Bay occurrence**	**4**
	Unspecified marble occurrence	**5**

Table 4.2A: South to North section of lithologies surrounding the west extremity of the diopsidite band, Spinel Island, Markham Bay.

Thickness (m)	Rock	Description
> 10	Marble (1A-M)	Medium-grained, dolomite-bearing calcite marble with subordinate phlogopite and forsterite. Contains sparsely distributed layers (< 10 cm) containing very coarse-grained clots of phlogopite. A representative sample of pale grey marble contains 5% phlogopite, subordinate forsterite, and trace pyrrhotite.
1.5-2.5	Diopsidite	Medium- to coarse-grained, locally pegmatitic greenish gray diopsidite with subordinate phlogopite, locally common calcite, and rare spinel. Calcite occurs in randomly oriented veins up to 15 cm thick and 2 meters long, and pods up to 30 cm in maximum dimension.
1	White Kfs rock	Discontinuous mass of white K-feldspar rock containing a few small pods and veinlets of diopsidite.
0.4	Diopsidite	Diopsidite, in one area containing a 30 cm-thick pod of marble.
1	C. White Kfs rock	Coarse-grained white K-feldspar with trace apatite and allanite.
1.3	Pyroxene-bearing feldspar rock	Fine-grained, foliated rock composed, by volume, of 35 % albite, 35 % K-feldspar, 16 % clinopyroxene ($X_{Mg} \approx 0.5$), 12 % orthopyroxene ($X_{Mg} \approx 0.4$), 1.5 % ilmenite, 0.5 % pyrrhotite, trace apatite and zircon.
> 5	Lineated granitoid rock	Pale beige rock composed primarily of fine-grained feldspar (albite, K-feldspar), and coarser-grained quartz as masses elongated along the lineation. Some parts of the rock contain black calcic amphibole porphyroblasts averaging 1 cm ($X_{Mg} \approx 0.4$), or local enrichments in fine-grained ilmenite. Trace apatite, biotite, and rare monazite.

Table 4.2B: South to North section of lithologies surrounding the spinel-bearing zone of the diopsidite band, Spinel Island, Markham Bay.

Thickness (m)	Rock	Description
> 6	Marble	Medium- to coarse-grained phlogopite, and phlogopite-diopside marble.
≥ 0.1	Recrystallized marble	Very coarse to pegmatitic calcite containing up to 15 % euhedral greyish-green diopside prisms and phlogopite crystals. 3-4 cm crystals common. Contact with marble eroded.
1.5-2.5	Diopsidite (1A-SPL)	Medium-grained to pegmatitic diopside with phlogopite, calcite, local spinel, and anorthite. See text.
> 10	Syenogranite pegmatite (1A-SG)	Pegmatitic microcline (with some perthite) with subordinate quartz, commonly as graphic intergrowth, and plagioclase. Trace titanite, rutile, allanite, and scapolite. Titanite contains 0.5 wt. % Nb (EDS).

Table 4.3A: Average composition of spinel from Markham Bay, Waddell Bay, and Hall Peninsula. Normalized to 32 oxygen atoms per formula unit.

Locality	Spinel Island		Unnamed island		Waddell Bay		Hall Pen.	
Lithology	Spl diopsidite		Spl-bearing metasomatite		Cal-Di-Phl-Spl rock		Spl-bearing marble	
Color	Dark blue		Black		Blue-violet		Dark grey-violet	
Sample	1A-SPL		1B		4		5	
n	5	σ	4	σ	3	σ	4	σ
TiO_2 (wt.%)	0.01	0	0.01	0.01	< 0.01	0	0.01	0.01
ZnO	0.32	0.02	0.29	0.01	0.36	0.02	0.07	0.01
Al_2O_3	70.20	0.16	69.59	0.20	71.47	0.08	70.96	0.33
V_2O_3	< 0.02		< 0.02		< 0.02	0	0.04	0.01
Cr_2O_3	< 0.03		0.06	0.01	< 0.03		0.07	0.04
FeO	6.9	0.07	8.61	0.01	3.90	0.02	2.87	0.15
CoO	< 0.03		< 0.03		< 0.03		< 0.03	
NiO	< 0.03		< 0.03		< 0.03		< 0.03	
MnO	0.08	0.01	0.08	0.01	0.04	0.01	0.03	0.02
MgO	22.89	0.14	22.17	0.13	24.66	0.09	25.65	0.12
TOTAL	100.40		100.81		100.43		99.70	
Ti (*apfu*)								
Zn	0.046		0.042		0.051		0.010	
Al	16.114		16.040		16.172		16.093	
V							0.006	
Cr			0.009				0.011	
Fe	1.124		1.408		0.626		0.462	
Co								
Ni								
Mn	0.013		0.013		0.007		0.005	
Mg	6.646		6.463		7.058		7.358	

Table 4.3B: Average composition of spinel from Glencoe Island. Normalized to 32 oxygen atoms per formula unit.

Locality	Glencoe main		Glencoe main		Glencoe beach		Glencoe contact		Glencoe gulch	
Lithology	Spl-bearing pod		Spl-bearing pod		Spl-bearing marble		Spl diopsidite		Fo-Prg-Spl marble	
Color	Violet		Dark grey-violet		Dark blue		Dark grey-violet		Violet	
Sample	2A-SPL-1		2A-SPL-3		2B		2C		2D	
n	4	σ	3	σ	4	σ	3	σ	4	σ
TiO_2 (wt.%)	< 0.01		< 0.01		0.01	0.02	< 0.01	0	0.01	0.01
ZnO	2.32	0.04	4.25	0.07	0.13	0.03	0.41	0.01	< 0.03	
Al_2O_3	69.43	0.20	69.04	0.11	70.31	0.97	70.04	0.09	71.62	0.20
V_2O_3	< 0.02		0.04	0.02	< 0.02		< 0.02		0.03	0.02
Cr_2O_3	0.03	0.01	< 0.03		< 0.03		< 0.03		< 0.03	
FeO	4.88	0.09	4.23	0.05	7.34	0.08	7.27	0.05	1.72	0.05
CoO	< 0.03		< 0.03		< 0.03		< 0.03		< 0.03	
NiO	< 0.03		< 0.03		< 0.03		< 0.03		< 0.03	
MnO	0.06	0.01	0.04	0.01	0.09	0.02	0.10	0.01	0.04	0.01
MgO	22.72	0.13	22.12	0.12	22.67	0.27	22.26	0.02	26.65	0.14
TOTAL	99.44		99.72		100.55		100.08		100.07	
Ti (*apfu*)										
Zn	0.337		0.621		0.019		0.059			
Al	16.115		16.094		16.129		16.159		16.092	
V			0.006						0.005	
Cr	0.005									
Fe	0.804		0.700		1.195		1.190		0.274	
Co										
Ni										
Mn	0.010		0.007		0.015		0.017		0.006	
Mg	6.670		6.522		6.578		6.496		7.574	

Table 4.3C: Average composition of spinel from Soper Lake and Soper River area, near Kimmirut. Normalized to 32 oxygen atoms per formula unit.

Locality	Soper River		Soper Falls		Soper Lk camp		Soper Lk mine		Soper Lk mine	
Lithology	Spl-bearing marble		Humitite		Spl-bearing marble		Fo-Carb-Phl-Spl rock		Fo-Spl marble	
Color	Violet		Greyish violet		Violet		Dark greyish purple		Dark violet	
Sample	3A-2		3B		3C		3D-1		3D-M1	
n	5	σ	5	σ	4	σ	4	σ	3	σ
TiO_2 (wt.%)	0.02	0.01	0.01	0.01	0.02	0.01	0.01	0.01	< 0.01	
ZnO	0.05	0.02	< 0.03		0.04	0.02	0.12	0.01	0.18	0.01
Al_2O_3	70.76	0.18	71.79	0.15	72.01	0.18	71.36	0.25	71.08	0.14
V_2O_3	< 0.02		0.04	0	0.04	0.02	0.04	0.02	0.03	0.01
Cr_2O_3	0.05	0.02	< 0.03		0.07	0.02	0.14	0.02	0.05	0.01
FeO	1.74	0.11	2.04	0.03	1.37	0.02	2.65	0.05	3.33	0.07
CoO	< 0.03		< 0.03		< 0.03		< 0.03		< 0.03	
NiO	< 0.03		< 0.03		< 0.03		< 0.03		< 0.03	
MnO	< 0.03		0.04	0.02	0.03	0.01	0.05	0.01	0.05	0.01
MgO	26.69	0.07	26.38	0.09	26.62	0.10	26.06	0.06	25.62	0.05
TOTAL	99.31		100.30		100.20		100.43		100.34	
Ti (*apfu*)	0.003				0.003					
Zn	0.007				0.006		0.017		0.025	
Al	16.031		16.113		16.132		16.061		16.061	
V			0.006		0.006		0.006		0.005	
Cr	0.008				0.011		0.021		0.008	
Fe	0.280		0.325		0.218		0.423		0.534	
Co										
Ni										
Mn			0.006		0.005		0.008		0.008	
Mg	7.649		7.489		7.543		7.419		7.323	

Table 4.3D: Average composition of spinel from Qila and Trailside, Kimmirut area. Normalized to 32 oxygen atoms per formula unit.

Locality	Qila		Qila		Qila		Qila (area)		Trailside		Trailside	
Lithology	Spl-bearing calc-silicate		Prg-Cal rock		Spl-bearing marble		Dolomitic marble		Spl-bearing silicate rock		Cal-Phl-Spl rock	
Color	Cobalt-blue		Sky blue		Cobalt-blue		Pale violet		Cobalt-blue		Cobalt-blue	
Sample	3E-1		3E-2		3E-3-A		3E-M1		3F-1		3F-2	
n	5	σ	4	σ	3	σ	4	σ	4	σ	4	σ
TiO_2 (wt.%)	< 0.01	0	< 0.01		< 0.01		0.02	0	< 0.01	0	< 0.01	0
ZnO	0.16	0.01	0.05	0	0.05	0.02	0.09	0.01	0.05	0.02	0.13	0.02
Al_2O_3	71.39	0.26	71.75	0.04	72.42	0.23	71.72	0.23	70.84	0.27	70.56	0.25
V_2O_3	< 0.02		< 0.02	0	< 0.02		0.04	0.02	< 0.02		< 0.02	
Cr_2O_3	< 0.03		< 0.03		0.04	0.01	< 0.03		< 0.03		< 0.03	
FeO	3.55	0.11	2.25	0.03	2.45	0.07	1.64	0.06	5.20	0.09	5.12	0.02
CoO	0.07	0.01	0.03	0.02	0.03	0.01	< 0.03		0.06	0.01	0.06	0.01
NiO	0.04	0.01	< 0.03		0.03	0.02	< 0.03		< 0.03		< 0.03	
MnO	0.05	0.02	0.04	0.01	0.03	0.01	0.03	0.02	0.06	0.02	0.06	0.01
MgO	24.78	0.17	26.62	0.21	25.57	0.03	26.82	0.04	23.62	0.08	23.65	0.19
TOTAL	100.04		100.74		100.62		100.36		99.83		99.58	
Ti (*apfu*)							0.003					
Zn	0.023		0.007		0.007		0.013		0.007		0.019	
Al	16.184		16.059		16.223		16.070		16.199		16.180	
V							0.006					
Cr					0.006							
Fe	0.571		0.357		0.389		0.261		0.844		0.833	
Co	0.011		0.005		0.005				0.009		0.009	
Ni	0.006				0.005							
Mn	0.008		0.006		0.005		0.005		0.010		0.010	
Mg	7.106		7.536		7.246		7.601		6.832		6.860	

Table 4.4: Average composition of forsterite associated with spinel, southern Baffin Island. Normalized to 4 oxygen atoms per formula unit.

Locality	Soper Lk camp		Soper Lk mine		Soper Lk mine		Qila		Qila		Hall Pen.	
Lithology	Spl-bearing marble		Fo-Carb-Phl-Spl rock		Fo-Spl marble		Spl-bearing marble		Spl-bearing marble		Spl-bearing marble	
Sample	3C		3D-1		3D-M1		3E-3-A (green Fo)		3E-3-A (grey Fo)		5	
n	3	σ	4	σ	3	σ	3	σ	3	σ	4	σ
SiO_2 (wt.%)	42.61	0.10	42.21	0.41	41.38	0.28	42.52	0.44	42.18	0.36	43.33	0.19
TiO_2	0.01	0.01	0.01	0.01	< 0.01		< 0.01		0.01	0.01	< 0.01	
FeO	1.29	0.05	2.55	0.02	3.10	0.08	2.39	0.04	2.28	0.02	2.76	0.06
CoO	< 0.03		< 0.03		< 0.03		0.03	0.01	< 0.03		< 0.03	
MnO	0.05	0.02	0.09	0.02	0.09	0.01	0.05	0.01	0.07	0.01	0.07	0.01
MgO	56.96	0.05	55.72	0.22	54.58	0.34	55.66	0.42	55.40	0.48	56.07	0.23
CaO	0.02	0.01	0.02	0.01	0.01	0.01	0.02	0.01	0.01	0.01	0.01	0.01
TOTAL	100.97		100.61		99.19		100.70		99.99		102.26	
Si (*apfu*)	0.995		0.995		0.992		1		0.999		1.004	
Ti	0		0		0		0		0		0	
Fe	0.025		0.050		0.062		0.047		0.045		0.053	
Co	0		0		0		0.001		0		0	
Mn	0.001		0.002		0.002		0.001		0.001		0.001	
Mg	1.983		1.958		1.951		1.951		1.955		1.937	
Ca	0.001		0.001		0		0.001		0		0	
CATSUM	3.005		3.006		3.007		3.001		3.000		2.995	
Fo	0.99		0.98		0.97		0.98		0.98		0.97	

Below detection limit: Na_2O, V_2O_3 and Al_2O_3 (0.02 wt. %); Cr_2O_3, ZnO, NiO (0.03 wt. %).

Table 4.5A: Composition of diopside associated with spinel, Markham Bay and Glencoe Island. Normalized to 6 oxygen atoms per formula unit.

Locality	Spinel Island		Unnamed Island		Glencoe main		Glencoe beach		Glencoe contact	
Lithology	Spl diopsidite		Spl-bearing metasomatite		Spl-bearing pod		Spl-bearing marble		Spl diopsidite	
Sample	1A-SPL		1B		2A-SPL-3		2B		2C	
n	4	σ	4	σ	3	σ	3	σ	3	σ
SiO_2 (wt.%)	51.02	1.36	51.36	0.22	53.24	0.95	53.25	0.43	51.69	0.32
TiO_2	0.17	0.05	0.33	0.02	0.14	0.01	0.31	0.01	0.14	0.02
Al_2O_3	3.41	0.67	4.62	0.23	3.63	0.21	2.88	0.03	5.07	0.09
V_2O_3	< 0.02		< 0.02		0.05	0.02	< 0.02		< 0.02	
FeO	1.20	0.02	1.63	0.03	0.87	0.03	1.15	0.03	1.21	0.04
MnO	0.03	0.02	0.05	0.02	< 0.02		0.06	0.02	0.05	0.02
MgO	16.35	0.33	15.80	0.20	16.61	0.27	17.01	0.26	15.66	0.15
CaO	25.81	0.08	25.46	0.05	25.54	0.01	25.22	0.07	25.54	0.09
Na_2O	0.06	0.01	0.10	0.01	0.02	0	0.06	0.01	0.06	0.02
TOTAL	98.07		99.38		100.13		99.97		99.44	
Si (*apfu*)	1.896		1.882		1.924		1.930		1.887	
Ti	0.005		0.009		0.004		0.008		0.004	
Al	0.149		0.200		0.155		0.123		0.218	
V	0		0		0.001		0		0	
Fe	0.037		0.050		0.026		0.035		0.037	
Mn	0.001		0.002		0		0.002		0.002	
Mg	0.906		0.863		0.895		0.919		0.852	
Ca	1.028		1.000		0.989		0.980		0.999	
Na	0.004		0.007		0.001		0.004		0.004	
CATSUM	4.026		4.013		3.995		4.001		4.003	

Below detection limit: ZnO (0.04 wt. %); Cr_2O_3, CoO, and NiO (0.03 wt. %).

Table 4.5B: Average composition of diopside associated with spinel, Kimmirut area, Waddell Bay, and Hall Peninsula. Normalized to 6 oxygen atoms per formula unit.

Locality	Soper River		Soper River		Soper Falls		Qila	Waddell Bay		Hall Pen.
Lithology	Spl-bearing marble		Spl-bearing marble		Humitite		Spl-bearing calc-silicate	Cal-Di-Phl-Spl rock		Spl-bearing marble
Sample	3A-1		3A-1 (pseudomorph)		3B		3E-1	4		5
n	3	σ	2	σ	3	σ	1	4	σ	1
SiO_2 (wt.%)	55.52	0.32	55.6	0.23	56.01	0.08	52.71	52.83	0.57	53.85
TiO_2	0.06	0.01	< 0.01		0.05	0.01	0.06	0.09	0.01	1.03
Al_2O_3	0.63	0.04	0.07	0.02	0.62	0.02	3.71	5.53	0.43	2.75
V_2O_3	< 0.02		< 0.02		< 0.02		< 0.02	< 0.02		< 0.02
FeO	0.22	0.02	0.21	0.01	0.28	0.03	0.41	0.96	0.04	0.43
MnO	0.03	0	0.03	0.01	0.03	0.02	0.03	0.04	0.01	0
MgO	18.11	0.06	18.33	0.24	18.46	0.06	16.64	15.79	0.10	17.34
CaO	25.57	0.05	25.7	0.11	25.71	0.03	24.75	24.43	0.05	25.52
Na_2O	0.13	0.01	0.03	0.01	< 0.02		0.37	0.61	0.02	0.05
TOTAL	100.31		100.01		101.2		98.71	100.30		100.99
Si (*apfu*)	1.995		2.005		1.994		1.927	1.901		1.927
Ti	0.002		0		0.001		0.002	0.002		0.028
Al	0.027		0.003		0.026		0.160	0.235		0.116
V	0		0		0		0	0		0
Fe	0.007		0.006		0.008		0.013	0.029		0.013
Mn	0.001		0.001		0.001		0.001	0.001		0
Mg	0.970		0.985		0.980		0.907	0.847		0.925
Ca	0.984		0.993		0.981		0.969	0.942		0.978
Na	0.009		0.002		0		0.026	0.043		0.003
CATSUM	3.995		3.995		3.991		4.005	4.000		3.990

Below detection limit: ZnO (0.04 wt. %); Cr_2O_3, CoO, and NiO (0.03 wt. %).

Table 4.6A: Average composition of amphibole from Markham Bay, Glencoe Island, and Hall Peninsula. Results calculated using the spreadsheet of Locock (2014) for 24 anions.

Locality	Spinel Island		Glencoe gulch	Glencoe gulch		Hall	
Lithology	Altered Spl diopsidite		Fo-Prg-Spl marble	Fo-Prg-Spl marble		Spl-bearing marble	
Sample	1A-SPL-Alt		2D	2D		5	
n	4	σ	1	4	σ	4	σ
Species	Tremolite		Pargasite	Pargasite		Pargasite	
SiO_2 (wt.%)	56.48	0.87	42.65	44.36	0.18	44.75	0.65
TiO_2	0.05	0.05	2.64	1.69	0.09	1.81	0.37
Al_2O_3	2.22	1.15	15.29	14.21	0.29	14.26	1.25
V_2O_3	< 0.02		0.06	0.03	0.01	0.02	0.01
FeO	2.76	0.33					
Fe_2O_3			0.43	0.60	0.02	0.89	0.01
MnO	0.05	0.01	< 0.03	< 0.03		< 0.03	
MgO	21.74	0.30	19.21	19.12	0.11	19.23	0.21
CaO	13.52	0.08	12.71	13.56	0.04	13.08	0.09
BaO	< 0.06		< 0.06	0.21	0.04	< 0.06	
Na_2O	0.16	0.07	2.92	1.37	0.07	2.20	0.29
K_2O	0.09	0.09	0.44	1.05	0.03	0.48	0.09
Cl	0.01	0.01	0.14	0.16	0.01	0.04	0.01
F	< 0.12		< 0.12	< 0.12		< 0.12	
H2O (calc)	2.17		1.49	1.71		1.72	
O=F,Cl	0		-0.03	-0.04		-0.01	
TOTAL	99.25		97.95	98.03		98.47	
T							
Si (*apfu*)	7.808		6.122	6.340		6.345	
Al	0.192		1.878	1.660		1.655	
C							
Ti	0.005		0.285	0.182		0.193	
Al	0.169		0.708	0.733		0.728	
V			0.007	0.003		0.002	
Fe^{3+}			0.047	0.065		0.095	
Mn^{2+}	0.006						
Fe^{2+}	0.319						
Mg	4.480		3.953	4.017		3.982	
B							
Fe^{2+}							
Mg			0.157	0.056		0.083	
Ca	2.000		1.843	1.955		1.917	
Ba				0.012			
Na	0.000		0.000	0.000		0.000	
A							
Ca	0.003		0.112	0.121		0.070	
Na	0.043		0.813	0.380		0.605	
K	0.016		0.081	0.191		0.087	
W							
OH	1.987		1.395	1.597		1.604	
F							
Cl	0.002		0.034	0.039		0.010	
O	0.010		0.571	0.364		0.387	

Below detection limit (0.03 wt. %): ZnO, Cr_2O_3, CoO, NiO.

Table 4.6B: Average composition of amphibole from the Kimmirut area. Results calculated using the spreadsheet of Locock (2014) for 24 anions.

Locality	Soper River		Soper River		Soper Falls		Soper Falls	
Lithology	Spl-bearing marble		Spl-bearing marble		Humitite		Humitite	
Sample	3A-2		3A-1		3B		3B	
n	7	σ	4	σ	3	σ	3	σ
Species	Pargasite		Pargasite		Tremolite		Pargasite	
SiO_2 (wt.%)	46.03	1.07	45.10	0.93	56.54	0.53	46.39	0.50
TiO_2	0.23	0.09	0.58	0.44	0.10	0.03	0.14	0.04
Al_2O_3	14.03	1.78	14.00	1.05	3.98	0.45	14.20	0.95
V_2O_3	0.02	0.01	0.02	0.01	0.02	0.01	0.06	0.02
FeO	0.23	0.01			0.34	0.02	0.41	0
Fe_2O_3	0.25	0.01	0.58	0.05	0		0	
MnO	< 0.03		< 0.03		0.03	0.02	< 0.03	
MgO	20.68	0.52	19.89	0.27	22.94	0.23	20.34	0.19
CaO	12.42	0.31	13.10	0.30	13.92	0.06	13.91	0.14
BaO	< 0.06		< 0.06		< 0.06		0.07	0.02
Na_2O	3.00	0.25	2.61	0.23	0.06	0.03	3.61	0.26
K_2O	0.49	0.12	0.48	0.22	0.02	0.01	0.18	0.02
Cl	0.08	0.04	0.18	0.06	0.01	0.01	0.06	0.01
F	< 0.12		< 0.12		< 0.12		0.42	0.14
H_2O (calc)	2.09		1.97		2.18		1.91	
O=F,Cl	-0.02		-0.04		0		-0.19	
TOTAL	99.53		98.47		100.14		101.51	
T								
Si (*apfu*)	6.421		6.380		7.663		6.381	
Al	1.579		1.620		0.337		1.619	
C								
Ti	0.024		0.062		0.010		0.014	
Al	0.727		0.714		0.298		0.684	
V	0.002		0.002		0.002			
Fe^{3+}	0.026		0.062					
Mn^{2+}					0.003			
Fe^{2+}					0.039		0.047	
Mg	4.220		4.160		4.635		4.171	
B								
Fe^{2+}	0.026							
Mg	0.080		0.034					
Ca	1.856		1.966		2.000		2.004	
Ba							0.004	
Na	0.037						0.000	
A								
Ca			0.020		0.021		0.046	
Na	0.774		0.716		0.016		0.963	
K	0.087		0.087		0.003		0.032	
W								
OH	1.933		1.833		1.977		1.774	
F							0.183	
Cl	0.019		0.043		0.002		0.014	
O	0.048		0.124		0.020		0.029	

Below detection limit (0.03 wt. %): ZnO, Cr_2O_3, CoO, NiO.

Table 4.6C: Average composition of amphibole from the Kimmirut area. Results calculated using the spreadsheet of Locock (2014) for 24 anions.

Locality	Soper Lk camp		Qila		Qila	
Lithology	Spl-bearing marble		Spl-bearing calc-silicate		Prg-Cal rock	
Sample	3C		3E-1		3E-2	
n	3	σ	6	σ	4	σ
Species	Pargasite		Pargasite		Pargasite	
SiO_2 (wt.%)	42.50	0.20	41.97	0.38	42.5	0.35
TiO_2	2.64	0.05	0.20	0.02	0.20	0.02
Al_2O_3	15.29	0.28	18.41	0.42	16.47	0.03
V_2O_3	0.06	0.02	< 0.02		< 0.02	
FeO			0.82	0.02		
Fe_2O_3	0.43	0.02			0.70	0.01
MnO	< 0.03		0.03	0.02	< 0.03	
MgO	19.21	0.16	17.79	0.17	19.14	0.07
CaO	12.71	0.07	12.90	0.04	12.93	0.06
BaO	< 0.06		0.12	0.04	0.07	0.02
Na_2O	2.92	0.05	2.04	0.13	2.74	0.03
K_2O	0.44	0.03	2.23	0.26	2.02	0.03
Cl	0.14	0.01	0.15	0.01	0.14	0.01
F	< 0.12		0.20	0.07	< 0.12	
H_2O (calc)	1.49		1.95		2.05	
O=F,Cl	-0.03		-0.12		-0.03	
TOTAL	97.80		98.69		98.93	
T						
Si (*apfu*)	6.112		5.991		6.056	
Al	1.888		2.009		1.944	
C						
Ti	0.286		0.021		0.021	
Al	0.703		1.088		0.822	
V	0.007					
Fe^{3+}	0.047				0.075	
Mn^{2+}			0.004			
Fe^{2+}			0.098			
Mg	3.958		3.785		4.066	
B						
Fe^{2+}						
Mg	0.160					
Ca	1.840		1.973		1.974	
Ba			0.007		0.004	
Na	0.000		0.021		0.022	
A						
Ca	0.119					
Na	0.814		0.544		0.735	
K	0.081		0.406		0.367	
W						
OH	1.394		1.830		1.923	
F			0.090			
Cl	0.034		0.036		0.034	
O	0.572		0.043		0.043	

Below detection limit (0.03 wt. %): ZnO, Cr_2O_3, CoO, NiO.

Table 4.7A: Average composition of phlogopite from Markham Bay, Waddell Bay, and Hall Peninsula. Normalized on the basis of 12 anions per formula unit.

Locality	Spinel Island		Unnamed Island		Waddell Bay		Hall Pen.		Hall Pen.	
Lithology	Spl diopsidite		Spl-bearing metasomatite		Cal-Di-Phl-Spl rock		Spl-bearing marble		Spl-bearing marble	
Sample	1A-SPL		1B		4		5		5	
n	3	σ	4	σ	3	σ	2	σ	5	σ
SiO_2 (wt. %)	37.81	0.12	37.39	0.25	39.08	0.04	36.27	1.58	37.59	0.79
TiO_2	0.28	0.01	0.49	0.01	0.35	0.01	1.60	0.14	1.22	0.13
Al_2O_3	17.16	0.32	17.03	0.18	17.91	0.02	17.49	0.86	17.19	0.28
V_2O_3	<0.02		<0.02		<0.02		<0.02		<0.02	
FeO	1.91	0.08	2.28	0.06	1.12	0.05	0.91	0.02	0.86	0.02
MgO	24.50	0.21	24.21	0.16	24.95	0.06	24.38	0.64	24.67	0.14
BaO	0.85	0.10	0.99	0.06	0.11	0.05	6.64	1.53	4.30	1.07
Na_2O	0.20	0.01	0.54	0.01	0.88	0.06	0.47	0.01	0.56	0.03
K_2O	10.12	0.04	9.86	0.03	10.17	0.06	7.00	0.51	7.67	0.34
Cl	0.16	0.01	0.16	0.02	0.03	0.01	0.17	0.02	0.11	0.02
F	1.22	0.18	0.67	0.12	0.42	0.05	<0.12		<0.12	
H_2O_{calc}	3.51		3.75		4.04		4.06		4.12	
O=F,Cl	-0.55		-0.32		-0.19		-0.04		-0.02	
TOTAL	97.17		97.05		98.87		98.95		98.27	
Si (*apfu*)	2.746		2.727		2.758		2.651		2.720	
Ti	0.015		0.027		0.019		0.088		0.066	
Al	1.469		1.464		1.49		1.507		1.466	
V	0		0		0		0		0	
Fe	0.116		0.139		0.066		0.056		0.052	
Mg	2.652		2.632		2.625		2.657		2.661	
Ba	0.024		0.028		0.003		0.190		0.122	
Na	0.028		0.076		0.120		0.067		0.079	
K	0.938		0.917		0.916		0.653		0.708	
Cl	0.020		0.020		0.004		0.021		0.013	
F	0.280		0.155		0.094		0		0	
OH_{calc}	1.700		1.826		1.903		1.979		1.987	

Below detection limit (wt. %): CaO (0.02); Cr_2O_3, ZnO, MnO, CoO, NiO (0.03).

Table 4.7B: Average composition of phlogopite from Glencoe Island. Normalized on the basis of 12 anions per formula unit.

Locality	Glencoe main		Glencoe main		Glencoe contact		Glencoe gulch	
Lithology	Spl-bearing pod		Spl-bearing pod		Spl diopsidite		Fo-Prg-Spl marble	
Sample	2A-SPL-1		2A-SPL-2		2C		2D	
n	4	σ	4	σ	3	σ	4	σ
SiO_2 (wt. %)	38.13	0.07	38.81	0.22	36.96	0.08	37.81	0.74
TiO_2	0.92	0.02	0.28	0.02	0.30	0.01	1.02	0.12
Al_2O_3	17.30	0.05	16.78	0.11	18.90	0.12	16.60	0.24
V_2O_3	<0.02		0.04	0.01	<0.02		<0.02	
FeO	1.51	0.03	1.27	0.04	2.30	0.01	0.45	0.02
MgO	24.12	0.12	24.99	0.05	23.33	0.09	25.39	0.39
BaO	2.21	0.10	1.40	0.08	0.92	0.04	4.04	0.73
Na_2O	0.08	0.01	0.06	0.01	0.16	0.02	0.24	0.02
K_2O	10.04	0.06	10.38	0.02	10.33	0.07	8.75	0.18
Cl	0.31	0.03	0.27	0.06	0.26	0.02	0.14	
F	<0.12		<0.12		<0.12		0.25	0.15
H_2O_{calc}	4.09		4.11		4.07		3.99	
O=F,Cl	-0.07		-0.06		-0.06		-0.14	
TOTAL	98.64		98.33		97.47		98.54	
Si (*apfu*)	2.745		2.785		2.682		2.734	
Ti	0.050		0.015		0.016		0.055	
Al	1.468		1.419		1.616		1.415	
V	0		0.002		0		0	
Fe	0.091		0.076		0.140		0.027	
Mg	2.589		2.673		2.524		2.737	
Ba	0.062		0.039		0.026		0.114	
Na	0.011		0.008		0.023		0.034	
K	0.922		0.950		0.956		0.807	
Cl	0.038		0.033		0.032		0.017	
F	0		0		0		0.057	
OH_{calc}	1.962		1.967		1.968		1.926	

Below detection limit (wt. %): CaO (0.02); Cr_2O_3, ZnO, MnO, CoO, NiO (0.03).

Table 4.7C: Average composition of phlogopite from the Soper Lake mine, Kimmirut area. Normalized on the basis of 12 anions per formula unit.

Locality	Soper Lk mine		Soper Lk mine	
Lithology	Fo-Carb-Phl-Spl rock		Fo-Spl marble	
Sample	3D-1		3D-M1	
n	6	σ	4	σ
SiO_2 (wt.%)	39.80	0.35	39.11	0.34
TiO_2	1.20	0.02	0.94	0.01
Al_2O_3	15.73	0.14	16.12	0.02
V_2O_3	< 0.02		< 0.02	
FeO	0.59	0.05	0.70	0.03
MgO	26.09	0.14	25.82	0.24
BaO	0.16	0.03	0.28	0.03
Na_2O	0.99	0.02	1.26	0.05
K_2O	9.97	0.07	9.44	0.03
Cl	0.11	0.01	0.14	0.01
F	1.52	0.06	1.32	0.05
H_2O_{calc}	3.50		3.55	
O=F,Cl	-0.66		-0.59	
TOTAL	99.00		98.09	
Si (*apfu*)	2.807		2.783	
Ti	0.064		0.050	
Al	1.307		1.352	
V	0		0	
Fe	0.035		0.042	
Mg	2.743		2.739	
Ba	0.004		0.008	
Na	0.135		0.174	
K	0.897		0.857	
Cl	0.013		0.017	
F	0.339		0.297	
OH_{calc}	1.648		1.686	

Below detection limit (wt. %): CaO (0.02); Cr_2O_3, ZnO, MnO, CoO, NiO (0.03).

Table 4.7D: Average composition of phlogopite from Qila, Kimmirut area. Normalized on the basis of 12 anions per formula unit.

Locality	Qila		Qila		Qila	
Lithology	Spl-bearing calc-silicate		Prg-Cal rock		Spl-bearing marble	
Sample	3E-1		3E-2		3E-3-A	
n	6	σ	4	σ	3	σ
SiO_2 (wt.%)	41.58	0.26	39.42	0.21	39.46	0.15
TiO_2	0.60	0.07	0.29	0.01	0.39	0.01
Al_2O_3	13.85	0.27	16.19	0.06	16.33	0.08
V_2O_3	< 0.02		< 0.02		< 0.02	
FeO	0.89	0.05	0.51	0.04	0.57	0.01
MgO	26.35	0.24	26.30	0.04	25.69	0.11
BaO	0.51	0.03	0.95	0.05	0.8	0.06
Na_2O	0.11	0.02	0.72	0.02	0.63	0.03
K_2O	9.90	0.13	9.63	0.08	9.8	0.01
Cl	0.07	0.01	0.14	0	0.13	0.01
F	1.58	0.13	0.97	0.06	0.42	0.16
H_2O_{calc}	3.46		3.72		3.97	
O=F,Cl	-0.69		-0.44		-0.21	
TOTAL	98.21		98.40		97.98	
Si (*apfu*)	2.947		2.802		2.813	
Ti	0.032		0.016		0.021	
Al	1.157		1.356		1.372	
V	0		0		0	
Fe	0.053		0.03		0.034	
Mg	2.784		2.787		2.730	
Ba	0.014		0.026		0.022	
Na	0.015		0.099		0.087	
K	0.895		0.873		0.891	
Cl	0.008		0.017		0.016	
F	0.354		0.218		0.095	
OH_{calc}	1.637		1.765		1.890	

Below detection limit (wt. %): CaO (0.02); Cr_2O_3, ZnO, MnO, CoO, NiO (0.03).

Table 4.7E: Average composition of phlogopite from Trailside, Kimmirut area. Normalized on the basis of 12 anions per formula unit.

Locality	Trailside		Trailside		Trailside	
Lithology	Spl-bearing silicate rock		Spl-bearing silicate rock		Cal-Phl-Spl rock	
Sample	3F-1		3F-1		3F-2	
n	3	σ	4	σ	4	σ
SiO_2 (wt.%)	36.96	0.36	38.88	0.11	39.20	0.15
TiO_2	0.09	0.01	0.32	0.01	0.20	0.01
Al_2O_3	22.37	0.47	18.12	0.10	18.29	0.05
V_2O_3	< 0.02		< 0.02		< 0.02	
FeO	1.33	0.04	1.25	0.03	1.18	0.02
MgO	23.24	0.02	24.40	0.07	24.81	0.08
BaO	0.10	0.05	0.29	0.02	0.35	0.03
Na_2O	0.32	0.03	0.32	0.02	0.44	0
K_2O	10.53	0.07	10.49	0.05	10.25	0.03
Cl	< 0.01		0.02	0.01	0.07	0.01
F	< 0.12		< 0.12		< 0.12	
H_2O_{calc}	4.26		4.21		4.24	
O=F,Cl	0		0		-0.02	
TOTAL	99.20		98.30		99.01	
Si (*apfu*)	2.599		2.763		2.762	
Ti	0.005		0.017		0.011	
Al	1.854		1.517		1.519	
V	0		0		0	
Fe	0.078		0.074		0.070	
Mg	2.436		2.585		2.606	
Ba	0.003		0.008		0.010	
Na	0.044		0.044		0.060	
K	0.945		0.951		0.921	
Cl	0		0.002		0.008	
F	0		0		0	
OH_{calc}	2.000		1.998		1.992	

Below detection limit (wt. %): CaO (0.02); Cr_2O_3, ZnO, MnO, CoO, NiO (0.03).

Table 4.8: Average composition of humite from Soper Falls. Normalized on the basis of 3 Si atoms per formula unit.

Locality	Soper Falls
Lithology	Humitite
Sample	3B
n	5
SiO_2 (wt.%)	36.72
TiO_2	0.43
FeO	1.18
MnO	0.05
MgO	57.21
F	4.70
H_2O (calc)	2.72
TOTAL	103.07
Si (*apfu*)	3
Ti	0.026
Fe	0.081
Mn	0.003
Mg	6.968
F	1.214
OH (calc)	0.786

Below detection limit (wt. %): ZnO, Cr_2O_3, CoO, NiO (0.03); Al_2O_3, V_2O_3 (0.02); Cl (0.01).

Table 4.9: Average composition of scapolite from spinel-bearing calc-silicate rock at Qila. Normalized to Al+Si=12.

Locality	Qila
Lithology	Spl-bearing calc-silicate
Sample	3E-1
n	3
SiO_2 (wt.%)	47.76
Al_2O_3	26.98
MgO	0.04
CaO	16.52
Na_2O	4.14
K_2O	0.34
Cl	0.86
O=Cl	-0.19
TOTAL	96.45
Si (*apfu*)	7.204
Al	4.796
Mg	0.009
Ca	2.670
Na	1.211
K	0.065
Me%	69

Below detection limit (wt. %): TiO_2 (0.02); V_2O_3, Cr_2O_3, FeO, CoO, NiO, MnO (0.03); ZnO (0.04); BaO (0.06).

Table 4.10: Average composition of muscovite from spinel-bearing silicate rock at Trailside. Normalized to 12 anions per formula unit.

Locality	Trailside	
Lithology	Spl-bearing silicate rock	
Sample	3F-1	
n	3	σ
SiO_2 (wt.%)	45.83	2.39
Al_2O_3	35.83	2.93
FeO	0.08	0.04
MgO	1.65	1.18
CaO	0.73	0.19
BaO	0.09	0.03
Na_2O	0.25	0.10
K_2O	8.75	0.32
Cl	0.16	0.17
H_2O (calc)	4.43	
O=F,Cl	-0.04	
TOTAL	97.76	
Si (*apfu*)	3.071	
Al	2.829	
Fe	0.004	
Mg	0.165	
Ca	0.052	
Ba	0.002	
Na	0.032	
K	0.748	
Cl	0.018	
OH (calc)	1.982	

Below detection limit (wt. %): TiO_2 (0.01); V_2O_3 (0.02); Cr_2O_3, ZnO, MnO, CoO, NiO (0.03); F (0.12).

Table 4.11A: Average composition of calcite associated with spinel from Markham Bay and Glencoe Island.

Locality	Spinel Island	Unnamed Island	Glencoe main	Glencoe main	Glencoe main	Glencoe beach	Glencoe beach	Glencoe contact	Glencoe gulch
Lithology	Spl diopsidite	Spl-bearing metasomatite	Spl-bearing pod	Spl-bearing pod	Spl-bearing pod	Spl-bearing marble	Spl-bearing marble	Spl diopsidite	Fo-Prg-Spl marble
Sample	1A-SPL	1B	2A-SPL-1	2A-SPL-1	2A-SPL-3	2B	2B	2C	2D
n	4	3	2	2	3	2	2	3	3
FeO (wt.%)	< 0.03	0.17	0.17	0.14	0.17	0.27	< 0.03	0.21	0.05
MnO	< 0.03	0.03	0.06	0.05	< 0.03	0.09	< 0.03	0.06	< 0.03
MgO	0.03	1.53	2.36	2.44	2.96	2.95	0.35	1.84	2.62
CaO	57.43	54.40	53.19	53.63	52.45	52.62	56.01	53.54	53.29
CO_2	43.07	43.56	43.75	43.65	43.87	43.78	43.34	43.70	43.74
TOTAL	100.56	99.69	99.53	99.91	99.47	99.71	99.81	99.35	99.72

Table 4.11B: Average composition of calcite associated with spinel from Kimmirut, Waddell Bay, and the Hall Peninsula.

Locality	Soper River	Soper River	Soper Falls	Soper Lk mine	Soper Lk mine	Qila	Qila	Trailside	Trailside	Waddell Bay	Hall Pen.
Lithology	Spl-bearing marble	Spl-bearing marble	Humitite	Fo-Carb-Phl-Spl rock	Fo-Spl marble	Prg-Cal rock	Spl-bearing marble	Cal-Phl-Spl rock	Cal-Phl-Spl rock	Cal-Di-Phl-Spl rock	Spl-bearing marble
Sample	3A-2	3A-1	3B	3D-1	3D-M1	3E-2	3E-3-A	3F-2	3F-2	4	5
n	3	3	3	3	3	3	3	3	3	3	3
FeO (wt.%)	0.03	0.03	0.04	< 0.03	0.09	0.07	0.06	0.20	0.20	0.06	0.09
MnO	0.04	0.04	0.04	0.03	0.05	0.04	< 0.03	0.04	0.04	< 0.03	0.04
MgO	0.35	1.06	2.50	0.48	2.26	3.24	1.34	3.02	3.45	1.34	2.44
CaO	56.61	55.53	53.64	56.61	53.86	52.54	55.23	52.77	52.58	54.54	53.32
CO_2	43.21	43.39	43.67	43.20	43.63	43.84	43.42	43.77	43.77	43.58	43.74
TOTAL	100.24	100.05	99.89	100.32	99.89	99.73	100.07	99.8	100.04	99.53	99.63

Table 4.12A: Average composition of dolomite and dolomite exsolution in calcite associated with spinel from Baffin Island.

Locality	Glencoe main	Glencoe gulch	Soper River	Soper River	Soper River	Soper Falls
Lithology	Spl-bearing pod	Fo-Prg-Spl marble	Spl-bearing marble	Spl-bearing marble	Spl-bearing marble	Humitite
Sample	2A-SPL-1	2D	3A-2	3A-1	3A-1	3B
Detail	Exsolution	Exsolution	Exsolution		Di-Dol pseudomorph	Exsolution
n	2	3	3	3	2	3
FeO (wt.%)	0.74	0.18	0.25	0.23	0.26	0.24
MnO	0.07	0.03	< 0.03	0.05	0.04	0.05
MgO	20.40	21.13	21.56	21.08	20.89	21.28
CaO	31.11	31.46	30.86	30.78	30.68	31.09
CO_2	46.89	46.89	46.97	47.06	47.11	46.94
TOTAL	99.21	99.69	99.66	99.20	98.98	99.60

Table 4.12B: Average composition of dolomite and dolomite exsolution in calcite associated with spinel from Baffin Island.

Locality	Soper Lk mine	Soper Lk mine	Qila (area)	Qila	Qila	Hall Pen.
Lithology	Fo-Spl marble	Fo-Carb-Phl-Spl rock	Dolomitic marble	Spl-bearing marble	Spl-bearing calc-silicate	Spl-bearing marble
Sample	3D-M1	3D-1	3E-M1	3E-3-A	3E-1	5
Detail	Exsolution	Exsolution		Exsolution		Exsolution
n	2	3	3	2	3	3
FeO (wt.%)	0.39	0.34	0.18	0.36	0.55	0.36
MnO	0.07	0.07	< 0.03	0.06	0.06	0.03
MgO	21.06	21.03	21.44	20.82	20.58	21.19
CaO	30.82	30.77	30.54	31.01	30.74	30.62
CO_2	46.99	47.02	47.10	46.99	47.03	47.05
TOTAL	99.33	99.23	99.28	99.24	98.96	99.25

Table 4.13: Average composition of pyrrhotite and pyrite associated with spinel on Baffin Island.

Species	Pyrrhotite	Pyrrhotite	Pyrrhotite	Pyrrhotite	Pyrite
Locality	Glencoe main	Soper River	Soper Falls	Soper Lk camp	Trailside
Lithology	Spl-bearing pod	Spl-bearing marble	Humitite	Spl-bearing marble	Spl-bearing silicate rock
Sample	2A-SPL-1	3A-1	3B	3C	3F-1 (after Spl)
n	4	3	3	5	1
Fe (wt. %)	60.99	61.79	63.19	60.32	43.06
Co	0.07	0.11	0.06	0.09	1.79
Ni	0.21	0.10	< 0.03	0.04	< 0.03
S	38.59	38.03	36.81	38.62	52.75
TOTAL	99.86	100.05	100.08	99.09	97.61

Below detection limit (wt. %): Mn (0.03), Zn (0.04).

Table 4.14A: Major element composition of whole rock samples from Spinel Island, Glencoe Island, and the Hall Peninsula.

Locality	Spinel Island	Spinel Island	Spinel Island	Spinel Island	Glencoe main	Glencoe main	Glencoe main	Glencoe main	Glencoe main	Hall Pen.
Lithology	Monzogranite	Syenogranite	Phl marble	Spl diopsidite	Spl-bearing pod	Spl-bearing pod (w/ Po)	Serpentine marble	Sulphide-rich diopsidite	Psammite	Spl-bearing marble
Sample	1A-MG	1A-SG	1A-M	1A-SPL	2A-SPL-1	2A-SPL-2	2A-M	2A-DI	2A-PS	5
Wt. %										
SiO_2	72.5	75.1	7.96	45.5	38.1	34.9	20.8	46.8	71	3.93
Al_2O_3	14.75	13.6	1.67	10.4	17.85	12.6	1.48	4.91	11.8	1.13
TiO_2	0.31	0.03	0.07	0.13	0.28	0.3	0.04	0.2	0.34	0.05
Cr_2O_3	<0.01	<0.01	<0.01	<0.01	0.01	0.01	<0.01	0.01	0.01	<0.01
MnO	0.01	0.01	0.05	0.05	0.03	0.04	0.06	0.04	0.04	0.04
Fe_2O_3	1.24	0.54	0.59	2.02	1.11	1.8	0.94	5.36	4.89	0.43
MgO	0.48	0.19	10.8	17.55	11	17.35	21.7	16.25	3.7	8.02
CaO	0.81	0.47	41.9	22.3	22.2	21	26.6	21.9	6.18	47.6
SrO	0.02	0.01	0.01	<0.01	0.07	<0.01	0.01	<0.01	0.01	0.01
Na_2O	3.77	1.85	0.06	0.09	0.44	0.07	0.05	0.05	0.9	0.03
K_2O	7.07	9.07	1.1	0.23	1.02	2.29	0.81	0.65	0.49	0.03
BaO	0.14	0.12	0.12	0.02	0.32	0.56	0.17	0.1	0.06	0.02
P_2O_5	0.08	0.05	<0.01	0.01	0.23	0.18	0.03	0.02	0.03	<0.01
LOI	0.54	0.33	36.2	1.22	6.86	7.57	28.1	4.12	2.26	39.9
Total	101.72	101.37	100.53	99.52	99.52	98.67	100.79	100.41	101.71	101.19
C	0.08	0.03	9.83	0.23	1.77	2	5.87	2.11	0.57	10.9
S	<0.01	0.01	0.04	0.01	0.1	0.25	0.09	1.97	1.33	<0.01

Table 4.14B: Major element composition of whole rock samples from Soper River, Soper Lake, and Soper Falls, Kimmirut area.

Locality	Soper River	Soper River	Soper River	Soper Falls	Soper Lk camp	Soper Lk mine	Soper Lk mine	Soper Lk mine
Lithology	Spl-bearing marble	Lapis lazuli	Lapis lazuli	Humitite	Spl-bearing marble	Fo-Carbonate rock	Fo-Spl marble	Phl marble
Sample	3A-1	3A-LAPIS-1	3A-LAPIS-2	3B	3C	3D-2	3D-M1	3D-M2
Wt. %								
SiO_2	2.2	35.7	42.1	29.8	5.94	33.4	5.95	6.24
Al_2O_3	0.39	10.85	12.25	8.11	1.26	0.23	1.32	1.35
TiO_2	0.02	0.16	0.18	0.3	0.12	0.01	0.01	0.07
Cr_2O_3	<0.01	0.01	0.01	0.01	<0.01	<0.01	<0.01	<0.01
MnO	0.05	0.02	0.02	0.05	0.03	0.08	0.06	0.04
Fe_2O_3	0.31	0.39	0.29	1.55	0.83	2.58	0.75	0.63
MgO	16.75	8.16	10.2	46.4	11.85	43.2	10.75	7.56
CaO	37.5	24.1	19.25	3.79	42.8	6.08	44.5	46.3
SrO	<0.01	<0.01	<0.01	<0.01	0.01	0.01	0.02	0.02
Na_2O	0.04	6.33	6.96	0.06	0.03	0.04	0.06	0.08
K_2O	0.01	0.45	0.46	<0.01	<0.01	0.11	0.13	0.95
BaO	<0.01	<0.01	<0.01	<0.01	<0.01	<0.01	<0.01	0.02
P_2O_5	0.01	0.01	0.03	0.02	<0.01	0.04	0.02	0.04
LOI	44.2	11.5	5.5	6.99	37.4	13.6	37.8	38.3
Total	101.48	97.68	97.25	97.08	100.27	99.38	101.37	101.6
C	12.15	2.86	1.36	1.45	10.2	1.92	10.35	10.3
S	0.01	0.98	1.27	0.02	0.11	0.02	0.03	0.08

Table 4.14C: Major element composition of whole rock samples from Qila and Trailside, Kimmirut area.

Locality	Qila	Qila	Qila	Qila	Qila (area)	Trailside	Trailside	Trailside	Trailside (area)	Trailside (area)	Trailside (area)	Trailside (area)
Lithology	Calc-silicate*	Prg-Cal rock	Spl-bearing marble	Phl-richer, Spl-poor marble	Marble	Spl-bearing silicate rock (Spl-poor)	Cal-Phl-Spl rock	Diopsidite	Marble	Marble	Diopsidite	Diopsidite
Sample	3E-1	3E-2	3E-3-A	3E-3-B	3E-M2	3F-1	3F-2	3F-4	3F-M1	3F-M2	3F-CS2	3F-CS3
Wt. %												
SiO_2	40.9	27.4	7.37	7.85	5.28	32.6	21.6	48.6	8.86	3.84	49.6	46.6
Al_2O_3	14.4	10.75	0.95	1.04	0.73	21	13.65	1.9	1.88	0.92	4.39	7.31
TiO_2	0.15	0.12	<0.01	0.02	0.02	0.08	0.14	0.03	0.06	0.02	0.1	0.26
Cr_2O_3	0.01	<0.01	<0.01	<0.01	<0.01	<0.01	<0.01	<0.01	<0.01	<0.01	<0.01	<0.01
MnO	0.03	0.02	0.04	0.03	0.04	0.02	0.03	0.04	0.03	0.03	0.03	0.03
Fe_2O_3	0.82	0.54	0.56	0.33	0.53	0.44	1.14	0.88	0.72	0.31	1.51	1.39
MgO	15	13.75	11.5	8.16	7.33	8.08	16.35	16.3	9.02	3.06	16.2	18.15
CaO	12.9	26	43	46.3	48	15.6	21.4	23.5	43.4	50.1	19.95	16.55
SrO	<0.01	0.01	0.02	0.02	0.02	0.03	0.02	<0.01	0.03	0.04	<0.01	<0.01
Na_2O	1.58	1.41	0.04	0.06	0.03	0.69	0.24	0.63	0.07	0.16	0.9	1.06
K_2O	1.86	1.38	0.07	0.42	0.5	5.07	5.65	0.36	1.13	0.32	0.88	3.13
BaO	0.1	0.08	0.01	0.04	0.02	0.17	0.2	0.01	0.02	0.02	0.01	0.03
P_2O_5	0.65	0.08	0.03	0.03	0.03	0.01	0.02	0.01	0.01	0.07	<0.01	0.02
LOI	10.8	16.8	36.4	37.1	39.4	18.1	20.1	8.79	36.3	41.2	5.52	5.37
Total	99.2	98.34	99.99	101.4	101.93	101.89	100.54	101.05	101.53	100.09	99.09	99.9
C	2.35	4.66	9.9	10.05	10.75	3.36	4.94	2.32	9.66	11.2	1.24	1.05
S	0.01	0.01	<0.01	0.01	0.01	0.01	0.01	0.01	0.01	0.01	0.01	0.01

Table 4.15A: Trace element concentrations (µg/g) of whole rock samples from Spinel Island, Glencoe Island, and the Hall Peninsula. Below detection limit: Ge (< 5 µg/g).

Locality	Spinel Island	Spinel Island	Spinel Island	Spinel Island	Glencoe main	Glencoe main	Glencoe main	Glencoe main	Glencoe main	Hall Pen.
Lithology	Monzogranite	Syenogranite	Phl marble	Spl diopsidite	Spl-bearing pod	Spl-bearing pod (w/ Po)	Serpentine marble	Sulphide-rich diopsidite	Psammite	Spl-bearing marble
Sample	1A-MG	1A-SG	1A-M	1A-SPL	2A-SPL-1	2A-SPL-2	2A-M	2A-DI	2A-PS	5
Li	10	<10	<10	10	10	30	<10	10	20	<10
B	n.d.	n.d.	n.d.	n.d.	21	n.d.	n.d.	n.d.	n.d.	n.d.
F	n.d.	n.d.	n.d.	n.d.	1070	n.d.	n.d.	n.d.	n.d.	n.d.
Cl	n.d.	n.d.	n.d.	n.d.	820	n.d.	n.d.	n.d.	n.d.	n.d.
Sc	1	<1	2	3	9	12	1	7	4	1
V	19	<5	10	14	53	43	17	457	29	7
Cr	10	10	10	10	60	100	10	50	50	10
Co	2	<1	2	2	2	4	3	16	7	<1
Ni	1	<1	2	<1	11	23	4	149	35	<1
Cu	1	<1	2	1	6	17	4	55	62	<1
Zn	14	7	<2	98	230	308	242	231	67	2
Ga	18.4	18.3	2.5	20.2	17.5	19	2.2	8.7	17.6	1.4
As	0.4	0.4	0.2	0.3	0.8	0.7	<0.1	2.7	0.8	<0.1
Se	<0.2	<0.2	0.2	<0.2	0.3	1.2	0.2	2.8	0.3	<0.2
Rb	263	372	32.4	20.9	33.4	76.4	29.7	33.7	15	1.3
Sr	167.5	144.5	86.6	18.1	614	49.2	83.3	26.7	87.1	93.3
Y	2.5	2.8	6.6	14.1	11.2	9.4	7.2	16.4	9.3	2.7
Zr	120	3	43	116	284	212	11	86	209	17
Nb	5.8	0.8	2.5	2.2	4.6	9.1	2	8.6	11.1	2.5
Mo	<1	1	1	<1	1	4	2	48	3	<1
Ag	<0.5	<0.5	<0.5	<0.5	<0.5	<0.5	<0.5	0.7	<0.5	<0.5
Cd	<0.5	<0.5	<0.5	<0.5	0.9	1.2	0.9	1.5	0.6	<0.5
In	<0.005	<0.005	0.009	0.007	<0.005	0.007	<0.005	0.014	0.011	0.005
Sn	<1	<1	1	4	2	2	<1	2	1	<1
Sb	<0.05	<0.05	0.12	<0.05	0.07	0.1	<0.05	0.11	<0.05	<0.05
Te	<0.01	<0.01	0.01	<0.01	0.01	<0.01	<0.01	0.02	0.02	<0.01
Cs	0.46	1.05	0.33	0.56	1.18	3.08	1.22	1.09	0.17	0.11
Ba	1265	1075	1100	173.5	2970	5300	1540	937	565	189.5
La	20.2	17.6	10.5	15.5	10.2	6.9	14	8	29.4	4.1
Ce	30.9	26.4	19.9	47.1	19.8	16	21.8	21.2	47.6	8.4
Pr	3.27	2.76	2.36	7.31	2.87	2.31	2.61	3.27	5.23	1.02
Nd	10.3	8.9	8.3	27.5	10.6	9.5	8.7	12.9	15.9	3.9
Sm	1.66	1.39	1.5	5.44	2.45	2.26	1.37	2.69	2.81	0.57
Eu	0.88	1.01	0.27	0.43	0.31	0.23	0.23	0.4	0.62	0.09
Gd	0.82	1.03	1.24	3.6	1.81	1.71	1.05	2.37	1.74	0.6
Tb	0.12	0.11	0.17	0.52	0.32	0.26	0.13	0.39	0.26	0.09
Dy	0.54	0.57	0.97	2.74	1.82	1.51	0.84	2.44	1.31	0.5
Ho	0.08	0.09	0.2	0.53	0.42	0.32	0.18	0.56	0.31	0.09
Er	0.2	0.3	0.67	1.24	1.17	1	0.64	1.39	0.9	0.28
Tm	0.05	0.04	0.1	0.16	0.19	0.17	0.08	0.21	0.14	0.04
Yb	0.22	0.15	0.58	1.04	1.07	1.14	0.53	1.33	1.06	0.3
Lu	0.03	0.02	0.1	0.16	0.19	0.17	0.09	0.21	0.15	0.05
Hf	2.9	<0.2	1.1	3.4	7.6	6.9	0.3	2.1	5.6	0.5
Ta	0.3	0.1	0.2	0.4	0.7	0.9	0.1	0.4	0.9	0.2
W	<1	1	<1	<1	<1	1	1	5	1	<1
Re	<0.001	<0.001	<0.001	<0.001	0.003	0.006	0.002	0.116	0.002	<0.001
Hg	<0.005	0.005	<0.005	0.006	<0.005	0.007	0.007	<0.005	0.01	<0.005
Tl	0.06	0.03	0.02	0.08	0.34	0.91	0.15	0.48	0.05	<0.02
Pb	21	32	2	24	32	42	12	13	7	2
Bi	0.01	0.01	0.04	0.01	0.05	0.16	0.01	0.3	0.2	0.03
Th	4	4.19	2.64	101.5	25.6	16.85	0.84	2	15.05	1.99
U	0.86	2.24	0.18	47.8	32.7	27.1	0.67	1.51	2.92	0.34

Table 4.15B: Trace element concentrations (µg/g) of whole rock samples from Soper River, Soper Lake, and Soper Falls, Kimmirut area. Below detection limit (µg/g): Ge (5), Cd (0.5).

Locality	Soper River	Soper River	Soper River	Soper Falls	Soper Lk camp	Soper Lk mine	Soper Lk mine	Soper Lk mine
Lithology	Spl-bearing marble	Lapis lazuli	Lapis lazuli	Humitite	Spl-bearing marble	Fo-Carbonate rock	Fo-Spl marble	Phl marble
Sample	3A-1	3A-LAPIS-1	3A-LAPIS-2	3B	3C	3D-2	3D-M1	3D-M2
Li	<10	<10	<10	<10	<10	10	<10	<10
B	13	n.d.	17	304	n.d.	n.d.	129	n.d.
F	n.d.	n.d.	560	>20000	n.d.	n.d.	510	n.d.
Cl	n.d.	n.d.	3170	250	n.d.	n.d.	390	n.d.
Sc	<1	4	4	<1	1	1	1	1
V	5	30	38	35	10	5	8	11
Cr	10	30	50	40	10	10	10	10
Co	1	<1	<1	3	1	6	2	2
Ni	<1	<1	<1	<1	1	7	<1	3
Cu	6	<1	<1	1	5	1	3	4
Zn	<2	4	10	5	3	14	4	5
Ga	0.5	13.3	10.2	13.4	1.5	0.7	2.3	1.9
As	0.1	5.7	19.4	0.9	<0.1	0.3	0.2	<0.1
Se	<0.2	1	0.9	<0.2	0.4	<0.2	<0.2	0.3
Rb	<0.2	2.4	5.9	0.2	0.5	3.5	4.6	59.8
Sr	26.7	49.5	31.8	18.9	86.6	105.5	192	203
Y	0.9	6	3.9	<0.5	4.2	1.4	4.6	4.3
Zr	26	91	105	16	40	33	16	35
Nb	0.2	1.5	4.3	1.9	0.8	0.9	0.9	3.1
Mo	<1	5	22	<1	<1	<1	<1	<1
Ag	<0.5	<0.5	<0.5	<0.5	<0.5	<0.5	0.5	<0.5
In	<0.005	<0.005	<0.005	0.005	0.007	0.008	0.005	0.007
Sn	<1	1	1	<1	<1	<1	<1	<1
Sb	<0.05	<0.05	0.09	<0.05	<0.05	<0.05	<0.05	<0.05
Te	<0.01	<0.01	0.01	<0.01	0.01	<0.01	0.01	<0.01
Cs	0.01	0.15	0.23	0.02	0.02	0.28	0.65	6.4
Ba	6.4	15.6	15	6.8	19.2	18.9	42.4	205
La	1.1	3.7	2.2	<0.5	7.1	2.7	8.6	8.8
Ce	2.1	9.6	5.6	0.9	15.4	5.1	17.4	17.2
Pr	0.21	1.28	0.73	0.13	1.47	0.57	1.85	1.67
Nd	0.9	5.3	3.4	0.5	5.7	2.1	6.1	5.2
Sm	0.12	1.23	0.73	<0.03	1.04	0.34	1.23	0.87
Eu	0.03	0.18	0.13	<0.03	0.17	0.06	0.25	0.18
Gd	0.16	1.1	0.77	0.07	0.92	0.35	0.88	0.69
Tb	0.02	0.15	0.11	0.01	0.14	0.03	0.12	0.11
Dy	0.12	1.04	0.75	0.05	0.74	0.21	0.77	0.61
Ho	0.02	0.2	0.16	0.01	0.15	0.05	0.14	0.13
Er	0.1	0.69	0.45	<0.03	0.39	0.14	0.42	0.38
Tm	0.02	0.09	0.07	0.01	0.07	0.03	0.06	0.06
Yb	0.07	0.68	0.4	0.03	0.39	0.15	0.38	0.33
Lu	0.01	0.11	0.07	<0.01	0.06	0.02	0.06	0.05
Hf	0.7	2.6	3.1	0.7	0.9	1	0.4	0.9
Ta	<0.1	0.3	0.4	0.2	0.3	<0.1	<0.1	0.2
W	<1	1	5	1	<1	1	<1	<1
Re	0.001	0.001	0.003	<0.001	<0.001	<0.001	<0.001	<0.001
Hg	<0.005	<0.005	0.006	<0.005	0.007	0.014	0.009	0.008
Tl	<0.02	0.05	0.09	<0.02	<0.02	0.02	0.02	0.16
Pb	<2	<2	3	<2	4	5	5	5
Bi	<0.01	0.02	0.03	0.01	0.03	0.03	0.03	0.03
Th	0.1	1.21	0.92	0.11	1.47	0.52	3.5	3.97
U	<0.05	0.93	1.09	0.11	0.79	0.52	3.72	2.45

Table 4.15C: Trace element concentrations (µg/g) of whole rock samples from Qila, Kimmirut area. Below detection limit (µg/g): Ge (5); Ag and Cd (0.5); Re (0.001).

Locality	Qila	Qila	Qila	Qila	Qila (area)
Lithology	Calc-silicate*	Prg-Cal rock	Spl-bearing marble	Phl-richer, Spl-poor marble	Marble
Sample	3E-1	3E-2	3E-3-A	3E-3-B	3E-M2
Li	30	10	<10	<10	<10
B	n.d.	95	n.d.	n.d.	n.d.
F	n.d.	6960	n.d.	n.d.	n.d.
Cl	n.d.	1160	n.d.	n.d.	n.d.
Sc	5	4	1	1	1
V	13	13	<5	5	6
Cr	40	10	10	10	10
Co	29	9	15	10	3
Ni	47	11	25	12	4
Cu	1	2	1	1	2
Zn	2	2	2	<2	3
Ga	14.1	11	1.9	1.7	1
As	1.1	0.3	<0.1	0.2	<0.1
Se	<0.2	0.2	<0.2	0.2	<0.2
Rb	15	12.4	1.6	12.4	20.5
Sr	50.9	98.6	177.5	170	191.5
Y	6.3	4	3.6	4.2	3.8
Zr	126	125	5	13	15
Nb	17.7	13.4	0.4	0.9	1.4
Mo	<1	<1	3	3	<1
In	0.016	0.011	0.006	<0.005	0.006
Sn	4	4	<1	<1	<1
Sb	<0.05	<0.05	<0.05	<0.05	<0.05
Te	0.01	<0.01	<0.01	<0.01	<0.01
Cs	0.3	0.24	0.04	0.38	0.62
Ba	892	664	87.4	345	165.5
La	1	1.6	3.9	4.2	5.8
Ce	2.7	3.1	7.5	7.9	10.7
Pr	0.42	0.39	0.84	0.94	1.16
Nd	1.9	1.7	3.5	3.3	4.5
Sm	0.63	0.41	0.64	0.58	0.77
Eu	0.05	0.06	0.09	0.08	0.11
Gd	0.65	0.64	0.59	0.61	0.64
Tb	0.16	0.1	0.08	0.11	0.1
Dy	0.92	0.64	0.46	0.64	0.67
Ho	0.24	0.15	0.12	0.14	0.12
Er	0.73	0.48	0.33	0.4	0.37
Tm	0.15	0.09	0.05	0.06	0.05
Yb	0.85	0.48	0.29	0.39	0.31
Lu	0.12	0.06	0.04	0.06	0.05
Hf	5	3.9	0.2	0.4	0.5
Ta	1.6	1.2	<0.1	0.1	0.1
W	1	1	<1	<1	<1
Hg	0.082	<0.005	<0.005	<0.005	<0.005
Tl	0.04	0.03	<0.02	<0.02	0.04
Pb	99	6	2	3	2
Bi	0.04	0.02	0.01	0.01	0.01
Th	84.2	3.26	3.78	4.58	2.31
U	257	8.21	3.38	3.49	1.51

Table 4.15D: Trace element concentrations (µg/g) of whole rock samples from Trailside, Kimmirut area. Below detection limit (µg/g): Ge (5); Ag and Cd (0.5); Re (0.001).

Locality	Trailside	Trailside	Trailside	Trailside (area)	Trailside (area)	Trailside (area)	Trailside (area)
Lithology	Spl-bearing silicate rock (Spl-poor)	Cal-Phl-Spl rock	Diopsidite	Marble	Marble	Diopsidite	Diopsidite
Sample	3F-1	3F-2	3F-4	3F-M1	3F-M2	3F-CS2	3F-CS3
Li	50	30	<10	<10	<10	10	10
B	196	n.d.	n.d.	30	n.d.	n.d.	n.d.
F	2320	n.d.	n.d.	1970	n.d.	n.d.	n.d.
Cl	680	n.d.	n.d.	410	n.d.	n.d.	n.d.
Sc	1	1	4	2	1	6	3
V	7	17	16	10	6	33	22
Cr	10	20	10	10	10	30	20
Co	9	27	16	2	<1	5	8
Ni	10	35	11	2	<1	2	12
Cu	1	<1	1	1	1	1	1
Zn	<2	15	3	3	<2	14	9
Ga	7.4	14.6	3.6	2.7	1.4	7.7	9.4
As	1.6	0.1	0.5	0.2	<0.1	0.4	0.1
Se	0.2	<0.2	<0.2	<0.2	0.2	0.2	<0.2
Rb	85.1	143	8.8	29.4	9	33.8	91.2
Sr	316	217	42.4	276	373	33.5	32.8
Y	5.4	7.3	1.9	6.3	4	1.2	0.9
Zr	19	24	77	19	14	119	89
Nb	6.6	14.5	0.7	3.1	0.9	3.3	10.9
Mo	<1	<1	<1	<1	<1	<1	<1
In	<0.005	<0.005	<0.005	0.006	0.007	0.006	0.007
Sn	1	1	1	1	<1	2	2
Sb	0.05	<0.05	<0.05	<0.05	<0.05	<0.05	<0.05
Te	<0.01	<0.01	<0.01	0.01	<0.01	<0.01	0.01
Cs	1.96	3.88	0.28	0.77	0.19	0.99	3.34
Ba	1500	1800	72.3	175.5	152	74.4	279
La	2.6	3.8	0.5	5.8	6.1	<0.5	<0.5
Ce	5.6	8.3	1.2	12	12	1	0.8
Pr	0.68	0.97	0.19	1.48	1.26	0.16	0.11
Nd	3	4	0.9	5.6	4.9	0.7	0.5
Sm	0.63	0.94	0.3	1.29	1.1	0.18	0.08
Eu	0.09	0.1	0.03	0.12	0.15	0.03	0.03
Gd	0.71	0.96	0.32	1	0.89	0.19	0.14
Tb	0.11	0.17	0.05	0.15	0.11	0.04	0.02
Dy	0.74	1.09	0.38	1.02	0.64	0.22	0.17
Ho	0.2	0.24	0.07	0.22	0.13	0.05	0.04
Er	0.66	0.77	0.28	0.68	0.37	0.18	0.09
Tm	0.11	0.14	0.04	0.09	0.06	0.03	0.04
Yb	0.63	0.87	0.24	0.63	0.4	0.17	0.18
Lu	0.12	0.13	0.03	0.1	0.06	0.02	0.02
Hf	0.7	0.6	2.2	0.6	0.3	3.2	2.1
Ta	0.4	0.7	<0.1	0.2	0.1	0.2	0.9
W	1	1	<1	2	<1	<1	2
Hg	<0.005	<0.005	<0.005	<0.005	<0.005	<0.005	0.008
Tl	0.09	0.2	0.03	0.06	<0.02	0.12	0.32
Pb	2	<2	<2	<2	<2	<2	<2
Bi	0.01	0.01	0.01	0.01	0.02	0.01	0.01
Th	3.75	2.39	0.7	3.41	3.92	0.47	0.37
U	1.32	0.95	0.73	1.18	2.15	0.59	0.56

Table 4.16A: Estimated protolith composition of metacarbonate samples from Markham Bay, Glencoe Island.

Locality		Spinel Island	Glencoe main	Glencoe main	Glencoe main	Glencoe main	Glencoe main
Lithology		Phl marble	Spl-bearing pod	Spl-bearing pod (w/ Po)	Serpentine marble	Sulphide-rich diopsidite	Psammite
Sample		1A-M	2A-SPL-1	2A-SPL-2	2A-M	2A-DI	2A-PS
Al/Si (weight)		0.24	0.53	0.41	0.08	0.12	0.19
Siliciclastic component		Sand-rich mud	Muddy clay	Mud	Slightly muddy sand	Muddy sand	Mud-rich sand
Siliciclastic Ca-Mg[a] (wt. %)	CaO	0.55	0.93	2.43	1.45	3.25	4.93
	MgO	0.22	0.81	1.44	0.33	0.87	1.71
Original H_2O estimate (wt. %)[b]	H_2O	0.36	3.34	3.15	0.07	0.63	2.26
Original carbonate[c]	CaO	41.35	21.27	18.57	25.15	18.65	1.25
	MgO	10.58	10.19	15.91	21.37	15.38	1.99
Original carbonate	CO_2	44.00	27.82	31.95	43.08	31.42	3.15
Total[d]		108.73	123.92	126.45	115.93	130.31	106.19
Carbonate species (mol. %)	Magnesite	0	0	16	15	13	55
	Dolomite	36	67	84	85	87	45
	Calcite	64	33	0	0	0	0
Original rock composition estimate (wt. %)[e]							
Siliciclastic	Sand	4.9		2.4	21.3	39.0	52.9
	Mud	6.7	16.1	44.6	1.2	10.0	41.0
	Clay		35.8				
	Sili. Total	11.6	51.9	47	22.5	48.9	93.9
Carbonate		88.4	48.1	53	77.5	51.1	6.1

[a] Estimated based on reference averages and samples of modern sedimentary rocks (see text).
[b] Assuming 5 wt. % water in shales and claystones.
[c] Siliciclastic contribution subtracted from whole rock total.
[d] Whole rock composition excluding volatiles and with the addition of the estimated original CO_2, H_2O, and where applicable, Cl.
[e] Where the siliciclastic proportion is calculated assuming it contains all Al, Si, Ti, Cr, K, Na (except in lapis lazuli), and their calculated estimated contribution of Ca and Mg; and the carbonate proportion contains the remainder of Ca and Mg plus estimated original CO_2.

Table 4.16B: Estimated protolith composition of metacarbonate samples from Hall Peninsula and part of the Kimmirut area.

Locality		Beluga sapphire	Soper River	Soper Falls	Soper Lk camp	Soper Lk mine	Soper Lk mine	Hall Pen.
Lithology		Calc-silicate	Spl-bearing marble	Humitite	Spl-bearing marble	Fo-Spl marble	Phl marble	Spl-bearing marble
Sample		Belley *et al.* 2017	3A-1	3B	3C	3D-M1	3D-M2	5
Al/Si (weight)		0.35	0.2	0.31	0.24	0.25	0.24	0.33
Siliciclastic component		Sandy mud	Mud-rich sand	Sandy mud	Sand-rich mud	Sand-rich mud	Sand-rich mud	Sandy mud
Siliciclastic Ca-Mg[a] (wt. %)	CaO	3.18	0.15	2.07	0.41	0.41	0.43	0.27
	MgO	1.67	0.06	1.00	0.17	0.17	0.18	0.14
Original H_2O estimate (wt. %)[b]	H_2O	3.39	0.08	1.89	0.27	0.29	0.29	0.27
Original carbonate[c]	CaO	13.88	37.35	1.72	42.39	44.09	45.87	47.33
	MgO	8.48	16.69	45.4	11.68	10.58	7.38	7.88
Original carbonate	CO_2	20.15	47.54	50.93	46.02	46.15	44.06	45.75
Total[d]		117.96	104.91	142.93	109.27	110.04	107.73	107.31
Carbonate species (mol. %)	Magnesite	0	0	97	0	0	0	0
	Dolomite	85	62	3	38	33	22	23
	Calcite	15	38	0	62	67	78	77
Original rock composition estimate (wt. %)[e]								
Siliciclastic	Sand	10.8	1.6	7.9	3.5	3.2	3.9	1.3
	Mud	53.1	1.5	23.5	4.8	5.1	5.7	4.6
	Clay							
	Sili. Total	63.9	3.1	31.4	8.3	8.3	9.5	5.9
Carbonate		36.1	96.9	68.6	91.7	91.7	90.5	94.1

[a] Estimated based on reference averages and samples of modern sedimentary rocks (see text).
[b] Assuming 5 wt. % water in shales and claystones.
[c] Siliciclastic contribution subtracted from whole rock total.
[d] Whole rock composition excluding volatiles and with the addition of the estimated original CO_2, H_2O, and where applicable, Cl.
[e] Where the siliciclastic proportion is calculated assuming it contains all Al, Si, Ti, Cr, K, Na (except in lapis lazuli), and their calculated estimated contribution of Ca and Mg; and the carbonate proportion contains the remainder of Ca and Mg plus estimated original CO_2.

Table 4.16C: Estimated protolith composition of metacarbonate samples from Soper River and Qila, Kimmirut area.

Locality		Soper River	Soper River	Qila	Qila	Qila	Qila	Qila (area)
Lithology		Lapis lazuli	Lapis lazuli	Calc-silicate*	Prg-Cal rock	Spl-bearing marble	Phl-richer, Spl-poor marble	Marble
Sample		3A-LAPIS-1	3A-LAPIS-2	3E-1	3E-2	3E-3-A	3E-3-B	3E-M2
Al/Si (weight)		0.34	0.33	0.4	0.44	0.15	0.15	0.16
Siliciclastic component		Sandy mud	Sandy mud	Mud	Clay	Muddy sand	Muddy sand	Muddy sand
Siliciclastic Ca-Mg-Na[a] (wt. %)	CaO	2.48	2.93	2.84	1.84	0.51	0.55	0.37
	MgO	1.29	1.48	1.65	1.16	0.15	0.17	0.11
	Na_2O	0.52	0.59					
Original H_2O estimate (wt. %)[b]	H_2O	2.61	2.91	3.58	2.67	0.15	0.17	0.12
Original carbonate[c]	CaO	21.62	16.32	10.06	24.16	42.49	45.75	47.63
	MgO	6.87	8.72	13.35	12.59	11.35	7.99	7.22
Original carbonate	CO_2	24.46	22.34	22.46	32.71	45.73	44.64	45.26
Original evaporite[d]	Na	4.31	4.73					
	Cl	6.65	7.29					
Total[e]		119.38	123.92	114.45	116.93	109.47	109.12	107.92
Carbonate species (mol. %)	Magnesite	0	0	46	0	0	0	0
	Dolomite	44	74	54	72	37	24	21
	Calcite	56	26	0	28	63	76	79
Original rock composition (wt. %)[f]								
Siliciclastic	Sand	8	10.6	4.2		6.3	6.7	4.7
	Mud	38	41	55.5	39.1	2.7	3.1	2.4
	Clay				1.4			
	Kaol-rich clay							
	Sili. Total	46	51.5	59.6	40.5	9	9.7	7.1
Carbonate		44.7	38.7	40.4	59.5	91	90.3	92.9
Halite		9.3	9.8					

[a] Estimated based on reference averages and samples of modern sedimentary rocks (see text).
[b] Assuming 5 wt. % water in shales and claystones.
[c] Siliciclastic contribution subtracted from whole rock total.
[d] Siliciclastic contribution subtracted from whole rock total, for lapis lazuli only, assuming all excess Na is halite.
[e] Whole rock composition excluding volatiles and with the addition of the estimated original CO_2, H_2O, and where applicable, Cl.
[f] Where the siliciclastic proportion is calculated assuming it contains all Al, Si, Ti, Cr, K, Na (except in lapis lazuli), and their calculated estimated contribution of Ca and Mg; and the carbonate proportion contains the remainder of Ca and Mg plus CO_2.

Table 4.16D: Estimated protolith composition of metacarbonate samples from Trailside, Kimmirut area.

Locality		Trailside	Trails. (area)	Trails. (area)	Trailside	Trailside	Trailside (area)	Trailside (area)
Lithology		Spl-bearing silicate rock (Spl-poor)	Marble	Marble	Cal-Phl-Spl rock	Diopsidite	Diopsidite	Diopsidite
Sample		3F-1	3F-M1	3F-M2	3F-2	3F-4	3F-CS2	3F-CS3
Al/Si (weight)		0.73	0.24	0.27	0.72	0.04	0.1	0.18
Siliciclastic component		Kaolinite-rich clay	Sand-rich mud	Sand-rich mud	Kaolinite-rich clay	Sand	Slightly muddy sand	Mud-rich sand
Siliciclastic Ca-Mg[a] (wt. %)	CaO	0.32	0.62	0.27	0.21	2.79	3.45	3.24
	MgO	0.45	0.25	0.12	0.3	0.59	0.86	1.08
Original H_2O estimate (wt. %)[b]	H_2O	2.93	0.4	0.21	1.93	0	0.42	1.35
Original carbonate[c]	CaO	15.28	42.78	49.83	21.19	20.71	16.5	13.31
	MgO	7.63	8.77	2.94	16.05	15.71	15.34	17.07
Original carbonate	CO_2	20.32	43.15	42.32	34.16	33.41	29.71	29.08
Total[e]		107.05	108.79	101.43	116.54	125.68	123.71	124.97
Carbonate species (mol. %)	Magnesite	0	0	0	5	5	23	44
	Dolomite	69	29	8	95	95	77	56
	Calcite	31	71	92	0	0	0	0
Original rock composition (wt. %)[f]								
Siliciclastic	Sand		5.4	2.1		44.4	43.5	31.2
	Mud		7.5	4			6.7	21.2
	Clay	7.2			7.3			
	Kaol-rich clay	52.3			31.3			
	Sili. Total	59.5	12.9	6.1	38.6	44.4	50.2	52.4
Carbonate		40.5	87.1	93.9	61.4	55.6	49.8	47.6
Halite								

[a] Estimated based on reference averages and samples of modern sedimentary rocks (see text).
[b] Assuming 5 wt. % water in shales and claystones.
[c] Siliciclastic contribution subtracted from whole rock total.
[d] Siliciclastic contribution subtracted from whole rock total, for lapis lazuli only, assuming all excess Na is halite.
[e] Whole rock composition excluding volatiles and with the addition of the estimated original CO_2, H_2O, and where applicable, Cl.
[f] Where the siliciclastic proportion is calculated assuming it contains all Al, Si, Ti, Cr, K, Na (except in lapis lazuli), and their calculated estimated contribution of Ca and Mg; and the carbonate proportion contains the remainder of Ca and Mg plus CO_2.

Table 4.17A: “Expected” trace element composition of metasediment samples calculated based on mixing of sedimentary rock averages and comparison to actual values metasediments (calculated using averages for shale/clay, sandstone, and limestone and corrected for mass loss due to devolatilization; see text). Samples from Markham Bay, Glencoe Island, Hall Peninsula and part of the Kimmirut area.

Locality	Spinel Island	Glencoe main	Glencoe main	Glencoe main	Glencoe main	Glencoe main	Soper River	Soper Falls	Soper Lk camp	Soper Lk mine	Soper Lk mine	Hall Pen.
Lithology	Phl marble	Spl-bearing pod	Spl-bearing pod (w/ Po)	Serpentine marble	Sulphide-rich diopsidite	Psammite	Spl-bearing marble	Humitite	Spl-bearing marble	Fo-Spl marble	Phl marble	Spl-bearing marble
Sample	1A-M	2A-SPL-1	2A-SPL-2	2A-M	2A-DI	2A-PS	3A-1	3B	3C	3D-M1	3D-M2	5
"Expected" concentration (µg/g)												
Li	10	42	38	9	19	35	6	27	9	9	9	8
B	28	76	71	28	44	65	23	57	27	27	27	26
F	368	518	511	370	422	391	348	522	367	371	363	362
Cl	156	192	191	140	126	85	155	202	159	161	156	160
Sc	2	7	6	1	3	5	1	4	2	2	2	2
V	30	96	87	25	40	69	23	66	28	28	28	27
Cr	20	71	65	20	38	64	13	48	18	18	18	17
Mn	1100	1100	1100	1000	800	400	1100	1300	1100	1100	1100	1100
Fe	6600	23700	21600	6300	11800	20200	4500	16000	5900	6000	6100	5600
Co	2	13	11	0	3	9	0	7	1	1	1	1
Ni	26	73	67	20	27	44	22	52	25	26	25	25
Cu	8	39	35	6	13	28	5	24	7	7	8	7
Zn	26	63	59	23	32	45	22	48	25	25	25	24
Ga	7	22	20	7	13	20	5	15	6	6	6	6
Actual / Estimate												
Li	--	0.2	0.8		0.5	0.6	--	--	--	--	--	--
B		0.3					0.6	5.3		4.8		
F		2.1						> 38		1.4		
Cl		4.3						1.2		2.4		
Sc	1.2	1.3	1.9	0.8	2.8	0.8	--	--	0.6	0.6	0.6	0.7
V	0.3	0.6	0.5	0.7	11.3	0.4	0.2	0.5	0.4	0.3	0.4	0.3
Cr	0.5	0.8	1.5	0.5	1.3	0.8	0.8	0.8	0.6	0.6	0.5	0.6
Mn	0.3	0.2	0.3	0.5	0.4	0.8	0.3	0.3	0.2	0.4	0.3	0.3
Fe	0.6	0.3	0.6	1	3.2	1.7	0.5	0.7	1	0.9	0.7	0.5
Co	1.3	0.2	0.4		5.7	0.8		0.4	0.8	1.7	1.5	--
Ni	0.1	0.2	0.3	0.2	5.6	0.8	--	--	0	--	0.1	--
Cu	0.2	0.2	0.5	0.7	4.4	2.2	1.2	0	0.7	0.4	0.5	--
Zn	--	3.6	5.2	10.5	7.3	1.5	--	0.1	0.1	0.2	0.2	0.1
Ga	0.4	0.8	1	0.3	0.7	0.9	0.1	0.9	0.3	0.4	0.3	0.2

Table 4.17B: “Expected” trace element composition of metasediment samples calculated based on mixing of sedimentary rock averages and comparison to actual values metasediments (calculated using averages for shale/clay, sandstone, and limestone and corrected for mass loss due to devolatilization; see text). Samples from Qila and Trailside, Kimmirut area.

Locality	Qila	Qila	Qila	Qila	Qila (area)	Trailside	Trailside	Trailside	Trailside (area)	Trailside (area)	Trailside (area)	Trailside (area)
Lithology	Calc-silicate *	Prg-Cal rock	Spl-bearing marble	Phl-richer, Spl-poor marble	Marble	Spl-bearing silicate rock (Spl-poor)	Cal-Phl-Spl rock	Diopsidite	Diopsidite	Diopsidite	Marble	Marble
Sample	3E-1	3E-2	3E-3-A	3E-3-B	3E-M2	3F-1	3F-2	3F-4	3F-CS2	3F-CS3	3F-M1	3F-M2
"Expected" concentration (µg/g)												
Li	41	32	8	8	7	40	31	12	16	25	11	8
B	74	61	25	26	24	72	59	34	39	52	29	24
F	483	466	362	361	358	462	461	381	390	434	369	340
Cl	171	180	155	154	155	167	179	110	111	135	156	150
Sc	7	5	1	1	1	7	5	1	2	4	2	1
V	93	76	25	26	24	92	73	25	34	54	31	25
Cr	70	55	16	17	15	69	53	27	34	47	21	15
Mn	900	1100	1100	1100	1100	900	1100	800	800	900	1100	1100
Fe	23400	18400	5400	5600	5200	22900	17700	8100	10400	14900	6900	5200
Co	13	10	1	1	1	13	9	0.2	2	6	2	1
Ni	70	59	23	23	23	69	57	15	21	38	27	23
Cu	38	30	6	6	6	38	29	6	10	19	9	6
Zn	61	52	23	24	23	60	50	23	28	39	26	23
Ga	22	17	6	6	5	21	16	10	11	15	7	5
Actual / Estimate												
Li	0.7	0.3	--	--	--	1.2	1	--	0.6	0.4	--	--
B		1.5				2.7					1	
F		14.9				5					5.3	
Cl		6.4				4.1					2.6	
Sc	0.7	0.7	0.7	0.7	0.8	0.1	0.2	3.1	3	0.8	1.1	0.7
V	0.1	0.2	--	0.2	0.2	0.1	0.2	0.6	1	0.4	0.3	0.2
Cr	0.6	0.2	0.6	0.6	0.6	0.1	0.4	0.4	0.9	0.4	0.5	0.7
Mn	0.2	0.1	0.3	0.2	0.3	0.2	0.2	0.4	0.3	0.3	0.2	0.2
Fe	0.2	0.2	0.7	0.4	0.7	0.1	0.5	0.8	1	0.7	0.7	0.4
Co	2.3	0.9	21.4	12.5	5	0.7	3	80	2.6	1.5	1.2	--
Ni	0.7	0.2	1.1	0.5	0.2	0.1	0.6	0.7	0.1	0.3	0.1	--
Cu	0	0.1	0.2	0.2	0.4	0	--	0.2	0.1	0.1	0.1	0.2
Zn	0	0	0.1	--	0.1	--	0.3	0.1	0.5	0.2	0.1	--
Ga	0.7	0.6	0.3	0.3	0.2	0.4	0.9	0.4	0.7	0.6	0.4	0.3

4.8 Figures

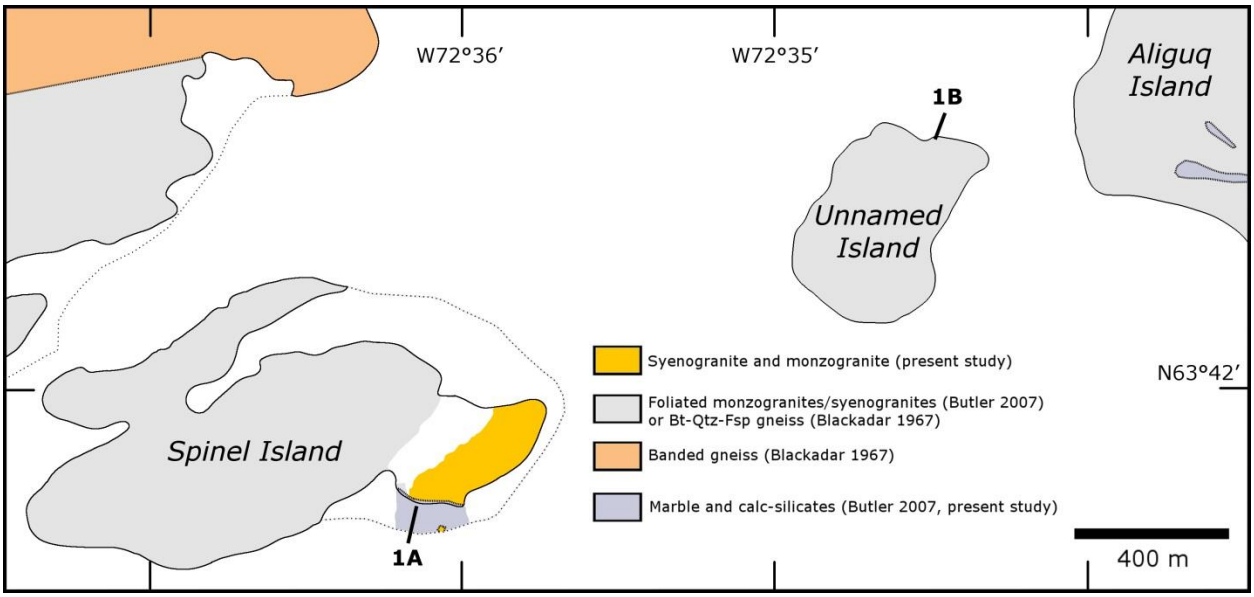

Figure 4.1: Location of the Markham Bay spinel localities (1A and 1B). Geology after Blackadar (1967) and Butler (2007). Only the southeastern part of "Spinel Island" was inspected in detail in the present study. Dotted lines represent the extent of exposure at low tide.

Figure 4.2: Spinel-bearing diopsidite band (*ca.* 2.5 m thick) seen looking West on Spinel Island, north of MacDonald Island, Markham Bay.

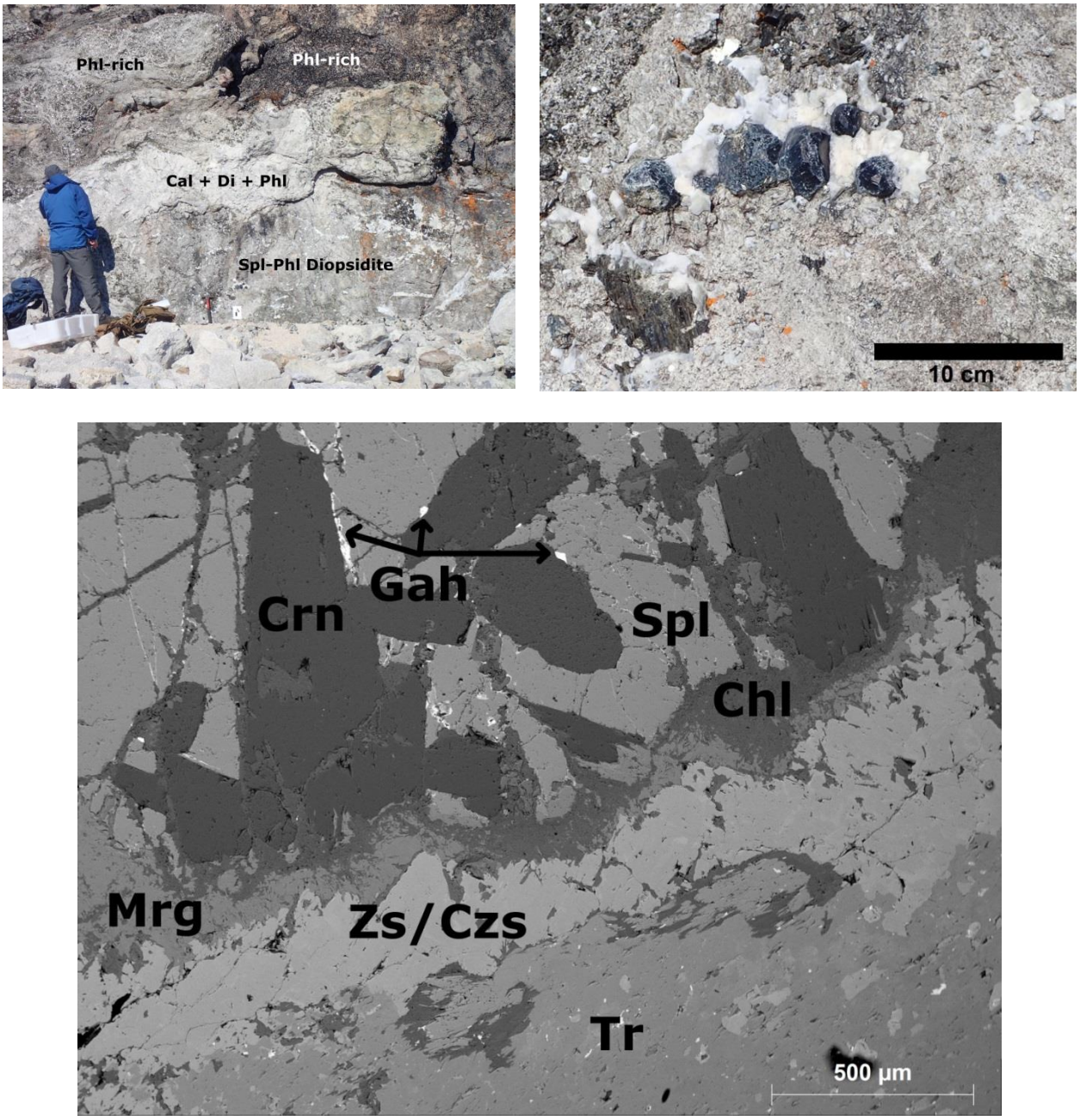

Figure 4.3: (A: top left) Main area of the diopsidite band at Spinel Island. Note the uneven distribution of phlogopite (Phl)-rich portions. Spinel (Spl) crystals occur in the lower part of the outcrop, where the diopsidite is poorer in phlogopite. Pale-colored calcite (Cal), diopside (Di), and phlogopite occur on the hanging wall of the diopsidite, where it probably grades into marble. (B: top right) Dark blue, euhedral spinel crystals up to 4 cm in size in white calcite, grey diopside, and brown phlogopite. (C: bottom) Spinel (Spl) partly replaced by corundum (Crn) and clinochlore (Chl). Trace gahnite (Gah). Lower part of image contains retrograde minerals margarite (Mrg), zoisite or clinozoisite (Zs/Czs), and tremolite (Tr). Spinel Island, Markham Bay. Backscattered electron image.

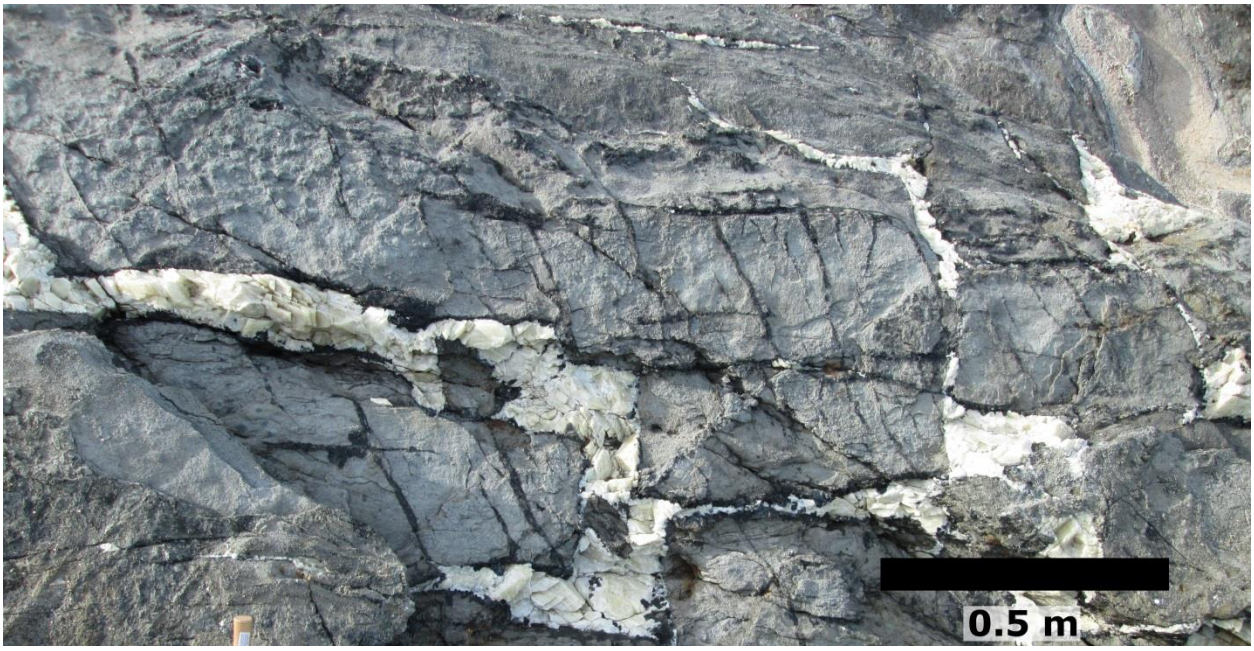

Figure 4.4: Yellowish-white amphibole-bearing calcite veins and dark amphibole veinlets cross-cutting diopsidite. Unnamed island, Markham Bay.

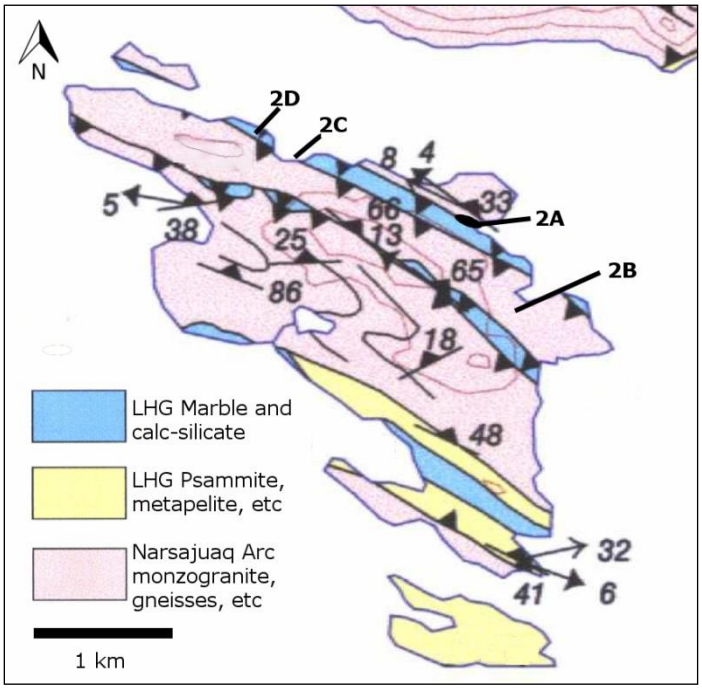

Figure 4.5: Location of spinel occurrences on Glencoe Island: (2A) Main occurrence, (2B) Marble beach, (2C) Contact, and (2D) Marble Gulch. All spinel occurrences are hosted in Lake Harbour Group (LHG) marbles and calc-silicate rocks. Modified after St-Onge *et al.* (1999b).

Figure 4.6: (A) Main spinel occurrence at Glencoe Island in a 2-meter thick band of marble. (B) Calc-silicate pod (disjointed boudins) at the Glencoe Main occurrence containing spinel (Spl), diopside (Di), calcite (Cal), and phlogopite (Phl) hosted in marble matrix.

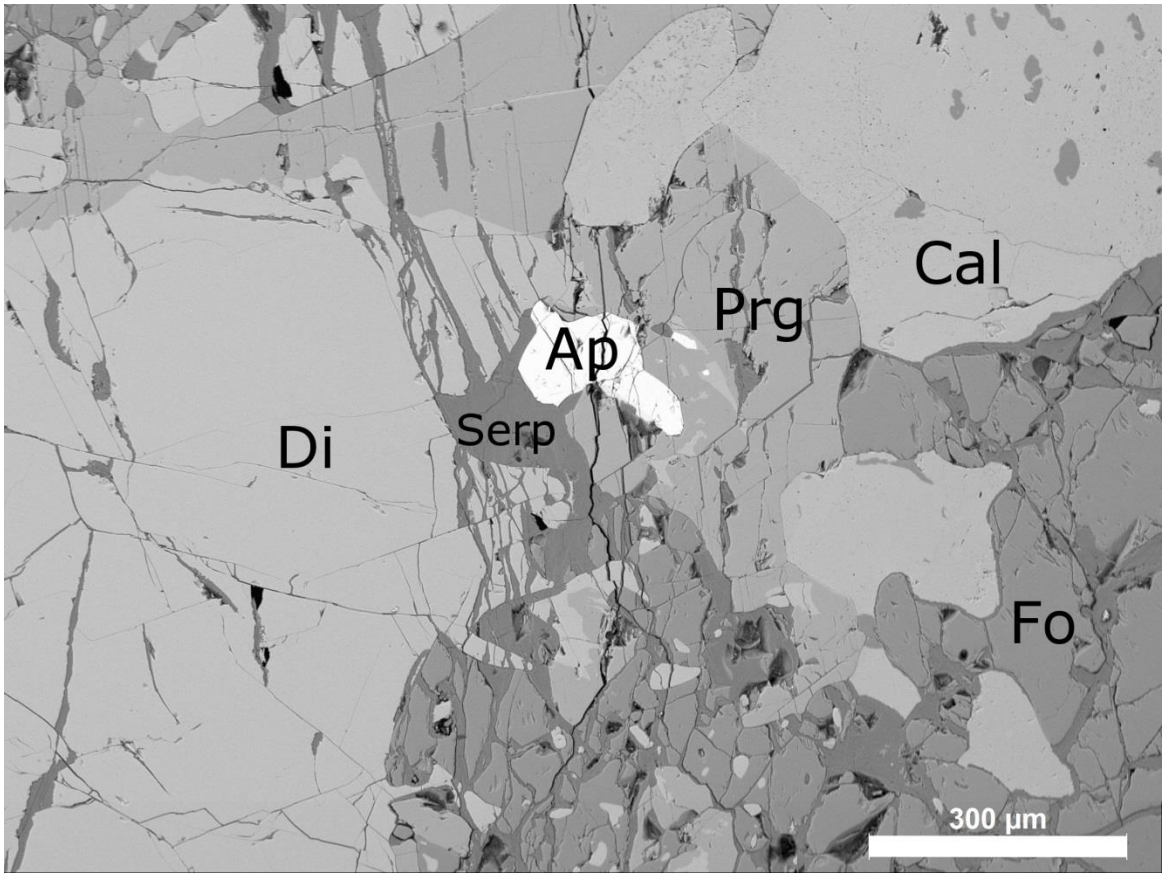

Figure 4.7: Embayed grain boundaries between forsterite (Fo), pargasite (Prg), and diopside (Di) with apatite (Ap) and retrograde serpentine (Serp). Marble gulch occurrence, Glencoe Island.

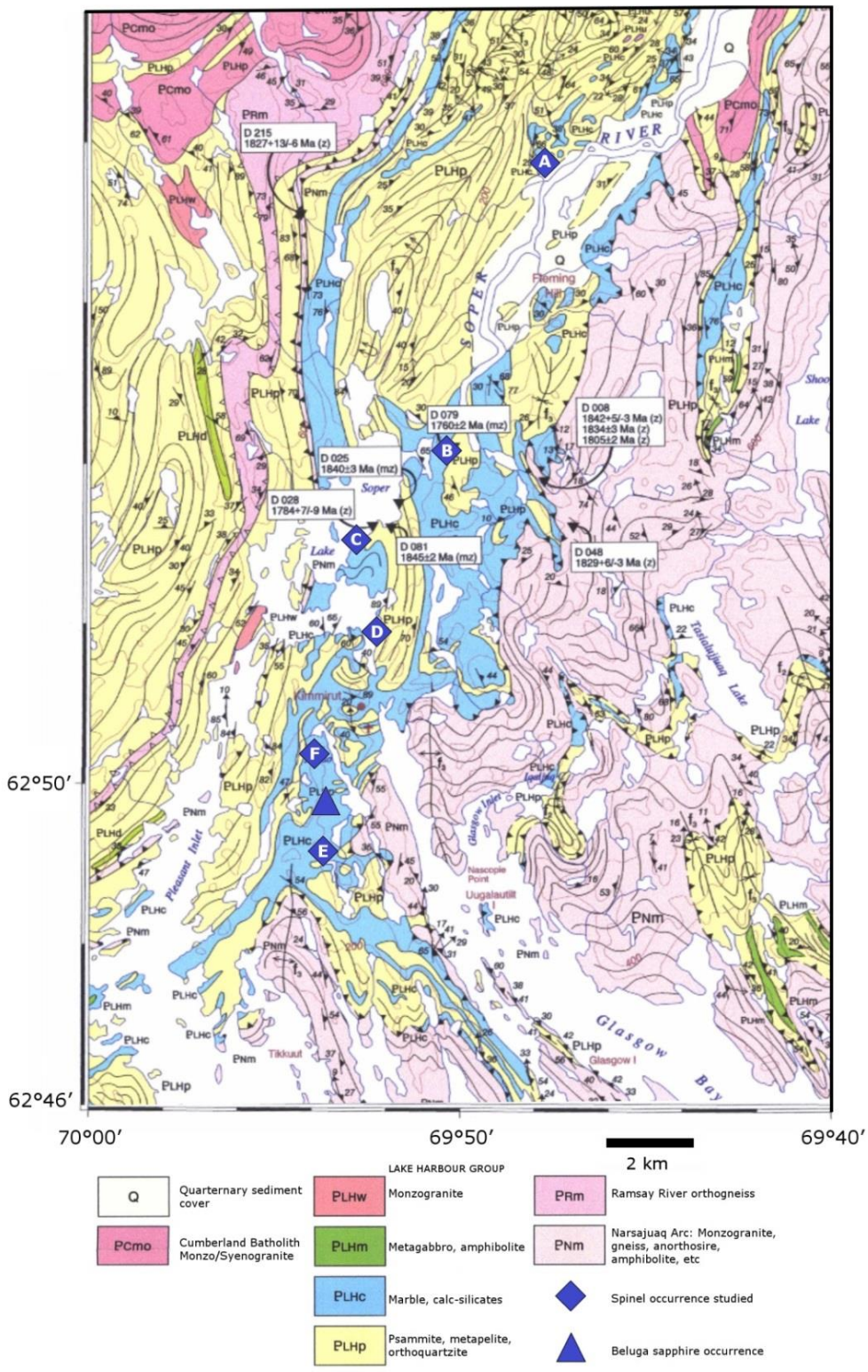

Figure 4.8: Location of spinel occurrences near Kimmirut sampled for this study (refer to Table 4.1 for localities). Modified after St-Onge *et al.* (1999a).

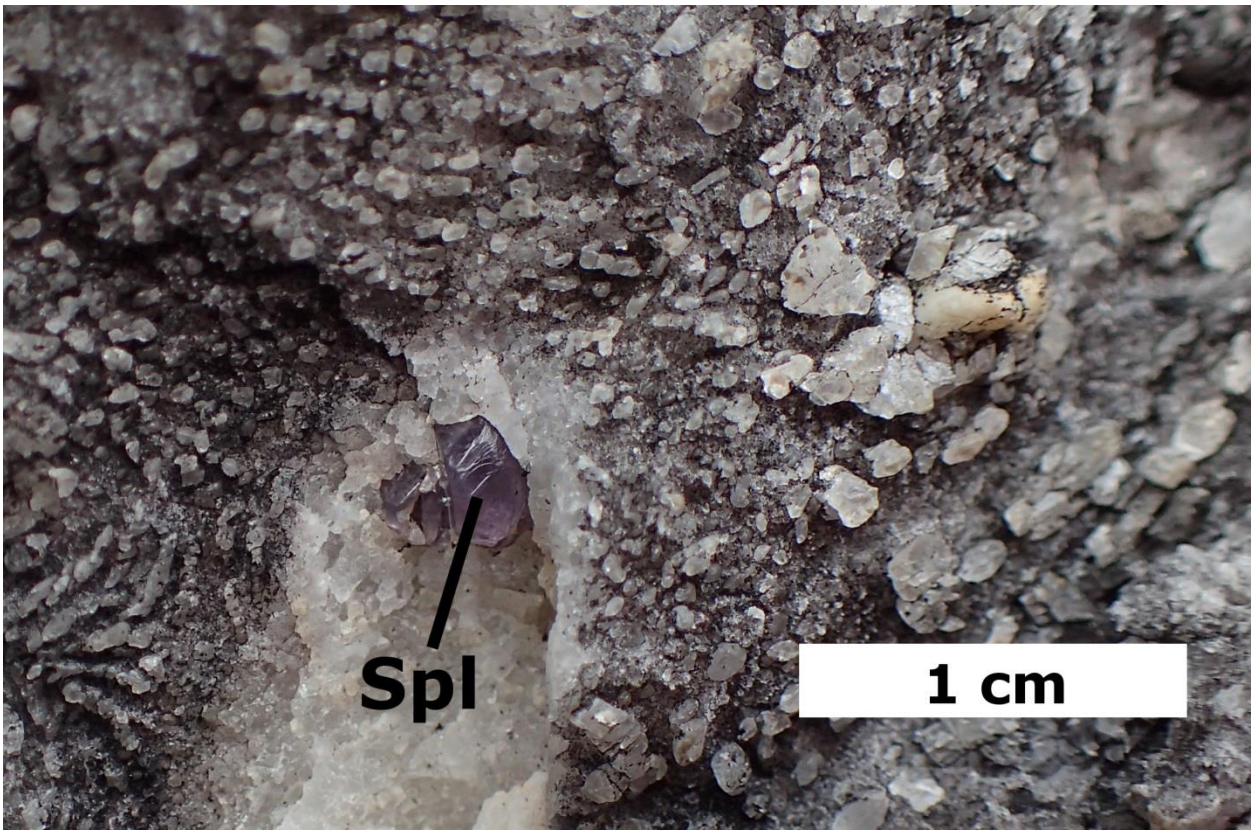

Figure 4.9: Spinel in dolomitic marble. Soper River spinel occurrence, Kimmirut area.

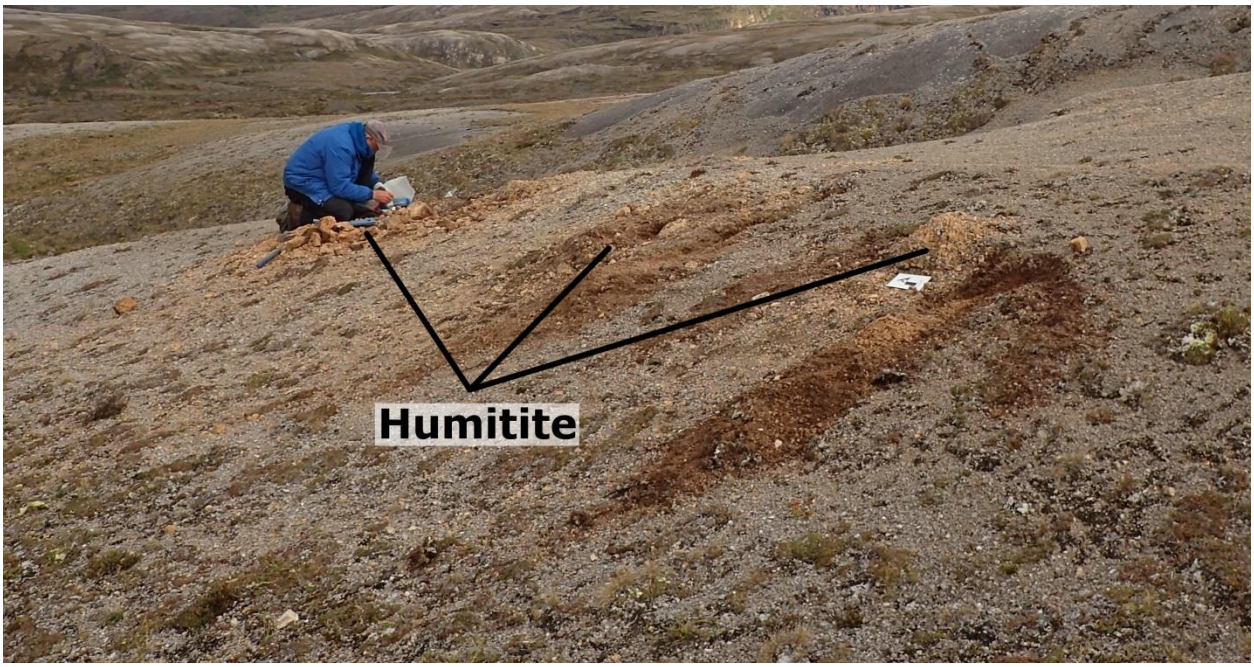

Figure 4.10: Spinel-bearing humitite pods (Hu) in weathered marble outcrop. Soper Falls spinel occurrence, Kimmirut area.

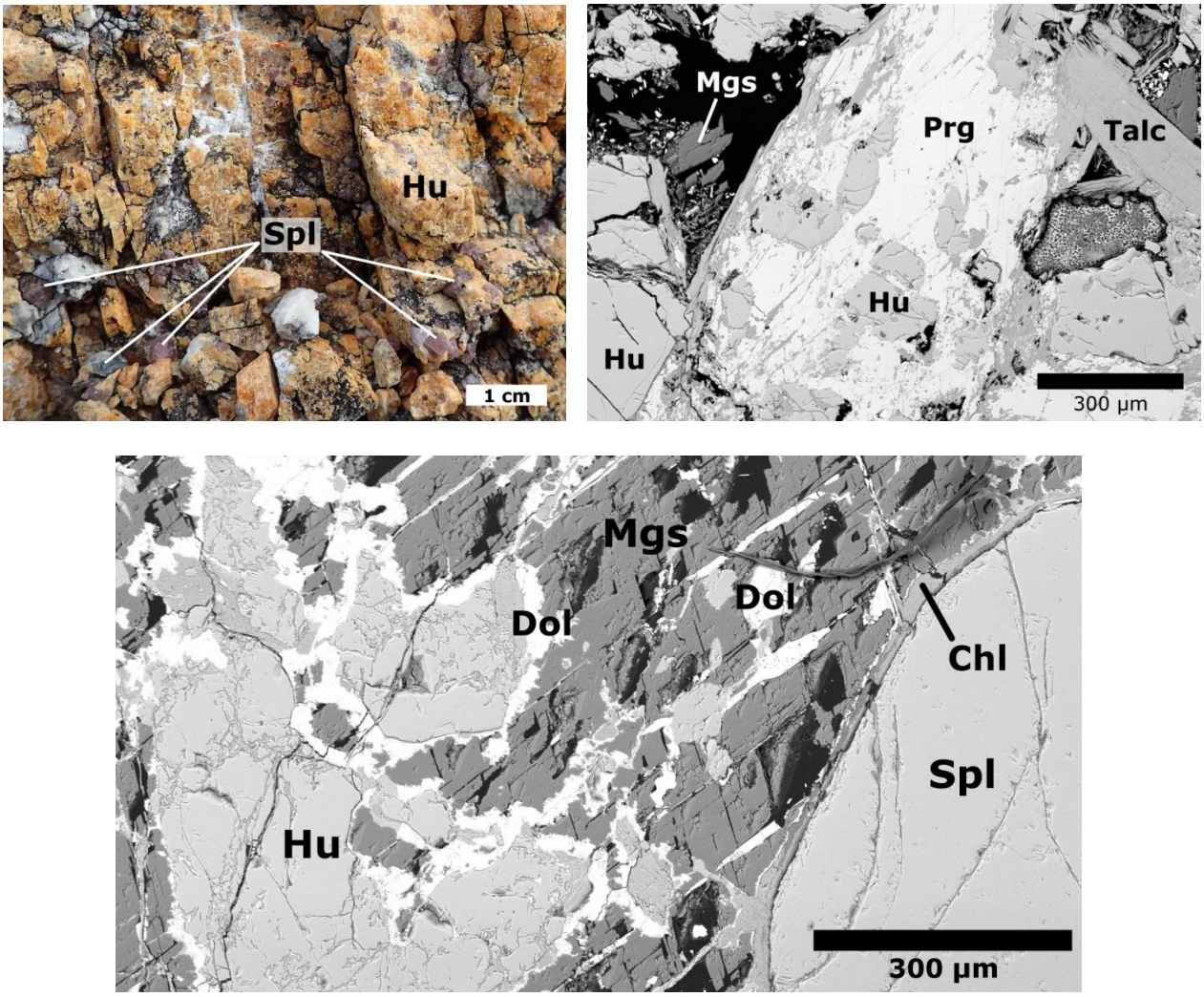

Figure 4.11: (A: top left) Spinel (Spl) and white carbonate in humite (Hu). (B: top right) Textural relationship between pargasite (Prg) and humite (Hu) suggesting replacement of the latter by the former. Sample contains talc and magnesite (Mgs). Backscattered electron image. (C: bottom) Dolomite (Dol) bordering magnesite (Mgs) and humite (Hu). Spinel (Spl) is surrounded by a thin rim of clinochlore (Chl). Soper Falls spinel occurrence, Kimmirut area.

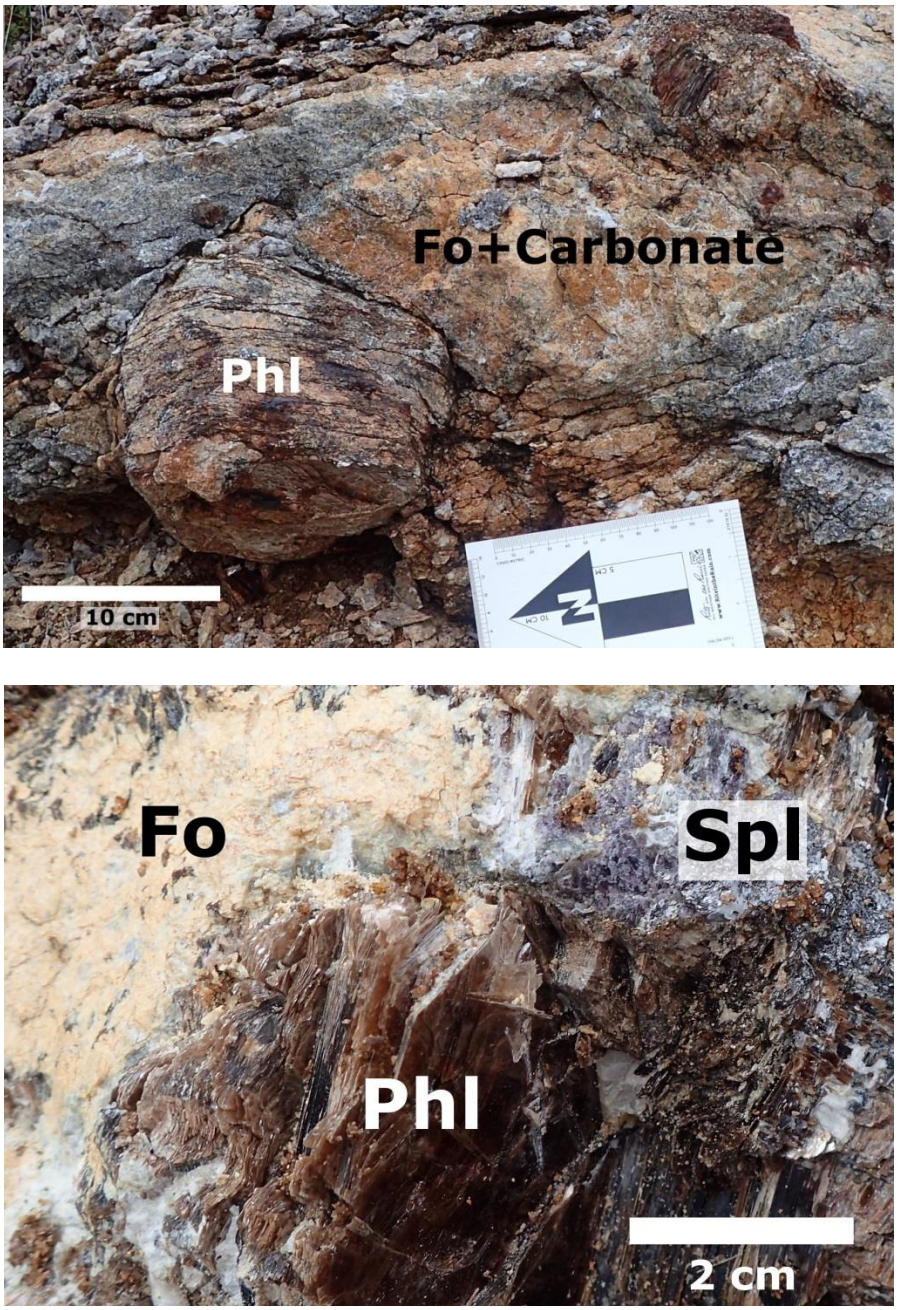

Figure 4.12: (A) Phlogopite (Phl) porphyroblast in coarse-grained forsterite (Fo) and carbonate rock in the rock face at the Soper Lake mica mine, Kimmirut area. (B) Purple spinel (Spl) with phlogopite (Phl) and forsterite (Fo) in the Soper Lake mica pit, Kimmirut area.

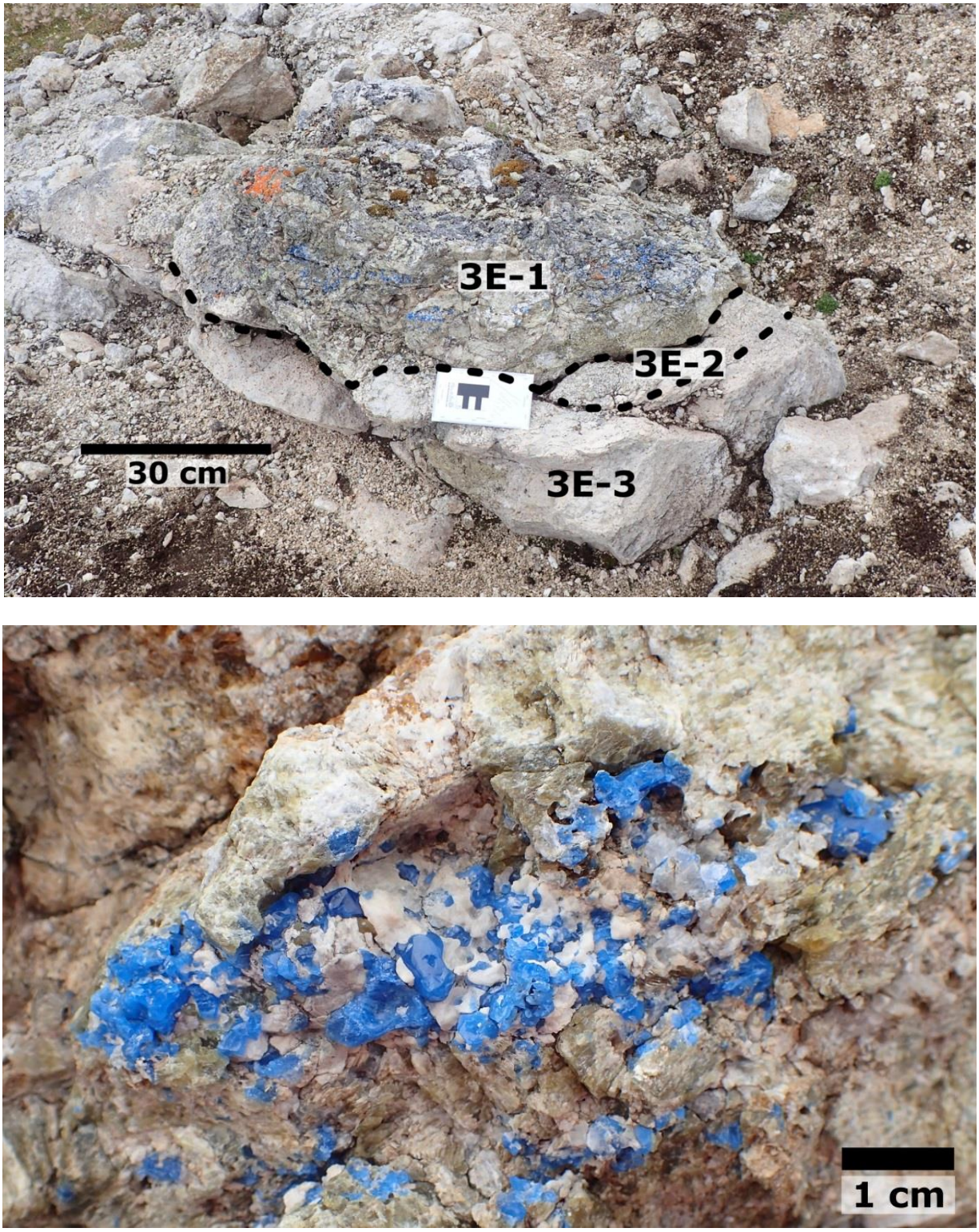

Figure 4.13: (A: top) Cobalt-blue spinel outcrop at the Qila occurrence: [3E-1] Calc-silicate pod; [3E-2] Pargasite-calcite rock; [3E-3] Marble. (B: bottom) Vivid blue spinel with white carbonate in calc-silicate rock composed of green pargasite with subordinate greyish scapolite. Qila occurrence [rock unit 3E-1], Kimmirut area.

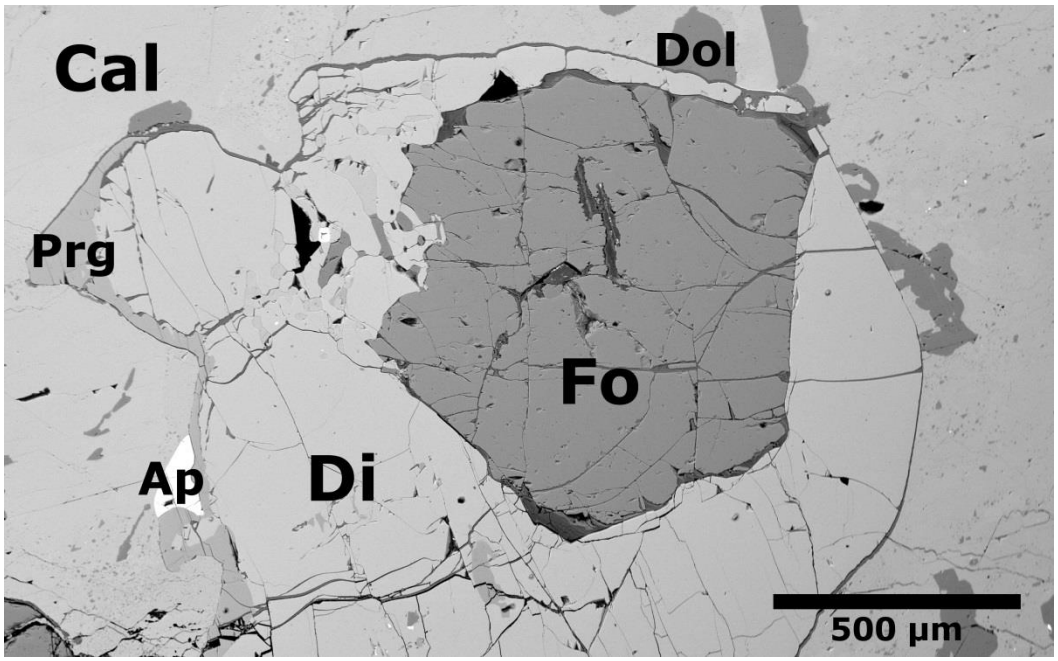

Figure 4.14: Forsterite (Fo) with a diopside (Di) interior corona and partial pargasite (Prg) exterior corona in calcite (Cal) and dolomite (Dol) marble. Trace apatite (Ap). Backscattered electron image. Qila cobalt-spinel marble (sample 3E-3-A), Kimmirut area.

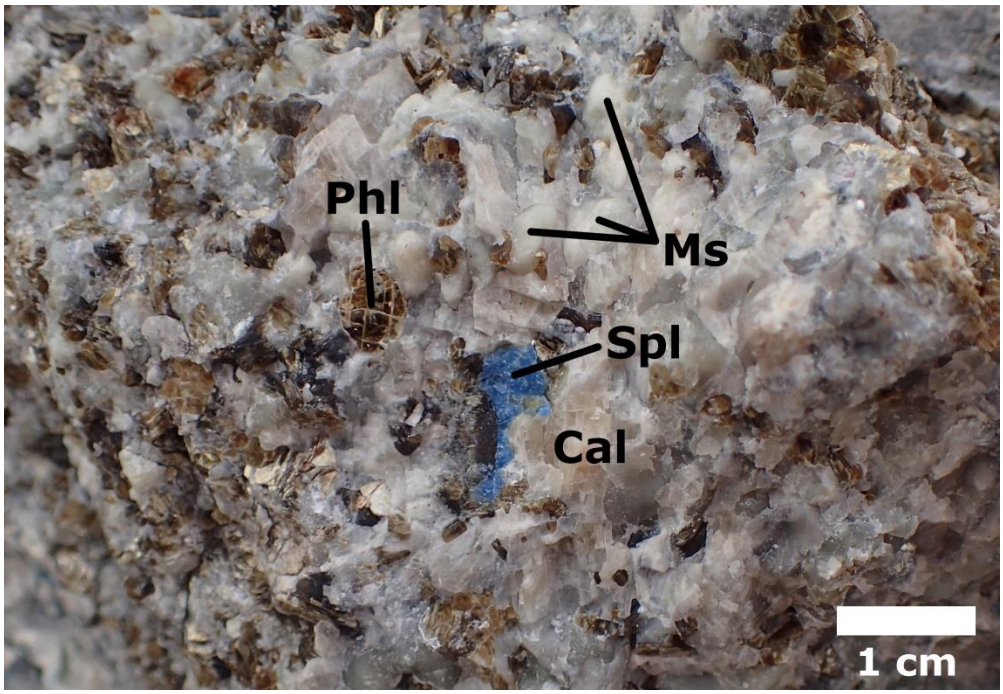

Figure 4.15: Silicate-rich spinel-bearing rock (*e.g.*, sample 3F-1), the predominant spinel-bearing unit at the Trailside occurrence, Kimmirut area. It is composed of fine-grained muscovite (Ms) pseudomorphs after an unknown mineral, coarse-grained phlogopite (Phl), calcite (Cal), and spinel (Spl).

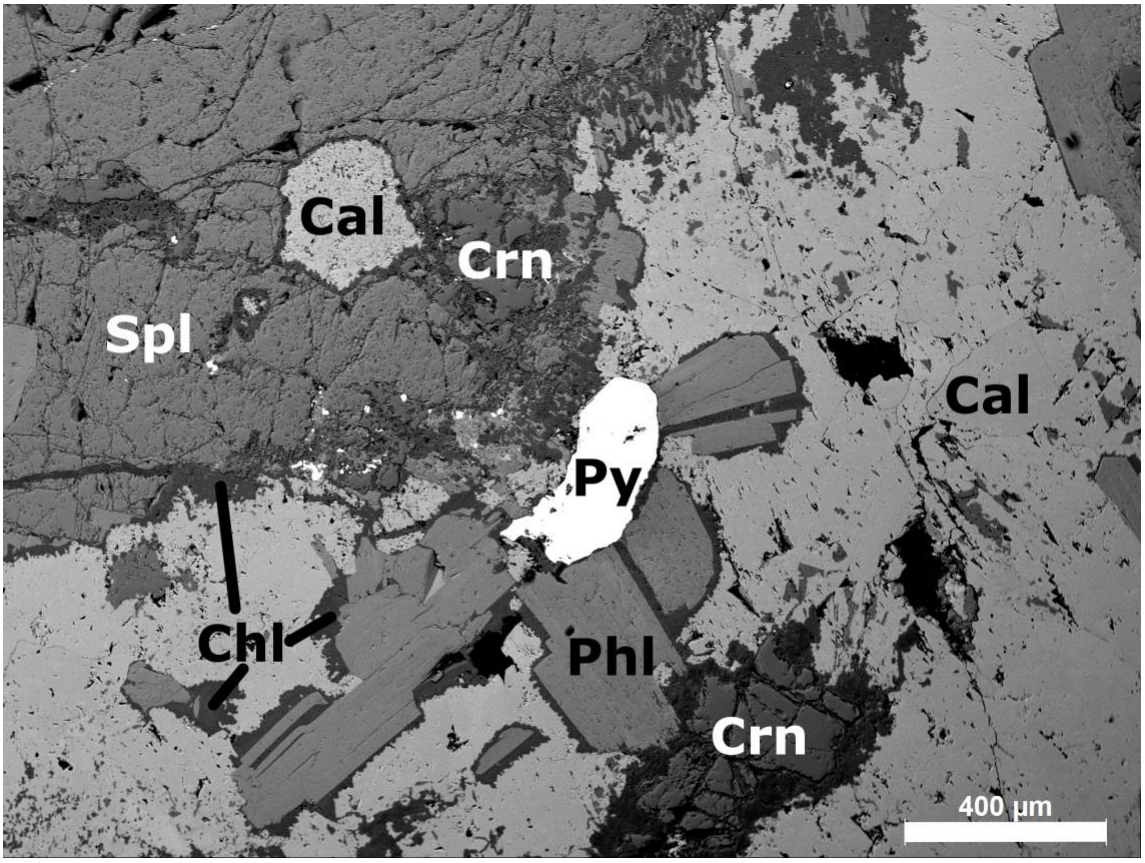

Figure 4.16: Spinel (Spl) partly altered to corundum (Crn) and clinochlore (Chl). Phlogopite (Phl) has rims of clinochlore. With accessory pyrite (Py) and hosted in calcite (Cal). Backscattered electron image. Trailside occurrence (Zone 3F-1), Kimmirut area.

Figure 4.17: Cobalt-blue spinel gemstone, 0.16 carats (0.032 grams) from the Trailside occurrence, Kimmirut area. B.S. Wilson photo. After Wilson (2014).

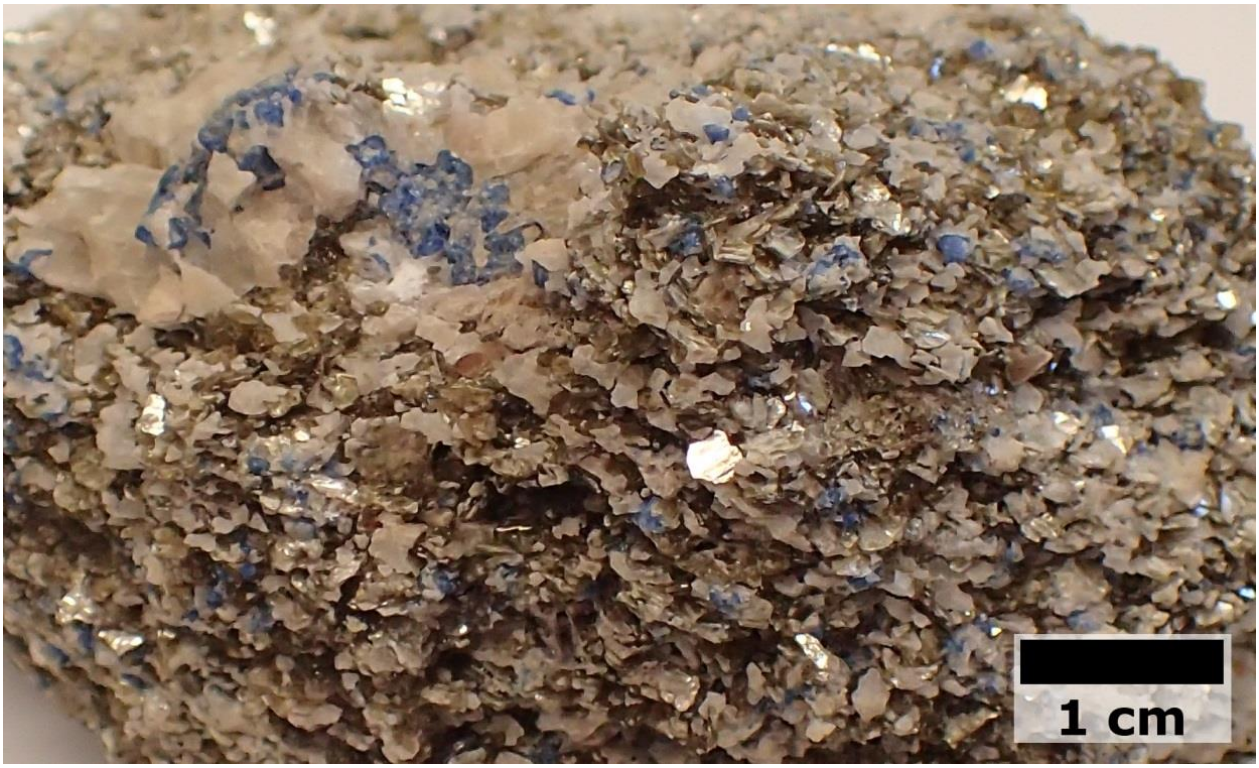

Figure 4.18: Foliated rock composed of pale yellow calcite, pale brown phlogopite, and cobalt-blue spinel (sample 3F-2) found as float above the main outcrop. Trailside occurrence, Kimmirut area.

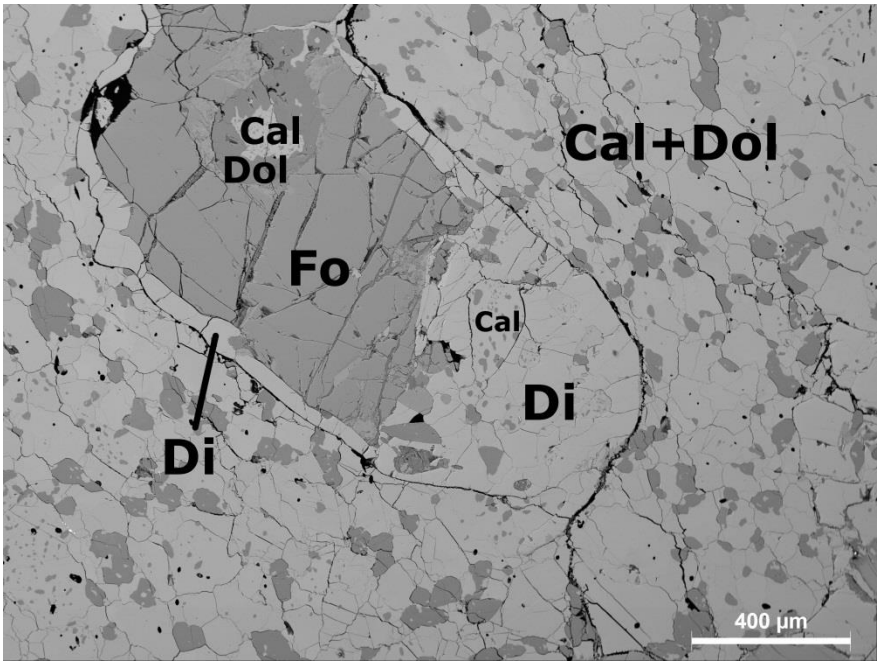

Figure 4.19: Apparent replacement of forsterite (Fo) by diopside (Di). Backscattered electron image. Sample 3F-M1 from the vicinity of the Trailside occurrence, Kimmirut area.

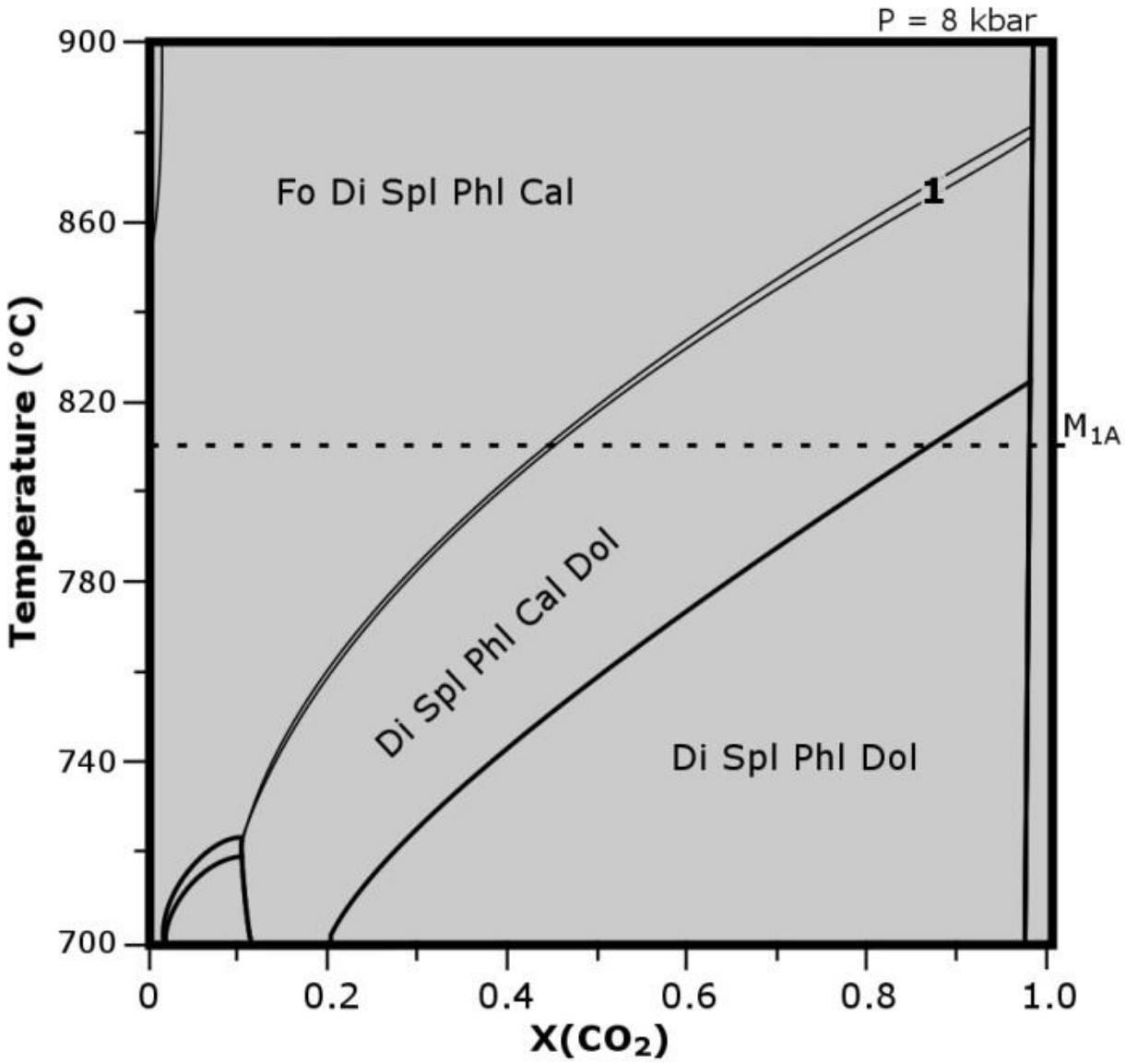

Figure 4.20: T-X(CO_2) pseudo-section for sample 2A-SPL-2, diopside-calcite-phlogopite-spinel rock from the Glencoe Main occurrence, Glencoe Island. Mineral assemblage "1" consists of forsterite (Fo), diopside (Di), spinel (Spl), phlogopite (Phl), calcite (Cal) and dolomite (Dol). Grey shading indicates conditions at which spinel is stable. M_{1A} represents peak metamorphic conditions after St-Onge *et al.* (2007).

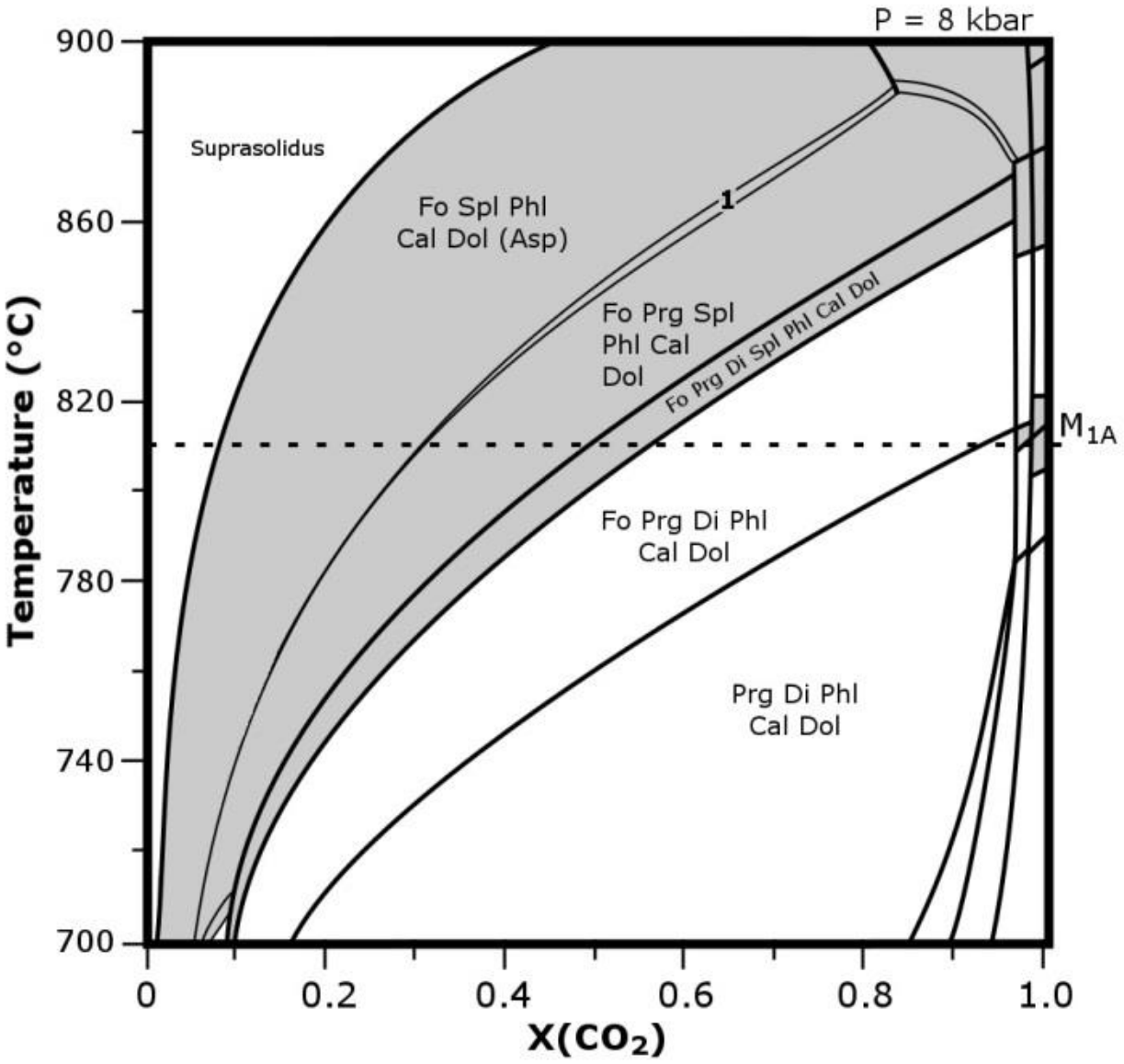

Figure 4.21: T-X(CO_2) pseudo-section for sample 3A-1, representative marble from the Soper River spinel occurrence near Kimmirut containing calcite (Cal) and dolomite (Dol) with subordinate spinel (Spl), pargasite (Prg), phlogopite (Phl), and fine-grained replacements of diopside (Di) and dolomite after an unknown mineral, probably forsterite (Fo). Mineral assemblage "1" consists of Fo, Prg, Spl, Phl, Asp, Cal and Dol. Aspidolite (Asp; Na-end-member of phlogopite) is predicted to occur, but the solution model for phlogopite/biotite does not account for substitution of Na for K. Grey shading indicates conditions at which spinel is stable. M_{1A} represents peak metamorphic conditions after St-Onge *et al.* (2007).

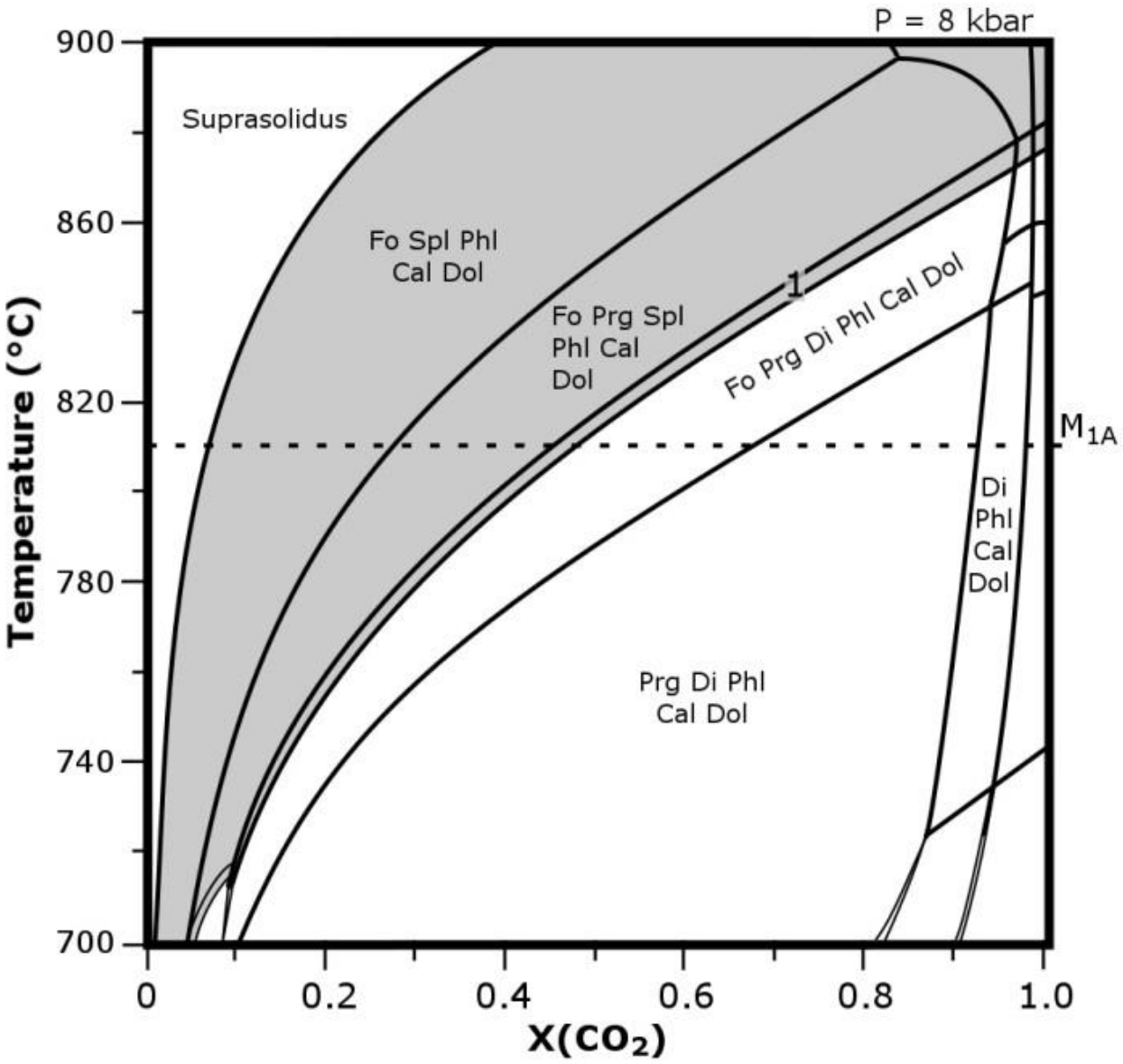

Figure 4.22: T-X(CO_2) pseudo-section for sample 3E-3-A, spinel-bearing marble from the Qila occurrence near Kimmirut. Mineral assemblage "1" consists of forsterite (Fo), pargasite (Prg), diopside (Di), spinel (Spl), phlogopite (Phl), calcite (Cal) and dolomite (Dol). Grey shading indicates conditions at which spinel is stable. M_{1A} represents peak metamorphic conditions after St-Onge *et al.* (2007).

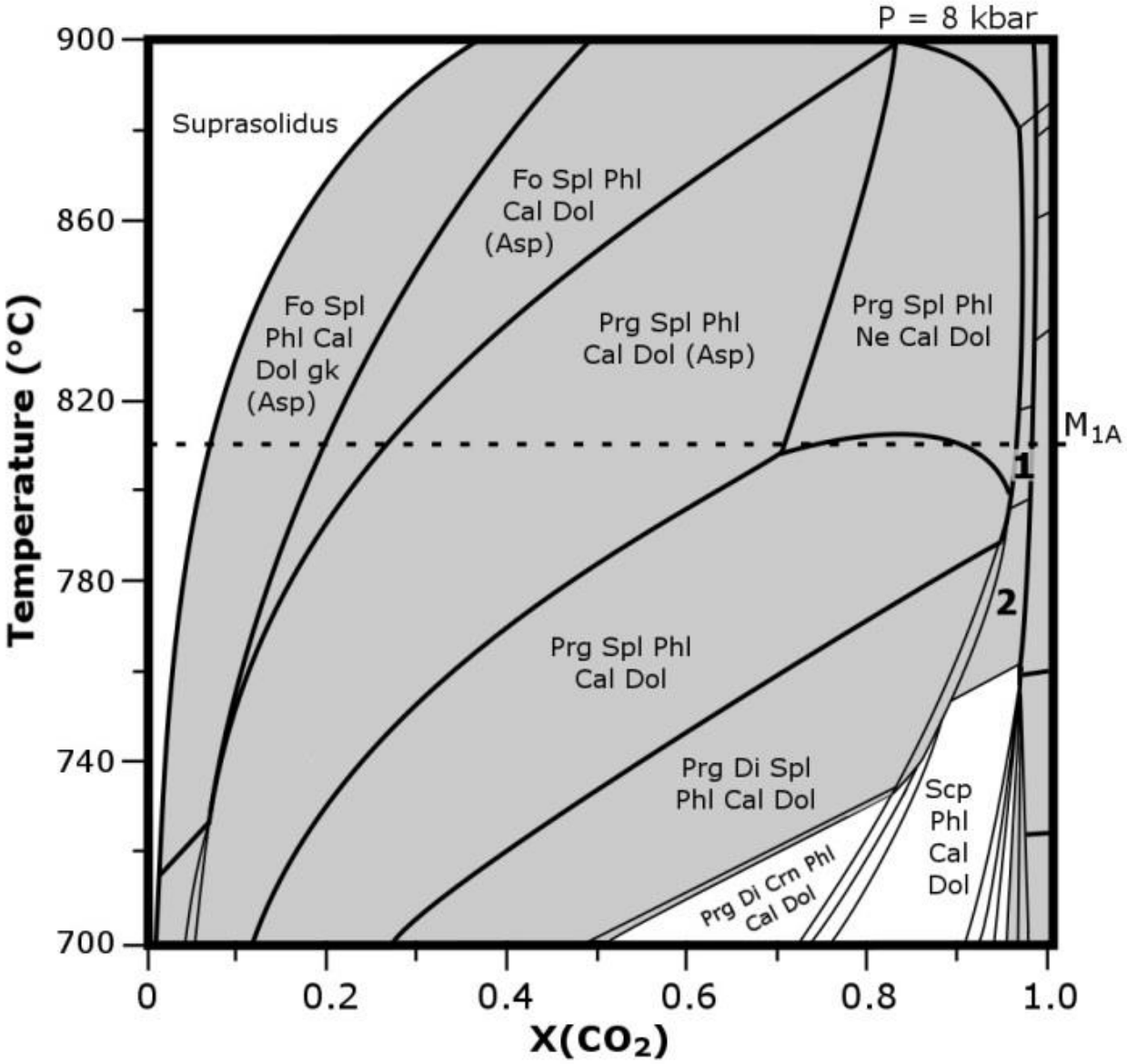

Figure 4.23: T-X(CO_2) pseudo-section for sample 3F-2, phlogopite-carbonate-spinel rock from the Trailside occurrence near Kimmirut. Mineral assemblage "1" consists of scapolite (Scp), spinel (Spl), phlogopite (Phl), nepheline (Ne), calcite (Cal), and dolomite (Dol). Assemblage "2" consists of Scp, Spl, Phl, Cal, and Dol. Also plotted are geikielite (gk), pargasite (Prg), and corundum (Crn) bearing assemblages. Aspidolite (Asp; Na-end-member of phlogopite) is predicted to occur, but the solution model for phlogopite/biotite does not account for substitution of Na for K. Grey shading indicates conditions at which spinel is stable. M_{1A} represents peak metamorphic conditions after St-Onge *et al.* (2007).

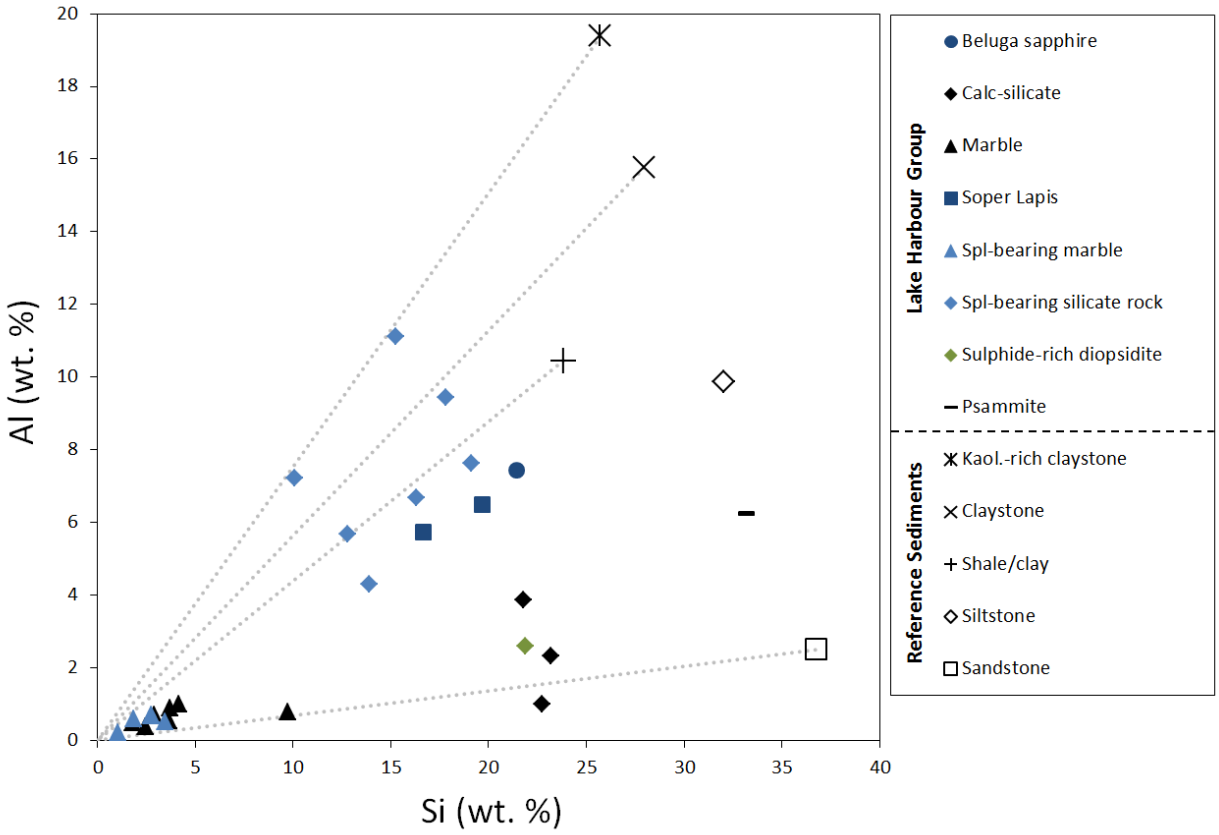

Figure 4.24: Aluminium and silicon content of LHG metasedimentary rocks and reference sedimentary rocks (kaolinite-rich claystone #AR-33, claystone and siltstone averages after López *et al.* 2005; average shale/clay after Parker 1967; average sandstone after Turekian & Wedepohl 1961). Dashed lines represent Al/Si for the reference sediment values used in protolith composition estimate calculations.

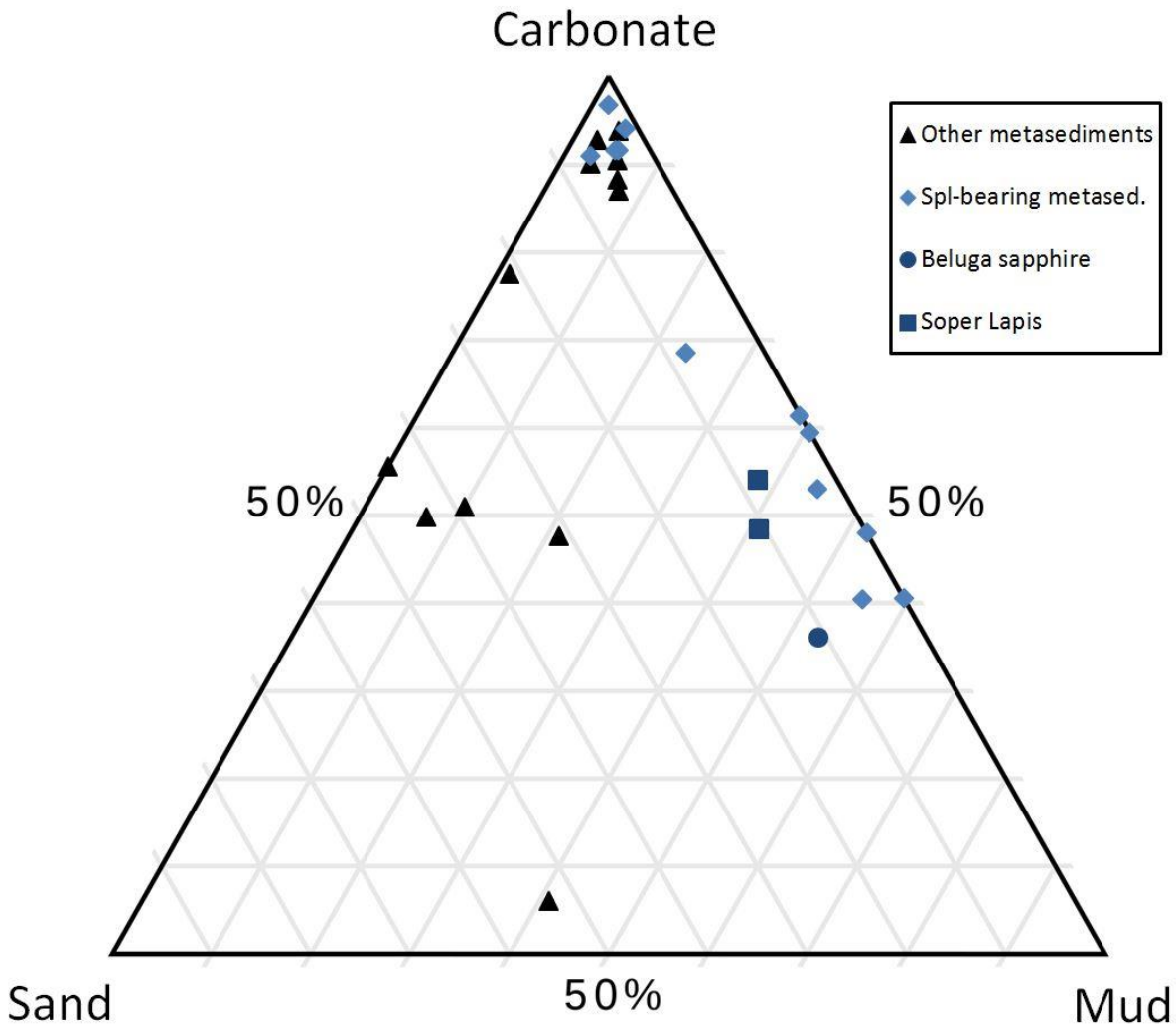

Figure 4.25: Ternary plot of the estimated protolith sedimentary composition (wt. %) for LHG spinel-bearing rocks, calc-silicate rocks, marble, Beluga sapphire calc-silicate rock, and Soper River lapis lazuli. For lapis lazuli, the evaporite component is included with carbonate.

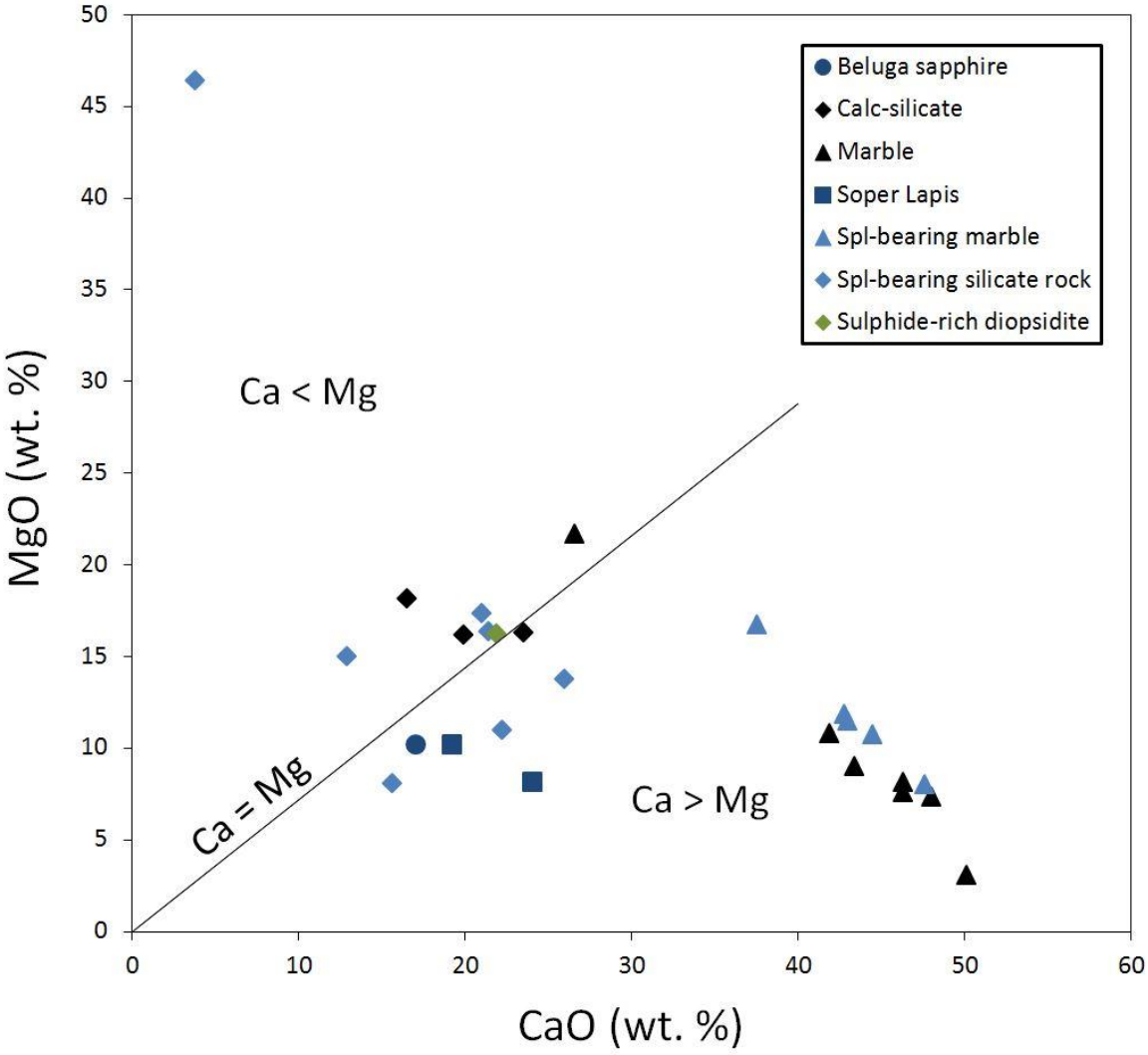

Figure 4.26: CaO and MgO content of LHG calc-silicate rocks, marbles, Beluga sapphire-bearing calc-silicate rock, and Soper River lapis lazuli.

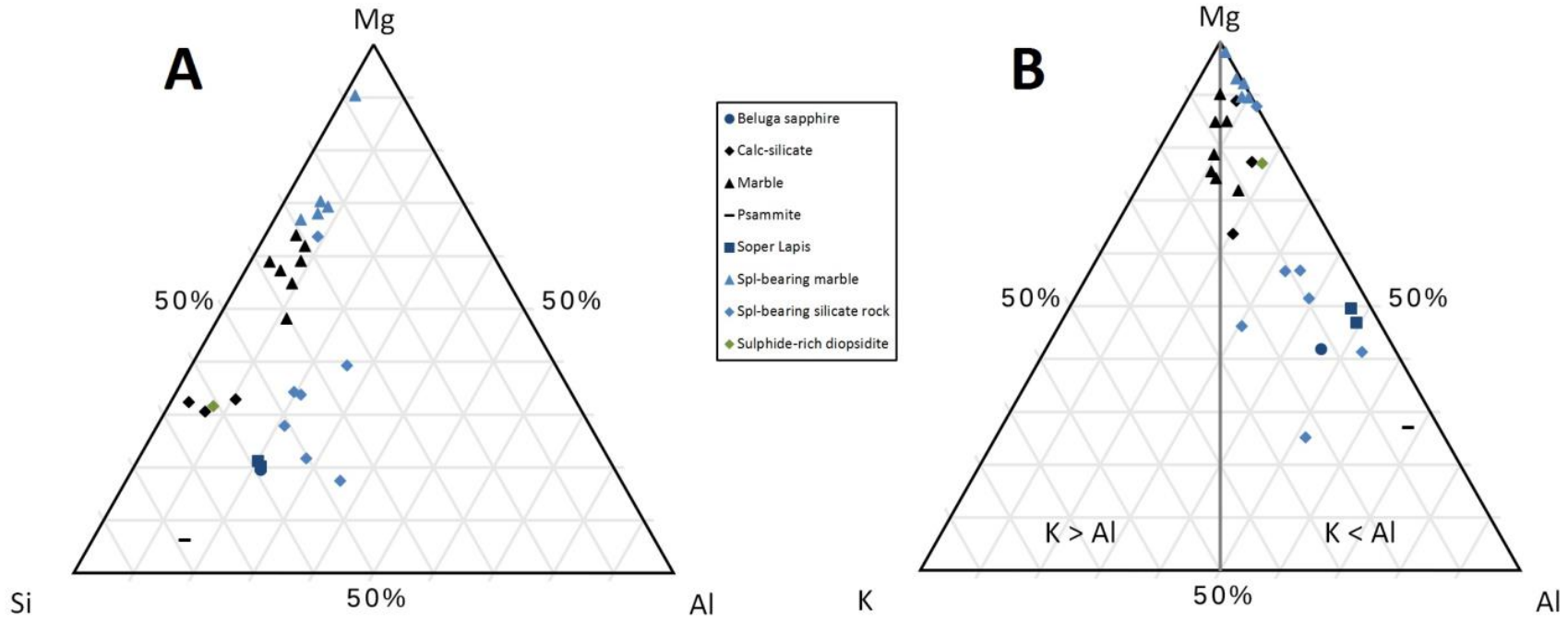

Figure 4.27: (A) Mg-Al-Si ternary diagram of LHG metacarbonate rocks and psammite (relative mol. %); (B) Mg-Al-K ternary diagram of LHG metacarbonate rocks and psammite (relative mol. %).

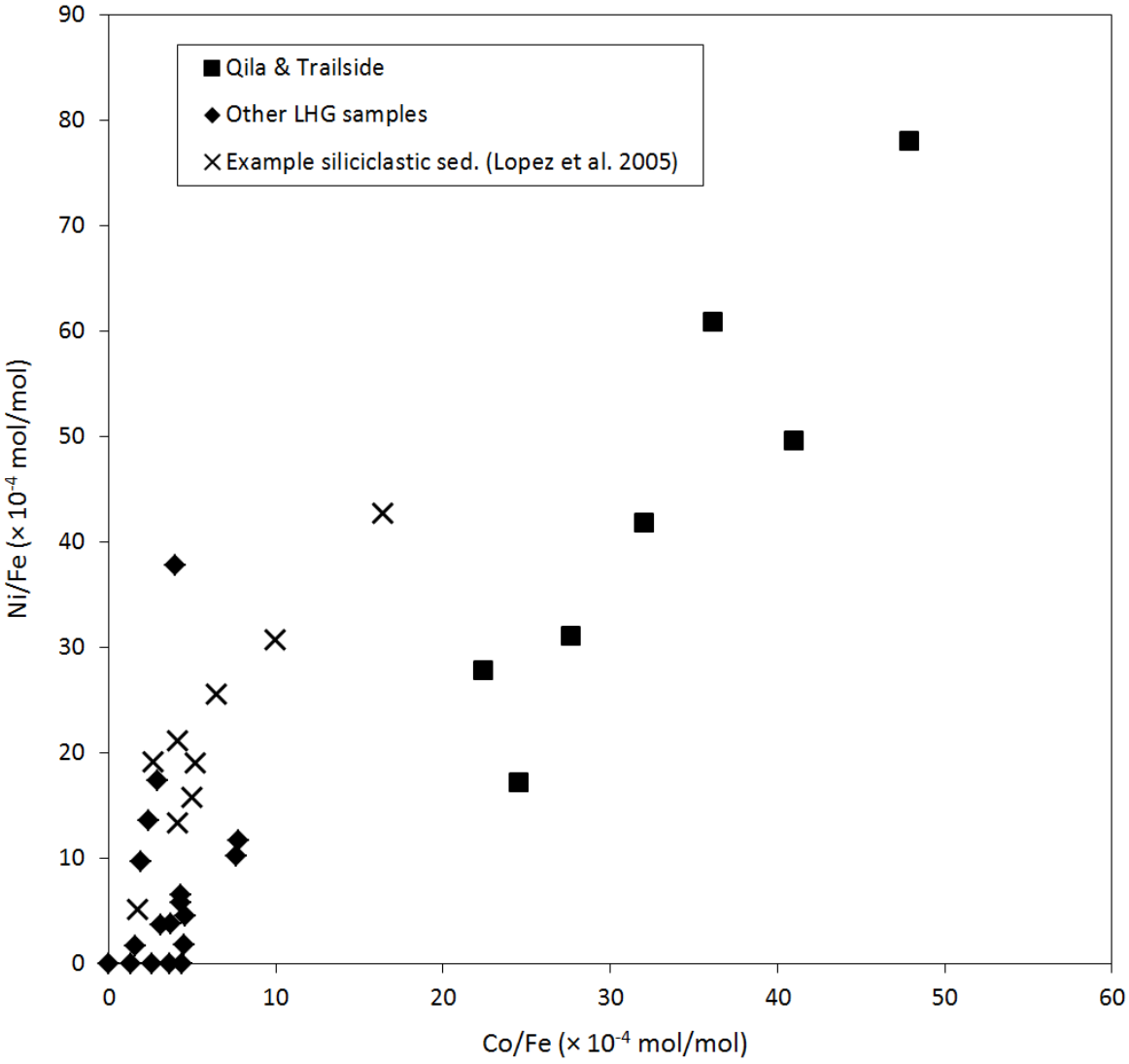

Figure 4.28: Whole rock Co/Fe plotted against Ni/Fe to illustrate the range of Qila and Trailside compared to other Lake Harbour Group metasediments (mostly calc-silicate metacarbonate and marble) and an example set of siliciclastic sedimentary rocks (López *et al.* 2005). LHG samples with Co or Ni below detection limit are excluded from the diagram.

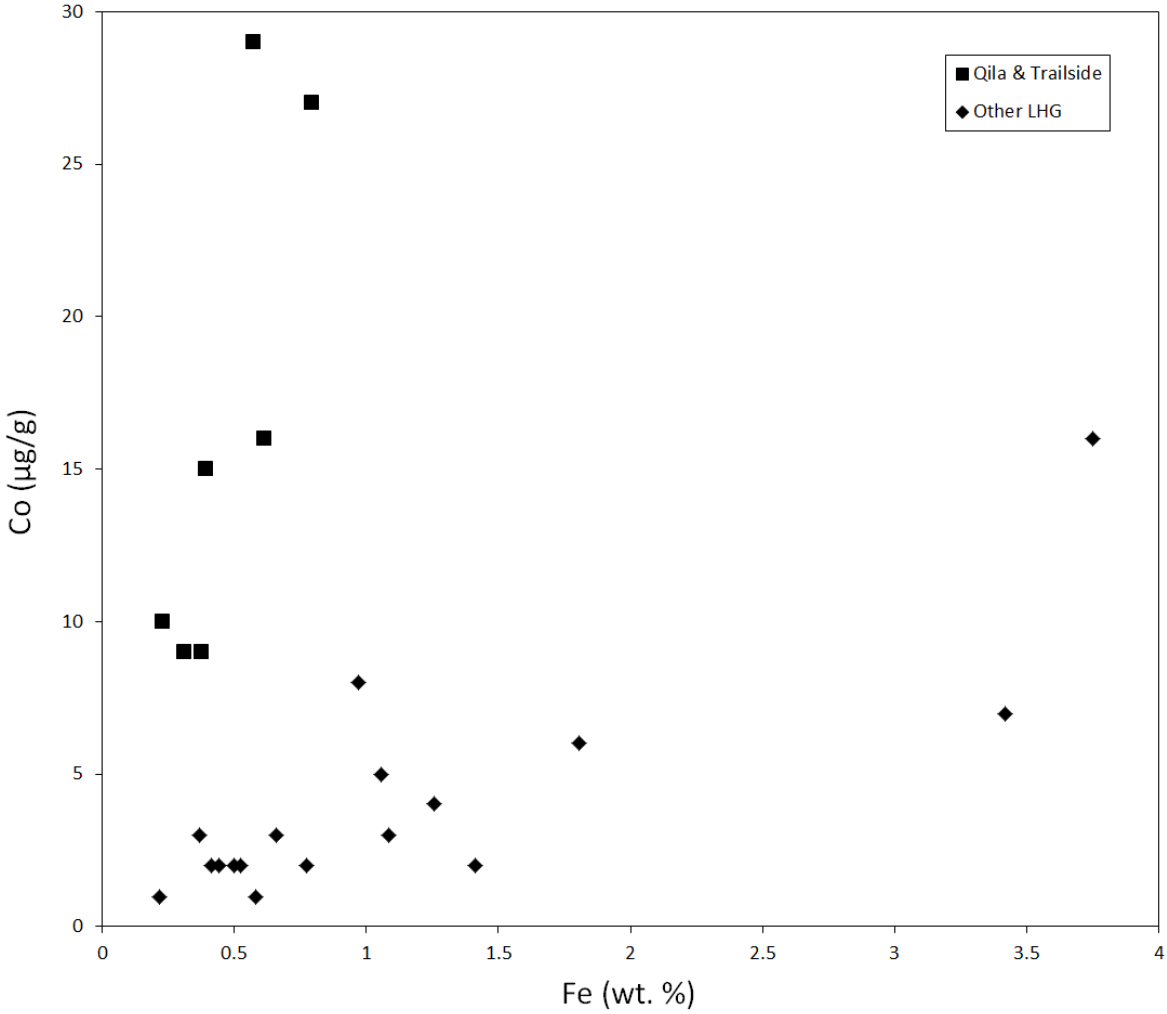

Figure 4.29: Whole rock concentrations of cobalt and iron illustrating the high level of Co enrichment relative to Fe in rocks from Qila and Trailside in comparison to other Lake Harbour Group metasediments analyzed in the present study. Samples with Co below detection limit are excluded from the diagram.

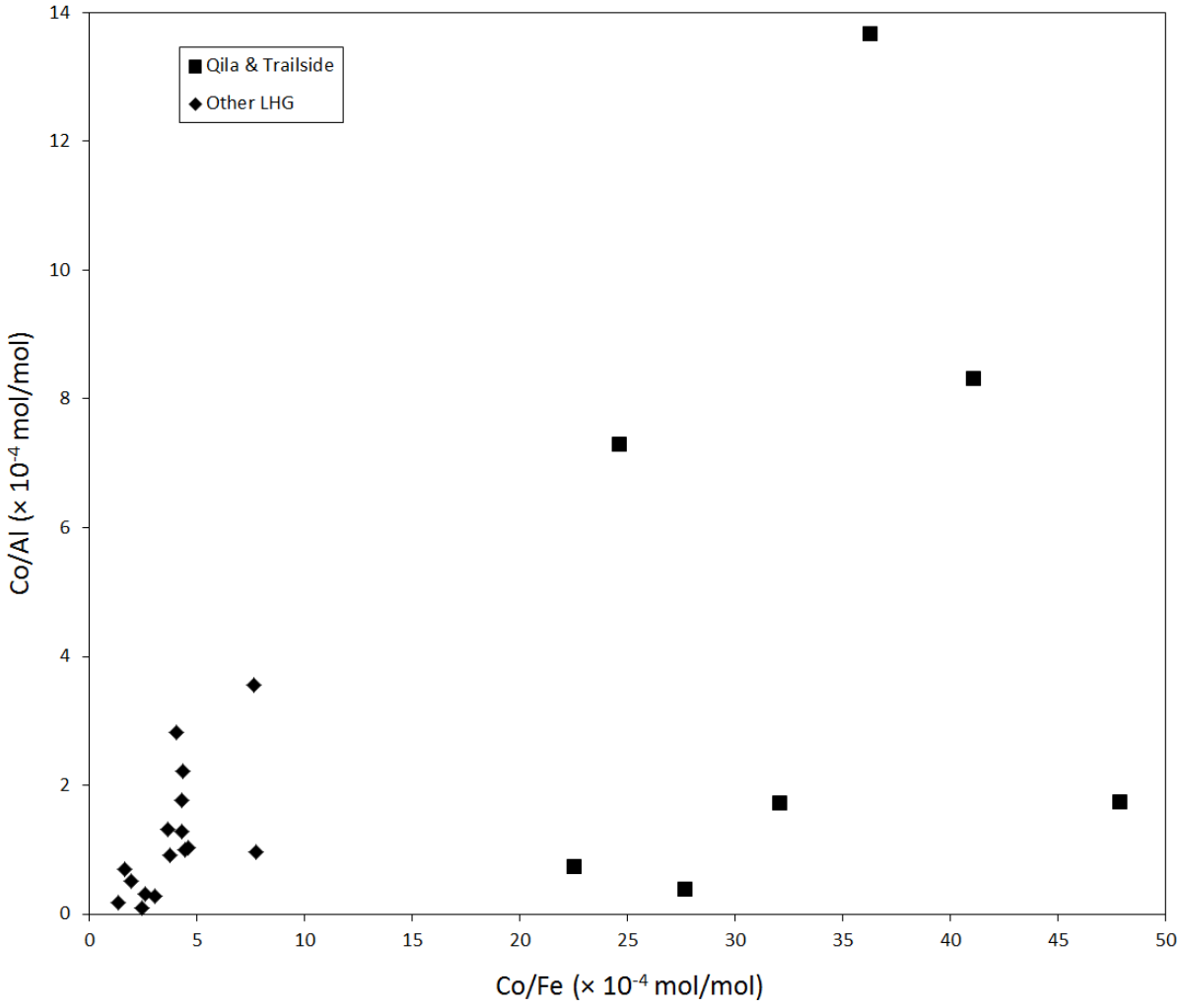

Figure 4.30: Whole rock Co/Al *vs.* Co/Fe in Lake Harbour Group metasediments illustrating the wide range in Co/Al at Qila and Trailside due to low Al contents in Qila Co-rich marble and Trailside Co-rich diopsidite. Sample 3D-2 is excluded due to significant under-representation of Al in the sample relative to the rock unit.

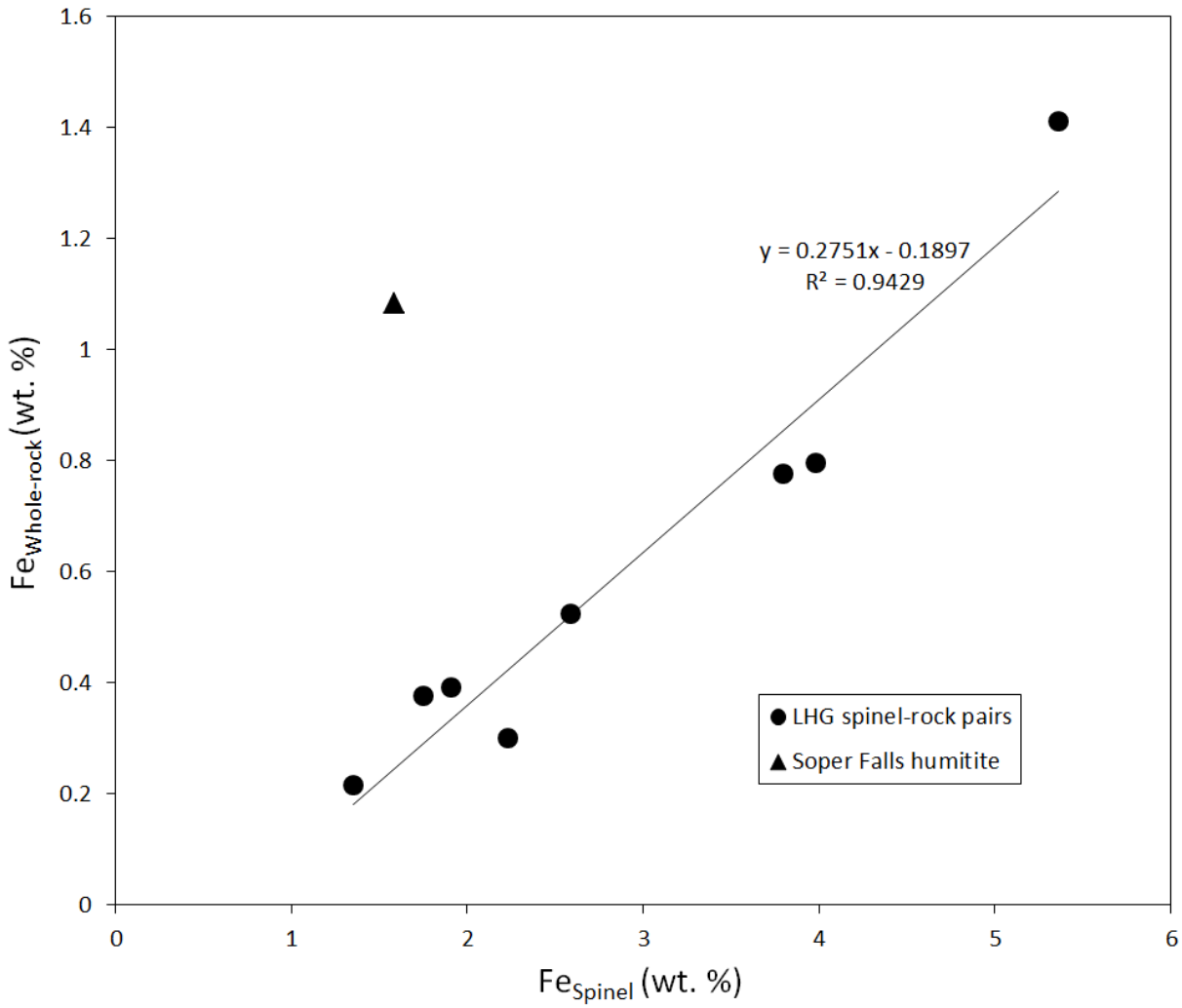

Figure 4.31: Iron content of spinel compared to its host rock. Samples insufficiently mineralogically representative of rock unit composition were excluded. Only the spinel-rock pair from Soper Falls humitite deviates from the trend (excluded from the linear regression trendline).

Chapter 5. Soper River lapis lazuli: Protolith and effect on quality

5.1 Chapter introduction

Bands of lapis lazuli described by Hogarth (1971) and Hogarth & Griffin (1978) occur in the same marble exposure as the Soper River spinel locality north of Kimmirut (Fig. 4.8). Hogarth & Griffin (1978) convincingly demonstrated that the lapis lazuli is a metamorphosed evaporite based on its well-developed layering parallel to regional foliation, the dearth of intrusive rocks in the area, and the elevated concentration of elements typically associated with evaporites. This chapter refines their interpretations of the lapis lazuli protolith and examines how the protolith composition has affected the suitability of Soper River lapis lazuli for use as a gem material.

5.2 Results

5.2.1 Mineralogical composition

Lapis lazuli rock samples from the main Soper River lapis lazuli occurrence (Fig. 5.1) were observed with a standard binocular microscope. The rock samples are medium-grained (Fig. 5.2) and dominantly composed of blue haüyne, pale grey diopside, and pale yellowish calcite with subordinate phlogopite and pyrite, consistent with the previous petrographic descriptions of Hogarth (1971).

5.2.2 Whole rock major element composition

The major element composition of Soper River lapis lazuli (Table 4.14B) is relatively similar to that of other calc-silicate rocks sampled in the Lake Harbour Group (see Chapters 3 and 4) with the exception of slightly low K concentrations (~ 0.5 wt. % K_2O) and exceptionally high Na concentrations (6.33 – 6.96 wt. % Na_2O *vs* ≤ 2.71 wt. % Na_2O in other sampled LHG calc-silicate rocks). The high Na concentrations reflect the high abundance of haüyne, a sodium-

rich feldspathoid. Soper River lapis lazuli contains 0.98 to 1.27 wt. % S, which is primarily incorporated in pyrite and haüyne, and is comparable in concentration only with sulphide-rich metamorphic rocks in the LHG (sulphide-rich diopsidite, psammite; see Chapter 4).

5.2.3 Whole rock trace element composition

Compared to other LHG marbles and calc-silicate rocks, the trace element composition of Soper River lapis lazuli rock (Table 4.15B) is characterized by high concentrations of As-Se-Mo (presumably due to the presence of pyrite), Cl, F, an average amount of B (17 µg/g), and very low Co-Ni-Cu. Relatively high sulphur contents (~ 1 wt. %) are due to the presence of haüyne (sulphate-bearing feldspathoid) and pyrite.

5.3 Discussion

5.3.1 Evaporitic origin and protolith

Previous work by Hogarth & Griffin (1978) demonstrated that Soper River lapis lazuli is a metamorphosed evaporite layer in marble (see Section 1.6.3). Indeed, the Na_2O concentrations in whole rock samples (~ 6 wt. %) are anomalously high; more than twice that in the LHG calc-silicate rock that is the second richest in Na_2O (Beluga sapphire-bearing calc-silicate, 2.71 wt. %); as is the concentration of chlorine, 3170 µg/g, almost thrice that of the Cl-bearing pargasite-rich Qila calc-silicate rock (1160 µg/g). Sodium and Cl could have been sourced from a halite component in the original lapis lazuli protolith, but could also be the result of evaporite-derived Na- and Cl-enriched fluid. The high abundance of haüyne (the Na-rich mineral phase) in the lapis lazuli bands over a large geographical area is more consistent with a halite-bearing protolith. Under this assumption, an estimation of the original protolith composition (method in Chapter 4; Table 4.16B; Fig. 4.25) is an evaporitic dolomitic marl, composed of *ca.* (by weight) 40% carbonate (dolomite ≈ calcite to dolomite > calcite), 10 % halite, and 50 % siliciclastic mud.

Hogarth (1971) proposed the presence of anhydrite in the protolith to explain the relatively high S concentrations (~1 wt. %), an element that is a fundamental component of haüyne. Therefore, lapis lazuli rock (and therefore the protolith) is relatively similar in major element composition (*i.e.*, characteristic of metamorphosed dolomitic marl) to spinel-bearing calc-silicates (Chapter 4) and Beluga sapphire-bearing calc-silicate rock (Chapter 3), but differs from the spinel-bearing rocks in lower Mg/Ca and Al/Si, and differs from both the spinel- and sapphire-bearing rocks in its high Na and S content. The abundance of Na and S, in this case interpreted to be due to the presence of halite and anhydrite evaporites in the dolomitic marl protolith, is key to forming lapis lazuli.

5.3.2 Composition of protolith vs. gem quality of lapis lazuli

Soper River lapis lazuli is not suitable as a commercial gem material due to its low haüyne concentration (*i.e.*, Fig. 5.2) relative to that of significantly higher quality materials from producing deposits (*e.g.*, Sar-e-Sang, Afghanistan). The small crystal size of haüyne at Soper River precludes the use of single crystals as gem materials. The high percentage of calcite and diopside are, therefore, detrimental to lapis lazuli gem quality, and the abundance of these minerals is interpreted to reflect the composition of the protolith (carbonate content, carbonate species, character of the siliciclastic component such as relative abundance of Al and Si).

Lapis lazuli formed by metasomatism at two of the three major deposits (Chile, Coenraads & Canut de Bon 2000; Russia, Deer *et al.* 2004 and references therein) and metasomatism possibly occurred at Sar-e-Sang, Afghanistan, especially for haüyne formed at the contact with granite/pegmatite (Faryad 2002 and references therein). While haüyne can occur in metasediments (*sensu stricto*), the protolith composition of lapis lazuli at Soper River is unsuitable for the genesis of gem grade lapis lazuli. Haüyne contains an equal molar abundance

of Al and Si (Al/Si = 1), but siliciclastic sediments generally have lower Al/Si (kaolinite-rich claystone Al/Si = 0.78 mol/mol, López *et al.* 2005; average shale/clay Al/Si = 0.46, Parker 1967). Two samples of Soper River lapis lazuli have Al/Si ≈ 0.32. Therefore, higher concentrations of haüyne in lapis lazuli rock would be favoured by higher proportions of Al relative to Si (*i.e.*, higher shale/clay siliciclastic component relative to silt/sand in protolith), an abundance of evaporites (*i.e.*, halite and anhydrite, providing the key elements Na and S, respectively, required for haüyne formation), and a lower proportion of carbonate. Metasedimentary (*sensu stricto*) gem-grade lapis lazuli is likely possible, but non-ideal proportions of Al/Si (siliciclastic component), carbonates, and potentially evaporites in the Soper River lapis lazuli protolith are expected to have prevented the genesis of high-quality gem lapis lazuli.

5.4 Conclusions

Soper River lapis lazuli is interpreted to consist of a metamorphosed dolomite-bearing to dolomitic marl that contained a significant evaporitic component (halite and subordinate anhydrite). The enrichment of Na and S from evaporite is required to form haüyne, the blue mineral that is the fundamental component of lapis lazuli rock. The Soper River lapis lazuli deposit is of relatively low gem quality due to its relatively low concentration of haüyne compared to commercial grade gem-quality lapis lazuli from other localities. Low Al/Si (interpreted to be a result of a silty siliciclastic component) and high carbonate content in the protolith prevented the genesis of high-quality gem lapis lazuli at Soper River.

5.5 Figures

Figure 5.1: Part of the weathered lapis lazuli band at the main Soper River occurrence, looking SE toward the violet spinel occurrence.

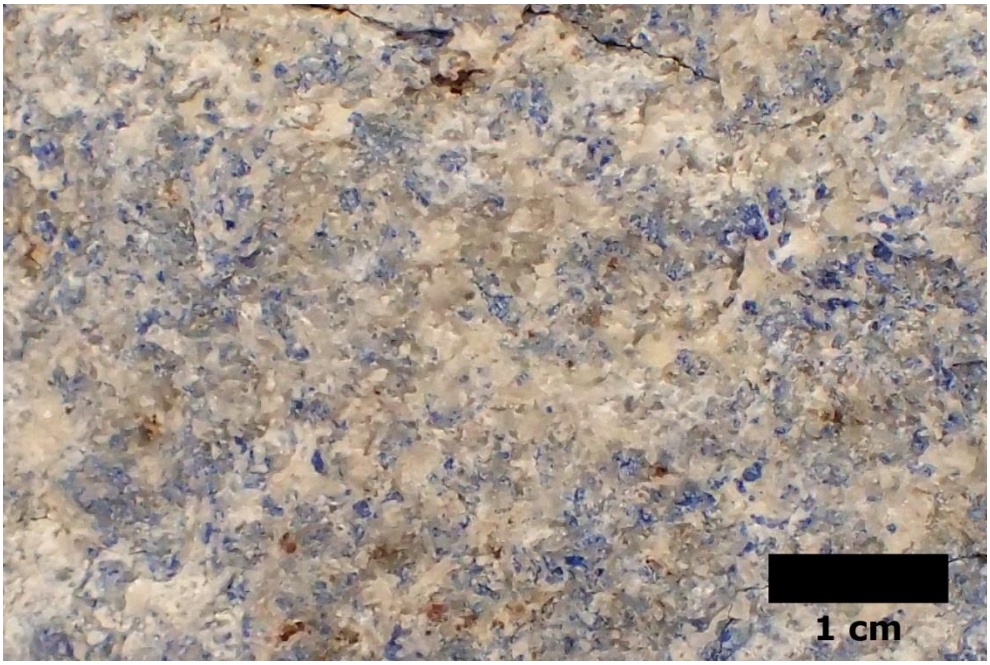

Figure 5.2: Lapis lazuli rock from Soper River. The rock is composed of pale yellowish calcite, grey diopside, and blue haüyne.

Chapter 6. General deposit model and exploration criteria

6.1 Fundamental assumptions about LHG metacarbonate protoliths

The Kimmirut calc-silicate-hosted sapphire occurrences and most spinel occurrences are interpreted to be metasedimentary on the basis of their isolation within a metacarbonate sequence with no proximal magmatic intrusions or textural/mineralogical evidence for metasomatism (Chapters 3 and 4). Most of these occurrences are sufficiently homogeneous (or show distinct separations between calc-silicates and marble) to warrant the assumption that their whole rock major element composition is representative of the original protolith composition, although the possibility of diagenetic and metamorphic transformations (especially with regards to more mobile elements) should not be discounted. It should be noted that deformation could also spatially redistribute rock-forming components, such that mineralogical/major element compositional zoning at some occurrences (*e.g.*, Trailside spinel occurrence, Chapter 4) may not be representative of the original protolith. However, hypothetical protolith compositions estimated from the metasedimentary rock bulk compositions would produce identical mineral assemblages if subjected to the same metamorphic conditions. Therefore, we consider the assumption that whole rock major-element compositions are representative of protolithic compositions, in most cases, to be a reasonable and useful new approach to understanding metasedimentary gem deposits.

Hogarth & Griffin (1978) supported the probable metasedimentary and evaporitic origin of Soper River lapis lazuli by citing the following evidence: (1) layering is well-developed and parallel to the regional foliation, suggesting that it is metasedimentary; (2) no intrusive rocks occur in the area, which argues against a contact metasomatic origin; and (3) the abundances of Na, K, S, Cl, Br, F, and Fe are consistent with evaporite-related sediments.

Using the aforementioned assumptions, estimates of protolith compositions were calculated for the following LHG rock types (Chapter 4): (1) marble and calc-silicate rocks barren of gem minerals; (2) spinel-bearing marble and calc-silicate rocks (including humite- and forsterite-rich metacarbonates); (3) sapphire-bearing calc-silicate rocks; and (3) lapis lazuli. Estimates were calculated by estimating the character of the siliciclastic component by comparing sample Al/Si to that of sedimentary averages and re-calculating the expected original concentration of carbonates (calcite, dolomite, magnesite) and, where applicable, halite.

6.2 Gem deposit model

6.2.1 Sedimentary protoliths and metasomatic occurrences

Corundum, spinel, and lapis lazuli occurrences in the LHG are all related to metasedimentary carbonates. More specifically, most occurrences are interpreted to have the following protoliths: (A) impure dolomite-bearing limestone to dolostone; (B) dolomitic marl; (C) magnesite-rich evaporitic marl; and (D) evaporite (halite and anhydrite)-bearing dolomite-rich marl (Fig. 6.1). Spinel at "Spinel Island" in Markham Bay formed from contact metasomatism of marble and syenogranite, which is probably related to the Cumberland batholith and, together with the metasomatic black spinel occurrence on a nearby unnamed island, are the most significant metasomatic spinel occurrences reported from the LHG, although the exact origin of the Soper River mica mine and Waddell Bay occurrences could not be assessed. The Contact occurrence on Glencoe Island is interpreted to have formed from the bimetasomatic reaction of contiguous gneiss and marble (Chapter 4). In metasedimentary occurrences, metacarbonates containing gem mineral species have carbonate-dominant protoliths (spinel) or mixed mud-carbonate(-evaporite) protoliths (corundum, spinel, lapis lazuli; Fig. 4.25).

6.2.2 Geochemical controls on gem mineral genesis

The gem minerals corundum, spinel, and haüyne (a feldspathoid) occur in silica undersaturated environments. Corundum near Kimmirut occurs in localized alteration zones within a calc-silicate rock, which formed during retrograde metamorphism. It should be noted that silica undersaturation in the whole rock at Kimmirut, during peak granulite facies metamorphism, was a key factor in forming the precursor assemblage containing nepheline, a key reactant in gem corundum genesis at the locality (Chapter 3). Therefore, silica undersaturation is a common feature of all LHG corundum-, spinel-, and haüyne-bearing rocks.

Silica undersaturation in LHG gem-mineral-bearing rocks is interpreted to have been achieved in three different ways (Chapters 3-5): (1) The mixing of siliciclastic and carbonate sediments in the protolith (*i.e.*, marl) with a high mud content, giving the rock a high alumina to silica ratio (*e.g.*, Kimmirut sapphire, metasedimentary spinel-bearing calc-silicates, lapis lazuli); (2) the occurrence of small amounts of siliciclastic impurities in a limestone or dolostone protolith (*e.g.*, spinel-bearing marbles); and (3) the bimetasomatic reaction of an Al-bearing, silica-rich rock with a contiguous marble (*e.g.*, syenogranite-marble on Spinel Island, gneiss-marble at the Glencoe Contact occurrence). In each case, decarbonation reactions led to the formation of various Ca- and Mg-silicate minerals and produced the Si-undersaturated conditions necessary for gem formation (oxide phase, spinel; feldspathoid, haüyne), or for generating a suitable precursor to corundum-bearing rock (nepheline-bearing calc-silicate rock).

A low potassium abundance (K/Al < 1 mol/mol) favors the formation of spinel, whereas high whole rock K/Al is hypothesized to result in the preferential incorporation of Al into phlogopite. The difference in K/Al between spinel-bearing and spinel-absent marbles is particularly significant in the LHG, likely due to the higher concentration of Si relative to Al

compared to the silicate-rich metacarbonates, in which Al/Si is the dominant differentiator between spinel-bearing and spinel-absent rocks (K/Al may also be a control on spinel concentration in calc-silicates; Chapter 4). However, in the case of bimetasomatic spinel- and phlogopite-bearing diopsidite on Spinel Island, Mg (*i.e.*, dolomite in the marble) rather than K is interpreted to have been the limiting element in the formation of spinel and additional diopside rather than phlogopite. X_{CO2} does not affect the presence of spinel in pseudo-sections of two silicate-rich metacarbonates, but it is an important control on the presence or absence of spinel in marbles at peak metamorphic conditions (Chapter 4).

In lapis lazuli, the contribution of Na and sulphate by evaporites, *i.e.*, halite and anhydrite, is required to form haüyne (Hogarth & Griffin 1978, Chapter 5). The Na content of Soper River lapis lazuli (~ 6 wt. % Na_2O) is considerably higher than that of other calc-silicate rocks in the LHG ($\leq$ 2.71 wt. % Na_2O; Chapter 5). Soper River lapis lazuli is unsuitable for use as a commercial gemstone due to its relatively high amount of calcite and diopside impurities; a protolith with a higher Al/Si fraction and lower carbonate content would be more favorable to gem lapis lazuli genesis.

6.2.3 Metamorphic controls on gem mineral genesis

In a broad sense, two conditions are required to form a metamorphic gem mineral occurrence. Firstly, a rock (or multiple rocks in the case of metasomatic occurrences) must be of favorable geochemistry and subjected to specific pressure and temperature in order to form the gem-bearing assemblage. Secondly, the gem mineral must not be significantly destroyed by subsequent metamorphic processes (*e.g.*, fluid influx during retrograde path at *P-T-x* where the mineral is not stable, or loss of gem quality from deformation of transparent gem materials). Calc-silicate hosted sapphires formed through a multi-step process requiring two retrograde

mineralization events at specific temperatures, while haüyne and metamorphic (*sensu stricto*) spinels are interpreted to have formed at granulite peak metamorphic conditions. None of the gem mineral species in the LHG studied thus far show significant levels of retrograde alteration; however spinel at a number of occurrences is heavily fractured.

Near Kimmirut, three sequential metamorphic reactions led to the formation of gem-quality corundum (Chapter 3). Granulite facies (peak) metamorphism of the dolomitic marl formed an assemblage of nepheline, diopside, and K-feldspar (inferred). This assemblage was partly retrogressed to phlogopite, oligoclase, calcite, and scapolite as a result of CO_2-, H_2O-, Cl-, and F-bearing fluid influx. The zircon U-Pb age from this first retrograde assemblage indicates crystallization ~30 Ma after the end of M_2 metamorphism (of St-Onge *et al.* 2007), and therefore at $P < 6.2$ kbar and $T < 720$ °C. The formation of scapolite in contact with nepheline is a necessary precursor to the second retrograde reaction, where corundum is formed:

Scapolite (Me_{57}) + 0.84 nepheline + 0.60 H_2O + 2.02 CO_2 → 0.76 corundum + 2.35 calcite + 2.14 albite + 0.60 muscovite + 0.66 Cl

The corundum-forming reaction occurs at lower *P-T* than the first retrograde assemblage. A thermodynamic model of the break-down of scapolite and nepheline to corundum, calcite, and albite (with scapolite modeled as end-member meionite) indicates that corundum can only form in a < 100 °C temperature window, bound by scapolite-nepheline stability at higher temperature and the formation of Al-silicate at lower temperature (Chapter 3).

Spinel studied at just over a dozen occurrences in the LHG (Chapter 4) is interpreted to have formed during granulite facies peak metamorphism based on stable mineral assemblages and, in several cases, thermodynamic modelling. Some occurrences (*e.g.*, Spinel Island) are assumed to have formed under these conditions based on the stability of similar assemblages that

were thermodynamically modeled (Glencoe Island main occurrence). The timing and *P-T* conditions of the Markham Bay unnamed island occurrence and the Waddell Bay occurrence could not be ascertained. Several, but not all, spinel-bearing assemblages in the Kimmirut area have peak metamorphic forsterite with subsequent (peak metamorphic or retrograde) diopside and/or pargasite, either as reaction rims or as well-developed crystals. Spinel at Spinel Island and the Trailside occurrence is locally, and in minor part, replaced by retrograde corundum in association with other minerals. The corundum alteration of spinel is not so significant as to affect the quantity or quality (*i.e.*, lack of impurities) of spinel at these occurrences, and there is no indication that the LHG has potential for gem corundum deposits formed from the retrograde break-down of spinel.

Haüyne / lapis lazuli at Soper River formed at or close to peak metamorphic conditions (granulite facies; Hogarth & Griffin 1978).

6.2.4 Controls on chromophore concentrations

Gem-quality corundum near Kimmirut varies from colourless to blue (Fe-Ti chromophore, Fritsch & Rossman 1988), commonly as oscillatory and sector zoning within single crystals but also as uniquely blue or colourless crystals, and yellow (Fe chromophore, Fritsch & Rossman 1988; Fig. 3.2). Iron and Ti activity varied during corundum crystallization, as evidenced by oscillatory zoning, however the cause of this variation is not known. Rare, pale greyish pink corundum found during exploration (True North Gems 2007) presumably contains small amounts of chromium (the chromophore in pink and red corundum, Fritsch & Rossman 1987). However, the dominant Cr-bearing phases (phlogopite and diopside) in Kimmirut corundum-bearing calc-silicate rocks are not part of the corundum-forming reaction; since corundum formed from the break-down of Cr-poor phases (scapolite, nepheline), the potential

for pink gem corundum (*i.e.*, pink sapphire) in these rocks is low. The whole rock Cr concentration in the Beluga sapphire occurrence is relatively high for a marl protolith (average 108 µg/g), but Cr/Al (0.00075 mol/mol) is substantially lower than that of ruby (red gem corundum) bearing rocks (*e.g.*, ruby mica schist Cr/Al = 0.002-0.006, Yakymchuk & Szilas 2018; ruby pargasite schist Cr/Al = 0.050, Wang *et al.* 2017).

Spinel in the LHG is blue, violet, purple, black, and rarely, cobalt-blue in colour. With increasing Fe content, spinel varies from colourless to pale lilac, sky blue, green, deep green and black (Kleišmantas & Daukšytė 2016, Hålenius *et al.* 2002; black spinel *e.g.*, Van Velthuizen 1993), and colour can vary with Fe coordination, charge, or interplay between Fe^{2+} and Fe^{3+} (D'Ippolito *et al.* 2015). In general, however, relatively high Fe concentrations in spinel do not result in attractive colours for use in the gemstone industry. Spinels from the LHG contain roughly four times the iron concentration of their host rocks, with some exceptions, and Chapter 4 discussed the importance of lower than expected Fe concentrations in spinel-bearing rocks relative to the Fe concentrations in a typical shale/carbonate protolith in order to favour spinel gem quality.

Vivid blue spinel at two occurrences near Kimmirut - Trailside and Qila - are cobalt-enriched (up to 0.07 wt. % CoO), which is responsible for its intense colouration (see D'Ippolito *et al.* 2015, Chauviré *et al.* 2015). The bright blue colour of spinel at these occurrences makes them of significant gemological and economic interest. Chapter 4 identified a localized enrichment of both Co and Ni at Qila and Trailside relative to other LHG metacarbonates (ranges of 9 to 29 µg/g *vs.* <1 to 6 µg/g cobalt; 10 to 47 µg/g *vs.* < 1 to 23 µg/g nickel, respectively), with limited diffusion of these trace elements (≤ 1 m scale) during metamorphism. The cobalt and nickel enrichment in these metacarbonates, which are isolated within a marble sequence, are

interpreted to be representative of the protolith composition. Concentrations of Co (especially) and Ni at Qila and Trailside are anomalously high for metacarbonate protoliths, at least double the estimates for similar protoliths of average composition, and the rocks are relatively impoverished in Fe, Mn, V, Cr, and Cu. The enrichment of Co and Ni, and depletion of V and Cr can take place under oxic early diagenetic conditions in the protolith sediment, the favoured hypothesis, but this is difficult to reconcile with a lack of coeval Mn enrichment, which is expected to occur under the same conditions (Chapter 4).

6.3 Exploration criteria & methods

6.3.1 Kimmirut-type sapphire deposits

Potential for Kimmirut-type sapphire deposits is strongly restricted by the *P-T* history of a metacarbonate-bearing terrane. On Baffin Island, potential for such deposits are expected to be proximal to the thrust fault separating the Lake Harbour Group and Narsajuaq terranes, where the retrograde amphibolite facies overprint of peak metamorphic assemblages is most pervasive. Known deposits have a relatively small footprint (calc-silicate pods up to 4.2 × 3.7 m), and occur throughout the True North Gems claim property (44 corundum showings discovered to date). Scapolite, a rock-forming constituent of calc-silicate pods in the area (of which approximately 0.5% contain corundum mineralization visible in outcrop), fluoresces bright yellow in long wave ultraviolet light. These fluorescing properties were used by True North Gems to explore for sapphire-bearing calc-silicate pods by prospecting the area with UV lamps in low light conditions (Lepage & Davison 2007). Interestingly, an occurrence of purplish-pink corundum in New York state, which also formed from scapolite-nepheline break-down, occurs in fluorescent scapolite (see Chapter 3). Ultraviolet light exploration has proven to be a valuable prospecting tool, however corundum could theoretically be found associated with non-fluorescent scapolite.

In normal light, the calc-silicate rocks have a distinctive mottled appearance caused by the contrast between darker minerals (purplish-brown diopside, brown phlogopite) and lighter ones (scapolite, calcite, albite-rich corundum-bearing zones).

Turner *et al.* (2017) successfully mapped distinct phlogopite, muscovite, scapolite, prehnite, and zeolite hyperspectral data domains using the Spectral Angle Mapper algorithm. Prehnite and zeolites represent low temperature alteration products closely associated with the corundum-bearing zone. Turner *et al.* (2017) suggested that these results could be used to conduct regional spectroscopic imaging in order to explore for Kimmirut-type gem corundum deposits in southern Baffin Island.

6.3.2 Gem spinel deposits

Spinel in the LHG occurs in two types of rock: (1) silicate-rich Mg-bearing metacarbonates with high Al/Si (rock forming minerals *i.e.*, diopside, pargasite, forsterite, phlogopite, humite, calcite, spinel); and (2) impure dolomite-bearing or dolomitic marbles (calcite/dolomite with subordinate silicates such as forsterite, pargasite, diopside, and phlogopite) with K/Al << 1. These rocks most commonly occur as pods within marble sequences, while some spinel-bearing diopsidites occur at the contact of marble and a silicate-rich rock (*e.g.*, syenogranite or gneiss) or within a calc-silicate rock (*i.e.*, metasomatic occurrence on unnamed island in Markham Bay). Magnesian marble sequences, especially where included by abundant calc-silicate pods (or other metamorphosed Mg-rich marls such as humitite or forsterite-rich rock), are expected to be the most prospective for spinel. Prospective rock units may be clustered together as a result of favourable geochemical compositions in the protolith stratigraphy. Local variations of K/Al in phlogopite-rich layers may lead to spinel formation. The highly localized nature of cobalt enrichment at cobalt-blue spinel occurrences make exploration

difficult, however the occurrence of two unique cobalt-enriched metacarbonates within 2 km is noteworthy. Whole rock geochemical sampling on a regional scale would be cost prohibitive for gemstone exploration, but regional geology surveys may happen to identify Co-enriched metacarbonates – good potential targets for gem spinel exploration.

6.3.3 Lapis lazuli deposits

Soper River lapis lazuli is interpreted to be metamorphosed evaporite-bearing dolomitic marl but this does not provide helpful exploration criteria because the whole rock composition of the rock at Soper River is unfavourable for its use in the commercial gemstone industry (*i.e.*, abundant diopside and calcite impurities). Lapis lazuli, relative to gem-quality sapphire and spinel, has a very low value per unit of volume. Therefore, larger volumes of high quality lapis lazuli are required to form a deposit. Considering the excellent level of rock exposure on southern Baffin Island, identification of bright blue rock within marble is currently the only viable exploration method.

6.3.4 Exploration using aerial surveys

Southern Baffin Island is an extremely remote region with limited infrastructure and a short (~two month) field season. The harsh climate offers one significant advantage: the rock is extraordinarily well-exposed and is scarcely covered by lichens, plants, or soil. This makes the area uniquely suited to exploration using aerial surveys. Harris *et al.* (2010) used airborne hyperspectral data to produce spectral maps identifying calcite-, dolomite-, and diopside-rich domains within a carbonate sequence in the LHG on southern Baffin Island. Turner *et al.* (2017) proposed the use of this method in combination with hyperspectral signatures of scapolite, phlogopite, muscovite, and other minerals to explore for gem corundum. These methods could be used in aerial surveys over marble-rich regions of Baffin Island to efficiently and thoroughly

seek out gem corundum and spinel exploration targets: magnesian marble sequences with abundant calc-silicate units. High resolution colour imagery could be collected simultaneously and be used to explore for blue lapis lazuli layers in marble.

Local-scale aerial surveys could also aid in exploration. The author used a DJI™ Mavic Pro unmanned aerial vehicle (UAV) video/photo camera to successfully explore for gem-quality olivine in the mountainous terrain of British Columbia, Canada. In good conditions, it was flown over 3 km away, 300 meters in elevation gain, and brought within 3 meters of basalt talus, where it successfully photographed *ca.* 10 cm wide mantle xenoliths in basalt blocks. Gem peridot exploration using this UAV took four days and saved roughly two weeks of field work when compared to traditional exploration. A portable UAV camera could help in field reconnaissance for calc-silicate units, potentially interesting mineralization, and blue lapis lazuli layers in southern Baffin Island.

6.4 Conclusions

Sapphire (gem corundum), spinel, and haüyne occurrences in the LHG are all genetically related to a metamorphosed carbonate sequence. Most occurrences of these gem minerals are uniquely metasedimentary (*i.e.*, formed from the metamorphism of a sedimentary protolith), while a few spinel occurrences formed from metasomatic reactions between Si-Al-rich rock (syenogranite or gneiss) and marble. Metasedimentary corundum, spinel, and haüyne occurrences have relatively similar protoliths: primarily dolomitic marls with a high Al/Si relative abundance (interpreted as sandy mud to clay siliciclastic fraction in the protolith). Kimmirut-type sapphire corundum deposits can only be formed by a multi-step metamorphic process under three different and specific *P-T* conditions (peak granulite facies assemblage transformed by two stages of subsequent retrograde metamorphism). Lapis lazuli formation at

peak or near-peak metamorphic conditions required the presence of evaporites to provide Na and S for the blue mineral haüyne. Spinel formed in Mg-bearing calc-silicates (high Al/Si) and in impure dolomitic marbles with very low K/Al (or subject to low X_{CO2}) during granulite facies peak metamorphism.

Potential for Kimmirut-type sapphire deposits is expected to be restricted to marbles proximal to the thrust fault separating the LHG from the Narsajuaq Arc, where retrograde upper amphibolite facies mineralization is most pervasive. Spinel and Kimmirut-type sapphire deposits are expected to likely be found in dolomitic marble sequences rich in calc-silicate layers. The potential occurrence of lapis lazuli is more difficult to predict. Aerial hyperspectral and photographic surveys are well-suited to gemstone exploration in this remote region thanks to excellent rock exposure with minimal sedimentary or plant/lichen cover. Spectral mapping of dolomite-, diopside-, phlogopite-, and scapolite-rich domains in LHG metacarbonate sequences is expected to provide exploration targets. Ground based exploration efforts could be aided by the use of a portable UAV.

6.5 Figures

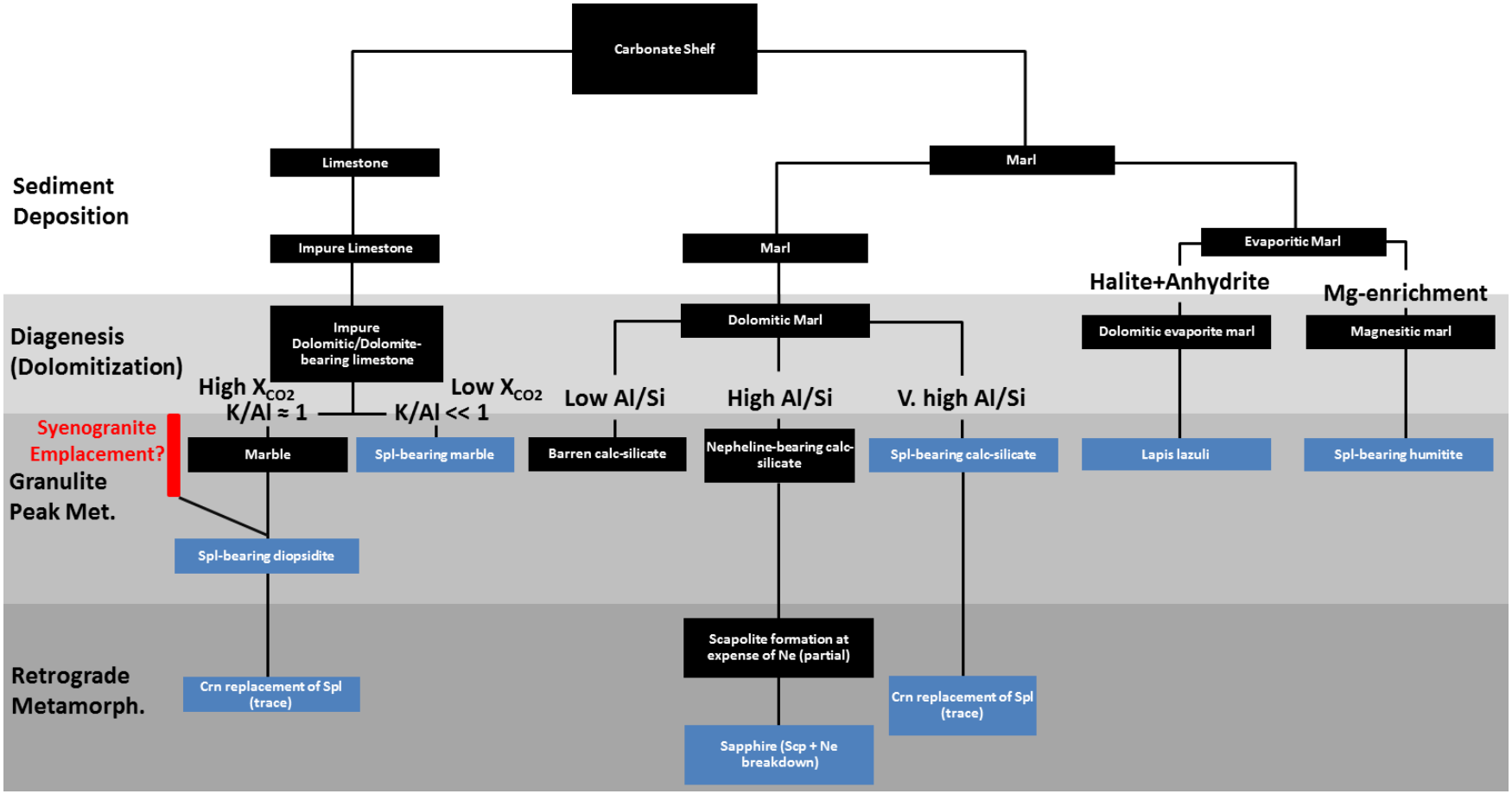

Figure 6.1: The proposed genetic model for Lake Harbour Group gem mineral occurrences. Stages containing gem minerals are represented in blue, and those devoid of gem minerals in black.

Chapter 7. Conclusions and future work

This dissertation presents new genetic models for Kimmurut-type sapphire (a new type of gem corundum deposit) and gem spinel, and a refined model for the genesis of lapis lazuli (haüyne). These three gem minerals occur in silica undersaturated rocks and generally occur in rocks with similar protoliths: dolomitic marls, transformed into silicate-rich metacarbonates by metamorphism. Spinel also occurs in dolomitic limestone, and a few metasomatic occurrences are known. Variations in the abundances of Na, K, Mg, Al, Si, and S play an important role in determining whether corundum, spinel, haüyne, or no gem minerals will form. The metamorphic *P-T-X* history of the terrane, including local variations in retrograde fluid influx, also plays a major role in gem genesis in the LHG. Haüyne and spinel formed at peak metamorphic conditions while gem corundum was formed by a three step metamorphic process involving two stages of retrogression.

The protolith for Beluga sapphire-bearing calc-silicate rock is interpreted to be dolomitic marl. New petrological and geochemical data indicated that this deposit does not consist of metamorphosed evaporite, as proposed by previous research. A model for the genesis of sapphire within this calc-silicate rock was established using a combination of petrography, thermodynamic modelling and zircon age dating. A peak metamorphic nepheline- and diopside-bearing assemblage was partly replaced by oligoclase-phlogopite-calcite-scapolite as a result of fluid influx shortly following M_2 retrograde metamorphism. This partial retrogression placed scapolite and nepheline in direct contact. A subsequent fluid influx, at yet lower metamorphic grade, produced corundum, albite, muscovite, and calcite from the break-down of scapolite and nepheline. Obscuring of the peak metamorphic assemblage by intense retrograde alteration has introduced some possibility for error in connecting the modeled reactions with observed mineral

assemblages; notably, K-feldspar is predicted to occur in the peak metamorphic assemblage, but it was not observed in the Beluga and Bowhead samples. Similarly, the formation of corundum from scapolite-nepheline break-down is inferred at Beluga, since no relict nepheline was found. However, new data from a similar locality in New York demonstrated an undeniable textural relation between corundum-albite-calcite formed from breaking down of nepheline and scapolite at their contact. The thrust fault separating the LHG and Narsajuaq terranes appears to be the most prospective for similar deposits, since the retrograde, amphibolite facies overprint of the granulite peak assemblages is most pervasive here. Future research and exploration may uncover new regions of sapphire-bearing potential.

Spinel occurrences in the LHG are interpreted to be metasedimentary, with the exception of two metasomatic occurrences (*e.g.*, syenogranite-marble bimetasomatism at Spinel Island). Spinel-bearing metacarbonate rocks are interpreted to have the following sedimentary protoliths: (1) impure dolomite-bearing and dolomitic limestone (marble); (2) dolomitic marl (calc-silicate rocks); and (3) evaporitic magnesitic marl (Soper Falls humitite). In Mg-bearing impure marbles, spinel genesis can be controlled by K activity and X_{CO2}, and is not significantly affected by Al/Si. In Mg-bearing calc-silicates, however, spinel only occurs at high Al/Si; higher than that for sapphire-, haüyne-, or non-gem-bearing metacarbonates. Spinel occurrences at Waddell Bay and Hall Peninsula were not studied in the field; doing so could provide additional, useful petrological data. Spinel is interpreted to have formed during granulite facies peak metamorphism. For multiple occurrences, this is supported by calculated *T-X* pseudo-sections. However, the very coarse grain size, very heterogeneous nature, and often limited surficial exposure of the spinel occurrences prevented the use of thermodynamic modelling in many cases. Interpretations on the timing of spinel genesis could be reinforced with a significantly

expanded sampling program exposing more rock and gathering larger samples, for both thermodynamic modelling and zircon extraction (U-Pb age dating).

This dissertation presents the first whole-rock geochemical dataset for cobalt-enriched spinel-bearing rocks, shedding new light on the possible origins of vivid blue Co-enriched spinel. The highly heterogeneous and localized nature of Co-enrichment in metacarbonates is interpreted to represent early enrichment (protolith, diagenesis, early metamorphism), and contradicts previous research for a similar locality in Vietnam suggesting transport in evaporitic fluids from either within marbles, or from regional Co-Ni-rich rocks. In all cases, the cobalt enrichment is associated with a coeval enrichment in nickel, and relatively low concentrations of Fe, Mn, V, Cr, and Cu. The trace metal composition of these rocks is distinctly different from most typical sources of Co-Ni enrichment, and most resembles (though not perfectly) the effects of oxic early diagenesis. Since the protoliths have undergone diagenetic, structural, and metamorphic transformations, such interpretations are ultimately speculative.

In agreement with previous authors, the exceptionally high Na content and relative S enrichment of haüyne-bearing rock (lapis lazuli) at Soper River supports a meta-evaporitic origin. Low Al/Si and high carbonate content in the protolith prevented the genesis of high-quality gem lapis lazuli, which has significantly higher haüyne concentrations.

The present research integrates data from multiple types of gem occurrences and compares them to similar rocks barren of gem minerals within the same metamorphic terrane. This new approach has yielded significant new contributions to the understanding of the metamorphic and geochemical conditions of gem genesis and successfully answered broad questions raised by previous authors (*i.e.*, conditions of spinel genesis in Giuliani *et al.* 2017). The estimation of protolith composition using whole rock concentrations of relatively immobile

elements presents a new approach to the analysis of gem deposits occurring in metamorphosed sedimentary rocks. The analysis of numerous whole rock trace element compositions helped set a reference benchmark for the assessment of unusual Co-enriched, vivid-blue-spinel-bearing rocks. Larger scale application of these methods could help better understand the trace element composition of individual gem minerals within metasedimentary rocks.

Excellent opportunities exist for future research. Firstly, an investigation of the distribution of gemstone occurrences within the context of structural geology would contribute important and practical information on the genesis of metamorphic gemstones. For example: does deformation of silicate-rich layers affect gem potential (*e.g.*, thinning of layers increasing the surface area with carbonates for metamorphic reactions)? Are gem occurrences traceable along stratigraphy or structural domains? To what degree has deformation modified the composition and distribution of formerly continuous layers (*i.e.*, sapphire-bearing calc-silicates)? The spinel deposit model would benefit from the addition of petrological/geochemical data from actively mined *in situ* gem spinel deposits. Lastly, the exact origin of cobalt enrichment in metacarbonates remains mysterious. Detailed petrological/geochemical studies on Vietnamese cobalt-blue spinel occurrences, using the methods presented in this dissertation, could shed new light on this phenomenon.

References

Armstrong, J.T. (1988): Quantitative analysis of silicates and oxide minerals: Comparison of Monte-Carlo, ZAF and Phi-Rho-Z procedures. *In:* Newbury, D.E. *Microbeam Analysis*, p. 239-246.

Baccar, M.B., Fritz, B., & Madé, B. (1993): Diagenetic albitization of K-feldspar and plagioclase in sandstone reservoirs: Thermodynamic and kinetic modeling. *Journal of Sedimentary Petrology* **63**, 1100-1109.

Belley, P.M. & Bourdeau, J. (2014): Blue calcite skarns as potential gem deposits: Examples from the Central Metasedimentary Belt, Grenville Province, Canada. *In*: Geological Society of America annual meeting, Vancouver, Canada, 19-22 October, 2014, abstract # 165-8.

Belley, P.M., Dzikowski, T.J., Fagan, A., Cempirek, J., Groat, L.A., Mortensen, J.K., Fayek, M., Giuliani, G., Fallick, A.E., & Gertzbein, P. (2017): Origin of scapolite-hosted sapphire (corundum) near Kimmirut, Baffin Island, Nunavut, Canada. *Canadian Mineralogist* **55**, 669-699.

Belley, P.M., O'Neil, J., & Hattori, K. (2016): Spinel and aspidolite from the Des Cèdres Dam occurrence, Notre-Dame-du-Laus, Québec, Canada. *Rocks & Minerals* **91**, 448-452.

Belley, P.M., Grice, J.D., Fayek, M., Kowalski, P.M. & Grew, E.S. (2014): A new occurrence of the borosilicate serendibite in tourmaline-bearing calc-silicate rocks, Portage-du-Fort marble, Grenville Province, Québec: evolution of boron isotope and tourmaline compositions in a metamorphic context. *Canadian Mineralogist* **52**, 595-616.

Beranek, L.P. & Mortensen, J.K. (2011): The timing and provenance record of the Late Permian Klondike orogeny in northwestern Canada and arc-continent collision along western North America. *Tectonics* **30**, TC5017, doi:10.1029/2010TC002849.

Berman, R.G. (1991): Thermobarometry using multiequilibrium calculations: a new technique with petrologic applications. *Canadian Mineralogist* **29**, 833-855.

Berman, R.G. (1988): Internally-consistent thermodynamic data for minerals in the system Na_2O-K_2O-CaO-MgO-FeO-Fe_2O_3-Al_2O_3-SiO_2-TiO_2-H_2O-CO_2. *Journal of Petrology* **29**, 445-522.

Blackadar, R.G. (1967): Geology of Mingo Lake-MacDonald Island map-area, Baffin Island, District of Franklin. *Geological Survey of Canada*, **Memoir 345**, 54 p.

Blauwet, D. (2006): The sapphire and spinel deposit of An Phu, Luc Yen Mining District, Yenbai Province, Vietnam. *Mineralogical Record* **37**, 225-2006.

Brandon, M.T., Roden-Tice, M.K., & Garver, J.I. (1998): Late Cenozoic exhumation of the Cascadia accretionary wedge in the Olympic Mountains, northwest Washington State. *Geological Society of America Bulletin* **110**, 985-1009.

Butler, J.P. (2007): Petrogenesis of nepheline- and scapolite-bearing metacarbonates from southwestern Baffin Island, Nunavut, Canada. B.Sc. thesis, Dalhousie University, Halifax, Nova Scotia, Canada.

Cabral, A.R., Wiedenbeck, M., Rios, F.J., Gomes, A.A.S. Jr, Filho, O.G.R. & Jones, R.D. (2012): Talc mineralisation associated with soft hematite ore, Gongo Soco deposit, Minas Gerais, Brazil: petrography, mineral chemistry and boron-isotope composition of tourmaline. *Mineralium Deposita* **47**, 411-424.

Carmichael, R.S. (1989): Physical properties of rocks and minerals. CRC Press, Inc., Boca Raton, Florida, USA. 741 p.

Catanzaro, E.J., Champion, C.E., Garner, E.L., Marinenko, G., Sappenfield, K.M., & Shields, W.R. (1970): Boric acid: isotopic and assay standard reference materials. *National Bureau of Standards (US) Special Publications*, **260-17**, 1–71.

Chamberlain, S.C., Walter, M., Bailey, D.G., & Robinson G.W. (2015): A new collecting site at the Rose Road Locality, Pitcairn, St. Lawrence County, New York. Rochester Mineralogical Symposium, Rochester, NY. Abstract. *Rocks & Minerals* **90**, 440-446.

Chaussidon, M. & Albarède, F. (1992): Secular boron isotope variations in the continental crust: An ion microprobe study. *Earth and Planetary Science Letters* **108**, 229–241.

Chauviré, B., Rondeau, B., Fritsch, E., Ressigeac, P., & Devidal, J.-L. (2015): Blue spinel from the Luc Yen District of Vietnam. *Gems & Gemology* **51**, 2-17.

Coenraads, R.R. & Canut de Bon, C. (2000): Lapis lazuli from the Coquimbo region, Chile. *Gems & Gemology* **36**, 28-41.

Connolly, J.A.D. (2009): The geodynamic equation of state: what and how. *Geochemistry, Geophysics, Geosystems* **10**, Q10014 DOI:10.1029/2009GC002540

Corriveau, L. (2013): Structure of the Central Metasedimentary Belt in Québec, Grenville Province; an example from the analysis of high-grade metamorphic terranes. *Geological Survey of Canada Bulletin* **586** (in French). 251 p.

D'Ippolito, V., Andreozzi, G.B., Hålenius, U., Skogby, H., Hametner, K., & Günther, D. (2015): Colour mechanisms in spinel: cobalt and iron interplay for the blue colour. *Physics and Chemistry of Minerals* **42**, 431-439.

Deer, W.A, Howie, R.A., Wise, W.S., & Zussman, J. (2004): Rock-forming minerals Vol. 4B: Framework Silicates, 2nd ed., p. 344-345.

Drake, M.J. & Weill, D.F. (1972): New rare earth element standards for electron microprobe analysis. *Chemical Geology* **10**, 179-181.

Dzikowski, T.J., Cempirek, J., Groat, L.A., Dipple, G.M., Giuliani, G. (2014): Origin of gem corundum in calcite marble: The Revelstoke occurrence in the Canadian Cordillera of British Columbia. *Lithos* **198-199**, 281-297.

Dzikowski, T.J. (2013): A comparative study of the origin of carbonate-hosted gem corundum deposits in Canada. Doctoral thesis, University of British Columbia, Vancouver, B.C., Canada. 259 p.

Eliopoulos, D.G. & Economou-Eliopoulos, M. (2000): Geochemical and mineralogical characteristics of Fe-Ni- and bauxitic-laterite deposits of Greece. *Ore Geology Reviews* **16**, 41-58.

Ellis, D.E. (1978): Stability and phase equilibria of chloride and carbonate bearing scapolites at 750 °C and 4000 bar. *Geochimica et Cosmochimica Acta* **42**, 1271-1281.

Emmett, J.L., Stone-Sundberg, J., Guan, Y., & Sun, Z. (2017): The role of silicon in the color of gem corundum. *Gems & Gemology* **53**, 42-47.

Faryad, S.W. (2002): Metamorphic conditions and fluid compositions of scapolite-bearing rocks from the lapis lazuli deposit at Sare Sang, Afghanistan. *Journal of Petrology* **43**, 725-747.

Fleet, M.E., Liu, X., Harmer, S.L., & Nesbitt, H.W. (2005): Chemical state of sulfur in natural and synthetic lazurite by S *K*-edge XANES and X-ray photoelectron spectroscopy. *Canadian Mineralogist* **43**, 1589-1603.

Fritsch, E. & Rossman, G.R. (1988): An update on colour in gems. Part 2: Colours involving multiple atoms and colour centers. *Gems & Gemology* **24**, 3-15.

Fritsch, E. & Rossman, G.R. (1987): An update on colour in gems. Part 1: Introduction and colours caused by dispersed metal ions. *Gems & Gemology* **23**, 126-139.

Garnier, V., Ohnenstetter, D., & Giuliani, G. (2004): L'aspidolite fluorée: role des évaporites dans la genèse du rubis des marbres de Nangimali (Azad-Kashmir, Pakistan). *Comptes Rendus Geoscience* **336**, 1245-1253.

Garnier, V., Giuliani, G., Ohnenstetter, D., Fallick, A.E., Dubessy, J., Banks, D., Hoang, Q.V., Lhomme, T., Maluski, H., Pêcher, A., Bakhsh, K.A., Long, P.V., Trinh, P.T., & Schwarz, D. (2008): Marble-hosted ruby deposits from Central and Southeast Asia: Towards a new genetic model. *Ore Geology Reviews* **34**, 169-191.

Gendron, A., Silverberg, N., Sundby, B., & Lebel, J. (1986): Early diagenesis of cadmium and cobalt in sediments of the Laurentian Trough. *Geochimica et Cosmochimica Acta* **50**, 741-747.

Genis, R. (2016): Retail gemstone price trends (1975-2015). *The Gemstone Forecaster* **34**. http://www.preciousgemstones.com/gfspring16.html ; Retrieved 20 December, 2016.

Gertzbein, P. (2003): The coloured gem potential of Baffin Island and Nunavut. *Canadian Gemmologist* **25**, 10-17.

Giletti, B.J. (1974): Studies in diffusion I: argon in phlogopite mica. *In:* Geochemical Transport and Kinetics. A.W. Hoffman, B.J. Giletti, H.S. Yoder, & R.A. Yund, editors. Carnegie Institution of Washington, publication 634, 107-115.

Giuliani, G., Dubessy, J., Ohnenstetter, D., Banks, D., Branquet, Y., Feneyrol, J., Fallick, A.E., & Martelat, J.-E. (2018): The role of evaporites in the formation of gems during metamorphism of carbonate platforms: a review. *Mineralium Deposita* **53**, 1-20.

Giuliani, G., Fallick, A.E., Boyce, A.J., Pardieu, V., & Pham, V.L. (2017): Pink and red spinels in marble: Trace elements, oxygen isotopes, and sources. *Canadian Mineralogist* **55**, 743-761.

Giuliani, G., Ohnenstetter, D., Fallick, A.E., Groat, L., & Fagan, A.J. (2014): The geology and genesis of gem corundum deposits. *In* Geology of Gem Deposits (L.A. Groat, ed.). Mineralogical Association of Canada short course volume 44 (29-112).

Giuliani, G., Fallick, A.E., Garnier, V., France-Lanord, C., Ohnenstetter, D., & Schwarz, D. (2005): Oxygen isotope composition as a tracer for the origins of rubies and sapphires. *Geology* **33**, 249-252.

Goldsmith, J.R. & Newton, R.C. (1977): Scapolite-plagioclase stability relations at high pressures and temperatures in the system $NaAlSi_2O_8$-$CaAl_2Si_2O_8$-$CaCO_3$-$CaSO_4$. *American Mineralogist* **62**, 1063-1081.

Graf, D.L. (1962): Minor element distribution in sedimentary carbonate rocks. *Geochimica et Cosmochimica Acta* **26**, 849-856.

Gregory, D.D., Large, R.R., Halpin, J.A., Baturina, E.L., Lyons, T.W., Wu, S., Danyushevsky, L., Sack, P.J., Chappaz, A., Maslennikov, V.V., & Bull, S.W. (2015): Trace element content of sedimentary pyrite in black shales. *Economic Geology* **110**, 1389-1410.

Grew, E.S., Yates, M.G., Swihart, G.H., Moore, P.B. & Marquez, N. (1991): The paragenesis of serendibite at Johnsburg, New York, USA: an example of boron enrichment in the granulite facies. *In* Progress in metamorphic and magmatic petrology; a memorial volume in honor of D.S. Korzhinskiy (L.L. Perchuk, ed.). Cambridge University Press, Cambridge, England (247-285).

Grice, J.D., Gault, R.A. & Waller, R. (1982): Spinel from Glencoe Island, Northwest Territories, Canada. *Rocks & Minerals* **57**, 155-157.

Grützner, T., Klemme, S., & Rohrbach, A. (2015) The effect of fluorine on the stability of humite-type minerals in the upper mantle and transition zone. *Presented at the 25th Goldschmidt conference, August 16-21, 2015.*

Hålenius, U., Skogby, H., & Andreozzi, G.B. (2002): Influence of cation distribution on the optical absorption spectra of Fe^{3+}-bearing spinel s.s.-hercynite crystals: Evidence for electron transitions in $^{VI}Fe^{2+}$-$^{VI}Fe^{3+}$ clusters. *Physics and Chemistry of Minerals* **29**, 319-330.

Hames, W.E. & Bowring, S.A. (1994): An empirical evaluation of the argon diffusion geometry in muscovite. *Earth and Planetary Science Letters* **124**, 161-167.

Hansen, M. (2008): A comparison of sapphire bearing and non-sapphire bearing lenses from the Lake Harbour Group, south-eastern Baffin Island. B.Sc. thesis, Carleton University, Ottawa, Ontario, Canada. 61 p.

Harris, J.R., McGregor, R., & Budkewitsch, P. (2010): Geological analysis of hyperspectral data over southwest Baffin Island: methods for producing spectral maps that relate to variations in surface lithologies. *Canadian Journal of Remote Sensing* **36**, 412-435.

Harrison, T.M., Célérier, J., Aikman, A.B., Hermann, J. & Heizler, M.T. (2009): Diffusion of ^{40}Ar in muscovite. *Geochimica et Cosmochimica Acta* **73**, 1039-1051.

Hassan, I., Peterson, R.C., & Grundy, H.D. (1985): The structure of lazurite, ideally $Na_6Ca_2(Al_6Si_6O_{24})S_2$, a member of the sodalite group. *Acta Crystallographica* **C41**, 827-832.

Heggie, D. & Lewis, T. (1984): Cobalt in pore waters of marine sediments. *Nature* **311**, 453-455.

Herd, C.D.K., Peterson, R.C., & Rossman, G.R. (2000): Violet-coloured diopside from southern Baffin Island, Nunavut, Canada. *Canadian Mineralogist* **38**, 1193-1199.

Hogarth, D.D. (1979): Afghanite: New occurrences and chemical composition. *Canadian Mineralogist* **17**, 47-52.

Hogarth, D.D. (1971): Lapis lazuli near Lake Harbour, Southern Baffin Island, Canada. *Canadian Journal of Earth Sciences* **8**, 1210-1217.

Hogarth, D.D. & Griffin, W.L. (1980): Contact-metamorphic lapis lazuli: The Italian Mountain deposits, Colorado. *Canadian Mineralogist* **18**, 59-70.

Hogarth, D.D. & Griffin, W.L. (1978): Lapis lazuli from Baffin Island – a Precambrian meta-evaporite. *Lithos* **11**, 37-60.

Hogarth, D.D. & Griffin, W.L. (1975): Further data on lapis lazuli from Latium, Italy. *Canadian Mineralogist* **13**, 89-90.

Holland, T. & Powell, R. (1998): An internally consistent thermodynamic data set for phases of petrological interest. *Journal of Metamorphic Geology* **16**, 309-343.

Holland, T. & Powell, R. (1991): A Compensated-Redlich-Kwong (CORK) equation for volumes and fugacities of CO_2 and H_2O in the range 1 bar to 50 kbar and 100-1600°C. *Contributions to Mineralogy and Petrology* **109**, 265-273.

Housley, R. (2012): History of Cascade Canyon lapis and corundum deposits, San Gabriel Mountains, CA. *Mindat.org* article #1575, www.mindat.org/article.php/1575 - retrieved 26 February, 2017.

Hughes, R.W. (1997): Ruby & sapphire. RWH Publishing, Boulder, Colorado, USA. 511 p.

Hughes, R.W. & Pardieu, V. (2006): Moon over the Pamirs: Chasing ruby and spinel in Tajikistan. http://www.ruby-sapphire.com/tajikistan_ruby_and_spinel.htm retrieved March 10, 2017.

Kievlenko, E.Y. (2003): Geology of gems, english edition. A. Soregaroli, editor. Ocean Pictures Ltd., Littleton, CO, USA. 468 pp.

Kleišmantas, A. & Daukšytė, A. (2016): The influence of Vietnam and Sri Lanka spinel mineral chemical elements on colour. *Chemija* **27**, 45-51.

LeCheminant, A.N., Groat, L.A., Mortensen, J.K., Gertzbein, P., & Rohtert, W. (2005): Sapphires from Kimmirut, Baffin Island, Nunavut, Canada. *Geochimica et Cosmochimica Acta* **69**, 10, supplement 280, Abstracts of the 15th annual V.M. Goldschmidt conference.

Leeman, W.P. & Tonarini, S. (2001): Boron isotopic analysis of proposed borosilicate mineral reference samples. *Geostandards Newsletter* **25**, 399-403.

Lepage, L. & Davison, J.G. (2007): Exploration advances with ultraviolet LED technology; Beluga sapphire, Nunavut. Abstracts with program, Geological Association of Canada – Mineralogical Association of Canada joint annual meeting, Yellowknife, Northwest Territories, 2007.

Lessing, P. & Grout, C.M. (1971): Haüynite from Edwards, New York. *American Mineralogist* **56**, 1096-1100.

Locock, A.J. (2014): An Excel spreadsheet to classify chemical analyses of amphiboles following the IMA 2012 recommendations. *Computers & Geosciences* **62**, 1-11.

López, J.M.G., Bauluz, B., Fernández-Nieto, C., & Oliete, A.Y. (2005): Factors controlling the trace-element distribution in fine-grained rocks: the Albanian kaolinite-rich deposits of the Oliete Basin (NE Spain). *Chemical Geology* **214**, 1-19.

Ludwig, K.R. (2003): Isoplot 3.09: A geochronological toolkit for Microsoft Excel. Berkeley Geochronology Center (bgc.org), Special Publication no. 4.

Ludwig, T., Marschall, H.R., Pogge von Strandmann, P.A.E., Shabaga, B.M., Fayek, M. & Hawthorne, F.C. (2011): A secondary ion mass spectrometry (SIMS) re-evaluation of B and Li isotopic compositions of Cu-bearing elbaite from three global localities. *Mineralogical Magazine* **75**, 2485-2494.

MacGregor, J.R., Grew, E.S., De Hoog, J.C.M., Harley, S.L., Kowalski, P.M., Yates, M.G. & Carson, C.J. (2013): Boron isotopic composition of tourmaline, prismatine, and grandidierite from granulite facies paragneisses in the Larsemann Hills, Prydz Bay, East Antarctica: Evidence for a non-marine evaporite source. *Geochimica et Cosmochimica Acta*, http://dx.doi.org/10.1016/j.gca.2013.05.030

Merlet, C. (1994): An accurate computer correction program for quantitative electron probe microanalysis. *Microchimica Acta* **114**, 363-376.

Moine, B., Sauvan, P., & Jarousse, J. (1981): Geochemistry of evaporite-bearing series: a tentative guide for the identification of metaevaporites. *Contributions to Mineralogy and Petrology* **76**, 401-412.

Möller, A., ÓBrien, P.J., Kennedy, A. & Kröner, A. (2003): The use and abuse of Th-U ratios in the interpretation of zircon. *In* EGS-AGU-EUG joint assembly, Nice, France, 6-11 April 2003. Abstracts with program, abstract # 12113.

Moore, T.P. & Woodside, R.W.M. (2014) The Sar-e-Sang lapis mines. *Mineralogical Record* **45**, 281-336.

Mora, C.I. & Valley, J.W. (1989): Halogen-rich scapolite and biotite: Implications for metamorphic fluid-rock interaction. *American Mineralogist* **74**, 721-737.

Mortensen, J.K., Ghosh, D., & Ferri, F. (1995): U-Pb age constraints of intrusive rocks associated with copper-gold porphyry deposits in the Canadian Cordillera. *In* Porphyry deposits of the northwestern Cordillera of North America. T.G. Schroeter, editor. Canadian Institute of Mining and Metallurgy, Special Volume **46**, 142-158.

Nockolds, S.R. (1954): Average chemical compositions of some igneous rocks. *Bulletin of the Geological Society of America* **65**, 1007-1032.

Palin, R.M., Weller, O.M., Waters, D.J., & Dyck, B. (2016): Quantifying geological uncertainty in metamorphic phase equilibria modelling; a Monte Carlo assessment and implications for tectonic interpretations. *Geoscience Frontiers* **7**, 591-607.

Palmer, M.R. (1991): Boron isotope systematics of hydrothermal fluids and tourmalines: A synthesis. *Chemical Geology (Isotope Geoscience Section)* **94**, 111-121.

Pardieu, V. (2014): Hunting for "jedi" spinels in Mogok. *Gems & Gemology* **50**, 46-57.

Pardieu, V. (2008): Tanzania, October 2007: a gemological safari, part 1. *FieldGemology.org*, http://www.fieldgemology.org/gemology%20tanzania%20ruby%20sapphire%20spinel%20tsavorite%20alexandrite%20emerald%20tunduru%20songea%20morogoro%20merelani.php ; retrieved June 10, 2015.

Pardieu, V., Hughes, R., & Boehm, E. (2008): Spinel: resurrection of a classic. *InColor Magazine* (Summer 2008 issue), 10-18.

Parker, R.L. (1967): Composition of the Earth's Crust. In: Michael Fleischer, editor. Data of Geochemistry, 6th ed. United States Government Printing Office, Washington. pp D1-D19.

Pham, V.L., Pardieu, V., & Giuliani, G. (2013): Update on gemstone mining in Luc Yen, Vietnam. *Gems & Gemology* **49**, 233-245.

Plimer, I.R. (1977): The origin of the albite-rich rocks enclosing the cobaltian pyrite deposit at Thackaringa, N.S.W., Australia. *Mineralium Deposita* **12**, 175-187.

Pouchou, J.L. & Pichoir, F. (1985): PAP φ(ρZ) procedure for improved quantitative microanalysis. *Microbeam Analysis Proceedings* (ed., J.T. Armstrong), San Fransisco Press, California, USA, p. 104-106.

Price, B.J. (1972): Minor elements in pyrites from the smithers map area, B.C. and exploration applications of minor element studies. Master's Thesis, University of British Columbia, Vancouver, Canada, 270 pp.

Renne, P.R., Swisher, C.C., Deino, A.L., Karner, D.B., Owens, T.L. & DePaolo, D.J. (1998): Intercalibration of standards, absolute ages and uncertainties in Ar-40/Ar-39 dating. *Chemical Geology* **145**, 117-152.

Rice, J.M. (1981) Phase equilibria involving humite minerals in impure dolomitic limestones: Part II – calculated stability of chondrodite and norbergite. *Contributions to Mineralogy and Petrology* **75**, 205-223.

Rivers, T. (2015): Tectonic setting and evolution of the Grenville Orogen: An assessment of progress over the last 40 years. *Geoscience Canada* **42**, 77-124.

Robbins, G.A. (1972): Radiogenic argon diffusion in muscovite under hydrothermal conditions. Master's thesis, Brown University.

Roddick, J.C. (1987): Generalized numerical error analysis with application to geochronology and thermodynamics. *Geochimica et Cosmochimica Acta* **51**, 2129-2135.

Rubatto, D., Williams, I.S. & Günther, D. (1999): Trace-element characterization of metamorphic zircons. *In* 9th Annual V.M. Goldschmidt conference, L.P.I. Contribution 971, Lunar and Planetary Institute, Houston. Abstract 7111.

Schropp, S.J. & Windom, H.L., eds. (1988): A guide to the interpretation of metal concentrations in estuarine sediments. Coastal Zone of Management Section, Florida Department of Environmental Regulation, Tallahassee, Florida, USA. 44 pp.

Scott, D.J. (1997): Geology, U-Pb, and Pb-Pb geochronology of the Lake Harbour area, southern Baffin Island: implications for the Paleoproterozoic tectonic evolution of northeastern Laurentia. *Canadian Journal of Earth Sciences* **34**, 140-155.

Scott, D.J., Stern, R.A., St-Onge, M.R. & McMullen, S.M. (2002): U-Pb geochronology of detrital zircons in metasedimentary rocks from southern Baffin Island: implications for the Paleoproterozoic tectonic evolution of Northeastern Laurentia. *Canadian Journal of Earth Sciences* **39**, 611-623.

Scott, D.J., St-Onge, M.R., Wodicka, N., & Hanmer, S. (1997): Geology of Markham Bay-Crooks Inlet area, southern Baffin Island, Northwest Territories. *In:* Current Research 1997-C, Geological Survey of Canada, 157-166.

Senoble, J.B. (2010): Beauty and rarity – a quest for Vietnamese blue spinels. *InColor* (Summer 2010 issue), 18-23.

Shaw, D.M. (1954): Trace elements in pelitic rocks: pt. I, Variation during metamorphism; pt. II, Geochemical relations. *Geological Society of America Bulletin* **65**, 1151-1182.

Shaw, T.J., Gieskes, J.M., & Jahnke, R.A. (1990): Early diagenesis in differing depositional environments: the response of transition metals in pore water. *Geochimica et Cosmochimica Acta* **54**, 1233-1246.

Shigley, J.E. & Stockton, C.M. (1984): 'Cobalt-blue' gem spinels. *Gems & Gemology* **20**, 34-41.

Shor, R. & Weldon, R. (2009): Ruby and sapphire production and distribution: a quarter century of change. *Gems & Gemology* **45**, 236-259.

Silva, K.K.M.W. & Siriwardena, C.H.E.R. (1988): Geology and the origin of the corundum-bearing skarn at Bakamuna, Sri Lanka. *Mineralium Deposita* **23**, 186-190.

Simonet, C., Fritsch, E. & Lasnier, B. (2008): A classification of gem corundum deposits aimed towards gem exploration. *Ore Geology Reviews* **34**, 127-133.

Skipton, D.R., St-Onge, M.R., Schneider, D.A., & McFarlane, C.R.M. (2016): Tectonothermal evolution of the middle crust in the Trans-Hudson Orogen, Baffin Island, Canada: Evidence from petrology and monazite geochronology of sillimanite-bearing migmatites. *Journal of Petrology* **57**, 1437-1462.

St-Onge, M.R., Scott, D.J., & Wodicka, N. (1999a): Geology, McKellar Bay, Nunavut; Geological Survey of Canada, Map 1981A, scale 1:100 000.

St-Onge, M.R., Scott, D.J., & Wodicka, N. (1999b): Geology, Crooks Inlet, Nunavut; Geological Survey of Canada, Map 1984A, scale 1:100 000.

St-Onge, M.R., Wodicka, N., & Lucas, S.B. (2000): Granulite- and amphibolite-facies metamorphism in a convergent-plate-margin setting: synthesis of the Quebec-Baffin segment of the Trans-Hudson Orogen. *Canadian Mineralogist* **38**, 379-398.

St-Onge, M.R., Scott, D.J. & Wodicka, N. (2001): Geology, Meta Incognita Peninsula, Baffin Island, Nunavut. Geological Survey of Canada, Map 2009A.

St-Onge, M.R., Wodicka, N., & Ijewliw, O. (2007): Polymetamorphic evolution of the Trans-Hudson Orogen, Baffin Island, Canada: Integration of petrological, structural and geochronological data. *Journal of Petrology* **48**, 271-302.

St-Onge, M.R., Van Gool, J.A.M., Garde, A.A., & Scott, D.J. (2009): Correlation of Archaean and Palaeoproterozoic units between northeastern Canada and western Greenland: constraining the pre-collisional upper plate accretionary history of the Trans-Hudson orogeny. *Geological Society of London Special Publication* **318**, 193-235.

St-Onge, M.R., Rayner, N.M., Liikane, D., & Chadwick, T. (2015): Mafic, ultramafic and layered mafic-ultramafic sills, Meta Incognita Peninsula, southern Baffin Island. *In*: Summary of Activities 2014, Canada-Nunavut Geoscience Office, 11-16.

Stacey, J.S. & Kramer, J.D. (1975): Approximation of terrestrial lead isotope evolution by a two stage model. *Earth and Planetary Science Letters* **26**, 207-221.

Steiger, R.H. & Jäger, E. (1977): Subcommission on geochronology: convention on the use of decay constants in geo- and cosmochronology. *Earth and Planetary Science Letters* **36**, 359-362.

Stockdale, A., Davison, W., Zhang, H., & Hamilton-Taylor, J. (2010): The association of cobalt with iron and manganese (oxyhydr)oxides in marine sediment. *Aquatic Geochemistry* **16**, 575-585.

Swihart, G.H. & Moore, P.B. (1989): A reconnaissance of the boron isotopic composition of tourmaline. *Geochimica et Cosmochimica Acta* **53**, 911-916.

Takahashi, Y., Hayasaka, Y., Morita, K., Kashiwabara, T., Nakada, R., Marcus, M.A., Kato, K., Tanaka, K. & Shimizu, H. (2015): Transfer of rare earth elements (REE) from manganese oxides to phosphates during early diagenesis in pelagic sediments inferred from REE patterns, X-ray absorption spectroscopy, and chemical leaching method. *Geochemical Journal* **49**, 653-674.

Tauson, V.L., Goettlicher, J., Sapozhnikov, A.N., Mangold, S., & Lustenberg, E.E. (2012): Sulphur speciation in lazurite-type minerals $(Na,Ca)_8[Al_6Si_6O_{24}](SO_4,S)_2$ and their annealing products: a comparative XPS and XAS study. *European Journal of Mineralogy* **24**, 133-152.

Taylor, S.R. & McLennan, S.M. (1985) The continental crust: its composition and evolution. Blackwell Scientific Publications, Oxford, 312 pp.

Themelis, T. (2008): Gems & Mines of Mogok. A & T Publishers, 356 p.

Thériault, R.J., St-Onge, M.R. & Scott, D.J. (2001): Nd isotopic and geochemical signature of the Paleoproterozoic Trans-Hudson Orogen, southern Baffin Island, Canada: implications for the evolution of eastern Laurentia. *Precambrian Research* **108**, 113-138.

True North Gems Inc. (2007): True North Gems recovers 139 carat sapphire from new Baffin Island discovery. *Press release, Dec. 17 2007*, http://www.marketwired.com/press-release/true-north-gems-recovers-139-carat-sapphire-from-new-baffin-island-discovery-tsx-venture-tgx-803810.htm retrieved December 20, 2016.

Turekian, K.K. & Wedepohl, K.H. (1961): Distribution of the elements in some major units of the Earth's crust. *Geological Society of America Bulletin* **72**, 175-191.

Turner, D.J., Groat, L.A., Rivard, B., & Belley, P.M. (2017): Reflectance spectroscopy and hyperspectral imaging of sapphire-bearing marble from the Beluga occurrence, Baffin Island, Nunavut. *Canadian Mineralogist* **55**, 787-797.

Tuttle, M.L., Klett, T.R., Richardson, M. & Breit, G.N. (2000): Geochemistry of two interbeds in the Pennsylvanian Paradox Formation, Utah and Colorado – A record of deposition and diagenesis of repetitive cycles in a marine basin. *US Geological Survey Bulletin* **2000-N**, 86 p.

van Hinsberg, V.J., Henry, D.J., & Marschall, H.R. (2011): Tourmaline: an ideal indicator of its host environment. *Canadian Mineralogist* **49**, 1-16.

Van Velthuizen, J. (1993): The Parker mine, Notre Dame du Laus, Quebec. *Mineralogical Record* **24**, 369-373.

Villa, I.M. (2010): Disequilibrium textures versus equilibrium modelling: geochronology at the crossroads. *In:* Advances in interpretation of geological processes: refinement of multi-scale data and integration in numerical modelling. M.I. Spalla, A.M. Marotta, G. Gosso, editors. *Geological Society of London Special Publication* **332**, 1-15.

Wang, K.K., Graham, I.T., Lay, A., Harris, S.J., Cohen, D.R., Voudoris, P., Belousova, E., Giuliani, G., Fallick, A.E., & Greig, A. (2017): The origin of a new pargasite-schist hosted ruby deposit from Paranesti, Northern Greece. *Canadian Mineralogist* **55**, 535-560.

Warren, J.K. (2016): Meta-evaporites. *In:* Evaporites: a geological compendium. Springer, pp. 1375-1478.

Wenger, L.M. & Baker, D.R. (1986): Variations in organic geochemistry of anoxic-oxic black shale-carbonate sequences in the Pennsylvanian of the Midcontinent, U.S.A. *Advances in Organic Geochemistry* **10**, 85-92.

Wilson, B.S. (2014): Coloured gemstones from Canada. *In:* Lee Groat (editor), Geology of Gem Deposits. Mineralogical Association of Canada, Short Course **44**, 375-405.

Yakymchuk, C. & Szilas, K. (2018): Corundum formation by metasomatic reactions in Archean metapelite, SW Greenland: Exploration vectors for ruby deposits within high-grade greenstone belts. *Geoscience Frontiers* **9**, 727-749.

Yardley, B.W.D. & Graham, J.T. (2002): The origins of salinity in metamorphic fluids. *Geofluids* **2**, 249-256.

Appendix A

Appendix A1: Argon data collected from phlogopite sample "A" (Beluga occurrence).

Step	$^{40}Ar/^{39}Ar$	2σ	$^{38}Ar/^{39}Ar$	2σ	$^{37}Ar/^{39}Ar$	2σ	$^{36}Ar/^{39}Ar$	2σ	Ca/K	Cl/K	$\%^{40}Ar$ (atm)	f ^{39}Ar	$^{40}Ar^*/^{39}Ar_K$	2σ	Age	2σ
Phlogopite-A																
1	86.792	0.008	0.083	0.135	0.041	0.130	0.139	0.040	0.160	0.010	47.07	0.76	45.993	1.675	1564.28	38.11
2	55.846	0.007	0.032	0.070	0.008	0.231	0.022	0.077	0.032	0.003	11.64	2.34	49.408	0.601	1640.31	13.11
3	50.105	0.005	0.018	0.087	0.001	0.767	0.003	0.142	0.004	0.001	1.96	8.27	49.185	0.272	1635.45	5.96
4	55.968	0.008	0.052	0.084	0.005	1.152	0.023	0.103	0.020	0.008	11.88	0.96	49.380	0.797	1639.71	17.38
5	49.880	0.005	0.017	0.098	0.001	1.319	0.002	0.392	0.004	0.001	1.27	5.39	49.307	0.363	1638.12	7.93
6	49.965	0.005	0.016	0.053	0.002	0.405	0.003	0.144	0.007	0.000	1.73	6.91	49.160	0.288	1634.90	6.29
7	49.821	0.006	0.014	0.155	0.001	1.245	0.001	1.207	0.005	0.000	0.59	5.57	49.590	0.469	1644.27	10.20
8	49.877	0.004	0.017	0.057	0.002	0.412	0.003	0.118	0.007	0.001	1.98	6.13	48.950	0.252	1630.30	5.52
9	49.820	0.005	0.016	0.077	0.001	0.361	0.002	0.182	0.005	0.000	1.36	8.99	49.205	0.269	1635.89	5.89
10	49.519	0.005	0.016	0.061	0.002	0.432	0.002	0.271	0.007	0.000	1.16	8.21	49.005	0.294	1631.51	6.43
11	49.787	0.006	0.016	0.115	0.002	0.403	0.001	0.430	0.006	0.000	0.86	6.22	49.419	0.347	1640.56	7.57
12	49.642	0.005	0.014	0.098	0.001	0.954	0.001	0.717	0.004	0.000	0.61	6.12	49.402	0.346	1640.20	7.54
13	49.536	0.005	0.015	0.084	0.002	0.386	0.001	0.769	0.007	0.000	0.47	6.86	49.364	0.323	1639.35	7.05
14	49.463	0.005	0.014	0.096	0.002	0.485	0.001	0.709	0.007	0.000	0.46	7.16	49.295	0.312	1637.84	6.81
15	49.466	0.006	0.015	0.124	0.000	2.291	0.001	0.892	0.002	0.000	0.47	4.67	49.293	0.377	1637.81	8.23
16	49.200	0.006	0.014	0.083	0.001	0.526	0.001	0.326	0.005	0.000	0.69	7.61	48.922	0.314	1629.69	6.88
17	49.049	0.004	0.015	0.085	0.001	0.787	0.001	0.618	0.003	0.000	0.36	7.83	48.931	0.249	1629.88	5.46
Total/Avg	50.227	0.001	0.017	0.011	0.004	0.029	0.003	0.024		0.001		100.00	49.205	0.047		
	J = 0.030003 ± 0.000060, Volume $^{39}Ar_K = 442.9 \times 10^{-13}$ cm^3															

Appendix A2: Argon data collected from phlogopite sample "A" (Beluga occurrence).

Step	$^{40}Ar/^{39}Ar$	2σ	$^{38}Ar/^{39}Ar$	2σ	$^{37}Ar/^{39}Ar$	2σ	$^{36}Ar/^{39}Ar$	2σ	Ca/K	Cl/K	$\%^{40}Ar$ (atm)	f ^{39}Ar	$^{40}Ar^*/^{39}Ar_K$	2σ	Age	2σ
Phlogopite-B																
1	60.154	0.009	0.037	0.312	0.007	0.580	0.040	0.133	0.227	0.004	19.73	0.48	48.175	1.634	1613.22	36.16
2	55.607	0.005	0.018	0.126	0.001	1.354	0.007	0.117	0.033	0.001	3.93	3.43	53.300	0.389	1723.25	8.10
3	52.427	0.005	0.016	0.072	0.001	0.396	0.002	0.128	0.043	0.000	1.32	6.74	51.619	0.296	1687.90	6.29
4	51.976	0.006	0.016	0.058	0.000	3.278	0.003	0.128	0.005	0.000	1.74	9.57	50.953	0.314	1673.70	6.72
5	50.200	0.004	0.015	0.053	0.000	1.188	0.001	0.166	0.006	0.000	0.71	16.03	49.730	0.226	1647.33	4.90
6	51.229	0.011	0.016	0.258	0.003	1.742	0.003	0.420	0.085	0.000	1.93	1.52	50.124	0.679	1655.87	14.67
7	49.842	0.005	0.014	0.061	0.000	1.596	0.001	0.308	0.009	0.000	0.48	15.88	49.488	0.257	1642.07	5.60
8	49.954	0.005	0.015	0.068	0.000	1.082	0.001	0.450	0.013	0.000	0.33	9.75	49.675	0.242	1646.13	5.25
9	50.105	0.007	0.015	0.091	0.001	0.922	0.001	0.735	0.026	0.000	0.56	7.68	49.709	0.399	1646.86	8.67
10	50.267	0.006	0.013	0.057	0.000	2.067	0.001	0.555	0.004	0.000	0.32	12.82	49.989	0.339	1652.94	7.34
11	50.588	0.006	0.015	0.099	0.000	1.444	0.001	0.300	0.000	0.000	0.60	7.97	50.167	0.294	1656.79	6.34
12	50.839	0.007	0.014	0.104	0.000	1.859	0.001	0.512	0.000	0.000	0.41	6.28	50.512	0.349	1664.23	7.50
13	51.765	0.011	0.014	0.222	-0.001	2.903	0.004	0.586	0.000	0.000	2.05	1.84	50.586	0.850	1665.81	18.28
Total/Avg	50.703	0.001	0.015	0.011	0.007	0.012	0.002	0.036		0.000		100.00	49.617	0.053		
	J = 0.030003 ± 0.000060, Volume $^{39}Ar_K = 269.57 \times 10^{-13}$ cm^3															

Appendix A3: Argon data collected from muscovite sample "A" (Beluga occurrence).

Step	$^{40}Ar/^{39}Ar$	2σ	$^{38}Ar/^{39}Ar$	2σ	$^{37}Ar/^{39}Ar$	2σ	$^{36}Ar/^{39}Ar$	2σ	Ca/K	Cl/K	$\%^{40}Ar$ (atm)	f ^{39}Ar	$^{40}Ar^*/^{39}Ar_K$	2σ	Age	2σ
Muscovite-A																
1	33.725	0.006	0.094	0.038	0.027	0.077	0.050	0.038	0.110	0.016	43.09	3.95	19.197	0.567	820.57	19.46
2	27.641	0.005	0.063	0.075	0.216	0.018	0.020	0.056	0.875	0.010	21.03	6.02	21.845	0.350	909.28	11.44
3	39.520	0.004	0.069	0.043	0.467	0.018	0.008	0.069	1.891	0.012	5.84	14.76	37.277	0.240	1354.19	6.13
4	42.220	0.005	0.019	0.050	0.004	0.113	0.001	0.395	0.017	0.001	0.50	14.25	42.057	0.249	1472.36	5.97
5	39.617	0.004	0.018	0.055	0.002	0.267	0.001	0.561	0.009	0.001	0.47	17.03	39.474	0.207	1409.47	5.14
6	43.683	0.006	0.013	0.098	0.002	0.489	0.000	0.741	0.006	0.000	0.32	15.75	43.593	0.285	1508.75	6.68
7	43.588	0.005	0.013	0.118	0.001	0.785	0.000	1.761	0.004	0.000	0.19	12.88	43.553	0.275	1507.81	6.45
8	44.105	0.005	0.011	0.201	0.001	2.321	0.000	2.832	0.002	-0.001	0.20	7.36	44.070	0.347	1519.90	8.09
9	44.153	0.007	0.012	0.122	0.003	0.419	0.001	0.999	0.010	0.000	0.64	6.02	43.920	0.414	1516.40	9.68
10	44.791	0.010	0.016	0.252	0.007	0.709	0.006	0.657	0.030	0.000	3.99	1.98	43.052	1.268	1496.02	29.94
Total/Avg	40.954	0.001	0.029	0.012	0.187	0.004	0.005	0.021		0.004		100.00	43.682	0.052		
	J = 0.030000 ± 0.000062, Volume $^{39}Ar_K$ = 311.75 × 10^{-13} cm^3															

Appendix A4: Argon data collected from muscovite sample "B" (Beluga occurrence).

Step	$^{40}Ar/^{39}Ar$	2σ	$^{38}Ar/^{39}Ar$	2σ	$^{37}Ar/^{39}Ar$	2σ	$^{36}Ar/^{39}Ar$	2σ	Ca/K	Cl/K	%^{40}Ar (atm)	f ^{39}Ar	$^{40}Ar^*/^{39}Ar_K$	2σ	Age	2σ
Muscovite-B																
1	10.793	0.009	0.060	0.026	0.009	0.082	0.023	0.040	0.286	0.010	63.18	13.23	3.937	0.280	201.43	13.55
2	55.429	0.006	0.056	0.025	0.113	0.037	0.047	0.022	3.691	0.008	24.93	4.88	41.568	0.393	1460.62	9.46
3	45.162	0.006	0.021	0.053	0.014	0.094	0.004	0.058	0.468	0.002	2.81	9.76	43.794	0.295	1513.46	6.91
4	43.847	0.008	0.013	0.046	0.000	1.104	0.001	0.411	0.010	0.000	0.53	18.74	43.511	0.344	1506.81	8.08
5	43.892	0.010	0.013	0.080	0.001	0.664	0.001	0.260	0.030	0.000	0.62	13.38	43.516	0.437	1506.94	10.26
6	43.660	0.008	0.013	0.092	0.000	2.164	0.001	0.559	0.011	0.000	0.41	15.62	43.376	0.356	1503.64	8.36
7	44.058	0.005	0.013	0.069	0.001	0.419	0.000	0.578	0.019	0.000	0.25	20.52	43.841	0.252	1514.55	5.88
8	46.009	0.014	0.014	0.369	0.004	0.847	0.003	0.978	0.136	0.000	1.79	1.76	45.082	1.028	1543.32	23.65
9	46.587	0.009	0.013	0.355	0.002	1.304	0.005	0.349	0.067	-0.001	3.37	2.10	44.911	0.677	1539.39	15.60
Total/Avg	40.213	0.001	0.022	0.009	0.152	0.002	0.006	0.014		0.002		100.00	43.607	0.064		

J = 0.030000 ± 0.000062, Volume $^{39}Ar_K = 198.62 \times 10^{-13}$ cm^3